1-1-1976

Optical studies of the stress-induced crystallization of rubbers.

Mitsuaki Hashiyama
University of Massachusetts Amherst

OPTICAL STUDIES OF THE STRESS-INDUCED CRYSTALLIZATION OF RUBBERS

A Dissertation Presented

by

Mitsuaki Hashiyama

Submitted to the Graduate School of the
University of Massachusetts in
partial fulfillment of the requirements for the degree of

DOCTOR OF PHILOSOPHY

April 1976

Major Subject: Polymer Science and Engineering

OPTICAL STUDIES OF THE STRESS-INDUCED CRYSTALLIZATION OF RUBBERS

A Dissertation Presented

by

Mitsuaki Hashiyama

Approved as to style and content by:

Richard S. Stein

Richard S. Stein, Chairman of Committee

William J. MacKnight, Member

Roger S. Porter, Member

Isaac C. Sanchez, Member

S. L. Aggarwal, Member

Roger S. Porter

Roger S. Porter, Head
Polymer Science & Engineering

April 1976

ACKNOWLEDGMENT

I wish to express my sincere thanks to Professor Richard S. Stein, thesis advisor, for his invaluable guidance, his continued inspiration and encouragement during the course of this work.

I also wish to extend my gratitude to other members of my Thesis Committee, Professors Roger S. Porter, William J. MacKnight, Isaac C. Sanchez and Dr. S. L. Aggarwal, for their invaluable comments and suggestions.

Appreciation is extended to Professor Richard J. Farris for his invaluable comments and suggestions on the problems presented in Appendix II and to Dr. S. D. Hong for his constructive comments and helpful discussion on the problem presented in Chapter II.

Thanks and sincere appreciation are further extended to the faculty and staff of the Polymer Science and Engineering Department.

Thanks also go to my colleagues in the Polymer Science and Engineering Department for many helpful discussions and for their collaboration in some of the work described in this thesis.

Finally, I also wish to express my gratitude to Professor Hiromichi Kawai of Kyoto University, Japan, who introduced and recommended me to this Department.

In addition, I wish to acknowledge with thanks the financial assistance from the General Tire and Rubber Company.

TABLE OF CONTENTS

ABSTRACT

OPTICAL STUDIES OF THE STRESS-INDUCED
CRYSTALLIZATION OF RUBBERS

(April 1976)

Mitsuaki Hashiyama

Directed by: Professor Richard S. Stein

There are only a few methods available to follow crystallization of a rubber sample under high deformation. In the present investigation development and improvement of one method is considered, examined and discussed. The change in the fraction crystallinity with time and elongation of synthetic cis-1,4-polyisoprene (PIP) was studied through simultaneous measurement of birefringence and stress. Several theories for birefringence and stress were applied and examined for their applicability and limitations. Results from various methods were compared including the one from x-ray measurement. The method described here proved to be a sensitive and convenient method for determination of crystallinity of such samples.

Thermal effects of rapid extension and crystallization were considered. For the case of PIP studied here, it was concluded that the effects were small and could be neglected.

The crystal intrinsic birefringence, Δ_c^o, of PIP, cis-1,4-polybutadiene and syndiotactic-1,2-polybutadiene were calculated from their crystal structures

using bond polarizabilities. The different values obtained using several sets of the polarizabilities were compared.

An experimental value of Δ_c° of PIP was determined as 0.224. This value was somewhat higher than the calculated values. A primary reason for this was attributed to the internal field effect after the effect had been deeply examined from the theoretical point of view.

The degree of crystallinity and orientation function of PIP were determined for samples at various elongations by x-ray measurement. The crystallinity was in the same range obtained for natural rubber. For example, 14.3% crystallinity was obtained for a sample stretched to 500%. The orientation function was determined to be very high ($f_c = 0.98$). The Krigbaum-Roe theory was applied to obtain theoretical orientation distributions of the crystalline c axis. From a comparison of the theoretical and experimental distribution of the axis, the size of the critical nucleus was determined at various elongations. The size becomes smaller with elongation.

Morphological studies for PIP samples under various conditions were carried out using a photographic light scattering technique. It was concluded that the scattering unit consisted of an assembly of crystals with its fibril axis parallel to the stretching direction but, at higher elongations, with the fibril axis at a slight angle to the stretching direction. There was an indication that at high elongation there may be some interference between the fibril-like superstructures. When a swollen sample (by nitrobenzene) was stretched, additional new patterns appeared in the H_V scattering whose

origin is not certain. The V_V scattering indicated the disorder within the superstructure because of the existence of the solvent. The four lobes in the V_V scattering arose from the secondary crystallization which was very slow after disruption of the superstructure by heating. When PIP sample under 250% strain was heated, the scattering pattern was observed until 87°C. For the sample under 320% strain, the scattering pattern persisted at 105°C. These temperatures are considered to be higher than the melting temperatures of these stretched samples. The origin of this scattering is not as yet certain.

DEDICATION

To my parents

who made many sacrifices for

the fulfillment of my education.

GENERAL INTRODUCTION

The study on crystallization in high polymers has been one of the major fields of polymer science since its foundations were established in the 1930's. Since then many brilliant achievements in this field have been done.

High polymers can exist as various phases, which is true not only for high polymers but also for almost any material. As observed in low molecular weight compounds, a crystalline phase and an amorphous phase can be observed in many high polymers. Because of the great length of the molecules, however, crystallization in high polymers is a more complex phenomenon than crystallization in ordinary low molecular weight compounds. There are important differences between both types of crystallization. One important difference, which has been well established now, between the structure of a crystallized polymer and that of a crystalline low molecular weight compound, is that the former has a significant amount of amorphous materials. Furthermore, in polymeric materials the crystals do not exist as a distinct phase, but the amorphous segments of molecular chains are connected with the crystallites.

The mechanical and optical properties of a crystalline polymer depend upon both the internal structure and interaction between the crystalline and the amorphous regions. The degree of crystallinity, orientation of amorphous and crystalline regions, morphology and perfection within crystalline regions are the important factors which determine the properties of polymers. To illustrate the importance of crystallinity, one property——modulus is given in Table 1. From this table it is obvious that crystallinity is a very important factor in changing the properties of a

Table 1

Values for the Modulus of a Polymer in the Rubbery, Glassy, and Crystalline States (1)

State	Approximate Modulus (dynes/cm^2)
Amorphous-rubbery	10^7
Amorphous-glassy	10^{11}
Crystalline	10^{12}

polymer whose amorphous state is rubbery.

Two models describing the structure of crystalline polymers have been proposed. The first model is a composite single-phase structure known as the fringed micelle model (2,3) which is shown in Figure 1. In this model the polymer chains are precisely aligned over distances corresponding to the dimensions of the crystallites, and more disordered segments form amorphous regions. Since chains are very long, it is considered that they penetrate into several crystalline and amorphous regions. The crystallites may be considered to be more or less cylindrical in shape. This concept satisfactorily accounts for many aspects of behavior of a polycrystalline polymer. In general, however, it is known to be too simple for a structure of crystalline polymer, and obviously does not account for more complex structures such as spherulites which are observed to grow in many crystalline polymers.

The second, and more recent model for the structure of crystalline polymers has been suggested right after the discovery of single crystals

from dilute polymer solutions, first from polyethylene solution (4-6). The concept is that a chain folding back and forth to form an intramolecular crystal lamella whose thickness is of the order of 100 Å. This idea is called the chain folding model and shown in Figure 2. Since then the formation of single crystals has been reported for many polymers, and it appears to be quite general and universal (7,8). Spherulites are considered as superstructures of folded chain lamellae, and found in many melt-crystallized polymers (9).

In summary, the fringed-micelle concept has largely been displaced especially for highly crystalline polymers. There are, however, many problems to solve such as the structure of polymers with low or intermediate crystallinity, in which the fringed-micelle model may still be the more appropriate one.

There are essentially two different types of crystallization. The first is so called "thermally induced crystallization", in which the amorphous melt is kept at temperatures between the glass transition temperature and melting point. The second is "stress-induced crystallization", in which rubbery polymer is sufficiently stretched to cause the crystallization (10).

The crystallization of rubber-like materials generally includes both aspects mentioned above. Low temperature crystallization occurs when rubber is cooled sufficiently in the unstretched state, and spherulitic structure is formed (11). The rate of low temperature crystallization of rubber in the unstretched state is generally markedly slower than that under strain. The axes of the crystallites are randomly oriented, and the x-ray diffraction pattern of such a crystallized rubber is similar to that shown by a crystalline powder. Andrews (12) showed that the spherulites

consist of crystalline islands dispersed with radiating crystalline filaments and amorphous material. This was called α-filament by Andrews and believed to be a folded chain type crystal. Recently Edwards (13) reported that a new type of spherulitic lamellar crystal in cis-polyisoprene has been identified, which was different in growth rate, lamellar thickness, and in direction of fold plane from those of α-filament. The α-lamellar crystal grows in prestrained films with the a axis perpendicular to the stretch direction. The new type of lamellar crystal was identified with the b axis perpendicular to the stretch direction, and named β-lamella. The multiple melting transitions for cis-polyisoprene have been related to these different morphological species.

In stress-induced crystallization the crystals had veen visualized as a system of parallel fringed micelles aligned along the stretching direction. The electron microscopic studies by Andrews (14), however, revealed structures such as those shown in Figure 3. The fibrous crystals apparently grew perpendicularly to the stress direction and they were connected by isolated columns whose direction was parallel to the stress direction. The former crystalline filament was considered as an α-filament and the latter was called a γ-filament.

This discovery was related to the independent result (15) from the crystallization of polymer melts under stress or flow. In this crystallization crystal nuclei are formed parallel to the stress or flow direction. The subsequent crystal growth is essentially confined to be normal to these lines. This is shown schematically in Figure 4 (16). If stress is low, this crystallization was be essentially as in spherulites; if the stress is high, the lamellae will be prevented from twisting and will align straight.

In Figure 3, the crystal structure of a stretched rubber is very similar to the shish-kebab (17) grown from stirred solutions. As with the case of solution-crystallized shish-kebabs, it has been suggested that also in the bulk a fibrous backbone (γ-filament) was first formed parallel to the stress direction, and that then untwisted folded chain lamellae (α-filament) grew normal to the stress direction from the backbone as nuclei. The backbone chain is considered to be partly or mostly extended-chain crystal, which is more thermodynamically stable.

Recently a new concept for the formation of shish-kebabs was suggested by Nagasawa and Shimomura (18). Their model is that the crystals grow first by a screw dislocation mechanism, like whiskers, and then later these are deformed by the shear stress to form the shish-kebab structure, which means that the shish and kebabs are formed simultaneously, and not in two steps.

The rubbery state of materials is characterized by their undergoing high elastic deformation. Especially in crosslinked three dimensional networks, this deformation is generally recoverable and reversible. The kinetic theory of rubber elasticity has been developed by Kuhn and Grün (19,20), and by Treloar (21), which can describe well the behavior of a crosslinked rubber at least qualitatively. An experimental stress-strain curve and theoretical predictions are shown in Figure 5.

However, when the rubber is stretched, the network entropy decreases, which causes an increase in the crystallization temperature and the ability of the rubber to crystallize increases. Consequently crystallization under strain may occur at higher temperatures than the melting temperature of the unstrained rubber. The crystallization accompanied by the crystal

orientation may cause substantial deviation from the kinetic theory of rubber elasticity. Treloar showed that (22) the hysteresis of the stress-strain curve and birefringence-stress curve of the crosslinked natural rubber was a consequence of the oriented crystallization. When the crystallites are formed during stretching, they may act as additional crosslinks. This means there is a rapid increase in the number of effective crosslinks with elongation. The increase causes the Young's modulus of rubber to increase drastically with increasing elongation. This phenomenon is often observed as causing the pronounced upward curvature in the stress-strain behavior (22,23). This is shown as curve 4 in Figure 5. Furthermore because of the increase of effective crosslinkages, the average degree of parallel alignment of amorphous chain molecules will increase markedly. As a result the crystallization will be accelerated by the elongation.

Crystallites formed by stress-induced crystallization have a tendency to align their c-axis parallel to the stretching direction. Consequently x-ray diffraction patterns show discrete spots superposed on an amorphous background such as shown in Figure 6.

The present theoretical understanding of crystallization in rubber-like polymers rest largely on studies of Flory (24). In his theory it is assumed that the chains which traverse the resulting crystallites are parallel to the stretching direction. The theory describes the relation between the equilibrium degree of crystallinity and the stress at a given elongation. This theory also predicts that the crystallization of pre-oriented polymers has the effect of reducing the applied stress.

The fact that stress-induced crystals orient along some preferential direction introduces the optical anisotropy, in addition to that

arising from the deformed amorphous regions. The increase in birefringence was observed during crystallization at high elongations by Treloar (25), which was proportional to the crystallinity determiend from the density measurement. Recently Smith (26) has developed an equation for birefringence in stress-induced crystallization using almost the same assumptions which Flory made in his theory (24). This theory predicts that the birefringence increases in the course of stress-induced crystallization.

Since crystal orientation and morphology in solid polymers are important to obtain specific properties appropriate for certain applications of commercial products, many studies (27-29) have been carried out on structures resulting from the industrial processes such as extrusion, spinning, blow and injection moldings, cold drawing, etc. Most of these processes include the solidification and deformation during flow of melt. These practical industrial processes may be complex, mainly because they are not under isothermal conditions. Therefore it is more simple and straightforward to study stress-induced crystallization under isothermal conditions.

The kinetic study of crystallization under stress may be carried out by the use of conventional methods such as dilatometry, calorimetry, and x-ray diffraction. In most systems, however, their use is difficult because of the long time required for measurement, or because of inconvenience for need of special experimental arrangements. Therefore, in many cases the crystallization in stretched natural rubber and synthetic rubber has been studied by observing the associated relaxation of tensile stress (30-33). Their results show that the rate of crystallization increases enormously with the applied strain. However, the degree of crystallinity of natural rubber is usually small and less than 30% even at very high exten-

sion. The Avrami index (34) decreases to values close to 1.0 at high elongation, which suggests one-dimensional crystal growth from pre-existing nuclei.

Since the birefringence of crystalline polymers depends upon the amorphous regions as well as the crystalline regions, the change in the birefringence during stress-induced crystallization may give a clue to understanding the crystallization process, just as the stress-relaxation does. One of the attempts to use the birefringence to follow crystallization has been proposed by Stein and Norris (35) and Yau (36), and applied to several polymers (37,38).

Traditionally, morphological studies of crystalline structure of a polymer has been carried out mostly by the optical and electron microscope. Since the sizes of the crystalline structure approach, in many cases, the limit of resolution of the optical microscope, it may be difficult to clearly distinguish the crystalline structures in a sample by optical microscopic study. The latter method may create possible misleading results, because samples for study under the electron microscope may be prepared in a manner much different from the condition in which the sample normally exists.

The light scattering technique (39,40) has been developed to study orientation and morphology of polycrystalline materials. It is a very sensitive and convenient method to provide morphological information about crystalline structure for many crystalline polymers. The light scattering study of the crystallization of natural rubber under stress has been carried out by Yau and Stein (41).

One of the purposes of this study is an attempt to develop an

optical (birefringence) method originally proposed by Stein and Norris (35) to follow crystallization with time, which should be convenient and accurate. Another purpose of the study is to obtain morphological information about crystalline structure during stress-induced crystallization by the light scattering investigation. Since the light scattering study of the crystallization of natural rubber (36), there have been further theoretical and technological developments. It may be a good time to study the stress-induced crystallization in light of these new developments. Finally the applicability and limitation of several theories (24,26,42) for the stress-induced crystallization are closely examined qualitatively and quantitatively.

Most parts of this work deal with the problems of the crystallization of synthetic cis-1,4-polyisoprene under large deformations. We may, however, hope that it will help to obtain an insight into the many relevant problems of stress-induced crystallization of other rubber-like materials.

References

1. A. Sharples, "Crystallinity", in Polymer Science, Ch. 4, Ed. by A. D. Jenkins.
2. K. Herrman and O. Gerngross, Kautschuk, 8, 181 (1932).
3. W. M. D. Bryant, J. Polym. Sci., 2, 547 (1947).
4. E. W. Fischer, Z. Naturforsch., 12a, 753 (1957).
5. A. Keller, Phil. Mag., 8, 2, 1171 (1957).
6. P. H. Till, Jr., J. Polym. Sci., 24, 301 (1957).
7. P. H. Geil, "Polymer Single Crystals", Interscience, New York, 1963.
8. A. Keller, Kolloid Z., and Z. Polymere, 197, 98 (1964).
9. A. Keller, J. Polym. Sci., 39, 151 (1959).
10. L. R. G. Treloar, "The Physics of Rubber Elasticity", 2nd ed., Oxford, 1967.
11. W. H. Smith and C. P. Saylor, J. Res. Nat. Bur. Stds., 21, 257 (1938); Rubber Chem. Tech., 12, 18 (1939).
12. E. H. Andrews, Proc. Roy. Soc., A270, 232 (1962).
13. B. C. Edwards, J. Polym. Sci., Polym. Phys. Ed., 13, 1387 (1975).
14. E. H. Andrews, Proc. Roy. Soc., A277, 562 (1964); J. Polym. Sci., A-2, 4, 668 (1966).
15. A. Keller, J. Polym. Sci., 15, 31 (1955).
16. M. J. Hill and A. Keller, J. Macromol. Sci.-Phys., B3, 153 (1969).
17. A. J. Pennings, Proc. Int. Conf. on Crystal Growth, Boston (Oxford: Pergamon Press), pp. 389.
18. T. Nagasawa and Y. Shimomura, J. Polym. Sci., Polym. Phys. Ed., 12, 2291 (1974).
19. W. Kuhn, Kolloid Z., 76, 258 (1936).

20. W. Kuhn and F. Grün, Kolloid Z., 101, 248 (1942).

21. L. R. G. Treloar, Trans. Faraday Soc., 43, 277 (1947).

22. L. R. G. Treloar, Trans. Faraday Soc., 43, 284 (1947).

23. P. J. Flory, Ind. Eng. Chem., 38, 417 (1946).

24. P. J. Flory, J. Chem. Phys., 15, 397 (1947); J. Chem. Phys., 17, 223 (1949).

25. L. R. G. Treloar, Trans. Faraday Soc., 37, 84 (1941).

26. K. J. Smith, Jr., J. Polym. Sci., A-2, 6, 1723 (1968).

27. E. C. Bernhardt, "Processing of Thermoplastic Materials", Reinhold, New York, 1959.

28. E. S. Clark, SPE Journal, 23, 46 (1967); ACS Papers, Organic Coatings and Plastics Chemistry, 32, 19 (1972).

29. A. Peterlin, "Man-Made Fibers", Vol. 1, H. F. Mark et al., ed., Interscience, New York (1967).

30. A. N. Gent, Trans. Faraday Soc., 50, 521 (1954); J. Polym. Sci., 3, 3787 (1965).

31. J. J. Arlman and J. M. Goppel, Appl. Sci. Res., A2, 1 (1951).

32. L. A. Wood and F. C. Roth, J. Appl. Phys., 15, 781 (1944).

33. H. G. Kim and L. Mandelkern, J. Polym. Sci., A-2, 6, 181 (1968).

34. M. Avrami, J. Chem. Phys., 7, 1103 (1939); ibid, 8, 212 (1940); ibid, 9, 177 (1941).

35. R. S. Stein and F. Norris, J. Polym. Sci., 21, 381 (1956).

36. W. C. Yau, Ph.D. Thesis, University of Massachusetts, 1966.

37. G. Kraus and J. T. Gruver, J. Polym. Sci., Polym. Phys. Ed., 10, 2009 (1972).

38. Y. Akana, M.S. Thesis, University of Massachusetts, 1973.

39. P. Debye and A. M. Bueche, J. Appl. Phys., 20, 518 (1949).

40. M. B. Rhodes and R. S. Stein, J. Appl. Phys., 31, 1873 (1960).

41. W. C. Yau and R. S. Stein, J. Polym. Sci., PT. B, 2, 231 (1964); J. Polym. Sci., A2, 6, 1 (1968).

42. W. R. Krigbaum and R. J. Roe, J. Polym. Sci., A, 2, 4391 (1964).

Captions for Figures

1) A fringed micelle model.

2) A model for the lamellar crystal.

3) Row nucleated or "shish-kebab" structure in strained natural rubber [from E. H. Andrews (14)].

4) Schematic diagram illustrating crystallization under (a) low stress and (b) high stress for polyethylene [from A. Keller (16)].

5) Experimental and theoretical stress-strain curves: 1. Experimental curve of an amorphous sample. 2,3. Gaussian and non-Gaussian predictions for the sample given in 1. 4. Experimental curve of a crystallizable sample.

6) X-ray diffraction pattern of a PIP sample stretched to $\alpha = 6.2$ at room temperature.

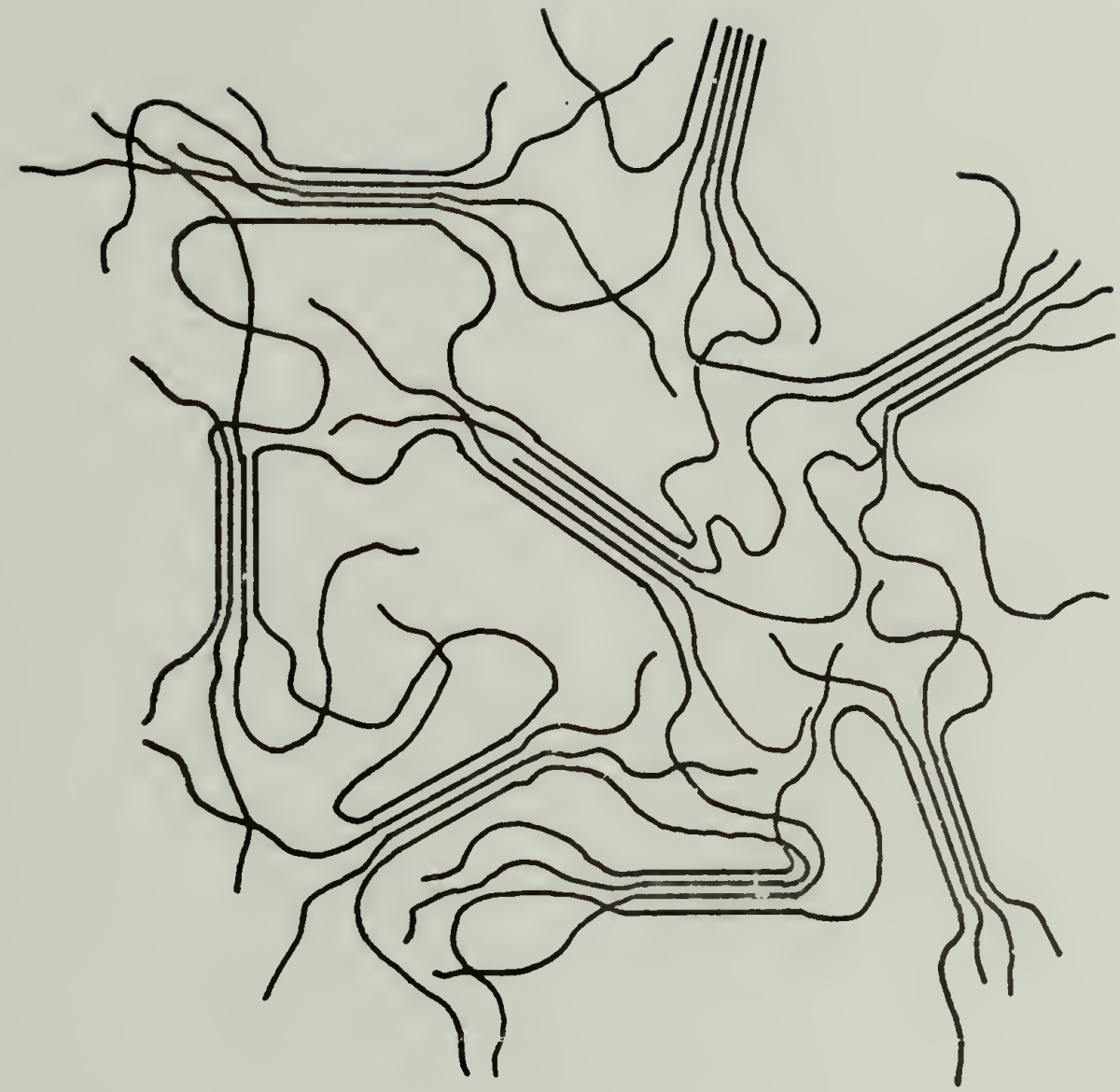

Figure 1

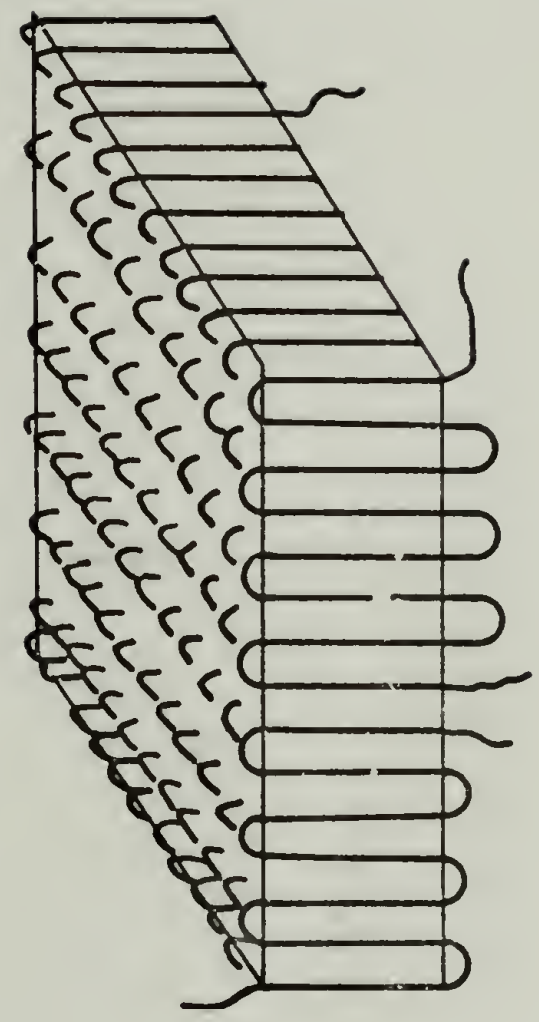

Figure 2

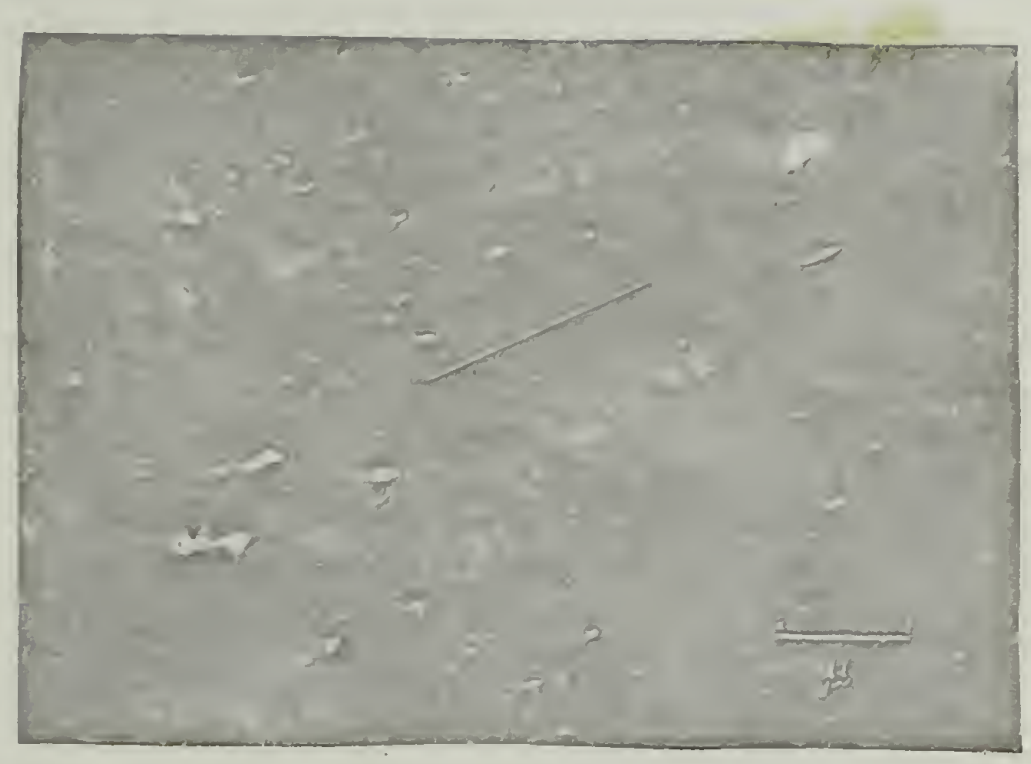

Figure 3

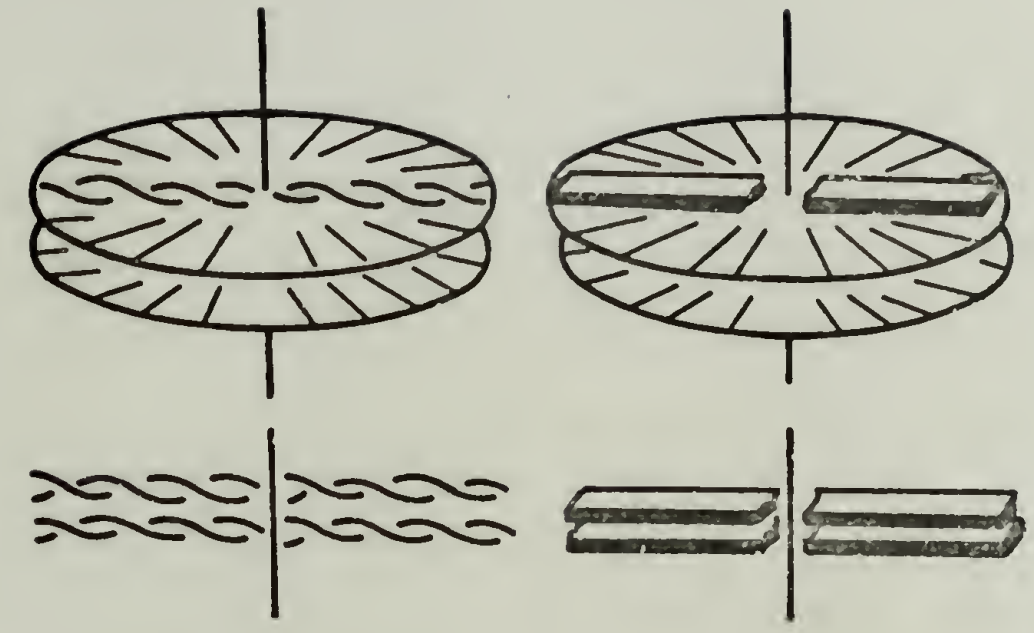

Low stress High stress

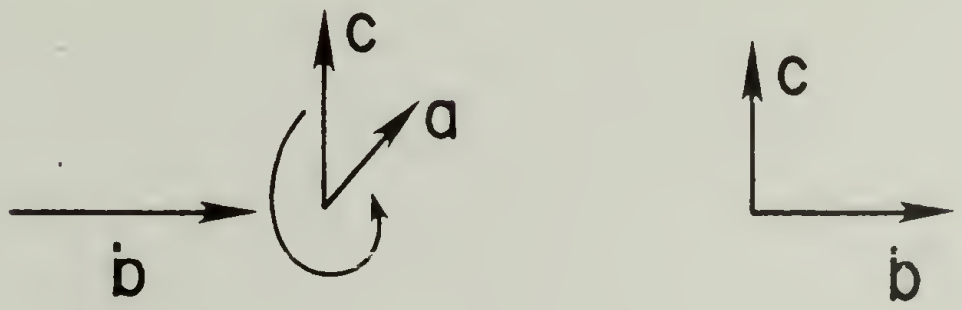

Figure 4

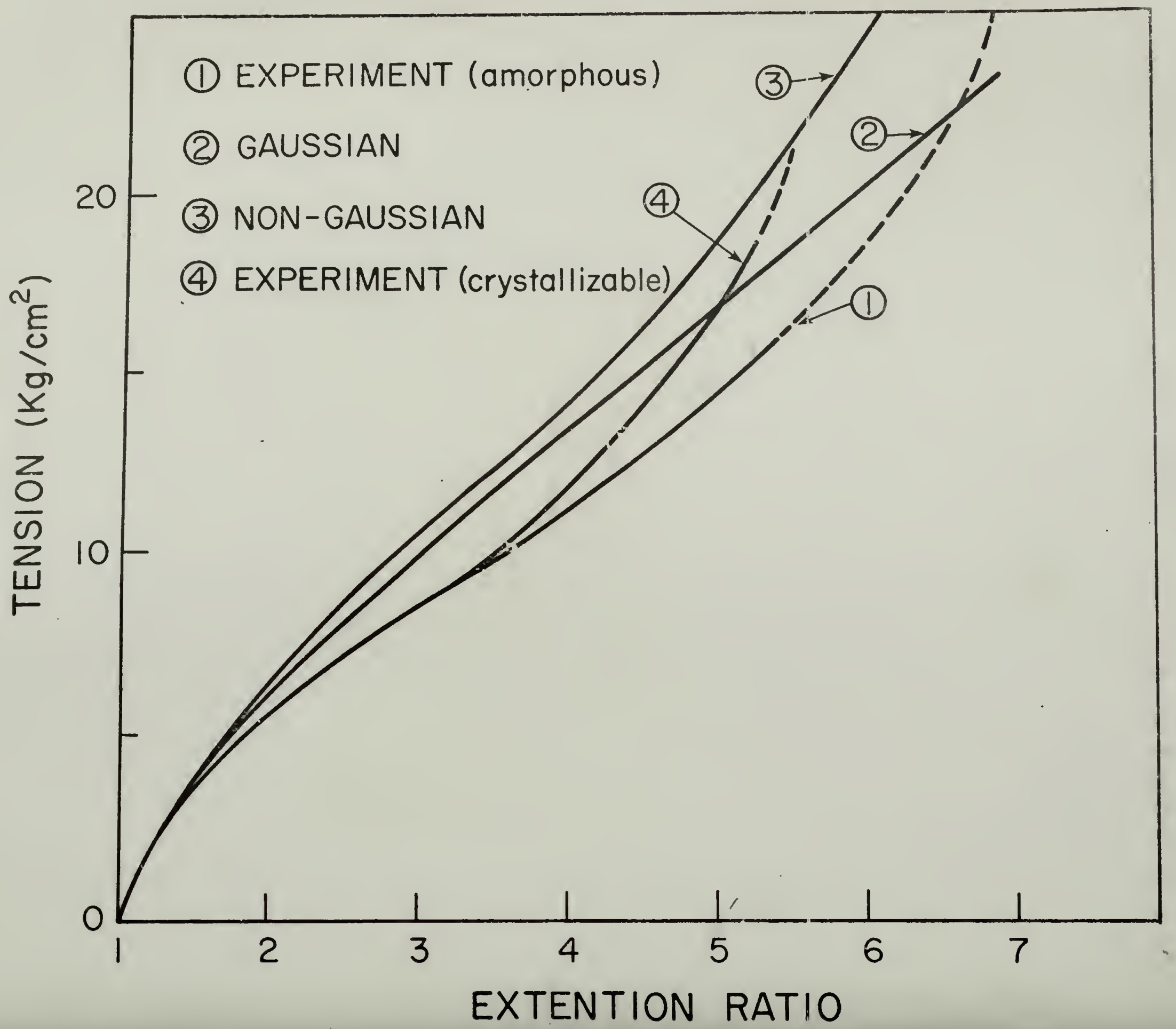
① EXPERIMENT (amorphous)
② GAUSSIAN
③ NON-GAUSSIAN
④ EXPERIMENT (crystallizable)
TENSION (Kg/cm²)
0
10
20
1
2
3
4
5
6
7
EXTENTION RATIO

Figure 5

Figure 6

CHAPTER I

BIREFRINGENCE STUDIES*

Summary

The change in the fraction crystallinity with time and elongation of synthetic cis-1,4-polyisoprene is studied through simultaneous measurement of birefringence and stress. Results are compared with values estimated from the decrease in stress arising from the crystallization. Various methods for calculating the crystallinity from the data are compared. This method proves to be a sensitive, convenient method for determination of crystallinity of such samples.

Introduction

The crystallization of natural rubber in the unstrained and uniaxially stretched states has been discussed in detail by many authors (1-5). Theoretical interpretations have also been tried by some authors (7,8). These theories give the degrees of crystallinity at a constant elongation and constant temperature. However, differing results are obtained using different theories.

For determining the crystallinity of the rubber the x-ray diffraction method is one of the best absolute methods. It may, however, be impossible to follow the crystallization by observing the change in x-ray diffrac-

---

*Acknowledgements. Most of the parts in CHAPTER I appeared in the paper titled "Birefringence Studies of the Strain-Induced Crystallization of Rubbers", in Die Makromolekulare Chemie, Suppl. 1, 579 (1975), which is authored with R. Gaylord and R. S. Stein.

tion intensity with time because of the long time required for the x-ray measurements. Consequently, it becomes necessary to develop other methods to follow crystallization under stress. A part of this work is to obtain and develop one of these methods.

W. Kuhn, working along with F. Grün (9) laid down the foundations of theory of birefringence of stretched rubbers leading to the equation for the stress-optical coefficient C in the Gaussian approximation

$$C = \Delta/\sigma = \frac{2\pi}{45} \frac{(\bar{n}^2 + 2)^2}{\bar{n}kT} \Gamma_s \qquad (1)$$

where Δ is the birefringence, σ the stress (based upon the actual cross-sectional area), $\bar{n}$ the average refractive index, k Boltzmann's constant, T the absolute temperature and Γ_s the anisotropy of the statistical segment of the polymer chain. More recent molecular theories of Flory, et al. (10) and Nagai (11) have yielded expressions for Γ_s in terms of bond polarizability tensors, factors describing molecular geometry, and bond rotation potentials. The validity of this equation has been extensively explored by Treloar (12), Gent (13), Stein (6), and others and has been shown to be essentially correct, provided the polymer is sufficiently above its T_g, is not crystalline and not too highly crosslinked or too highly elongated. The value of C is a property of the nature of the monomer unit constituting the chain and should be independent of the degree of crosslinking and elongation. The value of Γ_s may depend upon temperature in a predictable way because of the changing freedom of bond rotation with temperature. The slight elongation dependence of birefringence may be described in terms of an equation (11,13)

$$\Delta/(\alpha^2 - 1/\alpha) = 2B_1 + 2B_2/\alpha \qquad (2)$$

where α is the elongation ratio, which is analogous to the Mooney-Rivlin equation (14,15)

$$\sigma/(\alpha^2 - 1/\alpha) = 2C_1 + 2C_2/\alpha \qquad (3)$$

Thus the stress-optical coefficient is given by

$$C = \frac{B_1 + B_2/\alpha}{C_1 + C_2/\alpha} \qquad (4)$$

Since, generally $B_2/B_1 \neq C_2/C_1$, C varies with α. However upon swelling, both B_2 and C_2 become small and C becomes α independent. Also, it has been shown (16) that for rubbers crosslinked in the swollen state and then dried B_2 as well as C_2 are small.

It is noteworthy to observe (17) that values of C measured in the swollen state agree well with values obtained from streaming birefringence measurements in dilute solution in the same solvent. Consequently, the value of C measured in the swollen state appears to be a molecular property quite accurately described by the Kuhn-Grün theory. Deviations which are observed with unswollen rubbers are a consequence of short range interactions between molecules not considered in the theory as well and network complication arising from such factors as chain entanglements.

The enhancement of the birefringence arising from crystallization of rubbers was described by Treloar (12) and discussed by P. H. Hermans (18) for the contribution of the crystals to the birefringence of cellulose fibers. Following him, Stein and Norris (19) proposed that the birefringence

of polyethylene could be described by the equation

$$\Delta = \phi_c \Delta_c + (1 - \phi_c)\, \Delta_a + \Delta_f \qquad (5)$$

where ϕ_c is the volume fraction crystallinity, Δ_c and Δ_a are the birefringence values per unit volume of the crystalline and amorphous phases, and Δ_f is the form birefringence arising from the interface between the phases. Its value may be estimated using the technique of Weiner (20) of swelling with solvents of differing refractive index and found to be of the order of a 5% contribution. This result is consistent with the conclusions of a recent theory by Stein and coworkers (21) for the form birefringence of spherulitic polyethylene. The value of Δ_c may, in turn, be given by

$$\Delta_c = \Delta_c^{\,o}\, f_c \qquad (6)$$

for uniaxially birefringent crystals $\Delta_c^{\,o}$ is the intrinsic birefringence of the crystal. f_c is the crystal orientation function defined by

$$f_c = [3 \ \langle \cos^2 \theta_c \rangle - 1]/2 \qquad (7)$$

where θ_c is the angle between the stretching direction and the crystal optic axis.

Equation (5) has been used extensively by Stein and coworkers (19, 22) for polyethylene and by Samuels (23) for polypropylene for resolving the total birefringence into contributions from the crystalline and amorphous parts. The crystalline orientation function, f_c, was calculated from x-ray

diffraction, while the value of Δ_c^o for polyethylene was equated to microscopically measured values for n-paraffin crystals. The amorphous birefringence can be given by a corresponding equation

$$\Delta_a = \Delta_a^o f_a \tag{8}$$

By using the value of Δ_a^o obtained from stress-birefringence measurements on crosslinked polyethylene above the melting point of the crystals, one may then use this equation to obtain f_a the orientation function of the amorphous segments, which may then be favorably compared with values obtained using other methods (24).

The extension of this approach to the quantitative study of rubber crystallization was made by Stein and Yau (25) and later applied to the study of the stress induced crystallization of trans-polypentenamer by Kraus and Gruver (26). They assumed that stress-induced crystals are perfectly oriented so that $f_c = 1$. They also assumed that the amorphous birefringence could be given by the equation

$$\Delta_a = C\sigma \tag{9}$$

where C is the stress-optical coefficient of the amorphous rubber, and σ is the total stress. The application of this equation involves two assumptions: (1) The amorphous phase of the crystallized rubber is identical with that of the completely amorphous rubber. This neglects the possible perturbation of the amorphous phase by the presence of crystals, and (2) The stress on the amorphous phase equals the total stress. This neglects the stress

concentrating effect of the crystals. Both of these assumptions are probably fair approximations at low degrees of crystallinity, and will be considered in greater detail later in the paper. Upon including these assumptions in Equation (5) and neglecting the form birefringence, one obtains

$$\Delta = \phi_c \Delta_c^o + (1 - \phi_c) C\sigma \qquad (10)$$

which may be solved for ϕ_c to give

$$\phi_c = (\Delta - C\sigma)/(\Delta_c^o - C\sigma) \qquad (11)$$

Kraus and Gruver assumed that $\Delta_c^o > C\sigma$ so that the denominator of Equation (11) could be assumed constant. The crystallization rate of transpolypentenamer was sufficiently slow so that it was possible to stretch the polymer prior to crystallization and then observe changes in crystallinity with time for the polymer held at constant length. The value of $\Delta_c^o = 0.27$ was obtained by calibrating against an independent measure of crystallinity and was also found to be in agreement with values calculated from bond polarizabilities.

In this paper, we apply this method to the study of the crystallization of synthetic cis-1,4-polyisoprene, consider its limitations and improvement and compare the results with other methods for following the crystallization.

Experimental

The sample of synthetic cis-1,4-polyisoprene (PIP) was a Goodyear Natsyn 200 material with an $\overline{M}_n$ of about 350,000. The cis 1,4 content was in the range of 97-98%, with the remaining 2-3% being principally vinyl. It was purified by precipitation by methanol from a 5 g/200 ml solution in benzene. It was then dried in vacuum at room temperature for 24 hours, redissolved in benzene (20 g/l) along with dicumyl peroxide (DCP) as a cross-linking agent and with an antioxidant of 2,6-di-tert-butyl-p-cresol in the propirtions, PIP, 100 pts. by weight, DCP, 1 pt., and antioxidant, 0.5 pts. The solution was cast on a teflon coated pan to give films approximately 400 μm thick. These films were then cured for 30 minutes at 140°C at 5000 psi in a small laboratory press, holding the films between sheets of cellophane.

Samples were studied using an Instron tensile tester equipped with a constant temperature chamber and an optical bench for birefringence measurements using a filtered mercury light source and a Babinet compensator (27). The birefringence was calculated from the retardation R (in numbers of wavelengths) using the equation

$$\Delta = \lambda_o R/d \qquad (12)$$

where λ_o is the wavelength of the mercury green line in vacuum (5461 Å) and d is the thickness of the sample which is calculated from the initial thickness d_o assuming uniaxial stretching and incompressibility from

$$d = d_o \alpha^{-1/2} \qquad (13)$$

Forces were also measured with the Instron and stresses were caluclated on the basis of the actual (calculated) cross-sectional areas.

Two types of experiments were conducted. In the first, samples were stretched rapidly at room temperature at a rate of about 2000 % per min. to their final elongations after which birefringence and stress were observed as a function of time. In the second type of experiment, the sample was stretched at a high enough temperature (90°C) so that crystallization did not occur. Then after holding the sample at constant length and temparature for about 20 min. during which time the stress and birefringence slightly decreased and approached constant values, the temperature was lowered rapidly to room temperature (in less than a minute) and changes in stress and birefringence were observed as a function of time.

The first method suffered from the fact that the crystallization of PIP was sufficiently rapid so that crystallization may have occurred during stretching and that crystals were characteristic of a wide range of elongations during stretching. While under these conditions, Equation (11) and its modifications are believed to give the correct value of ϕ_c, the crystallization process is not one occurring at constatn elongation, which complicates the kinetic analysis. Furthermore, equations for describing the force on the crystallizing rubber such as that proposed by Flory (7) are based upon the assumption that crystals grow in a network held at fixed elongation. This assumption is not valid for the first procedure.

Results and Interpretation

Two different rubber samples were used in this investigation which differed slightly in their degree of crosslinking. Sample A was used

at elongations of α = 2.87 and 3.98 while B was used for α = 5.0 and 6.0. The stress-optical coefficient was derived from data obtained at elongations sufficiently low so that crystallization did not occur. The plots of stress vs $(\alpha^2 - 1/\alpha)$ for stretching samples A and B rapidly to the indicated elongations are shown in Figures 1 and 2, respectively. Deviations are seen from the straight line that would be expected if the rubber obeyed kinetic rubber elasticity theory. Mooney-Rivlin type plots for these samples for the stress and birefringence made according to Equations (2) and (3) are given in Figures 3 and 4 for samples A and B, respectively. From such plots, the stress-optical coefficient, according to Equation (4) is given by

$$C = \frac{4.494 + 2.799/\alpha}{2.263 + 1.128/\alpha} \times 10^{-4} \text{ cm}^2/\text{kg} \qquad (14)$$

for sample A, and

$$C = \frac{3.104 + 3.862/\alpha}{1.690 + 1.498/\alpha} \times 10^{-4} \text{ cm}^2/\text{kg} \qquad (15)$$

for sample B. The difference reflects a somewhat higher degree of cross-linking for sample A.

For comparisons of the stress-birefringence behaviors of different polymers Mooney-Rivlin plots for natural rubber samples are given in Figure 5. Natural rubber (NR) was obtained from the General Tire and Rubber Company (Akron, Ohio). NR samples used here were prepared by the same method as described for PIP samples. The stress-birefringence behavior for cis-1,4-polybutadiene (28) is also given in Figure 6. All figures indicate that the stress-birefringence behaviors can be described by Equations (2) and (3). In Figure 5, the upturns from the straight lines are observed

when α becomes larger than two. This phenomenon may be caused by finite chain extensibility rather than crystallization as shown by Smith and co-workers (29,30). For PIP, there is no upturn at least in the range shown in the figures. This difference may be considered as one of the characteristic features for NR and PIP. The fact that the stress-birefringence behaviors of PIP are described over the broad range by Equations (2) and (3) indicates that PIP may, probably, be a better polymer to study by the method used here.

Plots of the variation of stress and birefringence following the rapid stretching (approximately 2000 % per minute) of these PIP samples by the designated amounts are given in Figures 7-10.

It is seen that at the lower elongation, there is negligible variation of both stress and birefringence with time while at α = 3.89 a slight increase in birefringence and decrease in stress is detectable. This trend becomes appreciable at α = 5.0 and α = 6.0 and is clearly a consequence of crystallization.

In applying Equation (11) a correction factor was incorporated to account for the difference between the total stress and that on the amorphous phase by dividing the total stress by a factor $F(\phi_c)$ proposed by Guth (31) and Smallwood (32) as

$$F(\phi_c) = 1 + 2.5\ \phi_c + 14.1\ \phi_c^2 \qquad (16)$$

in which the crystals are approximated as spherical filler particles. This factor was first applied by Akana (31) in the studies of trans-polybutadiene. This correction was found to amount to about 30% for the higher

degrees of crystallinity. It is probable that a more correct $F(\phi_c)$ would approximate the crystals as rod-like inclusions, but the use of the extra parameter of an axial ratio that this would require did not seem warrented at this time.

The volume fraction crystallinities obtained by substituting (14) or (15) in Equation (11) were calculated. These were converted to weight fractions using

$$X_c = \rho_c \phi_c / [\rho_c \phi_c + \rho_a (1 - \phi_c)] \qquad (17)$$

where ρ_c and ρ_a are the densities of the crystalline and amorphous phases. The value of ρ_c for PIP was calculated from its crystal structure as 1.007 g/cm^3. Values for X_c determined in this way are plotted as a function of elongation in Figures 11-14.

At $\alpha = 2.87$, birefringence indicates negligible crystallization, while increasing amounts of crystallization are obtained at higher elongation ratios. It is noted that crystallization is seen at quite early times, casting doubt on the assumption that the sample is stretched before crystallization begins. For these calculations, a value of intrinsic crystalline birefringence of $\Delta_c^o = 0.130$ was used which was calculated from Denbigh's bond polarizabilities and crystal structure parameters as described in Appendix I.

Values of the degree of crystallinity calculated from Flory's stress equation (7) are also included in Figures 11-14. This equation is

$$\sigma = \frac{N_c kT}{(1 - X_c)} \left\{ (\alpha^2 - 1/\alpha) - \alpha (6n_s/\pi)^{1/2} X_c \right\} \qquad (18)$$

where N_c is the number of network chains/cm^3, X_c is the weight fraction crystallinity and n_s is the average number of segments between crosslinks. N_c is obtained from the stress at low elongations when X_c is negligible from the initial slope (dashed line) of Figures 1 and 2. n_s is obtained by dividing the number of segments/cm^3, N_s, by N_c. N_s is in turn obtained from

$$N_s = \rho A/M_o q \tag{19}$$

where ρ is the density found to be 0.91 [in agreement with McPherson (34)], A is Avagadro's number, M_o is the molecular weight of the isoprene unit (C_5H_8 = 68) and q is the number of isoprene units per segment. This is approximated by

$$q = (b_\ell - b_t)_s/(b_\ell - b_t)_i \tag{20}$$

where $(b_\ell - b_t)_s = \Gamma_s$ is the anisotropy of the statistical segment given by Equation (1) and $(b_\ell - b_t)_i$ is the anisotropy of the isoprene unit in the amorphous state given by Treloar (35) as 2.71×10^{-24} cm^3. By using the SOC at α = 1 obtained from Equations (14) and (15), we obtain q = 1.95 and 1.98 for samples A and B, respectively, which agree within experimental error.

The degrees of crystallinity obtained using Equation (18) differ appreciably from those obtained from Equation (11) at lower elongations but agree better at higher elongations. In addition to the previously given reason of the inapplicability of Equation (18) to the description of crystallization occurring during stretching, deviations are believed to arise from two additional causes: Equation (18) presumes that in the absence of

crystallization, the stress is accurately given by the ideal rubber elasticity equation, so that the deviations from this behavior can be accurately associated with the effects of crystallization. Actually, a fraction of this deviation may result from non-ideal rubber behavior. Also, limitations are involved in Flory's derivation of Equation (18). The model implies a direct single pass model of crystallization with perfectly oriented crystals where a chain enters the crystal from the amorphous phase and passes through it without reversing direction. Actually, reverse passing of the chain through the crystal and multiple passing associated with chain folding is neglected. The effects of these limitations are considered next under the more readily treatable situation where the crystallization is accomplished following stretching.

Data for samples crystallized by the second method where the sample was heated to 90°C, stretched to α = 6.0 and then rapidly cooled to room temperature is given in Figure 15. Crystallization is believed to begin quite early, at about 0.002 hrs, and leads to an increase in birefringence and decrease in stress. Values of X_c obtained in this way from the birefringence are plotted in Figure (16).

In order to avoid the previously discussed difficulty in calculating crystallinity from the stress resulting from deviations from ideal rubber elasticity theory, a procedure for treating data first suggested by Gent (3) was adopted. Rather than depending upon rubber elasticity theory for calculating the stress on the amorphous network prior to crystallization which would be affected by the errors in this theory, the actual experimental value of the stress was employed. If this value, designated as σ_o, is used instead of the $N_c kT\ (\alpha^2 - 1/\alpha)$ term in Equation

(18), it may then be written as

$$\sigma = \frac{\sigma_o}{(1 - X_c)}\left[1 - \frac{\alpha}{(\alpha^2 - 1/\alpha)}\left(\frac{6n_s}{\pi}\right)^{1/2} X_c\right] \qquad (21)$$

which may then be used for the calculation of X_c. Such values are included in Figure (16) which agree quite well with those obtained from the birefringence data. n_s is obtained from N_c in the equation $\sigma_o = N_c kT(\alpha^2 - 1/\alpha)$.

The limitation of Equation (11) arising from the neglect of perturbation of the SOC of the amorphous phase may be explored using the equation proposed by Smith (8) for the birefringence of a semicrystalline network obtained using assumptions similar to those used in the derivation of the Flory equation of stress. This is

$$\Delta = \frac{2\pi N_c (\bar{n}^2 + 2)^2}{9\bar{n}}\left\{(b_\ell - b_t)_c\, n_s\, X_c + \frac{(b_\ell - b_t)_s}{5(1 - X_c)}\right.$$
$$\left.\left[(\alpha^2 - 1/\alpha) - 2X_c\alpha\,(6n_s/\pi)^{1/2} + 3n_s\, X_c^2\right]\right\} \qquad (22)$$

where $(b_\ell - b_t)_c$ and $(b_\ell - b_t)_s$ are the statistical segment anisotropies of the crystalline and amorphous phases. This equation presumes that the amorphous phase may be described by the ideal statistical theory up to the point of crystallization. It is seen that when $X_c = 0$, Equation (22) reduces to the Kuhn-Grun result. The application of this equation to the determination of X_c is found to lead to values differing appreciably from those obtained from Equations (11) and (21). The reason is believed to be primarily related to the non-ideal behavior of the amorphous phase. This deficiency may be overcome using the same approach as proposed by Gent for the stress;

that is, to utilize for the amorphous contribution, the birefringence just before crystallization commences, designated by Δ_o, to give

$$\Delta = \frac{5\Delta_o (b_\ell - b_t)_c n_s X_c}{(b_\ell - b_t)_s(\alpha^2 - 1/\alpha)} + \frac{\Delta_o}{(1 - X_c)(\alpha^2 - 1/\alpha)}$$
$$X \left[(\alpha^2 - 1/\alpha) - 2X_c\alpha(6n_s/\pi)^{1/2} + 3n_s X_c^2\right] \qquad (23)$$

Using the value of n_s obtained from the value of N_c which is calculated from Δ_o using the Kuhn-Grun result, $(b_\ell - b_t)_s$ obtained from Equation (1) at low elongation and calculated values of $(b_\ell - b_t)_c$, X_c may be calculated and is plotted in Figure (16). The values are in reasonably good agreement with those obtained using Equation (11) suggesting that at least at the relatively low degrees of crystallinity encountered in this study, the approximations inherent in Equation (11) are good.

Since the recent studies (29,30) of stress-strain isotherms for rubber above room temperature strongly indicate that non-Gaussian (N-G) behavior occurs at lower strains than does crystallization, it may be interesting to extend Flory's stress and Smith's birefringence theories by applying non-Gaussian network theory in place of Gaussian theory which is used in their derivation. These calculations have been carried out by Gaylord (36) (see Note 1 for the derivations).

The stress equation is described as

$$\sigma = \frac{N_c kT\,\alpha}{(1 - X_c)}\left[\left(\alpha - \frac{1}{\alpha^2}\right) - X_c\left(\frac{6n_s}{\pi}\right)^{1/2} - \frac{1}{20}X_c\left(\frac{6}{\pi n_s}\right)^{1/2}\right]\left[1 - \frac{1}{n_s(1 - X_c)}\right]$$

$$+ \frac{3N_c kT\,\alpha}{5n_s(1 - X_c)}\left[\alpha^3 - \frac{1}{\alpha^3} + n_s X_c^2\left(3\alpha - \frac{1}{\alpha^2}\right) + \frac{1}{3} - \frac{1}{3\alpha^3}\right.$$

$$\left. - 12X_c\left(\frac{n_s}{6\pi}\right)^{1/2}\alpha^2 - n_s X_c^3\left(\frac{6n_s}{\pi}\right)^{1/2}\right] \qquad (24)$$

and the birefringence is expressed by

$$\Delta = \frac{2\pi N_c(\bar{n}^2 + 2)^2}{9\bar{n}}\left\{(b_\ell - b_t)_c\, n_s X_c + \frac{(b_\ell - b_t)_a}{5(1 - X_c)}\left[\left(1 - \frac{2}{5n_s(1 - X_c)}\right)\right.\right.$$

$$(\alpha^2 - 1/\alpha) + 3n_s X_c^2 - 2\alpha X_c\left(\frac{6n_s}{\pi}\right)^{1/2} - \frac{\alpha X_c}{10}\left(\frac{6}{\pi n_s}\right)^{1/2}$$

$$+ \frac{35}{35(1 - X_c)^2}\left(\frac{1}{3n_s}\left(\alpha^4 - \frac{1}{\alpha^2}\right) + \frac{1}{9n_s}\left(\alpha - \frac{1}{\alpha^2}\right) + \frac{2}{3}X_c^2\left(3\alpha^2 + \frac{1}{2\alpha}\right)\right.$$

$$\left.\left.\left. + n_s X_c^4 - \frac{4}{3}\alpha X_c^3\left(\frac{6n_s}{\pi}\right)^{1/2} - \frac{2}{9}X_c(4\alpha^3 + 1)\left(\frac{6}{n_s\pi}\right)^{1/2}\right)\right]\right\} \qquad (25)$$

The crystallinity X_c may be calculated from Equations (24) and (25) by using the same approach as described previously to overcome the non-ideal behavior of the amorphous phase. The calculated values of X_c are also plotted in Figure 16.

There is a small difference in the values obtained from the Gaussian and non-Gaussian equations. The values, however, are considered to be in reasonably good agreement with those obtained using Equation (11).

We may attempt to fit this isothermal crystallization data to an

Avrami (37) type equation

$$X_c = X_\infty [1 - \exp(-k_c t^n)] \qquad (26)$$

where X_∞ is the ultimate crystallinity, k_c is the rate constant, and n is the Avrami exponent which is often associated with the dimensionality of the process. This equation may be written in the form

$$\ell n \left\{ -\ell n[1 - (X_c/X_\infty)] \right\} = \ell n k_c + n \ell n t \qquad (27)$$

The value of X_∞ was obtained from extrapolation to long times using values obtained from Equation (11) to give $X_\infty = 0.23$ at $\alpha = 6.0$. The data are plotted according to Equation (27) in Figure 17 to give a straight line during the initial period of crystallization with a slope giving a value of $n = 0.93$. Such a low value of n is often found for crystallization in oriented systems and is interpreted as unidirectional growth on predetermined nuclei.

As it is seen from Figure 17, as the crystallization progresses the deviation from the Avrami equation becomes prominent. One may conclude that (38) as the transition from amorphous phase to crystalline phase progresses, the rate of crystallization will become smaller than that predicted by the theory. The heat liberated by crystallization has been considered as one of the reasons for the deviation. The possibility was eliminated however after considering the heat balance within the sample as shown in Appendix II. Several possible reasons are mentioned by Mandelkern (38) and others (39). One of them is that if nucleation occurs only by limited

amount impurities which are activated accidentally with time, the rate of nucleation will decrease with time considerably because of consumption of the impurities. At any rate, as the crystallinity increases, the deviation from the theory appears to increase. The development of the theory for the region in which the crystallinity becomes large is strongly called for.

The variation of crystallinity with temperature on stepwise cooling was observed by stretching a sample at 90°C and after 30 min, lowering the temperature in 5° steps. The temperature was kept constant for 15 min at each temperature after which the stress and birefringence achieved a constant value. Values for the variation of stress and birefringence determined in this way are plotted in Figures (18) and (19) for different extension ratios. At low elongations, the stress is approximately proportional to temperature and the birefringence is independent of temperature as expected for amorphous rubbers. At higher elongations and lower temperatures, the stress decreases more rapidly with decreasing temperature and the birefringence increases as a consequence of crystallization. The arrows show the temperatures at which crystallization is believed to begin. Crystallization is seen to affect birefringence much more than stress.

The change in X_c with temperature was calculated using the modified Equation (11) and is plotted in Figure 20 at $\alpha = 4.98$ and $\alpha = 6.51$. For this purpose the stress-optical coefficient prior to crystallization was taken from values of stress and birefringence at the position of the arrows in Figures (18) and (19) and it was calculated at lower temperatures by assuming it to be inversely proportional to temperature. It is seen that the melting point of the crystals is greater at the higher elongation and that the degree of crystallinity increases as the temperature is lowered.

Conclusions

The variation in degree of crystallinity of a rubber during stretching, with time following rapid cooling of a stretched sample or with temperature during stepwise cooling of a stretched sample may be followed by simultaneous measurement of the birefringence and the stress. For samples isothermally crystallizing at constant length, the degree of crystallinity calculated from the stress decrease agrees well with that calculated from the birefringence. At moderate to low degrees of crystallinity errors resulting from the assumption that the stress-optical coefficient of the amorphous phase appear to be small.

Note I

An Expansion of Flory's Equation to Non-Gaussian Network*

The network is assumed to be first oriented well enough so that the subsequently formed crystallites will have their chain axes parallel to the direction of stretch. As the temperature is lowered, portions of the network chains enter crystallites. Because repeat units in the crystalline region traverse a greater distance than they do when free (or amorphous), the remaining amorphous units of the chains are deformed away from the posi-

---

*Acknowledgements. Most of Note I is taken from "Theories of Chain Coiling, Elasticity, and Viscoelasticity", by Prof. K. J. Smith, Jr., in Polymer Science, edited by A. D. Jenkins, American Elsevier, New York, 1972, and modified for the derivation of non-Gaussian equations. The derivation was carried out by Dr. R. Gaylord except the part of the melting temperature.

tions which they had when the entire chain was amorphous. This deformation must be taken into account; therefore the free energy of fusion can be written as the sum of two terms: one, the free energy of fusion of the units in the crystalline phase (calculated on the basis that they are free or unconstrained) ΔF_n, and two, the deformational free energy imposed on the remaining amorphous segments by the crystallites, ΔF_D,

$$\Delta F_T = \Delta F_n + \Delta F_D \tag{28}$$

The deformational free energy of a chain of n_s segments when stretched from r_o to r may be written to the order of n_s^{-1} as

$$\Delta F_D = kT\left(\frac{3r^2}{2n_s\ell^2} - \frac{3r^2}{2n_s^2\ell^2} + \frac{9r^4}{20n_s^3\ell^4} - \frac{3r_o^2}{2n_s\ell^2} + \frac{3r_o^2}{2n_s^2\ell^2} - \frac{9r_o^4}{20n_s^3\ell^4}\right) \tag{29}$$

After crystallization of m segments the amorphous chain contains only $n_s - m$ segments. Furthermore, if the initial deformation is great enough, say along x, the distance spanned by the $n_s - m$ amorphous segments will change from $r^2 = x^2 + y^2 + z^2 + r_c^2 = (x - m\ell)^2 + y^2 + z^2$, the y- and z- directions being essentially unaffected by the crystallization. Therefore, ΔF_D may be written as

$$\Delta F_D = \frac{3GkT}{2\ell^2}\int [(x - m\ell)^2 + y^2 + z^2]\left[\frac{1}{(n_s - m)} - \frac{1}{(n_s - m)^2}\right] W(\underset{\sim}{r})\, d\underset{\sim}{r}$$

$$+ \frac{9GkT}{20(n_s - m)^3\ell^4}\int [(x - m\ell)^4 + y^4 + z^4 + 2(x - m\ell)^2(y^2 + z^2) + 2y^2z^2]$$

$$W(\underset{\sim}{r})d\underset{\sim}{r} - \frac{3}{2\ell^2}\langle r_o^2\rangle\left[\frac{1}{(n_s - m)} - \frac{1}{(n_s - m)^2}\right] - \frac{9}{20(n_s - m)^3\ell^4}\langle r^4{}_o\rangle \tag{30}$$

where $\langle r^2_o \rangle$ is $(n_s - m)\ell^2$, $\langle r^4_o \rangle$ is $\frac{5}{3}(n_s - m)^2\ell^4$, and G is the number of active chains in the system.

The distribution $w(\underset{\sim}{r})\, d\underset{\sim}{r}$ is that of the chains before crystallization. For simple elongation along x by an amount α it is

$$W(\underset{\sim}{r})d\underset{\sim}{r} = \left[\frac{3}{2\pi n_s \ell^2}\right]^{3/2} \exp\left\{-\frac{3}{2n_s\ell^2}\left[\frac{x^2}{\alpha^2} + \alpha(y^2 + z^2)\right]\right\}\left\{1 - \frac{3}{4n_s}\right.$$

$$+ \frac{3}{2n_s{}^2\ell^2}\left[\frac{x^2}{\alpha^2} + \alpha(y^2 + z^2)\right] - \frac{9}{20n_s{}^3\ell^4}\left[\frac{x^4}{\alpha^4} + \alpha^2\right.$$

$$\left.\left.(y^4 + z^4) + \frac{2}{\alpha}(x^2y^2 + x^2z^2) + 2\alpha^2y^2z^2\right]\right\} dxdydz \qquad (31)$$

By carrying out the integration of Equation (31) one obtains

$$\Delta F_D = \frac{GkT}{2(1 - X_c)}\left\{\left[1 - \frac{1}{n_s(1 - X_c)}\right]\left[\alpha^2 + \frac{2}{\alpha}\right] - 2\alpha X_c\left(\frac{6n_s}{\pi}\right)^{1/2}\right.$$

$$- \frac{1}{10}\alpha X_c\left(\frac{6}{n_s\pi}\right)^{1/2} + \frac{2\alpha X_c}{(1 - X_c)}\left(\frac{6}{n_s\pi}\right)^{1/2} + \frac{\alpha X_c}{10n_s(1 - X_c)}$$

$$\left.\left(\frac{6}{n_s\pi}\right)^{1/2} + 3X_c{}^2n_s - \frac{3X_c{}^2}{(1 - X_c)}\right\} + \frac{36\ GkT}{20n_s(1 - X_c)^3}$$

$$\left\{\left(\alpha^4 + \frac{2}{\alpha^2}\right) + 2n_sX_c{}^2\left(3\alpha^2 + \frac{2}{\alpha}\right) + 3n_s{}^2X_c{}^4 + \frac{4}{3}\left(\alpha + \frac{1}{2\alpha^2}\right)\right.$$

$$\left. - 16X_c\left(\frac{n_s}{6\pi}\right)^{1/2}(\alpha^3 + 1) - 4n_sX_c{}^3\alpha\left(\frac{6n_s}{\pi}\right)^{1/2}\right\} \qquad (32)$$

where $X_c = m/n_s$ is the weight fraction of crystallinity.

In the absence of the constraints imposed by the term ΔF_D the m statistical segments would crystallize just as does any other substance.

Thus we can write

$$\Delta F_n = -mG[\Delta H_u - T\Delta S_u] \tag{33}$$

where ΔH_u and ΔS_u are the heat and entropy of fusion respectively, consequently

$$\Delta F_n = -mG\ \Delta H_u[1 - T/T^\circ_m] \tag{34}$$

since at the fusion point for unstretched chains $\Delta S_u = \Delta H_u/T^\circ_m$, T°_m being the crystallization temperature of unstrained chain. Thus

$$\Delta F_T = -mG\ \Delta H_u\ [1 - T/T^\circ_m] + \Delta F_D \tag{35}$$

which represents the change in free energy of a total of Gm statistical segments crystallizing at constant deformation α.

The stress-strain isotherm at equilibrium crystallization can be determined by noting that ΔF_T is a function of α and m, consequently,

$$d\Delta F_T = \left(\frac{\partial \Delta F_T}{\partial \alpha}\right)_m d\alpha + \left(\frac{\partial \Delta F_T}{\partial m}\right)_\alpha dm \tag{36}$$

At equilibrium $(\partial \Delta F_T/\partial m)\alpha = 0$ and

$$\frac{d\Delta F_T}{d\alpha} = \left(\frac{\partial \Delta F_T}{\partial \alpha}\right)_m \tag{37}$$

which is simply the retractive force per unit length of unstretched sample, hence

$$\frac{f}{GkT/L_o} = \frac{1}{(1 - X_c)}\left\{\left(\alpha - \frac{1}{\alpha^2}\right) - X_c\left(\frac{6n_s}{\pi}\right)^{1/2} - \frac{1}{20}\ X_c\left(\frac{6}{n_s\pi}\right)^{1/2}\right\}$$
$$\left\{1 - \frac{1}{n_s(1 - X_c)}\right\} + \frac{3}{5n_s(1 - X_c)^3}\left\{\alpha^3 - \frac{1}{\alpha^3} + n_s X_c{}^2\right.$$
$$\left.\left(3\alpha - \frac{1}{\alpha^2}\right) + \frac{1}{3} - \frac{1}{3\alpha^3} - 12X_c\left(\frac{n_s}{6\pi}\right)^{1/2}\alpha^2 - n_s X_c{}^3\left(\frac{6n_s}{\pi}\right)^{1/2}\right\} \tag{38}$$

where f is the refractive force and L_o is the length of unstrained sample. If the number of active chains per unit volume, N_c is used in place of G, one would obtain Equation (24).

On setting $(\partial\Delta F_T/\partial m)\alpha$ equal to zero and setting $X_c = 0$, one obtains an expression for the temperature of incipient crystallization T_m as

$$\frac{1}{T_m} - \frac{1}{T_m{}^o} = \frac{R}{2n_s\ \Delta H_u}\ F(\alpha, n_s) \tag{39}$$

where

$$f(\alpha, n_s) = \alpha^2 + 2/\alpha - 2\alpha\ (6n_s/\pi)^{1/2} - \frac{2}{n_s}\ (\alpha^2 + 2/\alpha) - \frac{\alpha}{10}\left(\frac{6}{n_s\pi}\right)^{1/2}$$
$$+ 2\alpha\left(\frac{6}{n_s\pi}\right)^{1/2} + \frac{\alpha}{10n_s}\left(\frac{6}{n_s\pi}\right)^{1/2} + \frac{54}{5n_s}\left\{\left(\alpha^4 + \frac{2}{\alpha^2}\right)\right.$$
$$\left. + \frac{4}{3}\ \left(\alpha + \frac{1}{2\alpha^2}\right)\right\} - \frac{288}{5n_s}\ (\alpha^3 + 1)\left(\frac{n_s}{6\pi}\right)^{1/2}$$

In $F(\alpha, n_s)$ the first three terms are corresponding to the Gaussian expression.

Note II

An Expansion of Smith's Theory to Non-Gaussian Networks*

The birefringence Δn may be obtained by differentiating the Lorentz-Lorenz equation as

$$\Delta n \simeq \frac{2\pi (\bar{n}^2 + 2)^2}{9\bar{n}} \Delta\gamma \tag{41}$$

where $\Delta\gamma = \gamma_1 - \gamma_2$ is the difference between the polarizabilities of two principle axes.

Both crystalline and amorphous regions contribute to the birefringence, hence $\Delta\gamma$ may be separated to yield

$$\Delta n = \frac{2\pi (\bar{n}^2 + 2)^2}{9\bar{n}} (\Delta\gamma_c + \Delta\gamma_a) \tag{42}$$

where the subscripts (c and a) denote the crystalline and amorphous contribution, respectively.

In the assumed model the crystallites are perfectly aligned along the direction of stretch, hence a statistical segment within a crystallite is also oriented in this direction. If we denote the longitudinal and the average transverse components of polarizability of a crystalline statistical

---

*Acknowledgements. Most part of the Note II is taken from the article titled "Birefringence of Semicrystalline Polymeric Networks", by Prof. K. J. Smith, Jr., in Journal of Polymer Science, A-2, Vol. 6 (1968), and modified for the derivation of non-Gaussian equations. The derivation was carried out by Dr. R. Gaylord.

segment as b_{1c} and b_{2c} respectively, we can write $\Delta\gamma_c$ as

$$\Delta\gamma_c = n_s G (b_{1c} - b_{2c}) X_c \tag{43}$$

where $n_s G X_c$ is the total number of segments making up the crystalline region.

If γ_x is the x component of polarizability of a chain in an ensemble of chains and γ_y is the y component of the polarizability, $(\gamma_x - \gamma_y)$ is given as

$$\gamma_x - \gamma_y = \frac{3(b_1 - b_2)}{5n_s\ell^2} \left[\left(1 - \frac{2}{5n_s}\right)(x^2 - y^2) + \frac{12}{35n_s^2\ell^2} (x^4 - y^4 + x^2z^2 - y^2z^2) \right] \tag{44}$$

where b_1 is the polarizability of an amorphous statistical segment along its long axis, b_2 is the average polarizability in the transverse direction, and ℓ is the length of a statistical segment.

The total polarizability $\Delta\gamma = \gamma_1 - \gamma_2$ may be obtained by summing the contribution of all chains

$$\Delta\gamma = \int (\gamma_x - \gamma_y)\, dG \tag{45}$$

where dG is the chain distribution function and is given by the theory of rubber elasticity. For the case of simple elongation along the x axis this function is expressed as

$$dG = G\, W(\underset{\sim}{\gamma})\, d\,(\underset{\sim}{\gamma}) \tag{46}$$

The above results are valid only for completely amorphous networks so their application to the amorphous portion of semicrystalline structure entails some modification.

If we let the subscript a denote the amorphous portion of the chain we have in lieu of Equation (45)

$$\Delta\gamma_a = \int (\gamma_x - \gamma_y)_a \, dG_a \tag{47}$$

Because the crystallites are presumed to lie with their chain direction along the direction of stretch x, x_a becomes

$$x_a = x - X_c n_s \ell \tag{48}$$

where $X_c \, n_s \ell$ is the distance traversed by the crystalline portion of the chain, but the Y, Z coordinates are unaffected, therefore

$$y_a = y$$

$$z_a = z \tag{49}$$

This means that an amorphous chain with one end located at the origin of a rectangular coordinate system and the other end located around the point (x,y,z) will have coordinates $(x - X_c n_s \ell, y, z)$ after $X_c n_s$ segments have crystallized. Furthermore, crystallization will reduce the number of segments in the amorphous portion of a chain spanning the distance $\gamma_a^2 = (x - X_c n_s \ell)^2 + y^2 + z^2$ is $n_a = n_s(1 - X_c)$. We have therefore

$$\Delta\gamma_a = \int [\gamma_x - \gamma_y]\, dG$$

$$= \frac{3(b_1 - b_2)}{5n_s(1 - X_c)\ell^2} G \left[\frac{3}{2\pi n_s \ell^2}\right]^{3/2} \int\int_{-\infty}^{\infty}\int \left\{\left[1 - \frac{2}{5n_s(1 - X_c)}\right]\right.$$

$$\left[(x - X_c n_s \ell)^2 - y^2\right] + \frac{12}{35n_s^2(1 - X_c)^2\ell^2} \left[(x - X_c n_s \ell)^4 - y^4\right.$$

$$\left.\left. + (x - X_c n_s \ell)^2 z^2 - y^2 z^2\right]\right\} \exp\left\{-\frac{3}{2n_s\ell^2}\left[\alpha(y^2 + z^2) + \frac{x^2}{\alpha^2}\right]\right\}$$

$$\left\{1 - \frac{3}{4n_s} + \frac{3}{2n_s^2\ell^2}\left[\alpha(y^2 + z^2) + \frac{x^2}{\alpha^2}\right] - \frac{9}{20n_s^3\ell^4}\right.$$

$$\left.\left[\alpha^2(y^4 + z^4) + \frac{x^4}{\alpha^4} + \frac{2}{\alpha}(x^2y^2 + x^2z^2) + 2\alpha^2y^2z^2\right]\right\} \qquad (50)$$

Integration of Equation (49) yields for amorphous anisotropy

$$\Delta\gamma_a = \frac{G(b_1 - b_2)}{5(1 - X_c)} \left\{\left[1 - \frac{2}{5n_s(1 - X_c)}\right]\right.$$

$$\left[(\alpha^2 - 1/\alpha) + 3n_s X_c^2 - 2\alpha X_c \left(\frac{6n_s}{\pi}\right)^{1/2} - \frac{\alpha X_c}{10}\left(\frac{6}{n_s\pi}\right)^{1/2}\right] + \frac{36}{35(1 - X_c)^2}$$

$$\left[\frac{1}{3n_s}\left(\alpha^4 - \frac{1}{\alpha^2}\right) + \frac{1}{9n_s}\left(\alpha - \frac{1}{\alpha^2}\right) + \frac{2}{3}X_c^2\left(3\alpha^2 + \frac{1}{2\alpha}\right) + n_s X_c^4 - \frac{4}{3}\alpha X_c^3\right.$$

$$\left.\left.\left(\frac{6n_s}{\pi}\right)^{1/2} - \frac{2}{9}X_c(4\alpha^3 + 1)\left(\frac{6}{n_s\pi}\right)^{1/2}\right]\right\} \qquad (51)$$

From Equations (42), (43) and (51) we obtain the expression for the birefringence of a semicrystalline network. Then the birefringence per unit volume may be expressed by Equation (25).

References

1. L. A. Wood and N. Bekkedahl, J. Appl. Phys., 17, 362 (1946).
2. G. M. Mortin and L. Mandelkern, J. Appl. Phys., 34, 2312 (1963).
3. A. N. Gent, Trans. Faraday Soc., 50, 521 (1954).
4. A. N. Gent, J. Polym. Sci., A-2, 3, 3787 (1965), 4, 447 (1966).
5. H. G. Kim and L. Mandelkern, J. Polym. Sci., A-2, 6, 181 (1968).
6. R. S. Stein and A. V. Tobolsky, Textile Res. J., 18, 201, 302 (1948).
7. P. J. Flory, J. Chem. Phys., 15, 397 (1947).
8. K. J. Smith, Jr., J. Polym. Sci., A-2, 6, 1723 (1968).
9. W. Kuhn and F. Grün, Koll. Z., 101, 248 (1942).
10. P. J. Flory, The Statistical Mechanics of Chain Molecules, Interscience, New York, 1969.
11. K. Nagai, J. Phys. Chem., 74, 3411 (1970); T. Ishikawa and K. Nagai, J. Polym. Sci., A2, 7, 1123 (1969).
12. L. R. G. Treloar, The Physics of Rubber Elasticity, Oxford, 1958.
13. A. N. Gent and V. V. Vickroy, Jr., J. Polym. Sci., A2, 5, 47 (1967).
14. M. Mooney, J. Appl. Phys., 19, 434 (1948).
15. R. S. Rivlin in Rheology, F. R. Eirich, Ed., Academic Press, New York, 1956, Vol. 1.
16. C. S. M. Ong and R. S. Stein, J. Polym. Sci., 12, 1599 (1974).
17. M. Fukuda, G. L. Wilkes and R. S. Stein, J. Polym. Sci., A2, 9, 1417 (1971).
18. P. H. Hermans, Contributions to the Physics of Cellulose Fibers, Elsevier, New York, 1946, p. 198.
19. R. S. Stein and F. H. Norris, J. Polym. Sci., 21, 381 (1956).

20. O. Wiener, Abhandl. kg. Sachs. Ges. Wiss., Math.-Phys. Klasse, 32, 509 (1912).

21. C. Chang, D. Peiffer and R. S. Stein, J. Polym. Sci., Polym. Phys. Ed., 12, 1441 (1974).

22. R. S. Stein in Annual Reviews of Physical Chemistry, H. Eyring, C. J. Christensen and H. S. Johnson, Eds., Ann. Rev. Inc., Palo Alto, Calif., 1973, Vol. 24, p. 207.

23. R. J. Samuels, J. Polym. Sci., A3, 1741 (1965).

24. G. L. Wilkes, Adv. in Polym. Sci., 8, 91 (1971).

25. W. Yau, Ph.D. Thesis, Univ. of Mass., Amherst, Mass. (1966).

26. G. Kraus and J. T. Gruver, J. Polym. Sci., Polym. Phys. Ed., 10, 2009 (1972).

27. D. A. Keedy, R. J. Volungis and H. Kawai, Rev. Sci. Instr., 32, 415 (1961).

28. C. Ong and R. S. Stein, J. Polym. Sci., Polym. Phys. Ed., 12, 1599 (1974).

29. K. J. Smith, Jr., A. Greene, and A. Ciferri, Kolloid Z., 194, 49 (1964).

30. K. J. Smith, Jr., and D. Puett, J. Appl. Phys., 37, 346 (1966).

31. E. Guth, J. Appl. Phys., 16, 20 (1945).

32. H. M. Smallw-od, J. Appl. Phys., 15, 758 (1944).

33. Y. Akana, M.S. Thesis, University of Mass., Amherst, Mass. (1973).

34. A. T. McPherson, J. Res. Nat. Bur. Stds., 8, 751 (1932).

35. R. J. Morgan and L. R. G. Treloar, J. Polym. Sci., A2, 10, 51 (1972).

36. R. Gaylord, unpublished work; see Note I for the derivations.

37. M. Avrami, J. Chem. Phys., 7, 1103 (1939); 8, 212 (1940); 9, 177 (1941).

38. L. Mandelkern, "Crystallization of Polymers", McGraw-Hill, New York 1964.

39. F. Gornick and J. L. Jackson, J. Chem. Phys., 38, 1150 (1963).

Captions for Figures

1) The variation of stress with $(\alpha^2 - 1/\alpha)$ for sample A. The dotted straight line would be expected for kinetic elasticity theory.
2) The variation of stress with $(\alpha^2 - 1/\alpha)$ for sample B.
3) Mooney-Rivlin type plots for stress and birefringence for sample A.
4) Mooney-Rivlin type plots for stress and birefringence for sample B.
5) Mooney-Rivlin type plots for stress and birefringence for natural rubber sample.
6) Mooney-Rivlin type plots for stress and birefringence for cis-1,4-polybutadiene [from Ong et. al (28)].
7) The variation of stress and birefringence with time following the rapid stretching of PIP samples at room temperature at elongation ratio of 2.87.
8) The variation of stress and birefringence at elongation ratio of 3.89.
9) The variation of stress and birefringence at elongation ratio of 5.0.
10) The variation of stress and birefringence at elongation ratio of 6.0.
11) The variation in weight fraction crystallinity with time following rapid stretching of PIP samples at room temperature at elongation ratios of 2.87. Values are given which are obtained from the birefringence Equation (11) and Flory's stress equation (18).
12) The variation in weight fraction crystallinity at elongation ratio of 3.89.
13) The variation in weight fraction crystallinity at elongation ratio of 5.0.
14) The variation in weight fraction crystallinity at elongation ratio of 6.0.

15) The variation of stress and birefringence with time following cooling of a sample of PIP to room temperature following stretching to α = 6 at 90°C.

16) The variation of weight fraction crystallinity with time following cooling a PIP sample to room temperature which had been stretched to α = 6 at 90°C calculated from birefringence using (a) Equation (11) and (b), (b') Equations (22), (25), respectively, and (c), (c') from stress using Equations (21), (24), respectively.

17) An Avrami plot of the isothermal crystallization data on PIP.

18) The variation of stress with temperature upon stepwise cooling samples of PIP stretched to various elongations at 90°C.

19) The variation of birefringence with temperature upon stepwise cooling samples of PIP stretched to various elongations at 90°C.

20) The variation in weight fraction crystallinity with temperature upon stepwise cooling samples of PIP stretched to α = 4.98 and 6.51 at 90°C.

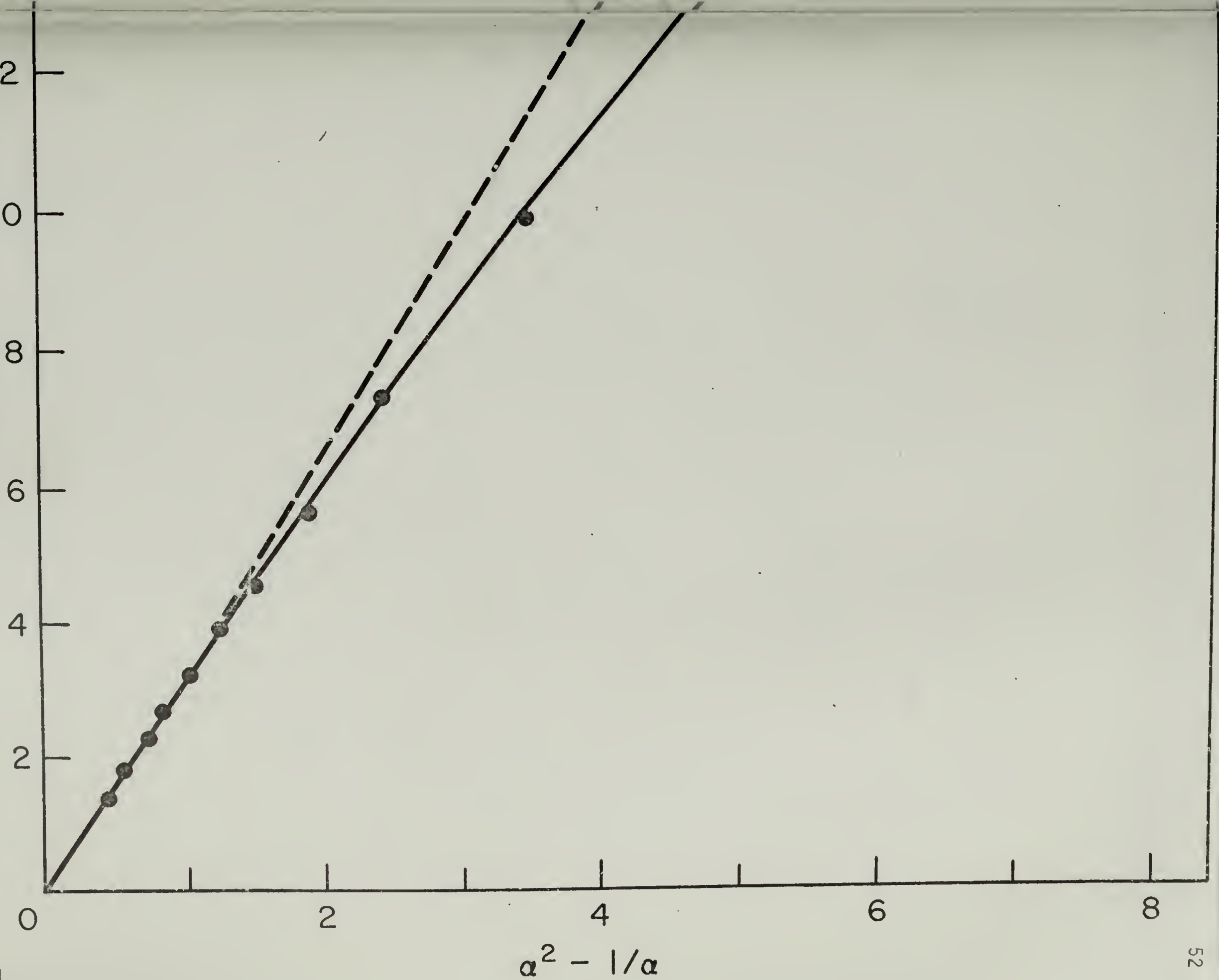

Figure 1

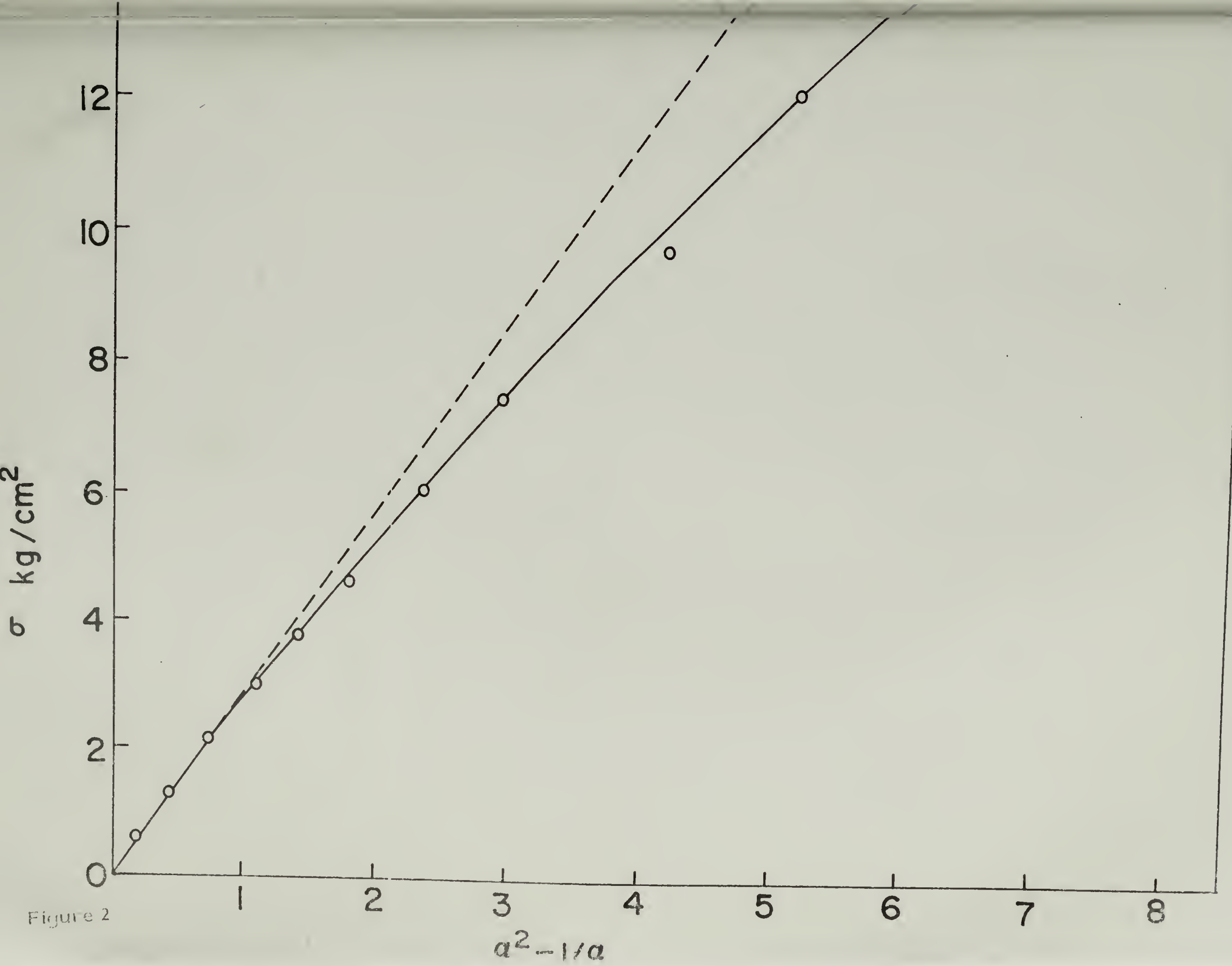

Figure 2

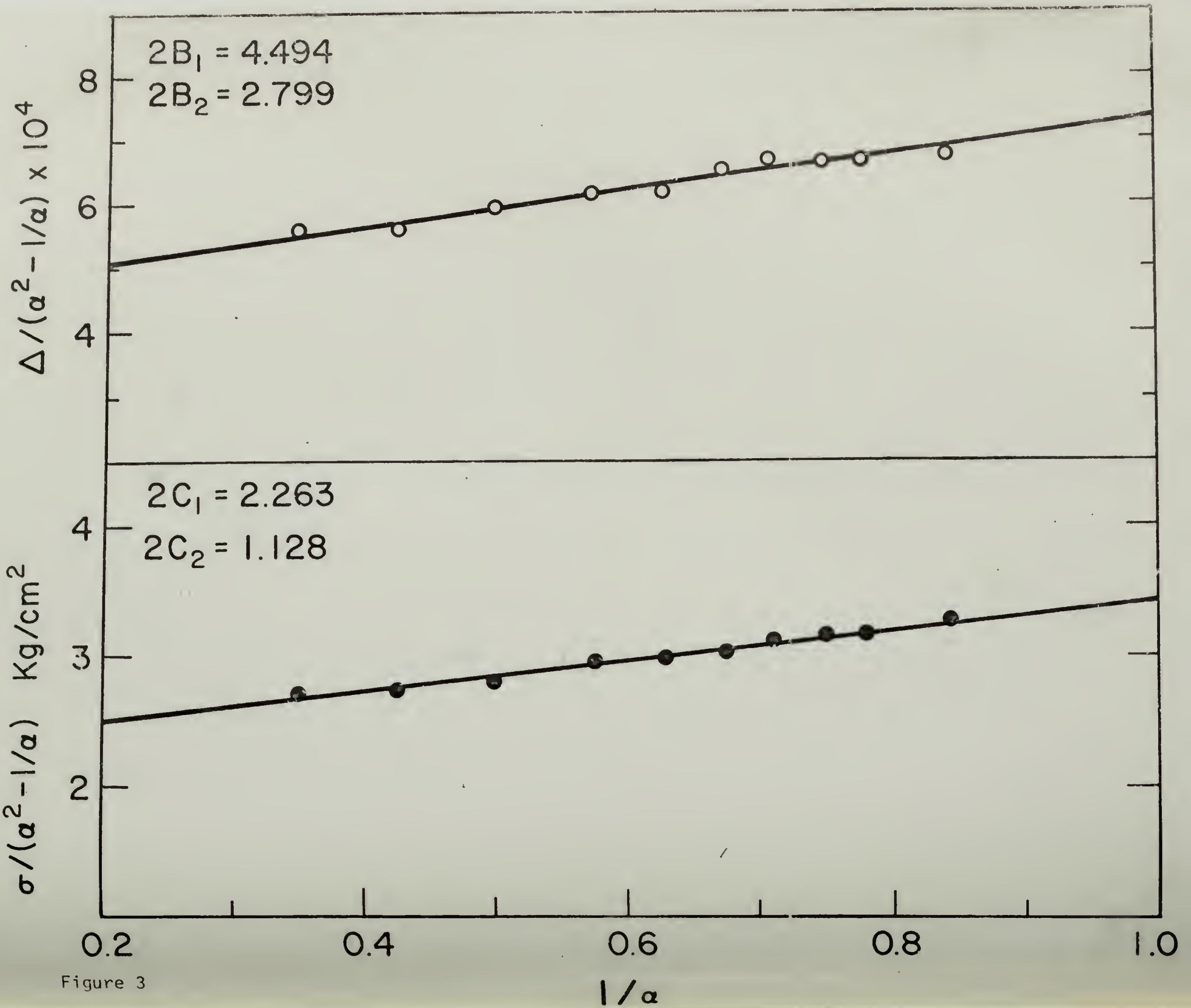
$2B_1 = 4.494$
$2B_2 = 2.799$
$2C_1 = 2.263$
$2C_2 = 1.128$
$\Delta/(\alpha^2 - 1/\alpha) \times 10^4$
$\sigma/(\alpha^2 - 1/\alpha)$ Kg/cm^2
8
6
4
3
2
0.2
0.4
0.6
0.8
1.0
$1/\alpha$

Figure 3

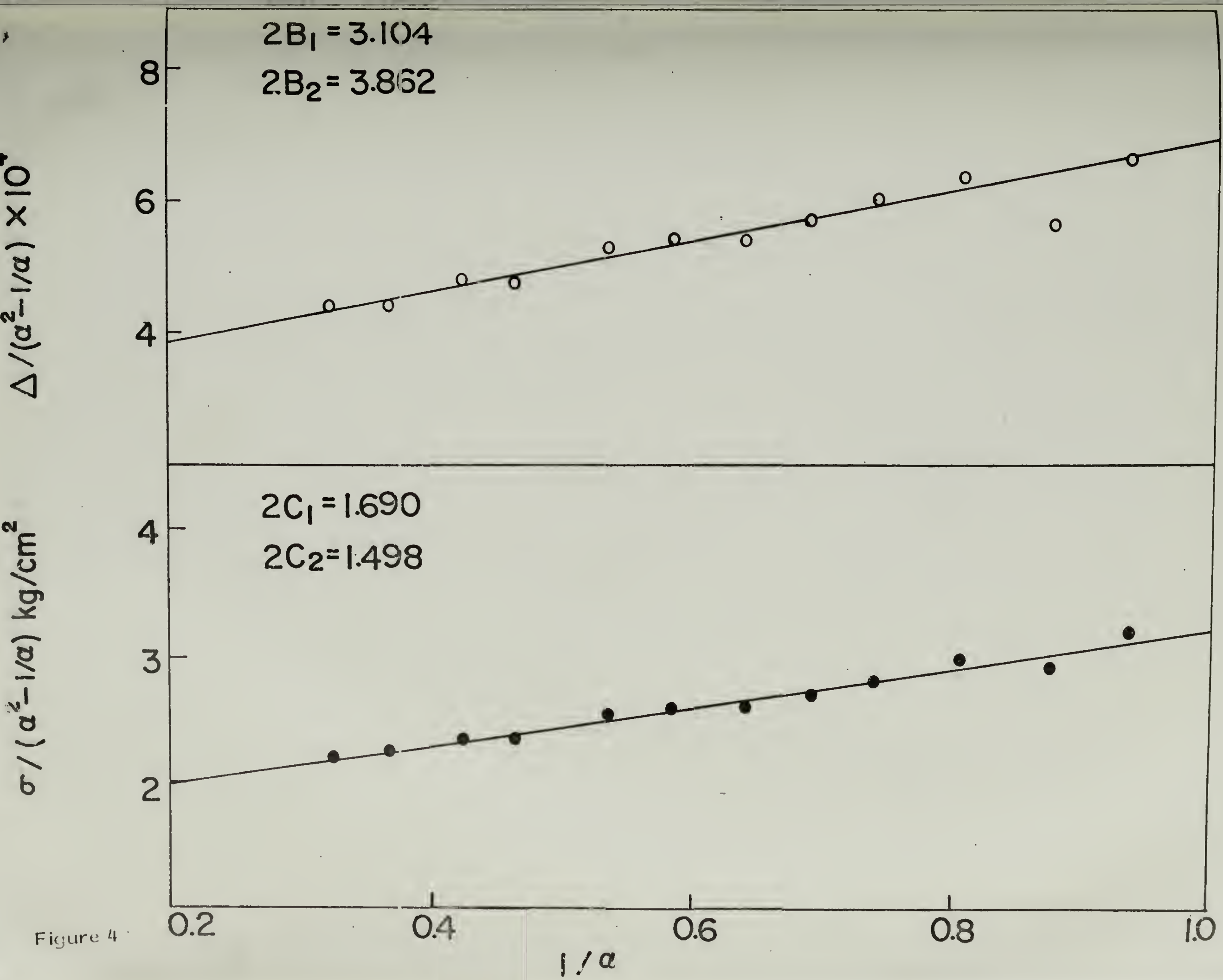
$2B_1 = 3.104$
$2B_2 = 3.862$
$\Delta/(\alpha^2 - 1/\alpha) \times 10^4$
8
6
4
$2C_1 = 1.690$
$2C_2 = 1.498$
$\sigma/(\alpha^2 - 1/\alpha)$ kg/cm^2
4
3
2
0.2
0.4
0.6
0.8
1.0
$1/\alpha$

Figure 4

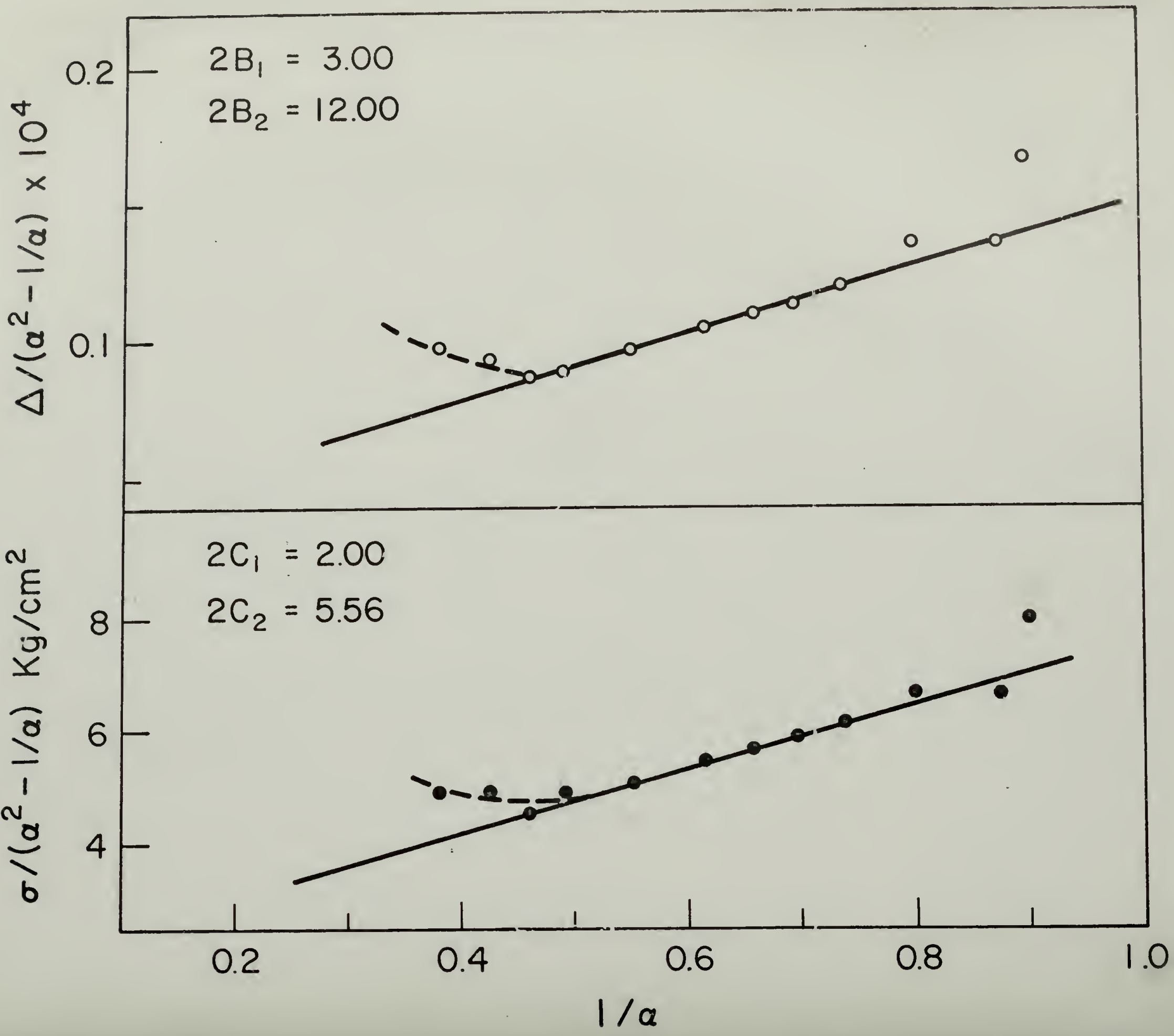
$2B_1 = 3.00$
$2B_2 = 12.00$
$\Delta/(a^2 - 1/a) \times 10^4$
0.2
0.1
$2C_1 = 2.00$
$2C_2 = 5.56$
$\sigma/(a^2 - 1/a)$ Kg/cm^2
8
6
4
0.2
0.4
0.6
0.8
1.0
$1/a$

Figure 5

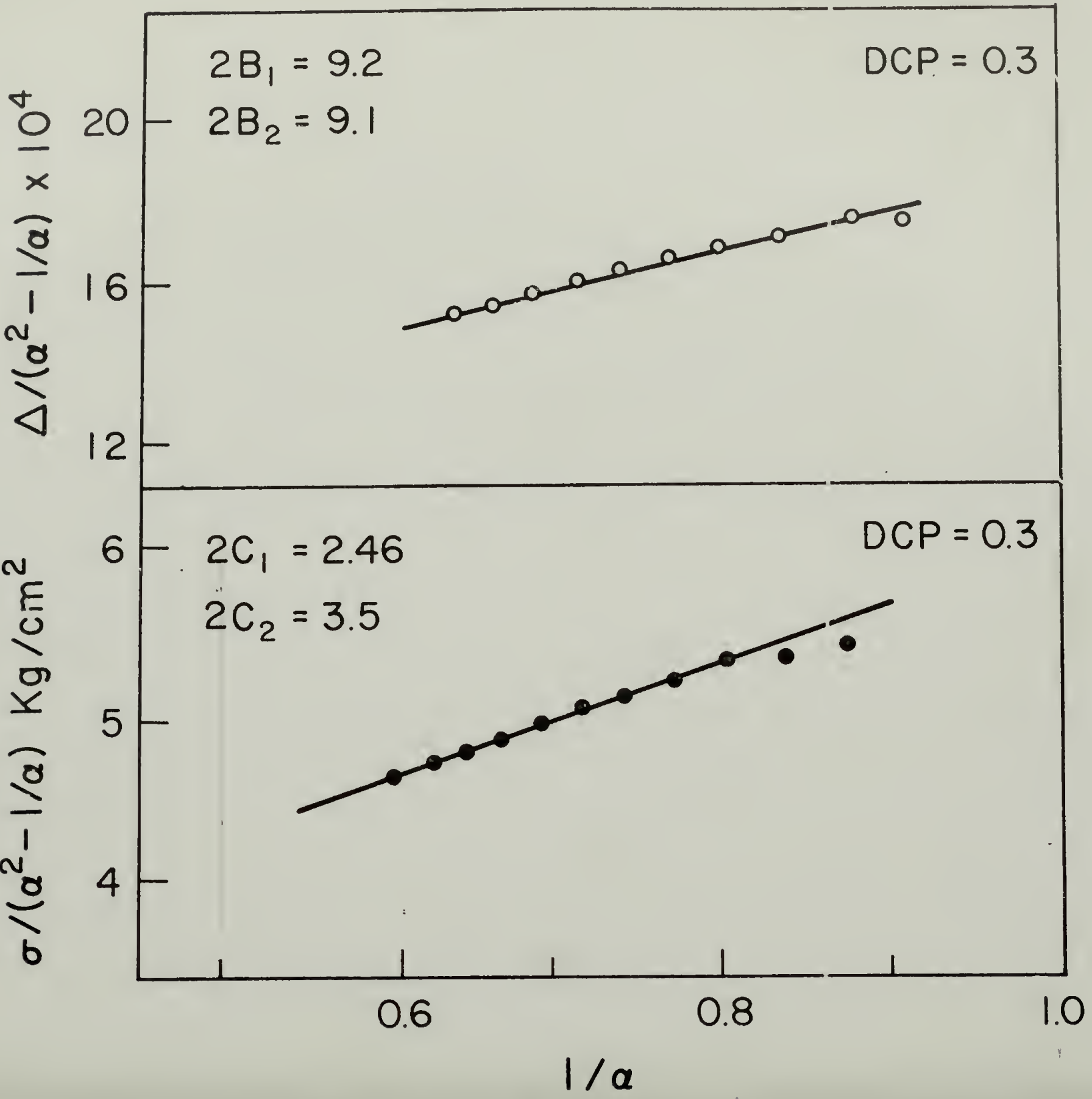
$2B_1 = 9.2$
$2B_2 = 9.1$
DCP = 0.3
$\Delta/(\alpha^2-1/\alpha) \times 10^4$
20
16
12
$2C_1 = 2.46$
$2C_2 = 3.5$
DCP = 0.3
$\sigma/(\alpha^2-1/\alpha)$ Kg/cm^2
6
5
4
0.6
0.8
1.0
$1/\alpha$

Figure 6

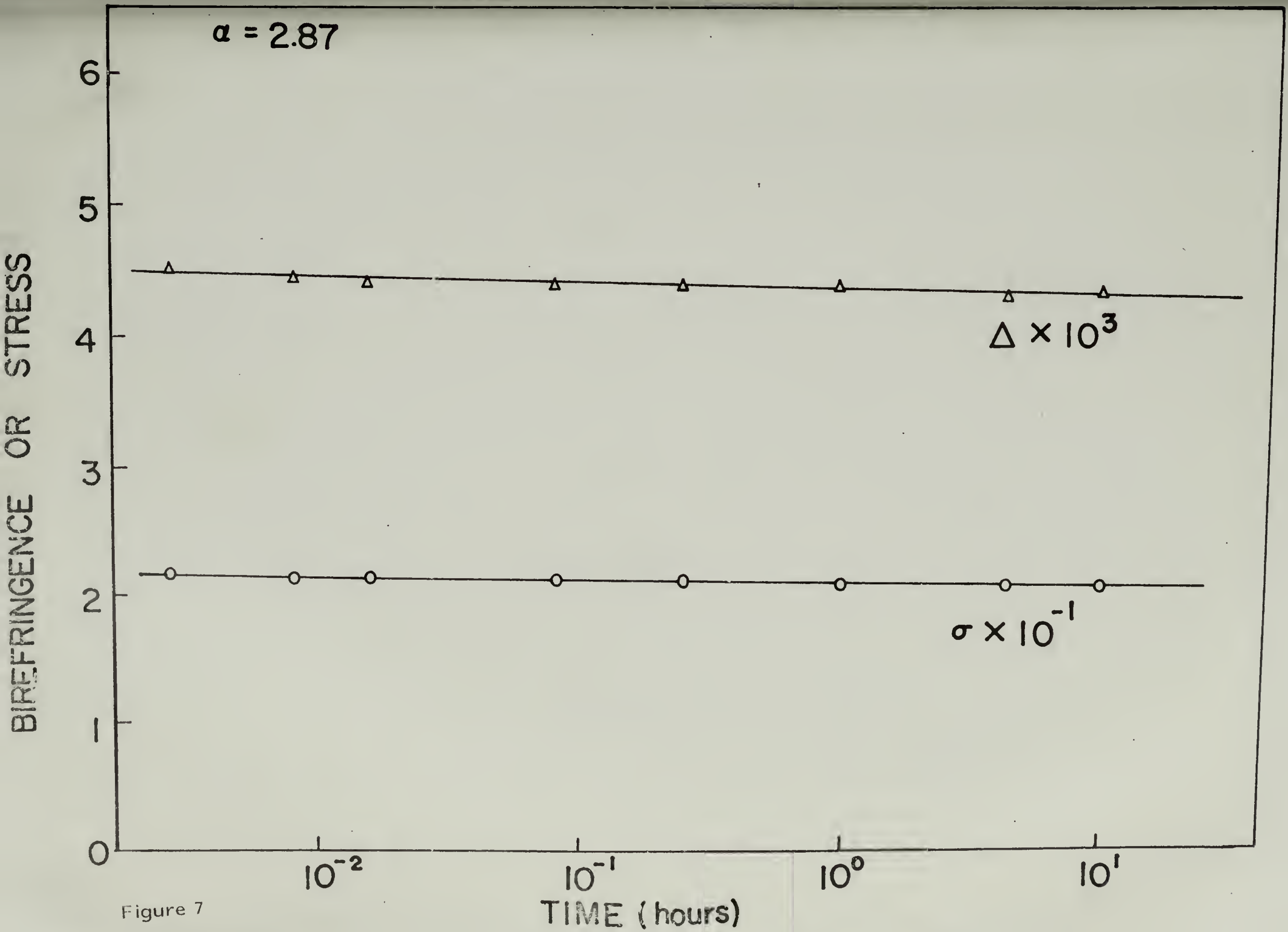
α = 2.87
6
5
4
3
2
1
0
BIREFRINGENCE OR STRESS
Δ × 10³
σ × 10⁻¹
10⁻²
10⁻¹
10⁰
10¹
TIME (hours)

Figure 7

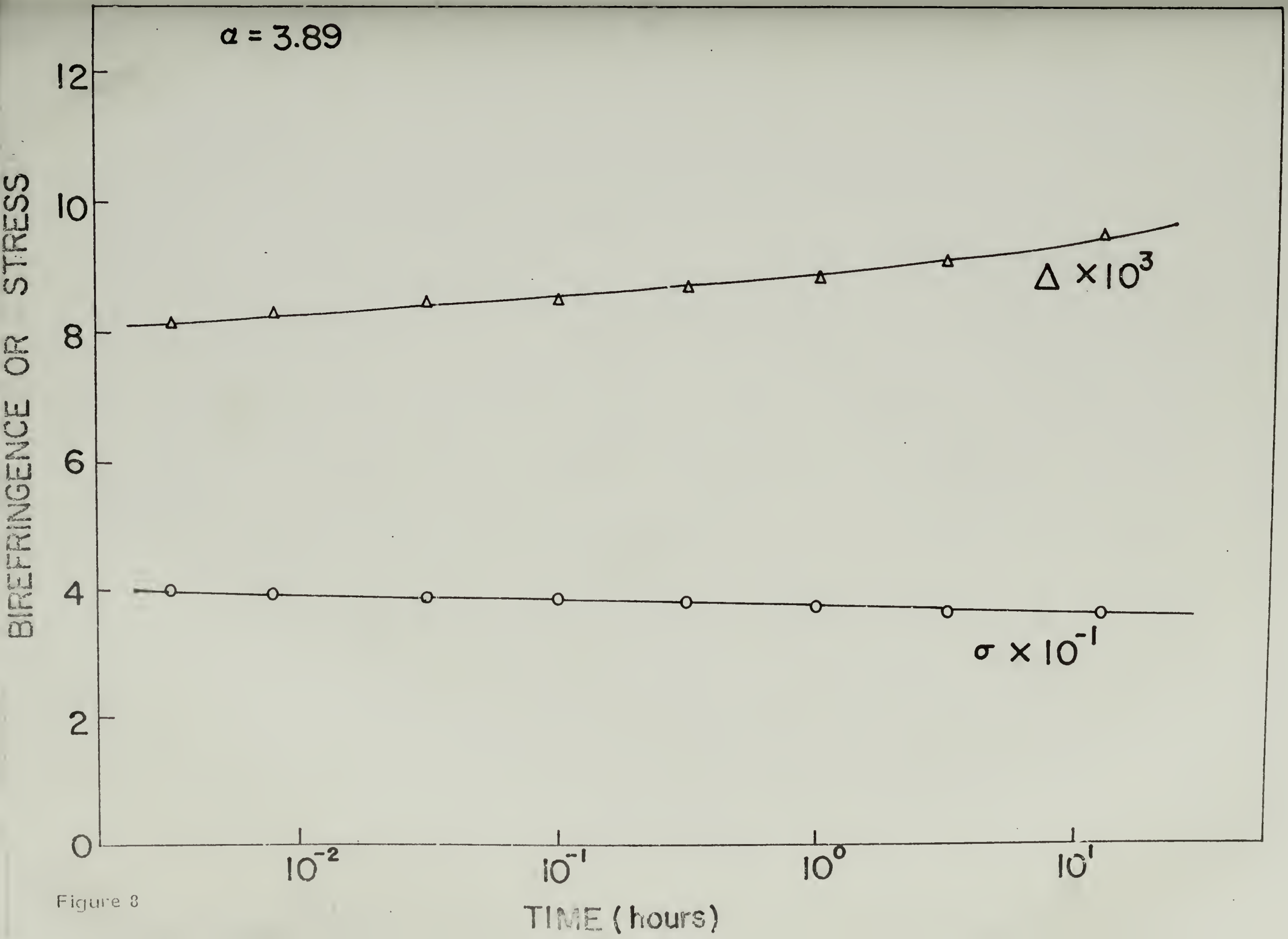
α = 3.89
12
10
8
6
4
2
0
BIREFRINGENCE OR STRESS
Δ ×10³
σ ×10⁻¹
10⁻²
10⁻¹
10⁰
10¹
TIME (hours)

Figure 8

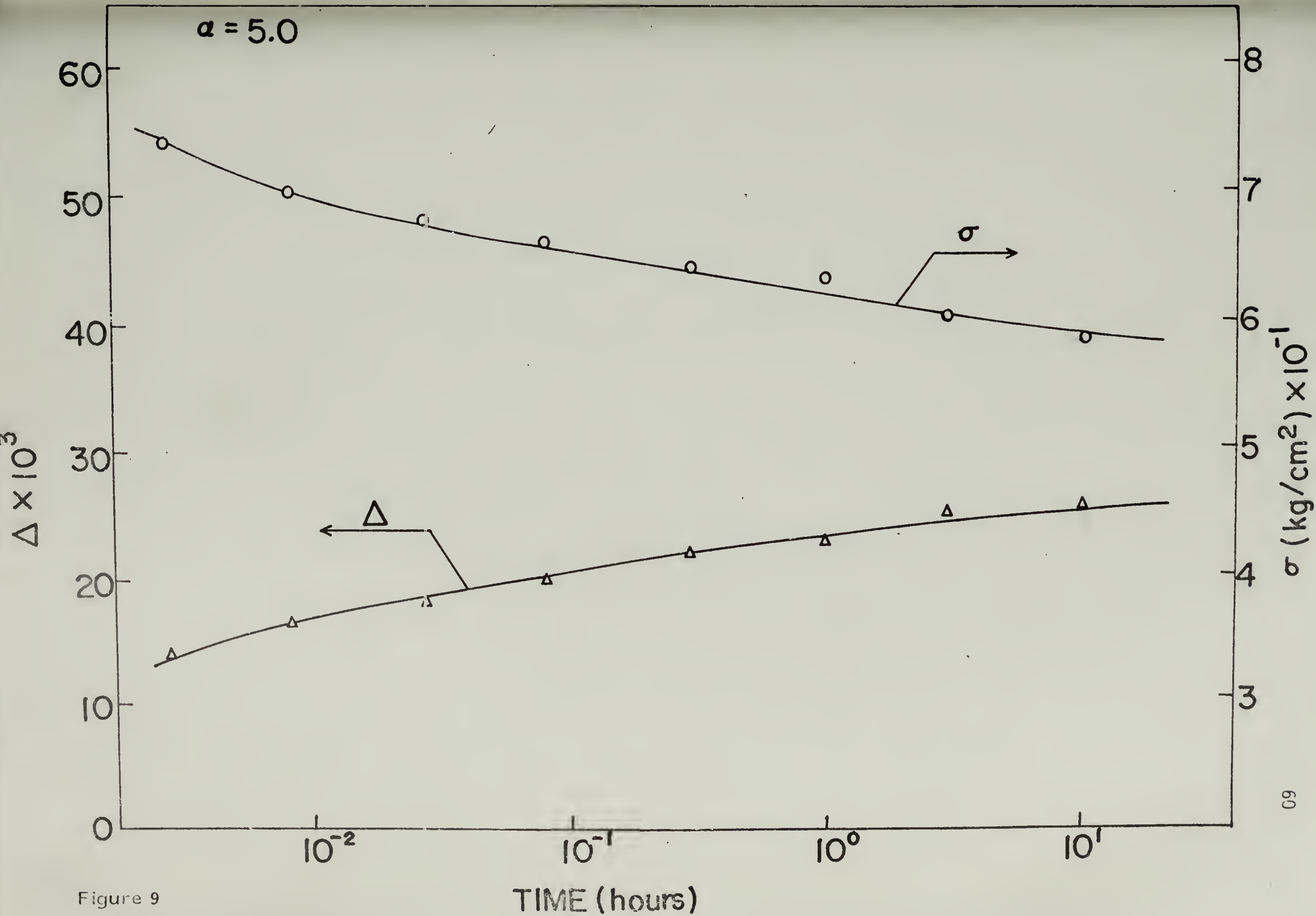
α = 5.0
σ
Δ
Δ x 10^3
σ (kg/cm²) x 10^-1
0
10
20
30
40
50
60
3
4
5
6
7
8
10^-2
10^-1
10^0
10^1
TIME (hours)

Figure 9

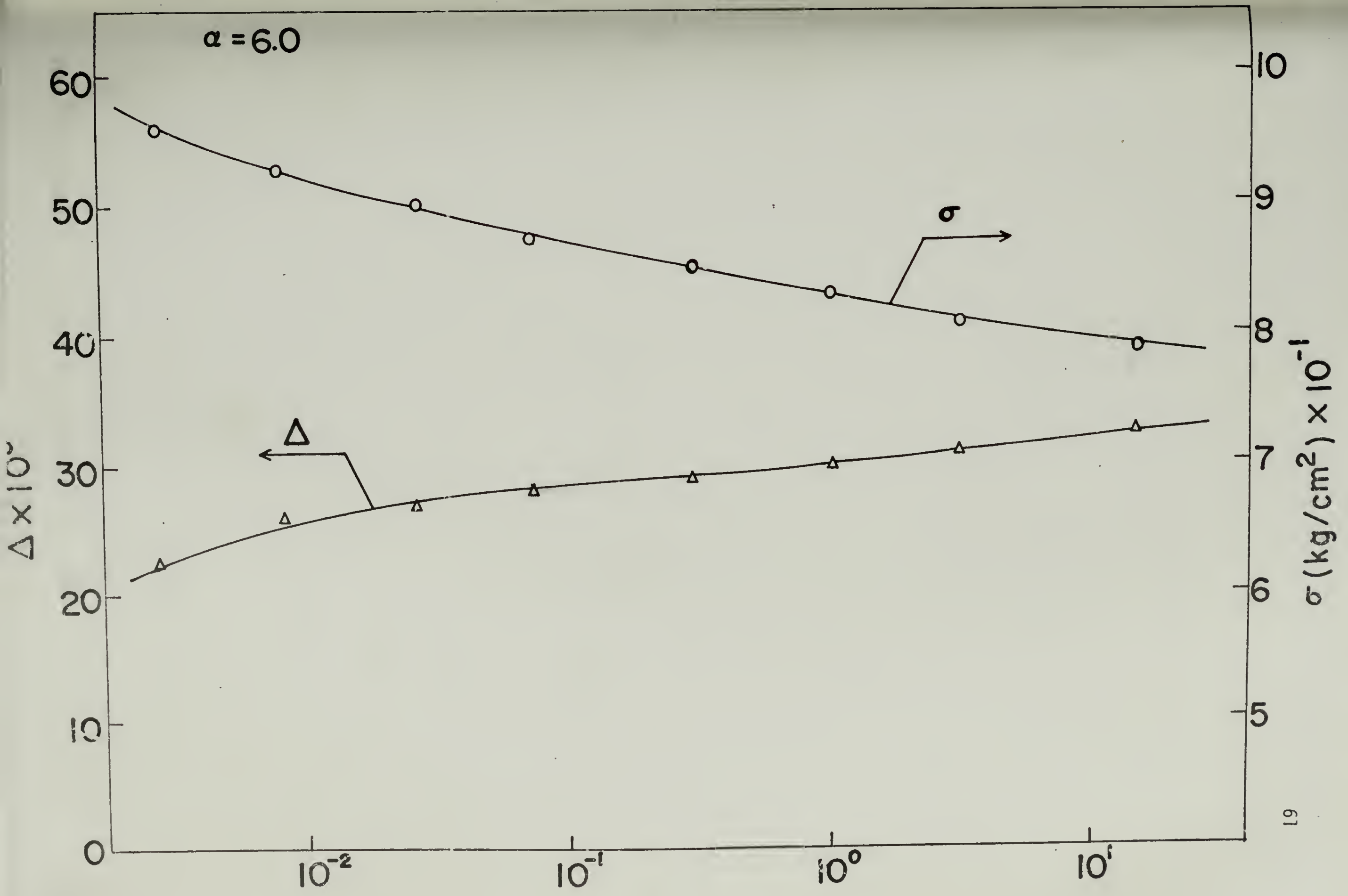
α = 6.0
σ
Δ
Δ x 10³
σ (kg/cm²) x 10⁻¹
60
50
40
30
20
10
0
10
9
8
7
6
5
10⁻²
10⁻¹
10⁰
10¹
TIME (hours)

Figure 10

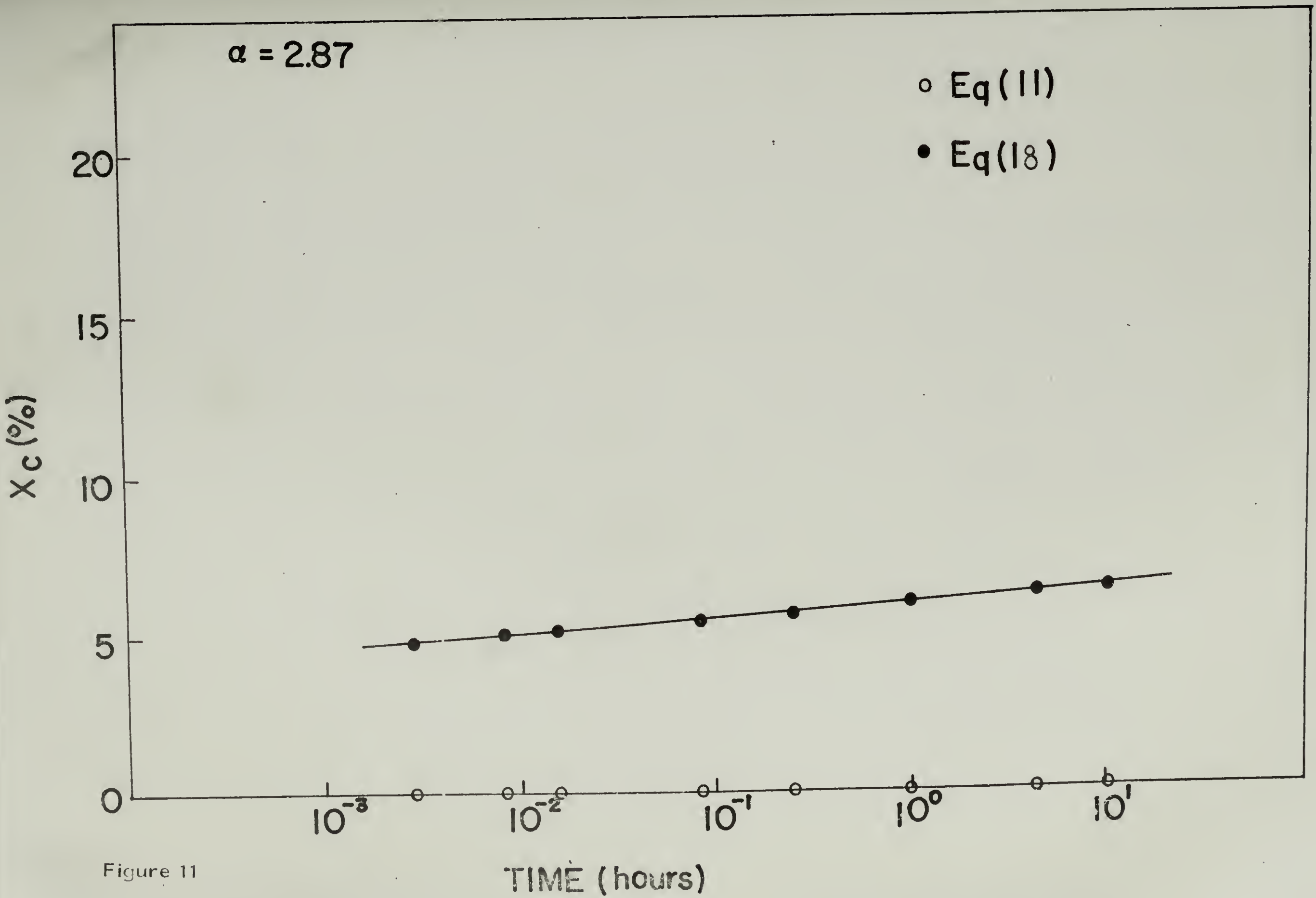

Figure 11

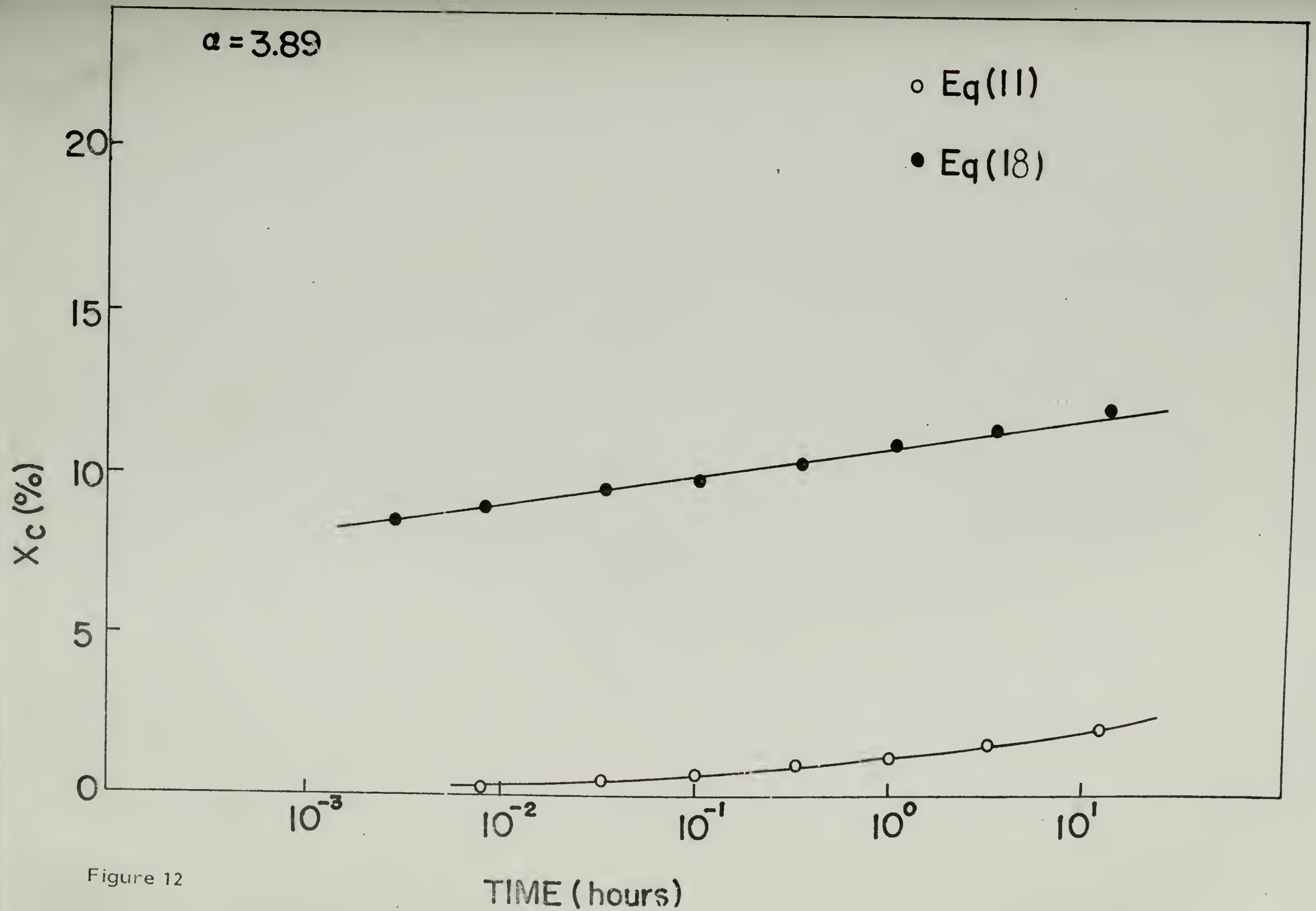

Figure 12

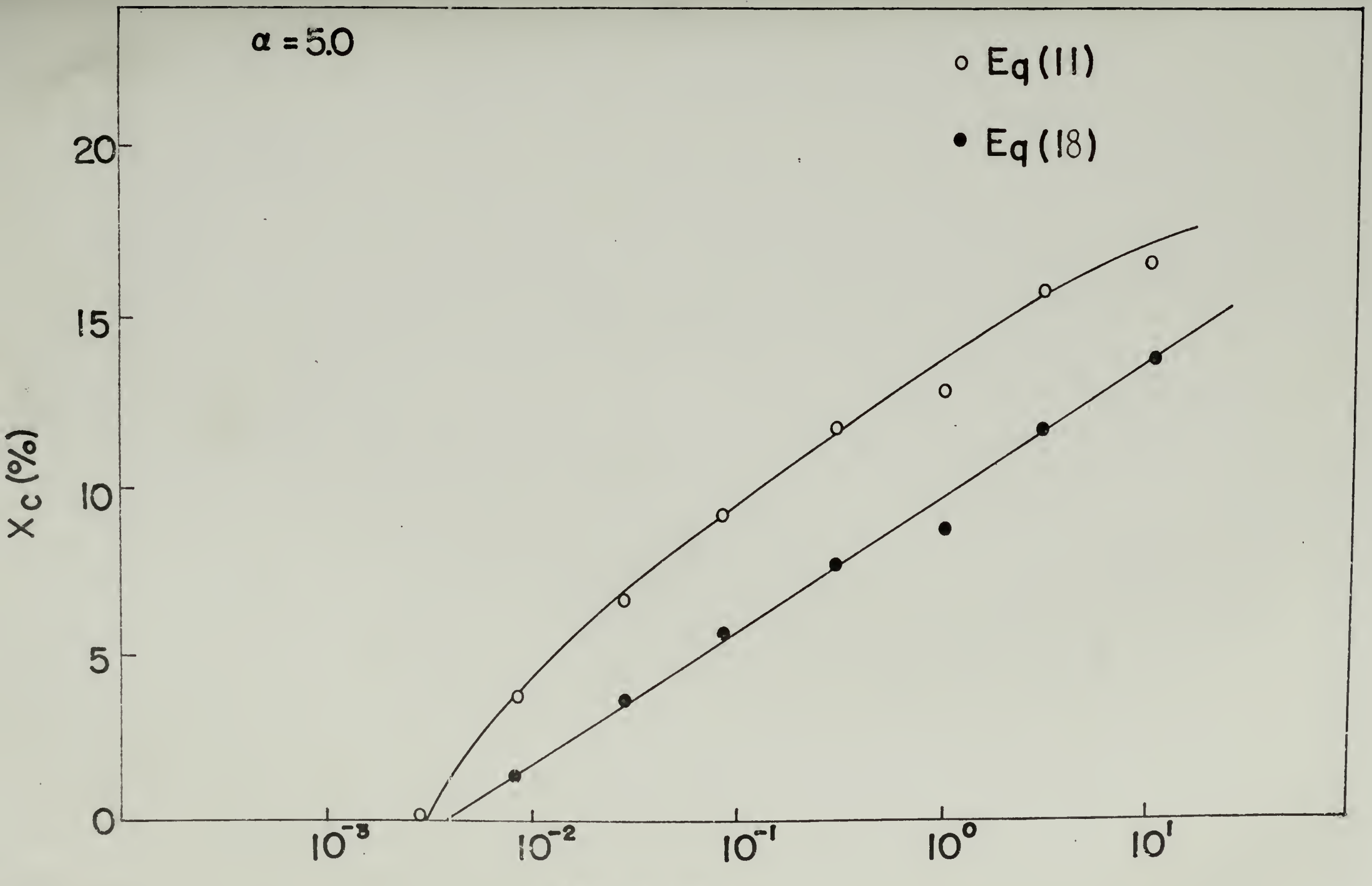

Figure 13

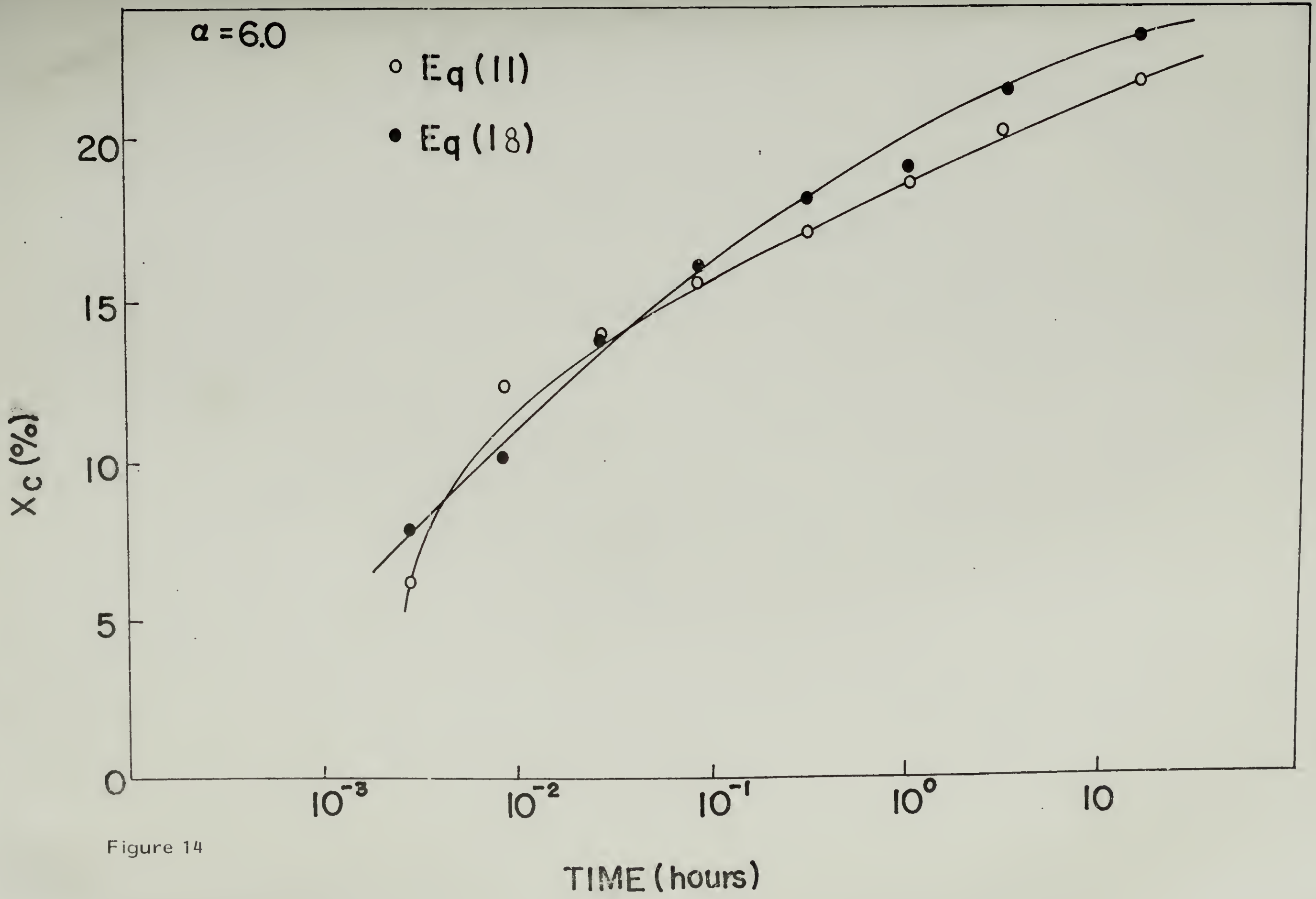

Figure 14

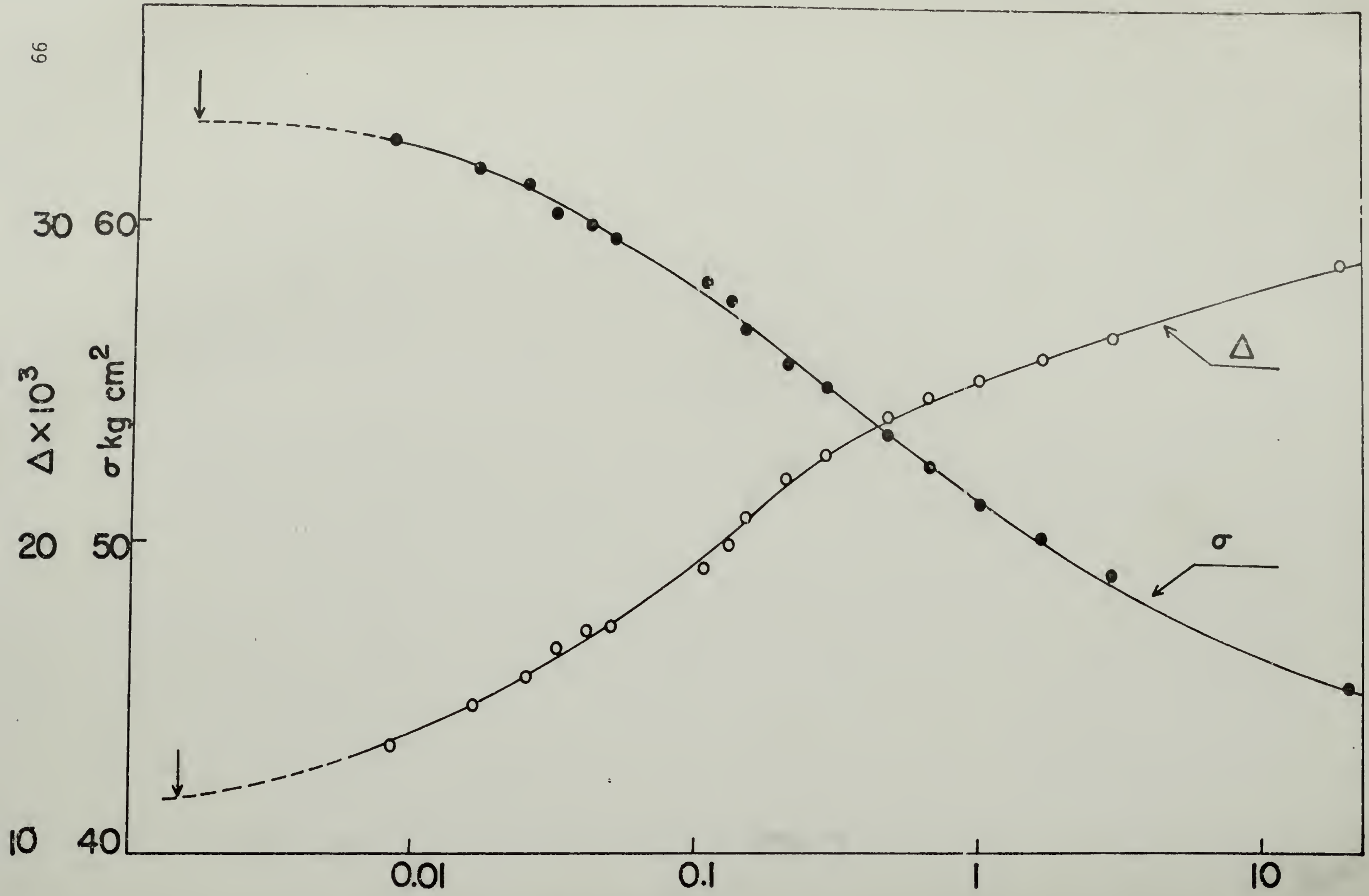

Figure 15

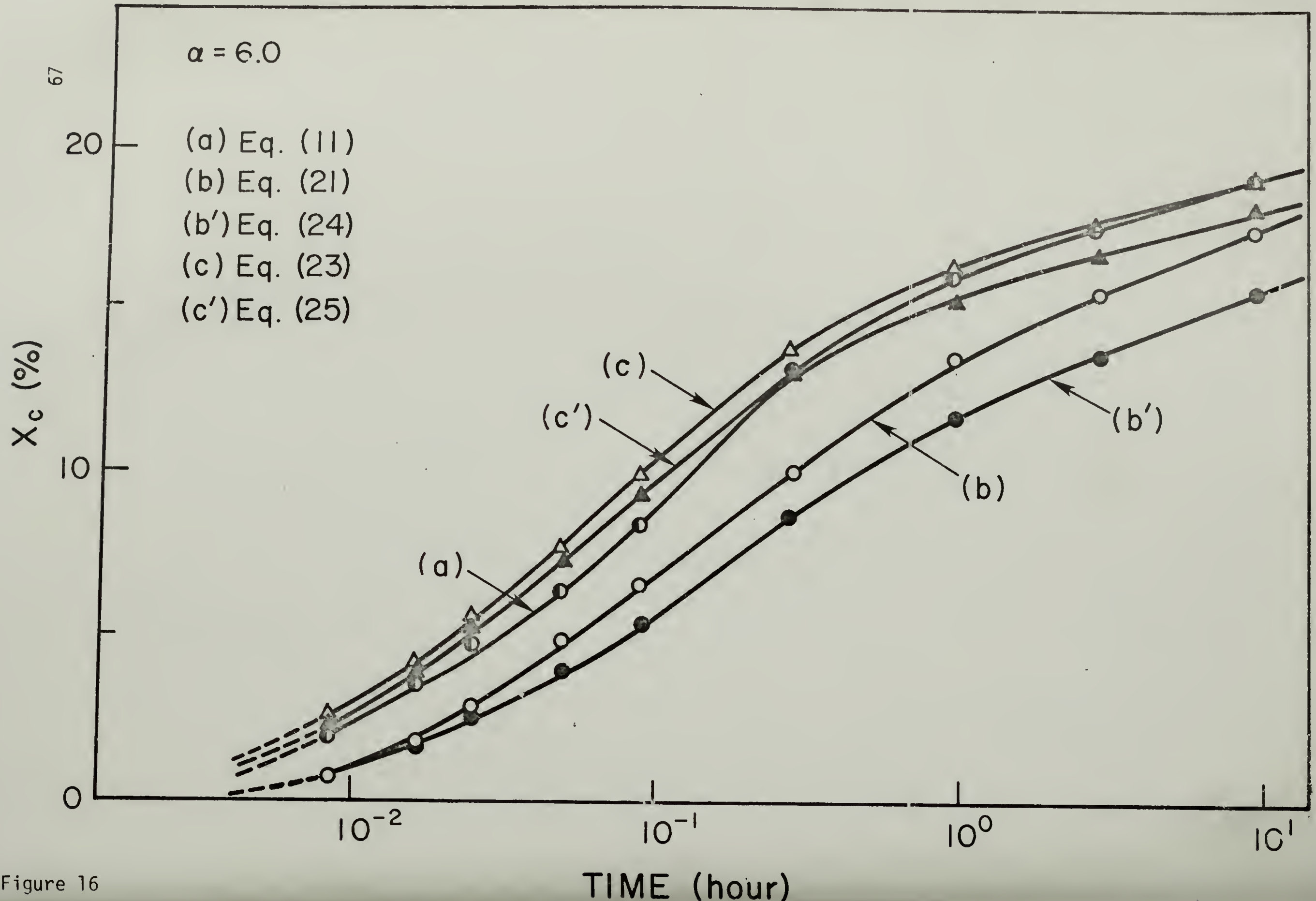
α = 6.0
(a) Eq. (11)
(b) Eq. (21)
(b′) Eq. (24)
(c) Eq. (23)
(c′) Eq. (25)
20
10
0
X_c (%)
(c)
(c′)
(b′)
(b)
(a)
10^{-2}
10^{-1}
10^{0}
10^{1}
TIME (hour)

Figure 16

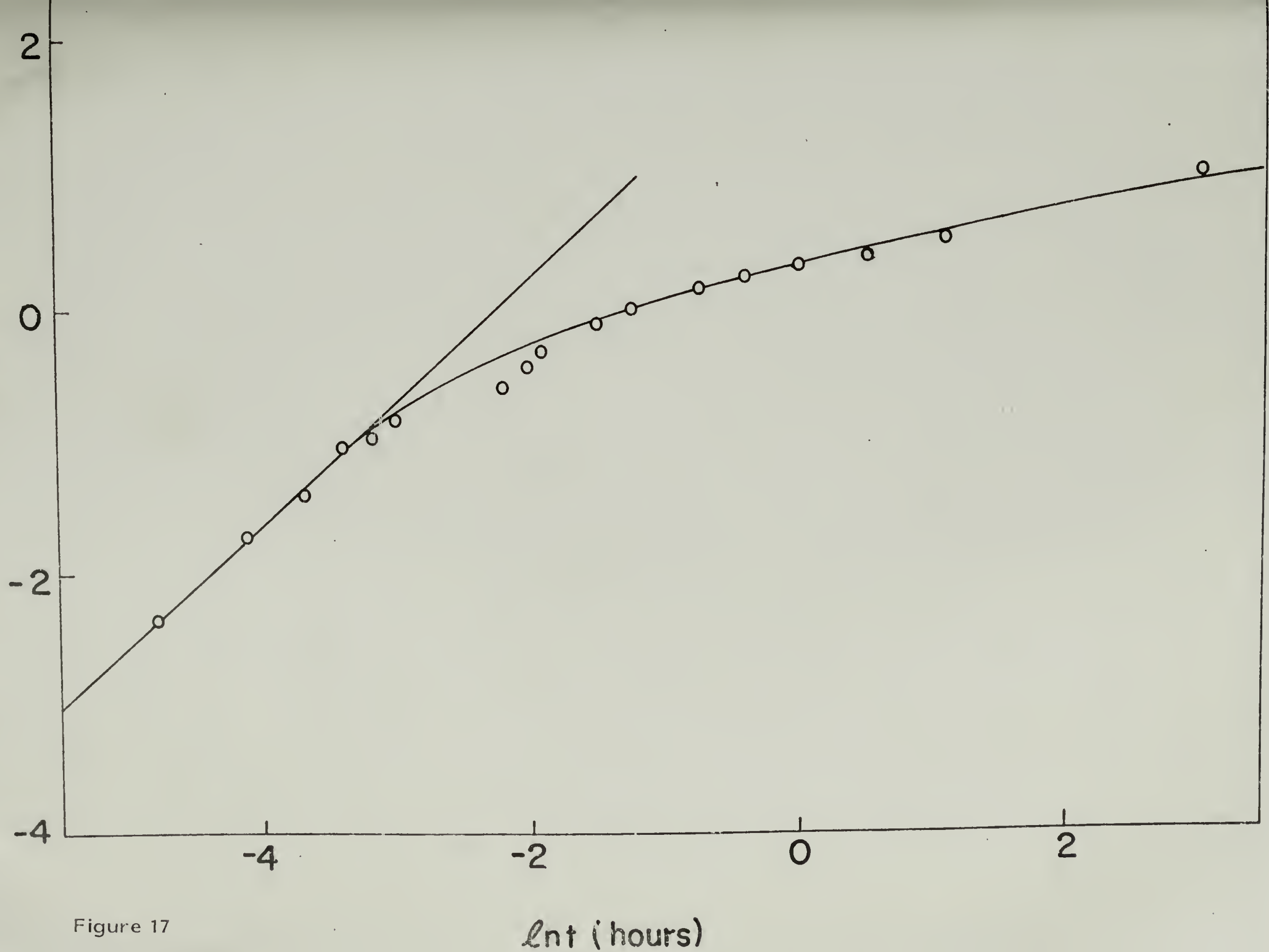

Figure 17

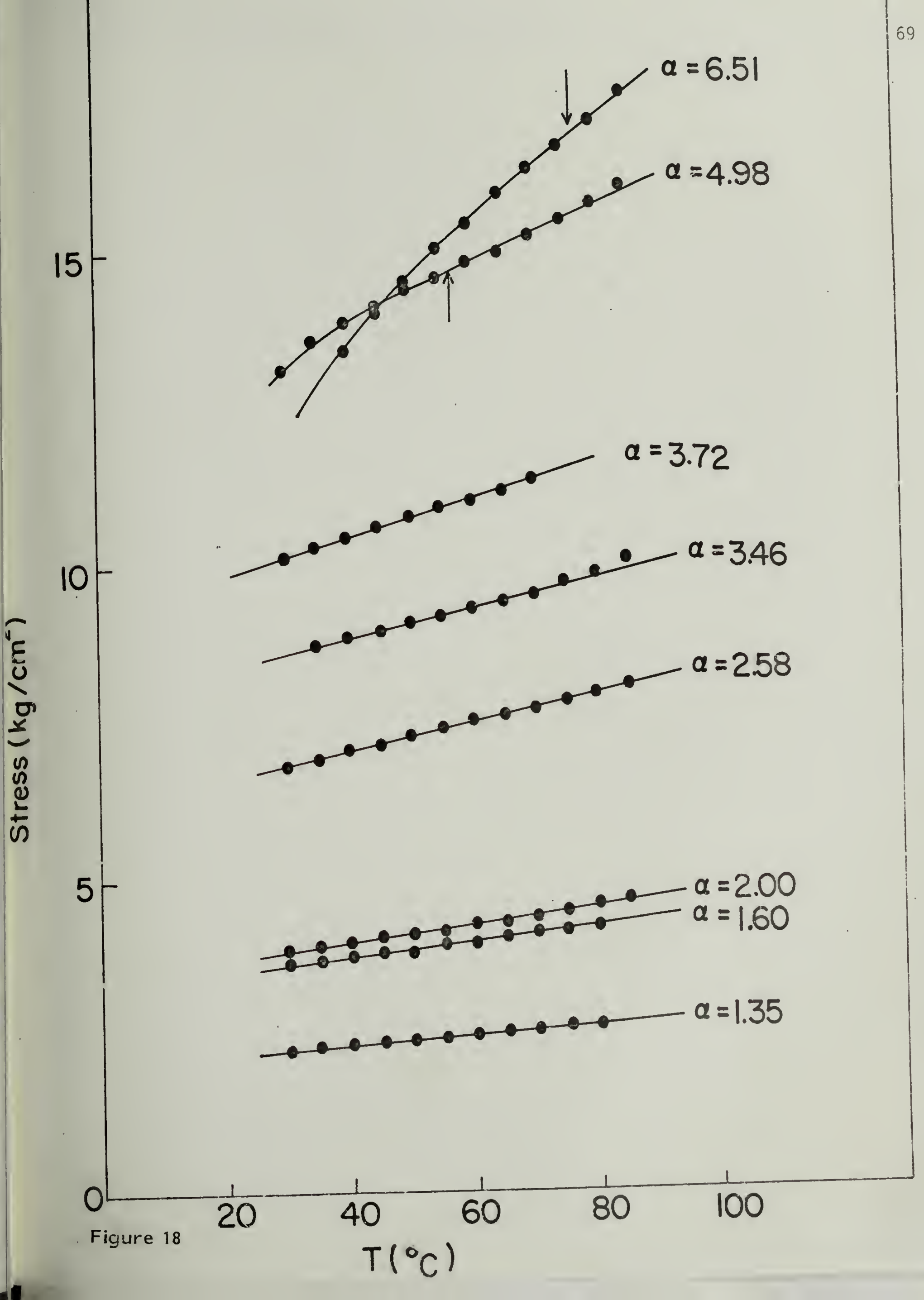
α = 6.51
α = 4.98
α = 3.72
α = 3.46
α = 2.58
α = 2.00
α = 1.60
α = 1.35
15
10
5
0
20
40
60
80
100
Stress (kg/cm²)
T(°C)

Figure 18

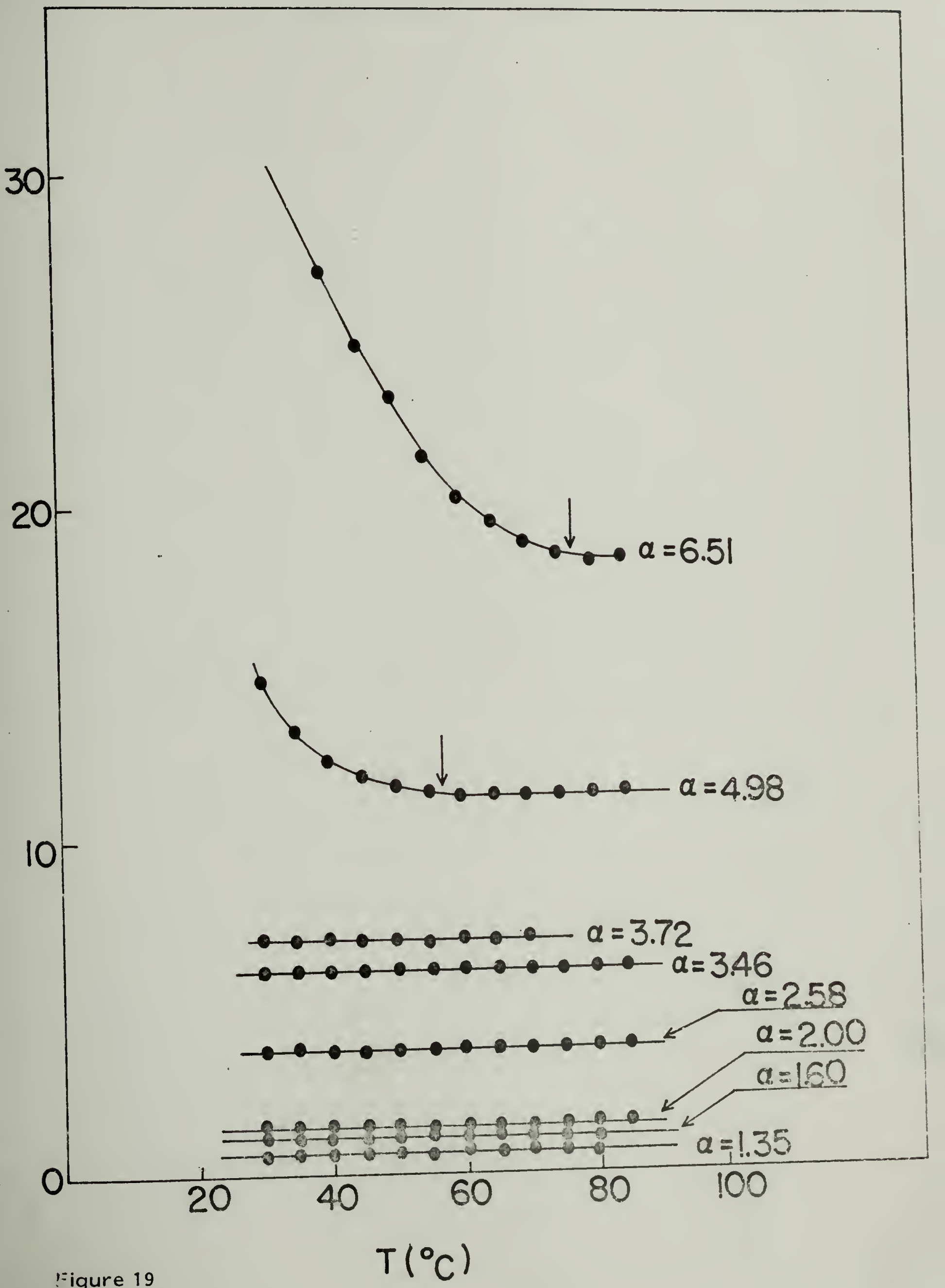
30
20
10
0
Δ x 10³
α = 6.51
α = 4.98
α = 3.72
α = 3.46
α = 2.58
α = 2.00
α = 1.60
α = 1.35
20
40
60
80
100
T(°C)

Figure 19

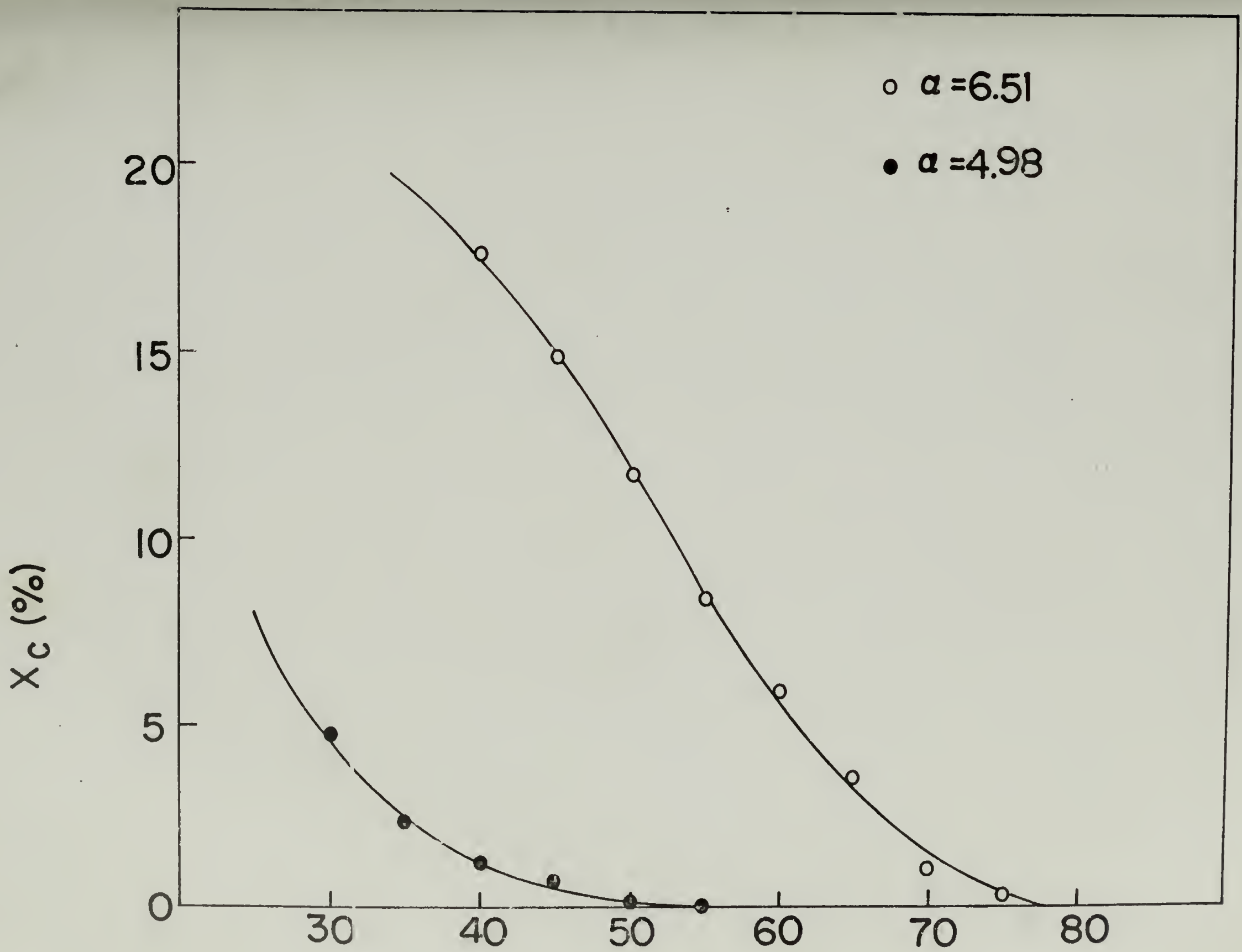

Figure 20

CHAPTER II

INTRINSIC BIREFRINGENCE AND INTERNAL FIELD

Introduction

The values of the bond polarizability vary considerably depending upon what state (gas or crystal) the system is in at the time of measurement (1-3). One of the reasons for the differences has been attributed to internal field effects. This effect is a result from interaction of the local neighboring fields of other bonds or molecules on the field of some specified bond.

Stein (4) has evaluated the internal field of a n-paraffin crystal. The results of his calculations indicate that the effective bond polarizabilities are affected by the internal field arising from the polarization of the rest of the molecules, and that their values will depend upon molecular configurations. Samuels (5) obtained the crystal intrinsic birefringence of isotropic polypropylene as 29.1×10^{-3} which is markedly small compared with the amorphous intrinsic birefringence, 61.5×10^{-3}. This is also attributed to the result from the strong internal field effect in the polypropylene crystal.

In Appendix I the crystal intrinsic birefringence was calculated from bond polarizabilities and in Chapter IV an experimental value was obtained. By comparing these values we feel that the calculated values may be somewhat underestimated. We also feel that the reason for this disagreement may be due to certain internal field effects, which indicate that the Lorentz-Lorenz equation used for the calculation may not be suitable for the polymer crystal. Because the author believes that the internal field

effect may be a very important factor on many optical problems, not only for cis-polyisoprene used here, but also for other polymers, in the following sections several internal field theories will be reviewed and their applicability and limitations will be considered.

Theories

For high-frequency radiation, the refractive index of a material is related to its polarization P as (6,7)

$$n^2 - 1 = 4\pi P/E_o \tag{1}$$

where E_o is the applied field. P is given by

$$P = N\alpha E_{eff} \tag{2}$$

where N is the number of molecules per unit volume, α is the molecular polarizability and E_{eff} is the effective field given by

$$E_{eff} = E_o + E_{int} \tag{3}$$

E_{int} denoting the internal field arising from all the surrounding molecules. If we assume a cavity in which a given molecule is located at the center, the internal field on the molecule may be described by (9)

$$E_{int} = E_S + E_I \tag{4}$$

where E_S is the contribution due to bond charge on the cavity surface and E_I is due to all of the dipoles inside of the cavity. There are a number of important cases for which this term, E_I vanishes. If there are a great many dipoles in the cavity, if they are oriented parallel but randomly distributed in position, and if there are no correlations between the positions of the dipoles, then $E_I = 0$ (8). This is the situation which might prevail in a gas or a liquid. Similarly, if the dipoles in the cavity are located at the regular atomic positions of a cubic crystal, then again $E_I = 0$ (8).

In the general case, however, E_I is not zero. Furthermore, if the material contains several species of molecules, E_I may differ at the various molecular positions.

In the Lorenz-Lorentz calculation, the molecules around a given molecule are treated as an isotropic dielectric continuum, and it is assumed that the molecule is located in the center of a spherical cavity in this continuum. E_S may be obtained by calculating the field arising from the polarization charge on the surface of the cavity as

$$E_S = (n - 1)\, E_o/3 \qquad (5)$$

E_I has been shown to be zero as described above. The effective field is then obtained as

$$E_{eff} = [(n^2 + 2)/3]\, E_o \qquad (6)$$

$$= kE_o$$

where k is the internal field factor. From Equations (1), (2), and (6) one

obtains

$$\frac{n^2 - 1}{n^2 + 2} = \frac{4\pi}{3} N\alpha \qquad (7)$$

which is the Lorenz-Lorentz equation. Equation (7) was used to calculate the crystal intrinsic birefringence of cis-1,4-polyisoprene in Appendix I.

The internal field in the crystal may, however, not be described by the model of the spherically-symmetrical Lorentz-Lorentz field, because the molecules take certain configurations in their crystal. A more realistic expression for the internal field has been proposed by Stein (4). His model is that the molecule resides in a cylindrical cavity instead of a spherical cavity. The cylindrical cavity model gives an explanation about the discrepancy between the values of the anisotropy of methylene groups determined from the refractive indices of n-paraffin crystals, from stress-optical data, and from gas and liquid light scattering depolarization.

In Stein's theory the field parallel to z axis in the center of the cavity whose symmetrical axis is in the z direction is described as

$$E_{int,z} = 4\pi P \left[1 - \frac{f}{(1 + f^2)^{1/2}}\right] \qquad (8)$$

where f is the axial ratio of the cylindrical cavity. The internal field of x (or y) direction is given by

$$E_{int,x} = 2\pi\ p \left[\frac{f}{(1 + f^2)^{1/2}}\right] \tag{9}$$

The internal field factor, k_z and k_x may be described as

$$k_z = 1 + (n_z^2 - 1) \left[1 - \frac{f}{(1 + f^2)^{1/2}}\right] \tag{10}$$

$$k_x = 1 + [(n_x^2 - 1)/2] \left[\frac{f}{(1 + f^2)^{1/2}}\right] \tag{11}$$

where n_z and n_x are the refractive indices in the z and x direction, respectively. If $n_x = n_z$ and f = 0.9, these equations are eventually equivalent to the Lorentz-Lorenz equation.

From Equations (1)-(3) and (8)-(11), one may obtain the following equations

$$(n_z^2 - 1) \left\{1 - 4\pi\ N\alpha_z \left[1 - \frac{f}{(Hf^2)^{1/2}}\right]\right\} = 4\pi\ N\alpha_z \tag{12}$$

for the z direction and

$$(n_x^2 - 1)\left\{1 - 2\pi N\alpha_x\left[\frac{f}{(1+f^2)^{1/2}}\right]\right\} = 4\pi N\alpha_x \qquad (13)$$

for the x (or y) direction.

From these equations the refractive indices, n_x, n_y and n_z may be calculated by using the values of N and α which are obtained in Appendix I and by assuming a value for f, the axial ratio of the cylindrical cavity. The intrinsic birefringence, $n_z - (n_x + n_y)/2$ may be obtained and compared with the experimental value, 0.224. By this manner one can find the value of f which gives the best fit to the experimental value. The results were obtained for Denbigh's (9) and Clement and Bothorel's (10) bond polarizabilities. They are given in Table 1; both values are reasonably close.

This approach by Stein indicates that the internal field effect may be one of the reasons for the disagreement between theoretical and experimental values. It should, however, be mentioned that Stein assumes that there is no contribution of dipoles within the cavity, i.e., $E_I = 0$. For a gas or liquid this may be a good assumption. For polymer crystals the contribution of E_I may be significant and should be taken into account

for quantitative studies.

Recently a more detailed calculation (designated as H-C-S theory) of the internal field has been proposed by Hong et. al (11). In their calculation a detailed summation of the dipolar field is carried out over a crystal. The molecules in their crystal are represented by thin anisotropic rods as shown in Figure 1. These anisotropic rods have different polarizabilities, α_a, α_b, and α_c in the directions of the a, b and c axes of the unit cell. By using this model they obtained the effective field of the central rod along the a-axis as

$$E_{eff} = \left[1 - \frac{k'_a \alpha_a}{L}\right]^{-1} E_o$$

$$= ka\ E_o \qquad (14)$$

where (α_a/L) is the polarizability per unit length in the a-axis direction and k_a is the internal field factor in the direction of the a-axis. k'_a is given as

$$k'_a = \sum_j \left\{ \frac{2x_j^2}{\varepsilon_{ja} C_j^4} (3\sin\omega_j - \sin^3\omega_j) - \frac{2\sin\omega_j}{\varepsilon_{ja} C_j^2} \right\} \qquad (15)$$

where x_j, ω_j and C_j are the paremeters which are defined in Figures 2 and 3. ε_{ja} is the dielectric constant of the j-th chain in the direction of the a-axis.

For the direction of b-axis

$$E_{eff,b} = \left[1 - \frac{k'_b \alpha_b}{L}\right]^{-1} E_o$$

$$= k_b E_o \qquad (16)$$

where

$$k_b' = \sum_j \left\{ \frac{2y_j^2}{\varepsilon_{jb} C_j} (3\sin\omega_j - \sin^3\omega_j) - \frac{2\sin\omega_j}{\varepsilon_{ja} C_j^2} \right\} \tag{17}$$

and for the direction of the c-axis

$$E_{eff,c} = \left[1 - \frac{k_c' \alpha_c}{L} \right]^{-1} E_o \tag{18}$$

$$= k_c E_o$$

where

$$k_c' = \left\{ \sum_j \frac{1}{\varepsilon_{jc}} \frac{2(\sin^3\omega_j - \sin\omega_j)}{C_j^2} \right\} \tag{19}$$

These results lead to

$$n_i^2 - 1 = 4\pi N \alpha_i k_i \tag{20}$$

where i is either a, b or c.

In order to calculate the intrinsic birefringence of the PIP crystal, the H-C-S internal field may be applied. The molecules of PIP in its crystal align along the c-axis. They may, therefore, be considered to be anisotropic rods as shown in Figure 1. The geometrical arrangement of these rods of PIP are similar to those of n-paraffin. The only difference is the distance between rods.

k_a', k_b' and k_c' were calculated as functions of R, the radius of a spherical region of the crystal within which all the induced dipoles are taken into account. The dielectric constants ε_{ja}, ε_{jb} and ε_{jc} are assumed to be unity. The curves in Figure 4 are very similar in shape to those

obtained for n-paraffin (11), but different in their values. The results indicate that the values of k'_a, k'_b and k'_c approach limiting values and change very slowly for R > 30 Å.

The values of k'_a, k'_b and k'_c for a crystal cylinder with various height-to-diameter ratios were also calculated. In the case of n-paraffin crystal, it is found that the values of k'_a, k'_b and k'_c versus the axial ratio can be plotted into master curves with negligible deviation. This is also the case for PIP. The master curves are shown in Figure 5. A difference between the cases of n-paraffin and PIP, however, is found at small values of (R/Z). The curves of k'_a, k'_b for PIP are very smooth and approach to certain limiting values, while those for n-paraffin change significantly in this region.

In practice, the dielectric constants ε_{ja}, ε_{jb} and ε_{jc} for the j-th chain will be unity only for the chains in the vicinity of the reference chain. As described by Hong et. al (11), the macroscopic dielectric constant was used in this work as an approximation. The corrected values of k'_a, k'_b and k'_c for dielectric constant are shown in Figure 6.

The internal field factors, k_a, k_b and k_c are calculated from Equations (14), (16) and (18). The polarizability of an isoprene monomer unit, α_i, is calculated in Appendix I for different sets of bond polarizability. L has been determined as 4.05 Å by x-ray diffraction (12,13). The calculated values of k_a, k_b and k_c considering the dielectric constant (ε = 2.4) are given in Table 2.

The change in refractive index corresponding to a small change in $\beta = \alpha k$ in Equation (20) can be found by differentiation

$$2n\,dn = 4\pi N\,d\beta \tag{21}$$

Thus for small refractive index differences

$$\Delta = \frac{2\pi\ N}{\bar{n}}\,\Delta\beta \tag{22}$$

where $\bar{n}$ is the average refractive index of the material. The crystal intrinsic birefringence can then be calculated from the difference in β, which is

$$\Delta\beta = \beta_c - \frac{\beta_a + \beta_b}{2} \tag{23}$$

$\bar{n}$ may be described as a first approximation as

$$\bar{n} = \frac{n_a + n_b + n_c}{3}$$

$$= \left\{ 2\sqrt{\pi N}\ \left(\sqrt{\beta_a} + \sqrt{\beta_b} + \sqrt{\beta_c}\right) + \frac{1}{4\sqrt{\pi N}}\left(\frac{1}{\sqrt{\beta_a}} + \frac{1}{\sqrt{\beta_b}} + \frac{1}{\sqrt{\beta_c}}\right)\right\} \Big/ 3 \tag{24}$$

The crystal intrinsic birefringence, Δ_c^o, of PIP was calculated for the sets (9,10,14) of polarizability and given in Table 3. The calculation for Δ_c^o of n-paraffin was made in the same manner using the values of k'_a, k'_b and k'_c obtained by Hong et. al (11). It is given in Table 4.

For n-paraffin the refractive indices were measured by Bunn and Daubeny (15) as

$$n_a = 1.514$$

$$n_b = 1.519$$

$$n_c = 1.575$$

The intrinsic birefringence is then

$$\Delta_c^o = n_c - \frac{n_a + n_b}{2} = 0.0585$$

In general the calculated values using H-C-S internal field theory are in good agreement with the experimental values, especially Denbigh's bond polarizabilities which give an excellent result. Keedy et. al (16) have reported that a better agreement was found between experimental and theoretical birefringence values of polypropylene using Denbigh's data rather than using that of Bunn and Daubeny.

For PIP however, the calculated values are significantly different from the value, 0.224, which was obtained experimentally in Chapter IV. A better agreement was obtained if the Lorentz-Lorenz internal field was used as shown in Appendix I.

These two opposite results may indicate a limitation of the applica-bility of the H-C-S theory. For PIP the fact that Δ_c^o from the H-C-S equation takes significantly small or negative values indicates that this theory may overestimate the internal field effect of the PIP crystal.

The author feels that one of the reasons for this significant disagreement may be due to an assumption made in the derivation of the H-C-S equations. Hong et. al assume that the induced dipole moments within a crystal are all the same at any position in the crystal. This may be a good assumption for n-paraffin. For a crystal of PIP, however, it is very likely that the induced dipole moment near the boundary of the crystal is not equal to that around the center of the crystal, because the surrounding conditions of these two points may be significantly different from each

other. Due to this reason the H-C-S equation probably overestimates the internal field effect.

If we consider a small domain within a crystal, in which the induced dipole moments can be considered to be equal to each other because of the small dimension of the domain compared with the dimension of the crystal. Then we assume that the domain has a size equivalent to that of the cylindrical cavity described before. As we have seen, Stein's internal field theory neglects the contribution from the induced dipoles within the cavity. Now we may evaluate the contribution using the H-S-C equation in which all induced dipole moments should be equal to each other.

By using Equation (4) the corresponding equations to Equations (12) and (13) may be given by

$$\left(n_z^2 - 1\right)\left\{1 - 4\pi N\alpha_z\left[1 - \frac{f}{(1 + f^2)^{1/2}}\right] - k'_z\left(\frac{\alpha_z}{L}\right)\right\} = 4\pi N\alpha_z \tag{25}$$

and

$$\left(n_x^2 - 1\right)\left\{1 - 2\pi N\alpha_x\left[\frac{f}{(1 + f^2)^{1/2}}\right] - k'_x\left(\frac{\alpha_x}{L}\right)\right\} = 4\pi N\alpha_x \tag{26}$$

By using Figure 5 one may obtain the coefficient k'_z (or k'_c), k'_x (or k'_a), and k'_y (or k'_b). Caution must be taken as f is defined by Z/R. The correction for the dielectric constant may be made by dividing the value without correctionby the macroscopic dielectric constant.

Following the same procedure described earlier, one can find a value of f which gives a best agreement between the theoretical and experimental crystal birefringence. They are given in Table 1. The two values for different sets of polarizabilities are reasonably close to each other.

The values from Equations (25) and (26) are smaller than those from Equations (12) and (13). These differences may imply the effect due to the induced dipoles within the cavity which are neglected in Equations (12) and (13).

The values of f indicate that the cavity is rather disk-like. If we further assume that the shape of the cavity is similar to the total crystal, the crystal in stress induced crystallized PIP sample has a disk-like shape. This shape may be equivalent to those of kebabs (17) as shown in Figure 4 in the General Introduction. It is, however, more likely that the shape of the crystal has nothing to do with the imaginary shape of the cavity.

We have considered, so far, only the internal field effect in the crystalline phase. In the real case, however, we may have to consider the effect due to the existence of the amorphous phase. For polymers like PIP this may be an important factor because small crystalline domains are surrounded by large amounts of amorphous phase. The effect due to the existence of amorphous phase may, therefore, not be neglected. For polymers like polyethylene the contribution from the amorphous phase may be relatively small because of the high crystallinity of the materials. These differences between PIP and polyethylene may be one of the reasons for the disagreement found here.

In conclusion it is evident that the internal field effect is the main reason for a large change in crystal birefringence. It has been demonstrated that the reason for this disagreement between the calculated and experimental crystal birefringence can be explained by the internal field effect.

References

1. R. J. W. LeFevre, J. Proc. Roy. Soc., New South Wales, 95, 1 (1961).
2. H. G. Bolton, Trans. Faraday Soc., 50, 1261 (1954).
3. D. W. Saunders, Trans. Faraday Soc., 53, 860 (1957).
4. R. S. Stein, J. Polym. Sci., A-2, 7, 1021 (1969).
5. R. J. Samuels, J. Polym. Sci., A-2, 6, 1101 (1968).
6. H. A. Lorentz, The Theory of Electrons, Dover, New York (1952).
7. L. Lorenz, Ann. Physik, 11, 70 (1880).
8. J. Reitz and F. Milford, Foundations of Electromagnetic Theory, Addison-Wesley, Mass., 1967.
9. K. G. Denbigh, Trans. Faraday Soc., 36, 936 (1940).
10. C. Clement and P. Bothorel, J. Chem. Phys., 61, 878 (1964).
11. S. D. Hong, C. Chang and R. S. Stein, J. Polym. Sci., Polym. Phys. Ed., 13, 1447 (1975).
12. C. W. Bunn, Proc. Roy. Soc., A180, 40 (1942).
13. S. C. Nyburg, Acta Crystal., 7, 385 (1954).
14. M. F. Vuks, Optika Spectroskopiya, 2, 494 (1957).
15. C. W. Bunn and R. deP. Daubeny, Trans. Faraday. Soc., 50, 1173 (1954).
16. D. A. Keedy, J. Powers and R. S. Stein, J. Appl. Physics, 31, 1911 (1960).
17. M. Hill and A. Keller, J. Macro. Sci., Phys., B3, 153 (1969).

TABLE 1

The Value of f which Gives an Agreement between Theoretical and Experimental Crystal Birefringence

Polarizability Used	From Equations (12) and (13)	From Equations (25) and (26)
Denbigh (9)	0.78	0.4
Clement and Bothorel (10)	0.89	0.5

TABLE 2

The Values of k_a, k_b and k_c of PIP Crystal
for Various Sets of Bond Polarizability
(Corrected for Dielectric Constant)

	Vuks (11)	Denbigh (12)	Clement and Bothorel (13)
k_a	0.9313	0.9265	0.934[illegible]
k_b	1.1971	1.1976	1.1885
k_c	0.8638	0.8584	0.8552

TABLE 3

The Intrinsic Birefringence, Δ_c^o, of
PIP Calculated from the H-C-S Internal Field

	Vuks (11)	Denbigh (12)	Clement and Bothorel (13)
Δ_c^o	-0.0124	-0.0036	0.0305

TABLE 4

The Intrinsic Birefringence of n-Paraffin
Calculated from the Lorenz-Lorentz and the H-C-S Internal Fields

Δ_c^o	Vuks (14)	Denbigh (19)	Clement and Bothorel (10)
Lorenz-Lorentz Field	0.2697	0.3316	0.2138
Hong Field	0.0422	0.0516	0.0209

Captions for Figures

1) Thin rod model used for the calculation of the internal field.
2) Dipole induced in the molecular chain when the electric field of the radiation is at thedirection of the chain axis.
3) Dipole induced in the molecular chains when the electric field of the radiation is perpendicular to the chain axis.
4) The coefficients of k'_a, k'_b and k'_c vs. the radius of the crystal sphere R. The dielectric constants are taken as unity.
5) The coefficients of k'_a, k'_b and k'_c vs. the axial ratio of the crystal cylinder. The dielectric constants are taken as unity.
6) The corrected values of k'_a, k'_b, and k'_c for the dielectric constant.

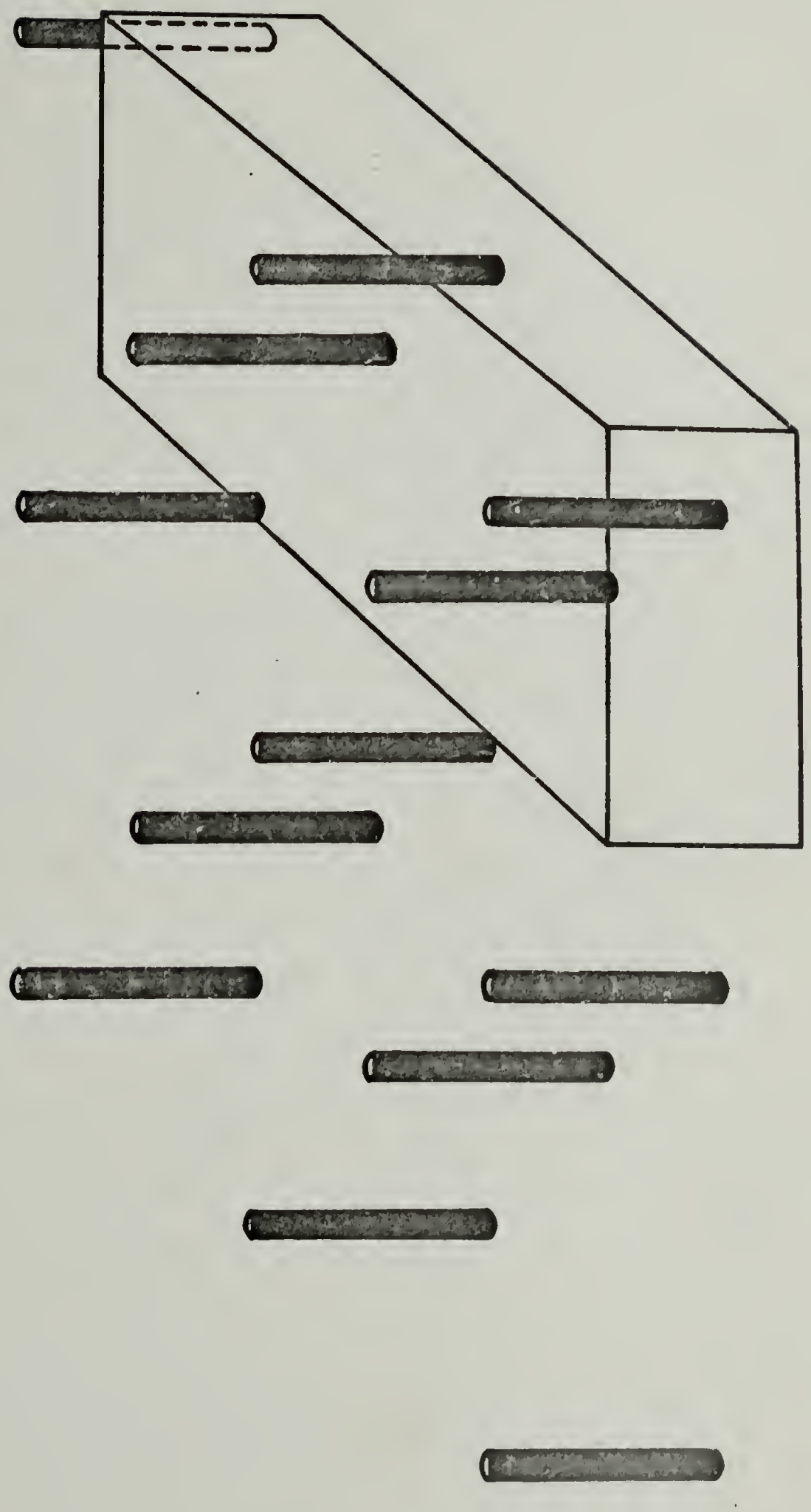

Figure 1

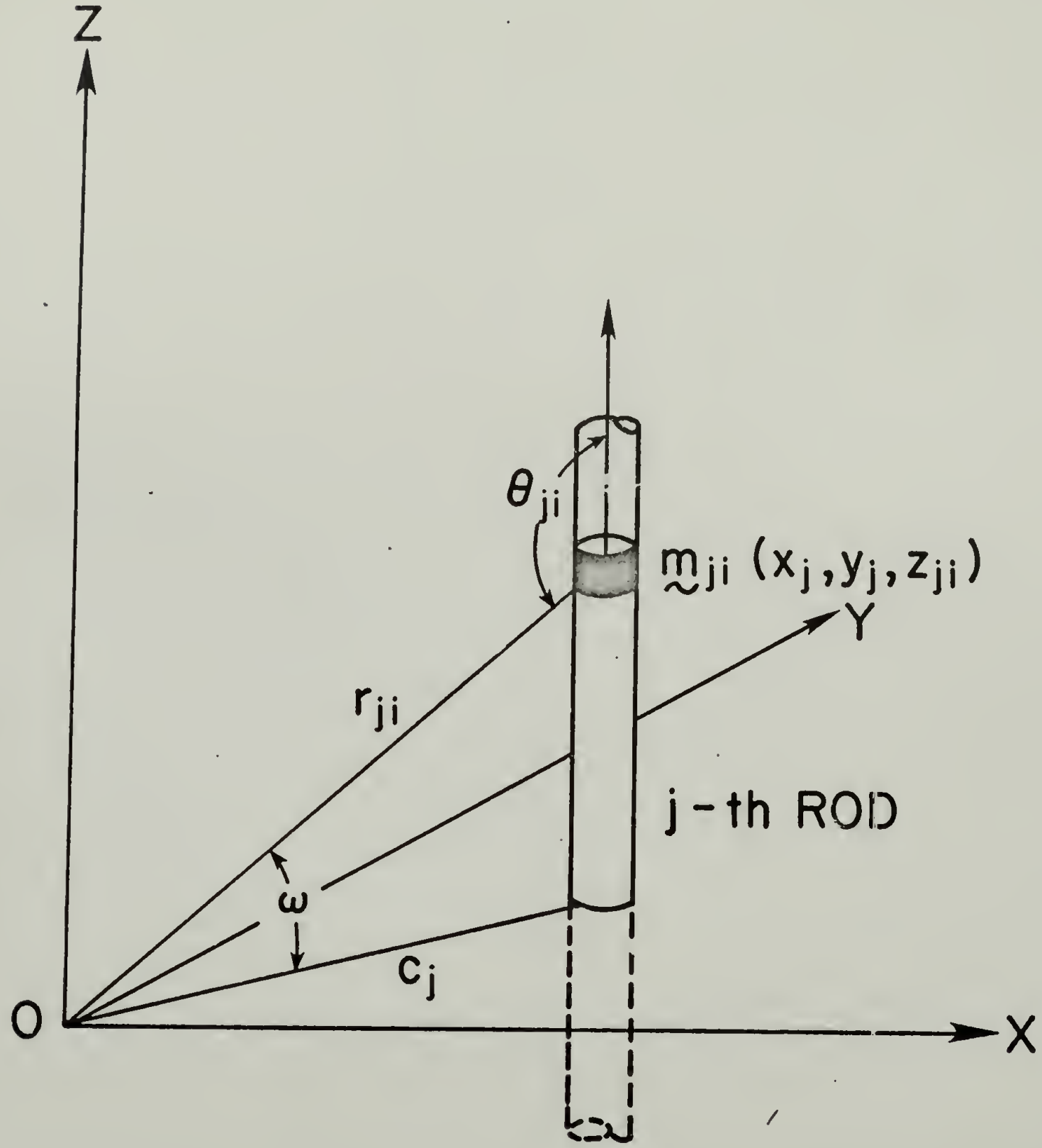

Figure 2

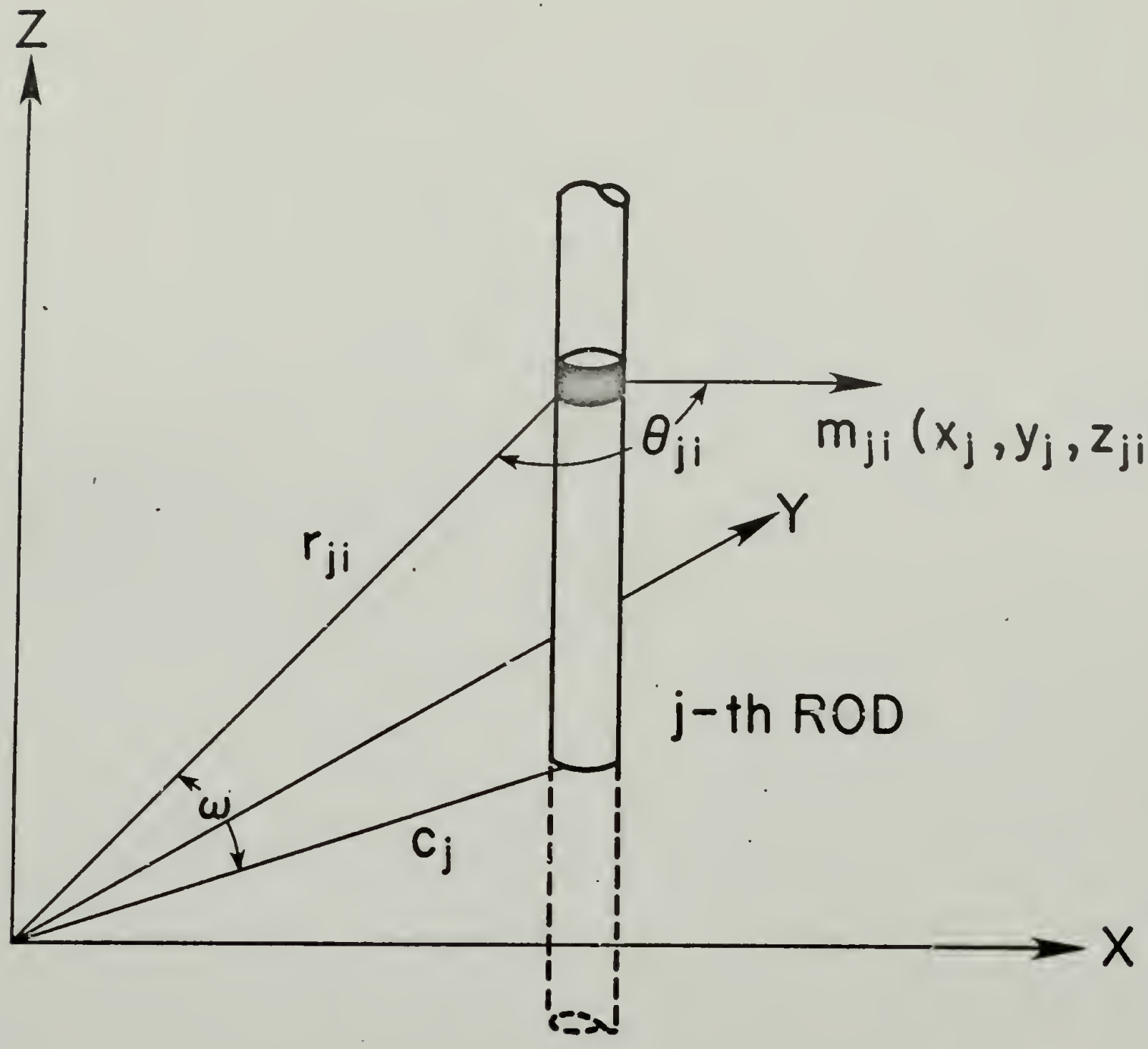

Figure 3

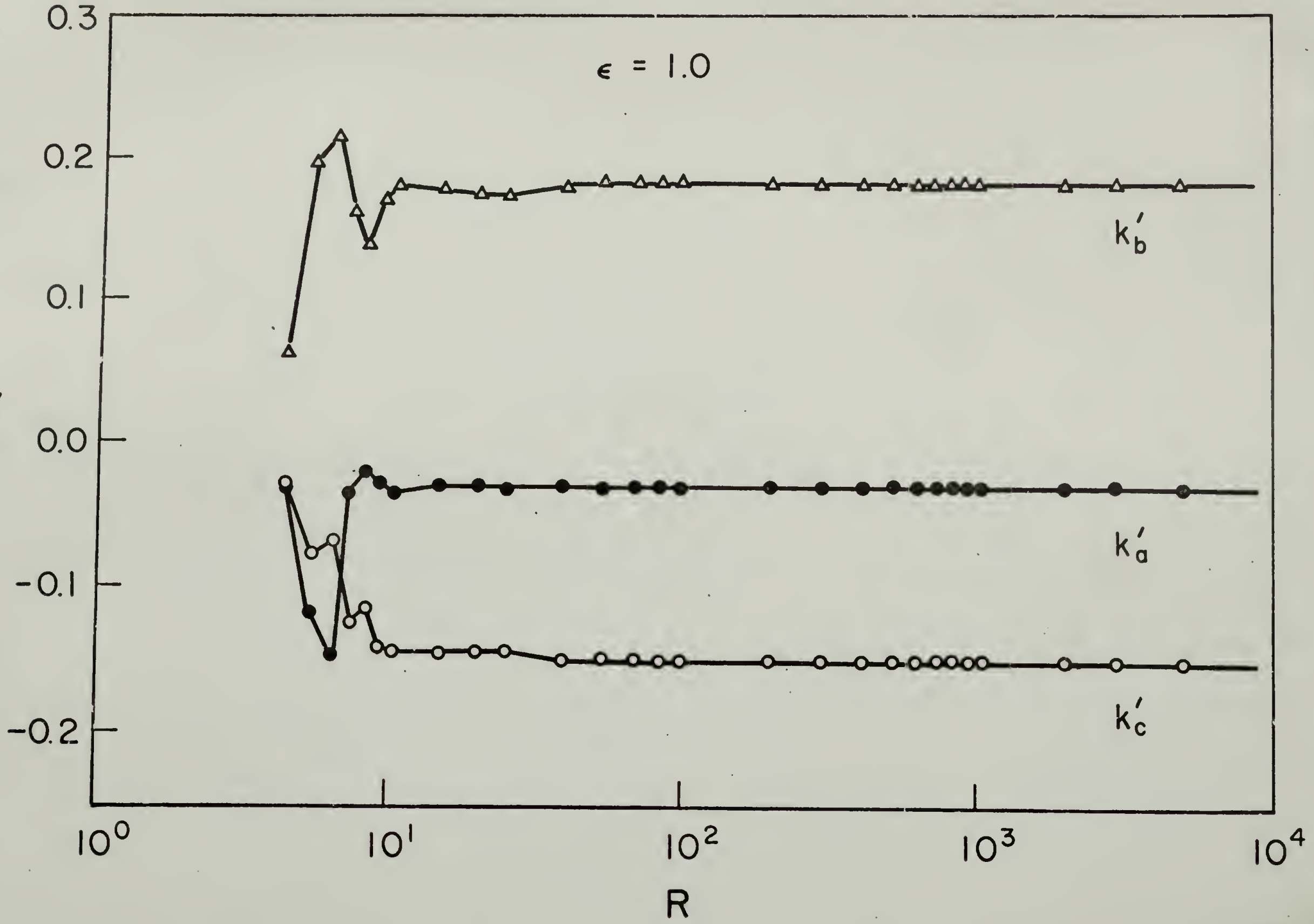

Figure 4

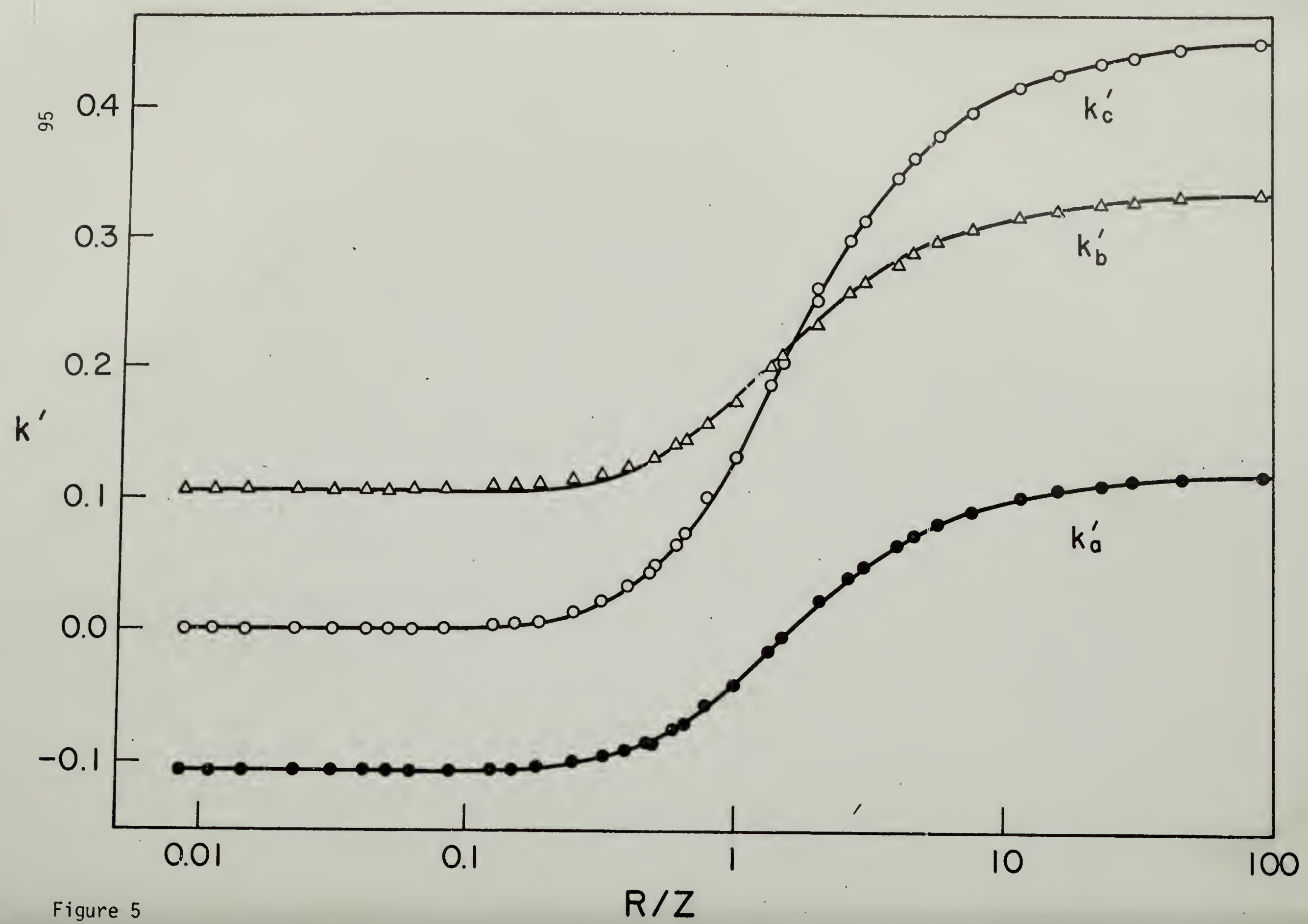

Figure 5

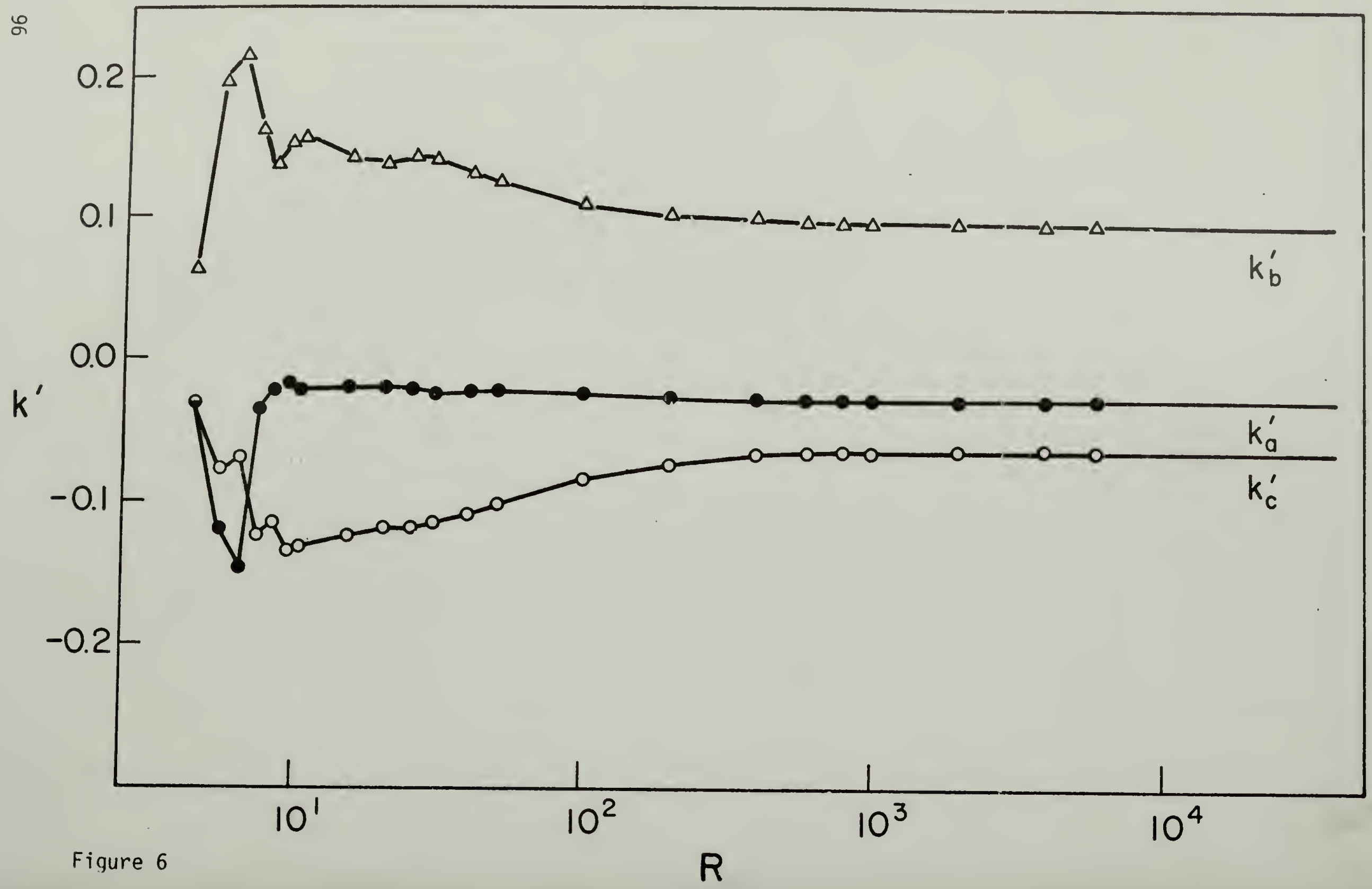

Figure 6

CHAPTER III

X-RAY STUDIES

Introduction

The mechanical and optical properties of a crystalline polymer depend upon several factors which are determined by the internal structure of the polymer (1). Among them the orientation of the crystal and the crystallinity are probably the most important factors. Therefore it is very desirable to know these factors.

The crystallinity may be determined by a number of methods such as density measurement (2), calorimetry (3), x-ray diffraction (4), NMR (5), and infrared spectrometry (6). These methods have both advantages and disadvantages in the time required of measurement and in the instrumental arrangement etc. For the time independent study of crystalline phase of a sample under stress, the x-ray diffraction technique is surely the most absolute and best established method.

The orientation of the crystal may also be measured by those methods described above. The x-ray diffraction method is, however, the best for this purpose as well as for the measurement of the crystallinity.

X-ray pictures of PIP samples are shown in Figure 1. They were taken at room temperature. There is only an amorphous halo at unstrained state and at low elongation which means zero or negligible crystallinity in the samples. As the elongation ratio α increases, the diffraction intensity increases and the diffraction peaks become more discrete, indicating higher crystallinity and higher orientation.

The quantitative determination of their values will be discussed in the following sections.

Measurement of the Degree of Crystallinity

There are several methods to determine crystallinity by x-ray measurement. One of the easy and convenient ways is that (7) the measurement is made at the positions of the intensity peaks as a function of the azimuthal angle Ω. (The coordinate system for x-ray diffraction is shown in Figure 12). For i-th diffraction peak, an integration over azimuthal angle is defined by

$$A_i = \int_0^{\pi/2} I_i(\Omega) \sin\Omega \, d\Omega \qquad (1)$$

may be calculated. The degree of crystallinity is then approximately given as

$$X_c = \frac{\sum_i A_i}{\text{Amorphous} + \sum_i A_i} \qquad (2)$$

Ruland (8) has proposed a more correct approach considering disorder of crystals. The crystallinity is described as

$$X_c = \frac{\int_0^{\infty} S^2 I_{cr} \, ds}{\int_0^{\infty} S^2 I \, ds} \quad \frac{\int_0^{\infty} S^2 \overline{f^2} \, ds}{\int_0^{\infty} S^2 \overline{f^2} \, Dds} \qquad (3)$$

where S is $(2/\lambda)\sin\theta$, λ is the wavelength of the x-rays, θ is the Bragg angle, I_{cr} is the coherent scattering from the crystalline phase at S, I is the total coherent scattering. $\overline{f^2}$ is the weighted mean-square atomic-scattering factor of the sample described by

$$\overline{f^2} = \frac{\sum N_i \, f_i^2}{\sum N_i} \tag{4}$$

N_i being the number of atoms of type i in the stoichiometric formula of the polymer and f_i being the atomic scattering factor of type i. D is an imperfection factor which includes the loss of intensity concentrated at reciprocal lattice points due to displacement of the atoms from their ideal positions. As a first approximation for unoriented systems, this may be described as exp $(-kS^2)$ in which k is the total disorder due to thermal motion and to lattice imperfection.

The integration of Equation (3) is usually taken over a finite range (say S_o to S_p) which gives

$$X_c = K \frac{\int_{S_o}^{S_p} S^2 \, I_{cr} \, ds}{\int_{S_o}^{S_p} S^2 \, I \, ds} \tag{5}$$

where

$$K = \frac{\int_{S_o}^{S_p} S^2 \, \overline{f^2} \, ds}{\int_{S_c}^{S_p} S^2 \, \overline{f^2} \, D \, ds} \tag{6}$$

A value of K is taken to produce a value of X_c which is independent of the integration range.

For a uniaxially oriented sample, the diffracted intensity is dependent upon the azimuthal angle Ω as well as the Bragg angle. In this case

$$I(S) = \int_0^{\pi/2} I \, (S,\Omega) \, \sin\Omega \, d\Omega \tag{7}$$

The intensities of diffracted x-ray are corrected for polarization, absorption, background intensity and incoherent scattering using (9)

$$I_{corr} = \left[I_{exp} - I_{exp\ back}\, e^{-\mu d \sec\theta}\right]\left[\frac{2}{1+\cos^2 2\theta}\right]\left[\frac{e^{\mu d \sec\theta}}{\sec\theta}\right] - I_{incoh} \qquad (8)$$

where

I_{corr} = corrected intensity

I_{exp} = (total) experimental intensity

$I_{exp\ back}$ = background intensity with no sample

I_{incoh} = incoherent intensity

μ is the linear absorption coefficient and d is the thickness of the sample. The value of μ may be calculated from the equation (10)

$$\mu = \rho \sum W_i\, (\mu/\rho)_i \qquad (9)$$

where ρ is the density of the sample, W_i is the weight fraction of the ith element in the sample and $(\mu/\rho)_i$ is the mass absorption coefficient. For cis-1,4-polyisoprene in this work 3.8 (cm^{-1}) is used as the value of μ. The calculation is shown in Table 1.

The incoherent scattering (Compton scattering) is given by the equation (11)

$$I_{inc} = R\left(Z - \sum_n |f_{nn}|^2 - \sum_{m \neq n}\sum |f_{mn}|^2\right) \qquad (10)$$

where

$$f_{mn} = \int \psi_m^* \exp\,(i\, \underset{\sim}{P} \cdot \chi)\, \psi_n\, dv \qquad (11)$$

Z is the atomic number, f_{nn} is the scattering factor of the nth electron, f_{mn} is an exchange term due to the interaction of the mth and nth electrons, $\underset{\sim}{P}$ is the reciprocal-lattice vector, γ is the position vector within the atom, ψ_m^* and ψ_n are electronic wavefunctions, and R is the Breit-Dirac electron recoil factor, which has a value close to unity except for elements of low atomic number. The calculation of the incoherent scattering for polyisoprene is given elsewhere (9). In practice the incoherent scattering intensity may be obtained by assuming that (7,12,13) the diffraction at a sufficiently high Bragg angle is entirely incoherent. The incoherent intensity at lower angles are then estimated from the calculated curve of the incoherent scattering. Although Krimm and Tobolsky (14) showed that the coherent intensity did not entirely vanish even at large Bragg angle, this procedure for the evaluation of the incoherent scattering is a good and convenient approximation in a practical sense. The angle $2\theta = 50$ was used as such an angle. While a somewhat greater angle would have been desirable, this angle was chosen because of instrument limitations.

Samples of PIP were prepared by the same manner described in Chapter I. They were a little thicker than the previous ones for the birefringence study to make the x-ray measurements easier (about 50 mils at unstretched state). The samples were stretched to certain elongations at room temperature and held by sample holders for about 40 hours. X-ray measurements were made using the dynamic diffractometer (15) of our laboratory in a static mode using $CuK\alpha$ radiation. The measurement of intensities was done at various azimuthal angles such as 0°, 5°, 15°, 28°, 39°, 50°, 70°, 85° and 90°.

The corrected intensity of the diffracted x-ray from the samples of PIP at various elongations are shown in Figures 2-4. It is noted that $S^2Ids = (8/\lambda^3)\ I(\theta,\Omega) \times \sin^2\theta \cos\theta d\theta$. A typical plot of $I(\theta,\Omega) \sin^2\theta \cos\theta$ vs θ at several values of Ω for a sample stretched 420% is given in Figure 6. Each of these plots was resolved into its crystalline and amorphous contributions and the areas of the total intensity and the amorphous parts considering the weighting factor $\sin\Omega$ are plotted as a function of azimuthal angle Ω as shown in Figures 6-8. The crystalline contribution was taken as the difference between both. The integration was taken from $\theta = 4.5$ ($S_o = 0.1$) to $\theta = 12$ ($S_p = 0.27$).

To determine the degree of crystallinity from the $S^2\ I_c$ and $S^2\ I$ curves of any specimen it may be useful to prepare a nomogram of K versus S_p for a range of values of coefficient k in the lattice-imperfection factor $D = \exp(-kS^2)$. By using Equations (4) and (6), a nomogram for $S_o = 0.1$ and for $\overline{f^2}$ corresponding to chemical composition of cis-1,4-polyisoprene, i.e., $(C_5H_8)_n$, was calculated using the atomic scattering factor in the International Table (11) and shown in Figure 9. As has been obtained for $(CH_2)_n$ composition by Ruland (8), the curves of K versus S_p are nearly linear. For a given polypropene sample Ruland could read the optimal value of k from the nomogram for $(CH_2)_n$ composition to make X_c as nearly constant as possible for independent S_p. In this manner he obtained k = 4 for polypropene sample, k = 3 ~ 5.6 for Nylon 6, and k = 3.6 ~ 7.7 for Nylon 7.

In this work the diffracted x-ray intensity was measured up to about S = 0.3. (It was desirable to go to a higher value, however, it was not done because of instrument limitations). It would not be practical to proceed with Ruland's method over this relatively small range. There-

fore, the integration was taken from $\theta = 4.5$ ($S_o = 0.1$) to $\theta = 12$ ($S_p = 0.27$). As seen in Figure 9, it is obvious that the value of K is very close to unity even at high values of k in the range over which the integrations were taken. Consequently it may be a good approximation to take K as one over this integration range. If the lattice-imperfection of PIP crystal is very high, that is high k values, the degree of crystallinity will only become about 20% higher than that obtained by the assumption of $K = 1$ or $k = 0$. Another important thing concerning the determination of X_c with elongation is whether or not K varies with elongation. While it is conceivable that (7) the degree of disorder may vary with elongation and lead to a variation of K, the assumption of $K = 1$ in this work is probably still applicable to the oriented system by the reason discussed above.

The degree of crystallinity X_c of PIP at different elongations is given in Table 2 and shown in Figure 10. The degree of crystallinity of natural rubber has been measured by several workers (4,16,17) and their results are also shown in Figure 10. It is noted that the crystallinity of PIP is comparable with that of natural rubber. It seems, therefore, that non cis-content (about 3%) in PIP (synthetic polyisoprene) does not have significant effects at least on the degree of crystallinity. The non cis-content, however, may have a significant effect on the rate of crystallization.

These values of X_c will be used later to determine the intrinsic birefringence of PIP crystal.

Measurement of the Orientation Function of Crystallites

Measurement of the Orientation Function

To describe the orientation of crystallites in crystalline fibers an orientation function was proposed first by Hermans and co-workers (18) as

$$f_{\phi} = \frac{1}{2} (3 \langle \cos^2\phi \rangle - 1) \qquad (12)$$

where $\langle \cos^2\phi \rangle$ represents the mean-square cosine (averaged over all the crystallites) of the angle ϕ between a given crystal axis and the reference direction. In this equation it is assumed that other crystallographic axes as well as the one specified are arranged with cylindrical symmetry about the reference direction (10).

Following Hermans' treatment Stein (19) has proposed the equations for uniaxial orientation

$$f_{a,z} = \frac{1}{2} (3 \langle \cos^2\phi_{a,z} \rangle - 1)$$

$$f_{b,z} = \frac{1}{2} (3 \langle \cos^2\phi_{b,z} \rangle - 1) \qquad (13)$$

$$f_{c,z} = \frac{1}{2} (3 \langle \cos^2\phi_{c,z} \rangle - 1)$$

where $\phi_{a,z}$, $\phi_{b,z}$ and $\phi_{c,z}$ are the angles between a, b and c crystal axes and the reference direction Z. The geometry is shown in Figure 11. For uniaxial oriented materials the symmetric (most likely stretching) direction is usually taken as Z direction and the angles σ_a, σ_b and σ_c may be considered as being uniformly distributed along the reference (symmetric) direction Z. The value of $\langle \cos^2\phi \rangle$ is 1 for perfect alignment with Z, 1/3 for random orien-

tations, and 0 for perpendicular orientation to Z direction.

If the crystal unit cell is orthogonal, one may obtain

$$\cos^2\phi_{a,z} + \cos^2\phi_{b,z} + \cos^2\phi_{c,z} = 1 \qquad (14)$$

and

$$f_{a,z} + f_{b,z} + f_{c,z} = 0 \qquad (15)$$

Thus, for an orthogonal crystal only two of the orientation functions are needed to describe the orientation in uniaxially oriented materials.

The orientation function of a and c axes of cis-polyisoprene crystal may be obtained directly from the measurements for the orientation of the plane-normal of the (200) and (002) plane, respectively. Because the crystal unit cell of PIP is orthorhombic (20,21) and because both diffraction intensities from the two reflections are strong enough for the measurements. Bragg angles which are corresponding to the major reflections of PIP are as follows (20,21)

hkℓ	Bragg Angle (2θ)
200	14.0
201/$\bar{2}$01	17.5
120	20.7
002	21.4

Averages of $\cos^2\phi_{hk\ell,z}$ may be calculated from the observed intensities according to the relation (22,23)

$$\langle\cos^2\phi_{hk\ell,z}\rangle = \frac{\int_0^{\pi/2} I_{hk\ell}(\phi)\,\cos^2\phi\,\sin\phi\,d\phi}{\int_0^{\pi/2} I_{hk\ell}(\phi)\,\sin\phi\,d\phi} \qquad (16)$$

where $I_{hk\ell}(\phi)$ is the relative intensity of the diffracted x-ray by ($hk\ell$) plane.

The inclination of the stretching direction from the horizontal plane is designated by the angle χ, and the samples are symmetrically tilted with respect to the incident and diffracted beams. The coordinate system used here is given in Figure 12.

If the sample is uniaxially oriented and if the symmetry axis is the stretching direction, the angle $\phi_{hk\ell,z}$ is equal to the angle χ provided that the Bragg angle θ is positioned at $\theta_{hk\ell}$ (24). Then, Equation (16) is rewritten as

$$\langle\cos^2\phi\rangle = \langle\cos^2\chi\rangle = \frac{\int_0^{\pi/2} I(\chi)\cos^2\chi\sin\chi\, d\chi}{\int_0^{\pi/2} I(\chi)\sin\chi\, d\chi} \qquad (17)$$

The measurements were performed with the diffractometer described before (15). The diffraction intensities at various elongations were measured as a function of azimuthal angle Ω (or $\pi/2 - \chi$) at $\theta = 7.0°$ for (200) reflection and at $\theta = 10.7°$ for (002) reflection. The intensities were corrected using Equation (8). They are shown in Figures 13-18. The intensity from each reflection plane was obtained by subtracting the amorphous intensity from the total intensity.

The values of $\langle\cos^2\phi_{hk\ell}\rangle$ were calculated from Equation (17) and the orientation functions for the a and c axes were obtained from Equation (13). The numerical values of them are given in Table 3 and $\langle\cos^2\chi\rangle$ is plotted in Figure 19. By using Equations (14) and (15) $\langle\cos^2\chi\rangle$ and the orientation function for b axis were calculated.

The values for the b axis are very close to those for the a axis as expected in axial orientation, which indicates random orientations of a and b axes around the c axis. It is also noted that the orientation function is very high even at $\alpha = 4.1$. This result shows that the assumption of $f_c = 1$ used in Chapter I may be very good and gives a justification for Flory's and Smith's theories (25,26) in which the perfect orientation is assumed. For natural rubber stretched at room temperature the values of 0.985 at $\alpha = 5.0$ and 0.982 at $\alpha = 7.5$ have been reported (4).

Because of the instrumental limitation it is considered there may be an error or $\pm$ 1 degree with respect to the angle χ. For a system with very high orientation such as that discussed in this work, this one degree could be a source of large experimental errors. The fluctuation of the incident x-ray beam is about 10%. However, since this fluctuation is random, the error caused by this fluctuation can be minimized if many experimental points are taken. The possible experimental error may, therefore, be considered to be about 2-5%.

The plane-normal distribution function $Q(\chi)$ may also be obtained from the intensity by normalization:

$$Q(\chi) = I(\chi) \Big/ \int_0^{\pi} I(\chi) \sin\chi \, d\chi \qquad (17a)$$

$Q(\chi)$ for (200) and (002) planes are calculated and shown in Figures 20 and 21. It should be mentioned that there is an appreciable difference in shape of the distribution curve for different elongation. On the hand the values of $\langle\cos^2\chi\rangle$ are almost the same for all elongations. This may be natural because of the fact that the function of $\cos\chi$ does not change significantly

if χ is smaller than 10°. It may, therefore, be difficult to say that there is some difference in the orientation for the samples at different elongations. The distribution function $Q(\chi)$ may, however, describe the differences clearly.

The Orientation Distributions of Crystallites and Statistical Chain Segment

Krigbaum and Roe (27) have proposed the orientation function for statistical segments in a strained amorphous network, using the Kuhn-Grun-Treloar (28) model of a network of flexible linked chains. Here χ is the angle specifying the orientation of a statistical segment with respect to the stretching direction. (In the definition this χ may be different from the χ described previously. Later in this section, however, this χ will be equivalent to one described before as will be seen). The distribution function is expressed in series form as (27)

$$W(\xi) = \sum_{\ell=0}^{\infty} W_\ell P_\ell (\xi) \tag{18}$$

where $\xi = \cos\chi$, $P_\ell(\xi)$ is normalized Legendre polynomials and W_ℓ is the coefficient. The first seven coefficients have been obtained as

$$(2)^{1/2} W_0 = 1$$

$$\left(\frac{2}{5}\right)^{1/2} W_2 = (1/5n_s)(\alpha^2 - 1/\alpha) + (36/875n_s^2)(\alpha^4 + \alpha/3 - 4/3\alpha^2)$$

$$+ (108/6125n_s^3)(\alpha^6 + 3\alpha^3/5 - 8/5\alpha^3)$$

$$\left(\frac{2}{9}\right)^{1/2} W_4 = (3/175n_s^{\,2})(\alpha^4 - 2\alpha + 1/\alpha^2) + (216/13475n_s^{\,3})$$

$$(\alpha^6 - 4\alpha^3/5 - 7/5 + 6/5\alpha^3)$$

$$\left(\frac{2}{13}\right)^{1/2} W_6 = (27/35035n_s^{\,3})(\alpha^6 - 3\alpha^3 + 3 - 1/\alpha^3)$$

$$W_\ell = 0 \quad (\text{if } \ell = \text{odd})$$

and

$$(2)^{1/2} P_o = 1$$

$$\left(\frac{2}{5}\right)^{1/2} P_2 = (3\xi^2 - 1)/2$$

$$\left(\frac{2}{9}\right)^{1/2} P_4 = (35\xi^4 - 30\xi^2 + 3)/8 \qquad (20)$$

$$\left(\frac{2}{13}\right)^{1/2} P_6 = (231\xi^6 - 315\xi^4 + 105\xi^2 - 5)/16$$

where n_s is the number of statistical segments between crosslinks.

From Equations (18)-(20) the distribution function $W(\chi)$ can be calculated at various elongations as a function of χ. The value of n_s may be obtained by the method described in Chapter I. In this calculation 57 is used as the value of n_s, which is the average value obtained in Chapter I. The distribution functions calculated at α = 4.1, 4.7 and 6.1 are shown in Figure 22. The average value of $\cos^2\chi$ may be given by

$$\langle\cos^2\chi\rangle = \frac{\int_0^\pi W(\chi)\cos^2\chi \sin\chi \, d\chi}{\int_0^\pi W(\chi)\sin\chi \, d\chi} \qquad (21)$$

The values of $\langle\cos^2\chi\rangle$ are plotted in Figure 19, designated as amorphous. It is noted that the orientation of the c axis is much higher than that of the statistical segments prior to crystallization.

To explain this difference Krigbaum and Roe further assume that the formation of a stable nucleus for crystallization requires the simultaneous alignment of ν amorphous segments (29). By invoking another assumption that the nucleation process controls the overall crystallite orientation distribution in the sample, they obtain the orientation distribution of the crystallite c axis as

$$Q_c(\chi) = \frac{[W(\chi)]^{\nu}}{\int_0^{\pi} [W(\chi)]^{\nu} \sin\chi \, d\chi} \tag{22}$$

then,

$$\langle\cos^2\chi\rangle = \int_0^{\pi} \cos^2\chi \, Q_c(\chi) \sin\chi \, d\chi \tag{23}$$

Now the critical volume of nucleus is represented by the value of ν. It may be interesting to estimate the size of the critical nucleus from x-ray measurements for the orientation.

One may determine the values of ν as they give an agreement between $\langle\cos^2\chi\rangle$ calculated according to Equations (22) and (23) and the value obtained for (002) reflection as given in Table 3. The values of ν can be obtained independently by a best fit between the theoretical and experimental distribution curves. In this calculation here the values of ν were determined by the former method and given in Table 4. The theoretical distribution curves were calculated using these values and shown along with the experimental ones in Figures 23-25. It is seen that both curves agree well,

which indicates that the values of ν from the best fit are probably close to those obtained here. Actually the differences between two values of ν are within 5, except the case of $\alpha = 4.1$, in which case the value from the best fit is about 20 less than that reported here. However, the general conclusions are believed to be valid in spite of this uncertainty.

From the values of ν the volume of a crystalline nucleus can be calculated. The dimensions of a unit cell of PIP are given as (20,21)

$$a = 12.46\ \text{Å},\quad b = 8.89\ \text{Å},\quad c = 8.10\ \text{Å}$$

and 8 isoprene monomer units in the unit cell. The number of monomer units per segment have been calculated as 1.97 in Chapter I. The volume of the nucleus changes from 35,800 Å^3 (33 Å cube) at $\alpha = 4.1$ to 18,100 Å^3 (26 Å cube) at $\alpha = 6.1$. Both the primary and secondary nuclei are considered to determine the crystal orientation distribution. As described by Krigbaum and Roe (29), however, the fact that the number of the latter greatly exceeds that of the former may suggest that the values given above probably refer to the volume of the secondary nuclei.

For polychloroprene (29) the size of the nucleus has been reported to be 29,000 Å^3 (30 Å cube) at $\alpha = 1.45$, 13,800 Å^3 (24 Å cube) at $\alpha = 4.44$, and 6,500 Å^3 (17 Å cube). The size of nucleus of PIP is relatively comparable with that of polychloroprene.

According to nucleation theories (30-33) the critical nucleus size is determined by its melting temperature and supercooling. One can, therefore, estimate the equilibrium melting temperature using an appropriate theory from the value of the critical nucleus obtained by the orientation

measurement. For bulk crystallization Hoffman et. al (34,35) have proposed an expression for the critical radius ρ^* of a cylindrical secondary nucleus of fixed length λ_o as

$$\rho^* = \left(\frac{\sigma_s}{\Delta h_f}\right)\left(\frac{T_m}{\Delta T}\right)\left(\frac{T_m}{T}\right)$$

$$\simeq \left(\frac{\sigma_s}{\Delta h_f}\right)\left(\frac{T_m}{\Delta T}\right) \qquad (24)$$

where σ_s and Δh_f are the lateral surface free energy and the heat of fusion per unit volume, respectively. T_m and T are the melting point and crystallization temperature, respectively. ΔT is the difference between T_m and T. It is well known that the melting point of a crosslinked polymer increases with elongation (36,37). ΔT becomes larger with elongation and, therefore, ρ^* becomes smaller. This may qualitatively explain the observed decrease in ν with α (29).

Following Krigbaum and Roe (29), if we consider the polymer segment to be cylindrical with radius γ_o, and identify λ_o with the length of a segment, then ν may be expressed by

$$\nu^{1/2} = \left(\frac{\sigma_s}{\gamma_o\ \Delta h_f}\right)\left(\frac{T_m}{\Delta T}\right)\left(\frac{T_m}{T}\right)$$

$$\simeq \left(\frac{\sigma_s}{\gamma_o\ \Delta h_f}\right)\left(\frac{T_m}{\Delta T}\right) \qquad (25)$$

The lateral surface free energy σ_s is not known for cis-polyisoprene under strain. As a first approximation the value of the average interfacial free energy $\bar{\sigma}$ for natural rubber at unstretched state is used as σ_s. It is 3 erg/cm^3 (38). The value of Δh_f is given as 6.8×10^8 erg/cm^3 (39-41).

From the dimension of the unit cell of PIP the radius of a segment is calculated as γ_o = 2.97 Å. T is taken as 298°K (room temperature).

The estimated values for T_m from Equation (25) are 28.6°C for α = 4.1, 29°C for α = 4.7 and 30°C for α = 6.1, which are considerably low as compared with the experimental values. The main reason for this may be attributed to the value of σ_s. We use the value for natural rubber at unstretched state. The surface free energy of a nucleus formed at oriented systems may not be equal to that at unoriented systems. Furthermore, the shape of a nucleus may also depend upon the degree of orientation of the mother phase (amorphous phase). It may, therefore, be questionable to use Equation (25) for this problem. If Equation (25) is still applicable to an oriented system, the value of the surface free energy has to be about ten times higher than that used here in order to give a comparable melting temperature with the melting temperature determined experimentally.

We should, however, not draw a definite conclusion from the limited data obtained here. More theoretical and experimental investigations will be needed to obtain a quantitatively satisfactory result.

References

1. A. Sharples, Chapter 4, "Crystallinity", in Polymer Science, ed. by A. D. Jenkins.
2. L. R. G. Treloar, The Physics of Rubber Elasticity, Oxford, 1958.
3. L. Mandelkern, Crystallization of Polymers, McGraw-Hill, New York, 1964.
4. L. E. Alexander, S. Ohlberg and G. R. Taylor, J. Appl. Phys., 26, 1068 (1955).
5. R. C. Hirst and H. Y. Chen, Rubber. Chem. and Tech., 46, 22 (1973).
6. B. E. Read and R. S. Stein, Macromolecules, 1, 116 (1968).
7. S. D. Hong, Ph.D. Thesis, Polymer Science and Engineering, University of Massachusetts, Amherst, Mass. (1975).
8. W. Ruland, Acta Crystallographica, 14, 1180 (1961).
9. H. P. Klung and L. E. Alexander, X-Ray Diffraction Procedures, John Wiley, New York, 1954.
10. L. E. Alexander, X-Ray Diffraction Method in Polymer Science, John Wiley, New York, 1969.
11. International Tables for X-Ray Crystaliography, Vol. III, 1962.
12. R. S. Stein, J. Powers and S. Hoshino, ONR Technical Report, No. 33, Univ. of Mass., Amherst, Mass. (1961).
13. Y. Akana, M.S. Thesis, University of Massachusetts, Amherst, Mass. (1973).
14. S. Krimm and A. V. Tobolsky, J. Polym. Sci., 7, 57 (1951).
15. T. Ito, T. Oda, H. Kawai, T. Kawaguchi, D. A. Keedy and R. S. Stein, Rev. Sci. Instr., 39, 1847 (1968).
16. J. M. Goppel and J. J. Arlman, Appl. Sci. Res., A1, 462 (1949).
17. S. C. Nyburg, British J. Appl. Phys., 5, 321 (1954).

18. P. H. Hermans and P. Platzek, Kolloid Z., 88, 68 (1939).

19. R. S. Stein, J. Polym. Sci., 31, 327 (1958).

20. C. W. Bunn, Proc. Roy. Soc., A180, 40 (1942).

21. S. C. Nyburg, Acta CRystall., 7, 385 (1954).

22. P. H. Hermans, Contribution to the Physics and Cellulose Fibers, Elsevier, Amsterdam, 1946.

23. Z. W. Wilchinsky, Advances in X-Ray Analysis, Vol. 6, Plenum Press, New York, 1963.

24. R. S. Stein, ONR Technical Report, No. 8, Nonv 2151, NR 356-378 (1958).

25. P. J. Flory, J. Chem. Phys., 15, 397 (1947).

26. K. J. Smith, Jr., J. Polym. Sci., A-2, 6, 1723 (1968).

27. R. J. Roe and W. R. Krigbaum, J. Appl. Phys., 35, 2215 (1964).

28. L. R. G. Treloar, Trans. Faraday Soc., 50, 881 (1954).

29. W. R. Krigbaum and R. J. Roe, J. Polym. Sci., Part A, 2, 4391 (1964).

30. N. Hirai, J. Polym. Sci., 42, 213 (1960).

31. F. P. Price, J. Polym. Sci., 42, 49 (1960).

32. F. P. Price, SPE Trans., 151 (1964).

33. J. Frenkel, Kinetic Theory of Liquids, Oxford Univ Press., 1964.

34. J. D. Hoffman and J. J. Weeks, J. Res. Natl. Bur. Std., 63A, 67 (1959).

35. J. D. Hoffman and J. J. Weeks, J. Chem. Phys., 37, 1723 (1962).

36. H. G. Kim and L. Mandelkern, J. Polym. Sci., A-2, 6, 181 (1968).

37. F. deCandia and V. Vittoria, Makromol. Chem., 155, 17 (1972).

38. G. M. Martin and L. Mandelkern, J. Appl. Phys., 34, 2312 (1963).

39. J. F. M. Oth and P. J. Flory, J. Am. Chem. Soc., 80, 1297 (1958).

40. D. E. Roberts and L. Mandelkern, J. Am. Chem. Soc., 77, 781 (1955).

41. F. deCandia, G. Romano and V. Vittoria, J. Polym. Sci., Polym. Phys. Ed., 11, 2291 (1973).

TABLE 1

Calculation of the Linear Absorption Coefficient
of Cis-1,4-Polyisoprene for CuKα Radiation

Chemical Composition: C_5H_8

Molecular Weight: $\sum_i n_i A_i = 68.119$

Densities (g/cm^3): Crystalline, 1.00
Amorphous, 0.91

Mass Absorption Coefficient: $\frac{\mu}{\rho} = \sum_i W_i \left(\frac{\mu}{\rho}\right)_i$

Atom	n	A	μ/ρ (cm^2/g)	$n_i A_i$	W_i	$W_i (\mu/\rho)_i$
Carbon	5	12.011	4.60	60.055	0.8816	4.055
Hydrogen	8	1.008	0.435	8.064	0.1184	0.052
				68.119	1.0000	4.107

Mass absorption coefficient (cm^2/g): 4.107

Linear absorption coefficient (cm^{-1}):

Crystalline, 1.00 x 4.107 = 4.107
Amorphous, 0.91 x 4.107 = 3.737

TABLE 2

The Degree of Crystallinity
at Various Elongations

α	X_c (%)
4.1	1.4^5
5.2	8.3^8
6.0	14.2^7

TABLE 3

The Values of $\langle\cos^2\chi\rangle$ (or $\langle\cos\varphi\rangle$)

α	$\langle\cos^2\chi_a\rangle$	$\langle\cos^2\chi_b\rangle$	$\langle\cos^2\chi_c\rangle$
4.1	0.012^2	0.002^7	0.985^1
4.7	0.010^6	0.003^9	0.985^5
6.1	0.006^3	0.007^1	0.986^6

The Values of the Orientation Functions, f_a, f_b and f_c

α	f_a	f_b	f_c
4.1	-0.48^2	-0.49^6	0.97^8
4.7	-0.48^4	-0.49^4	0.97^8
6.1	-0.49^1	-0.48^9	0.98^0

TABLE 4

The Values of ν and the Estimated Volume of Critical Nucleus

α	ν	V^* (A^3)
4.1	162	35800
4.7	127	28100
6.9	82	18100

Captions for Figures

1) X-ray patterns of PIP samples stretched at room temperature.

2) The corrected intensity of the diffracted x-ray of PIP at α = 4.1. Here, Ω is defined to be equal to χ in Figure 12.

3) The corrected intensity of the diffracted x-ray of PIP at α = 5.2.

4) The corrected intensity of the diffracted x-ray of PIP at α = 6.0.

5) The variation of $I(\theta, \Omega) \sin^2\theta \cos\theta$ with θ for a 420% stretched PIP sample at several azimuthal angles.

6) The variation of $S(\Omega) \sin\Omega$ with Ω for a 310% stretched PIP sample.

7) The variation of $S(\Omega) \sin\Omega$ with Ω for a 420% stretched PIP sample.

8) The variation of $S(\Omega) \sin\Omega$ with Ω for a 500% stretched PIP sample.

9) Nomogram of K values as a function of k and S_p calculated for the chemical composition $(C_5H_8)_n$ and S_0 = 0.1.

10) Crystallinity in PIP samples at room temperature along with that in natural rubber measured by others; (A) Alexander, et al. (4); (B) Goppel and Arlman (16); (c) Nyburg (17).

11) Stein's (19) coordinate system for specifying orientation modes in orthorhombic polymers.

12) (a) The geometrical relation between inxident x-ray, $\underset{\sim}{S}_0$, diffracted x-ray, $\underset{\sim}{S}_1$, sample S and detector B in the method of diffractometer. X axis indicates the normal of sample surface.

(b) Coordinate of rotation of a sample. Z is the diffractometer axis. X' is the direction of the incident x-ray. Z is the stretching direction. Note: Azimuthal angle Ω in the section of "Measurement of the Degree of Crystallinity" is defined to be equal to

χ. In the section, "Measurement of the Orientation Function of Crystallites", however, Ω is equal to $\pi/2 - \chi$.

13) The variation of I with Ω at $\theta = 7.0^{o}$ for a PIP sample at $\alpha = 4.1$.

14) The variation of I with Ω at $\theta = 10.7^{o}$ for a PIP sample at $\alpha = 4.1$.

15) The variation of I with Ω at $\theta = 7.0^{o}$ for a PIP sample at $\alpha = 4.7$.

16) The variation of I with Ω at $\theta = 10.7^{o}$ for a PIP sample at $\alpha = 4.7$.

17) The variation of I with Ω at $\theta = 7.0^{o}$ for a PIP sample at $\alpha = 6.1$.

18) The variation of I with Ω at $\theta = 10.7^{o}$ for a PIP sample at $\alpha = 6.1$.

19) The variation of $\langle \cos^2 \chi \rangle$ with elongation for PIP.

20) The (200) plane-normal distribution function $Q(\chi)$ obtained from x-ray measurement for PIP samples at various elongations.

21) The (002) plane-normal distribution function $Q(\chi)$ obtained from x-ray measurement for PIP samples at various elongations.

22) The variation of the distribution function with χ calculated from Equation (18) for various elongations.

23) The experimental (full curve) and theoretical (dotted curve) distribution function $Q(\chi)$ of the (002) plane-normal for a PIP sample stretched to $\alpha = 4.1$.

24) The experimental and theoretical distribution function $Q(\chi)$ of the (002) plane-normal for a PIP sample stretched to $\alpha = 4.7$.

25) The experimental and theoretical distribution function $Q(\chi)$ of the (002) plane-normal for a PIP sample stretched to $\alpha = 6.1$.

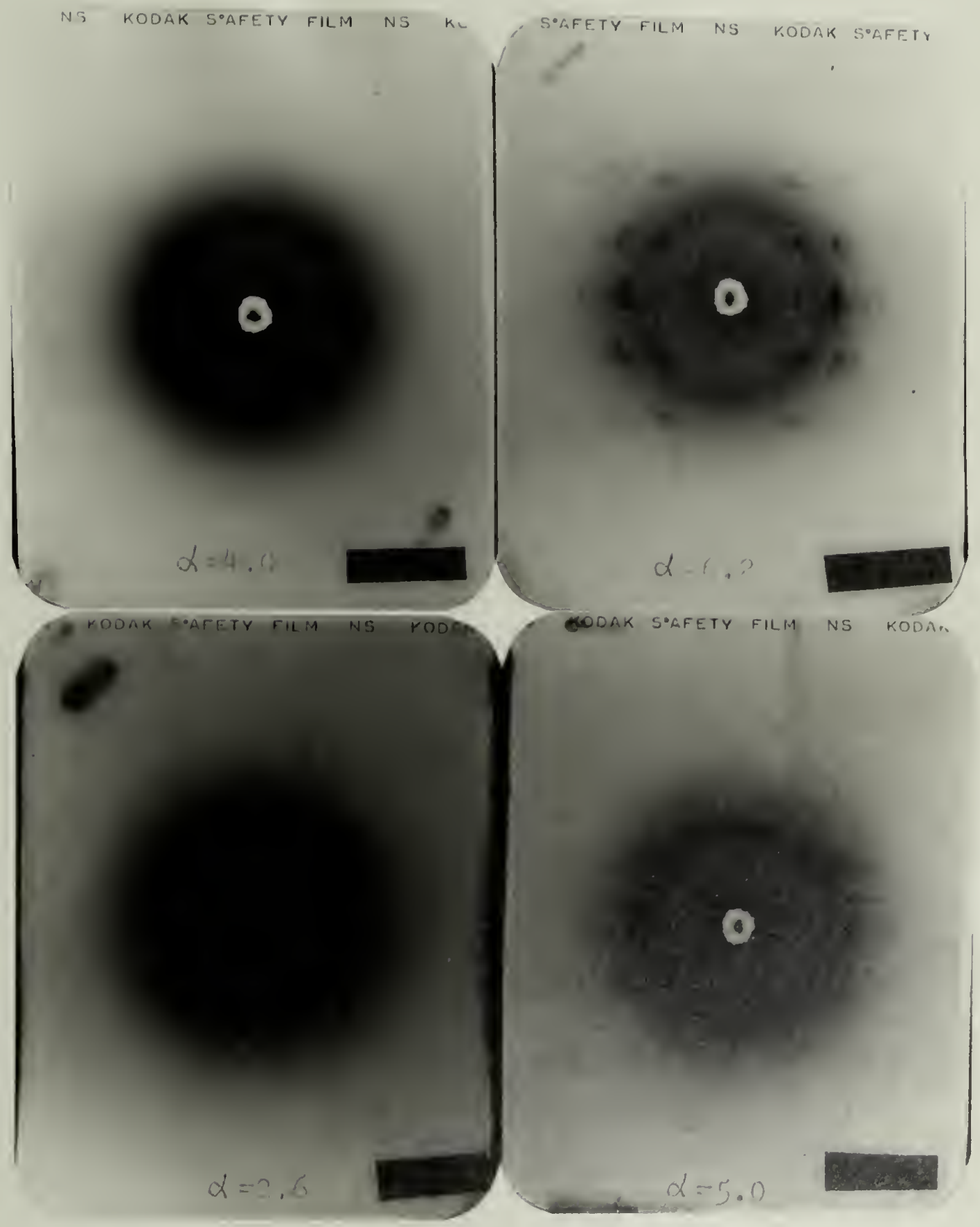

Figure 1

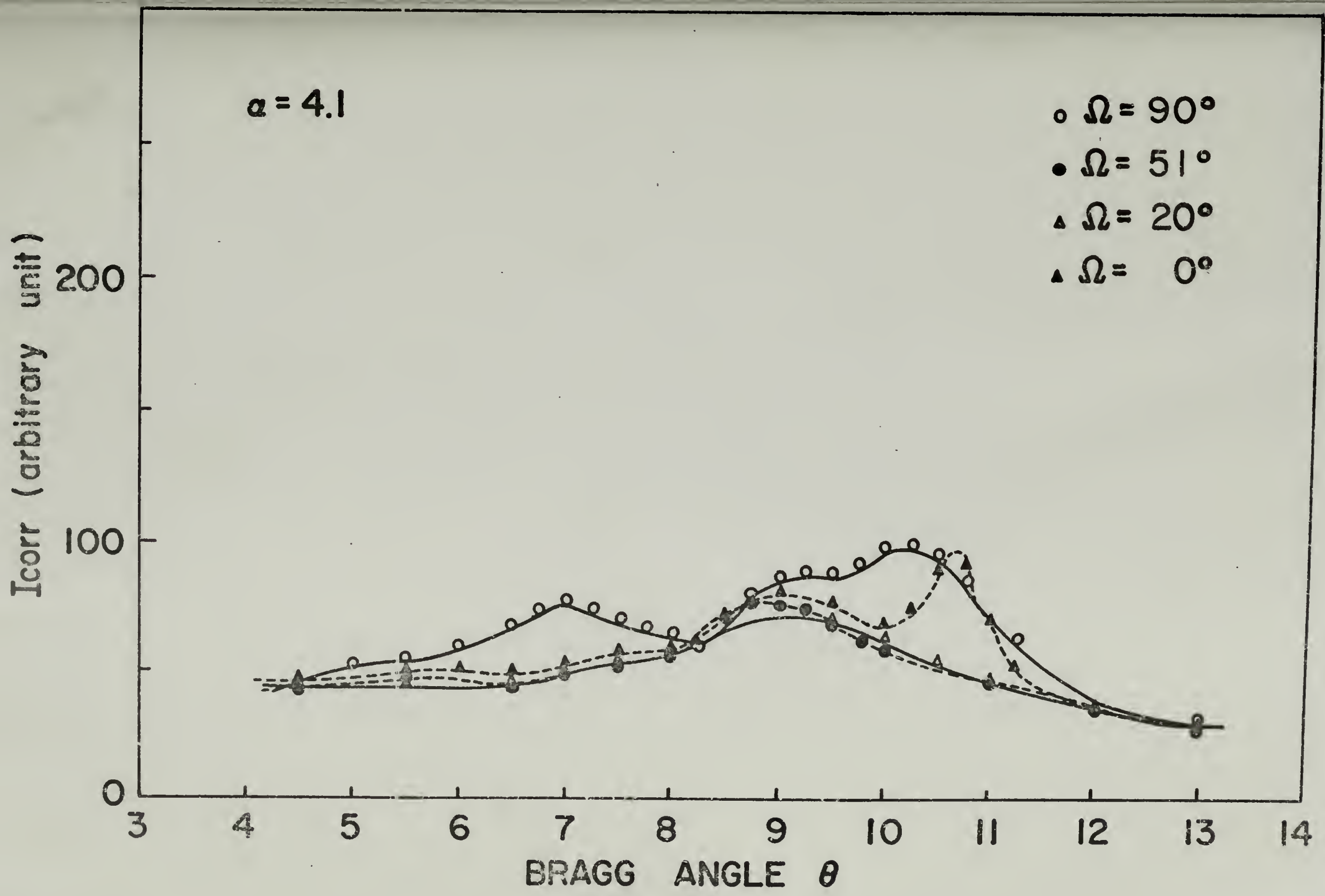
α = 4.1
○ Ω = 90°
● Ω = 51°
▲ Ω = 20°
▲ Ω = 0°
Icorr (arbitrary unit)
0
100
200
3
4
5
6
7
8
9
10
11
12
13
14
BRAGG ANGLE θ

Figure 2

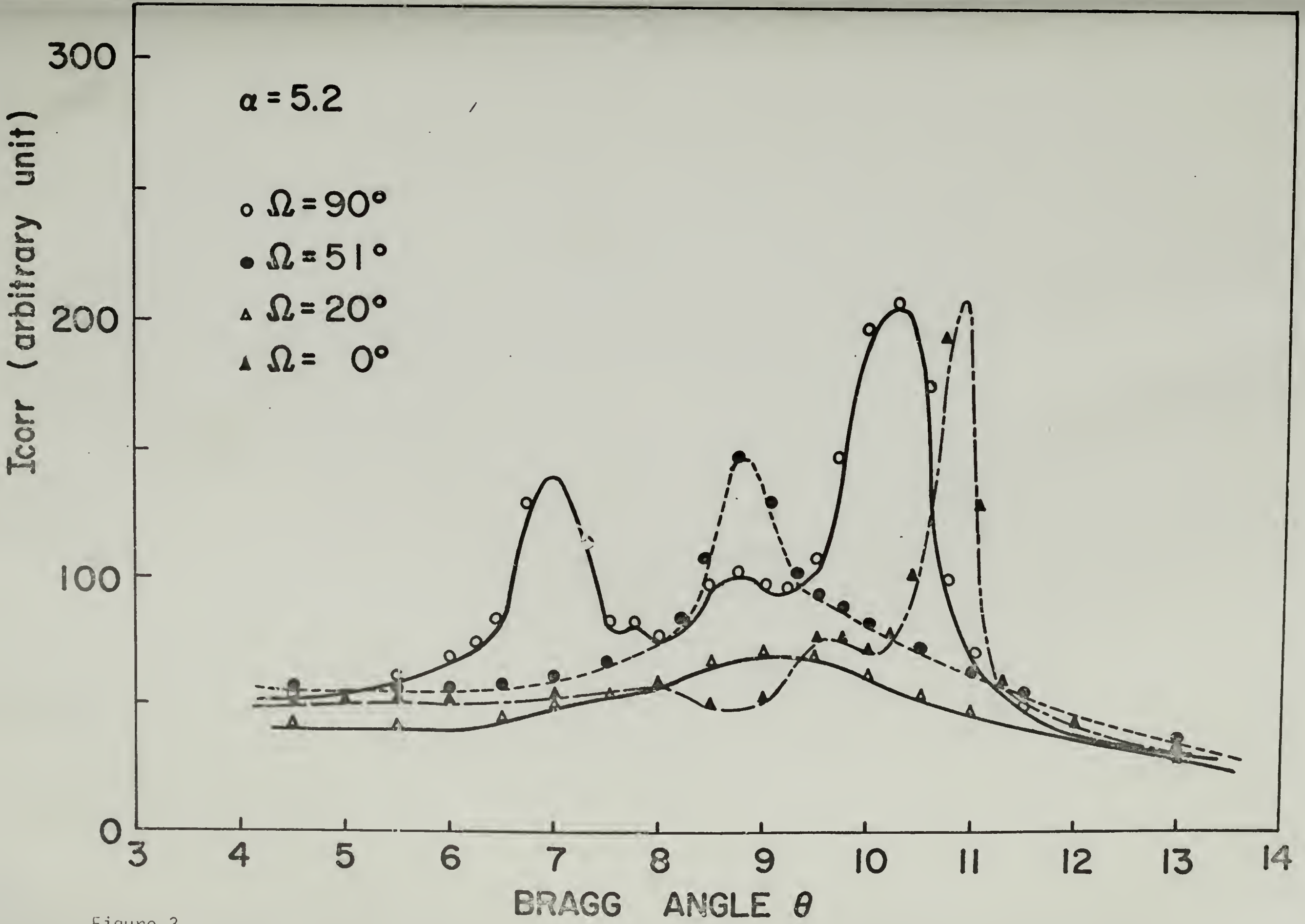
α = 5.2
○ Ω = 90°
● Ω = 51°
△ Ω = 20°
▲ Ω = 0°
Icorr (arbitrary unit)
300
200
100
0
3
4
5
6
7
8
9
10
11
12
13
14
BRAGG ANGLE θ

Figure 3

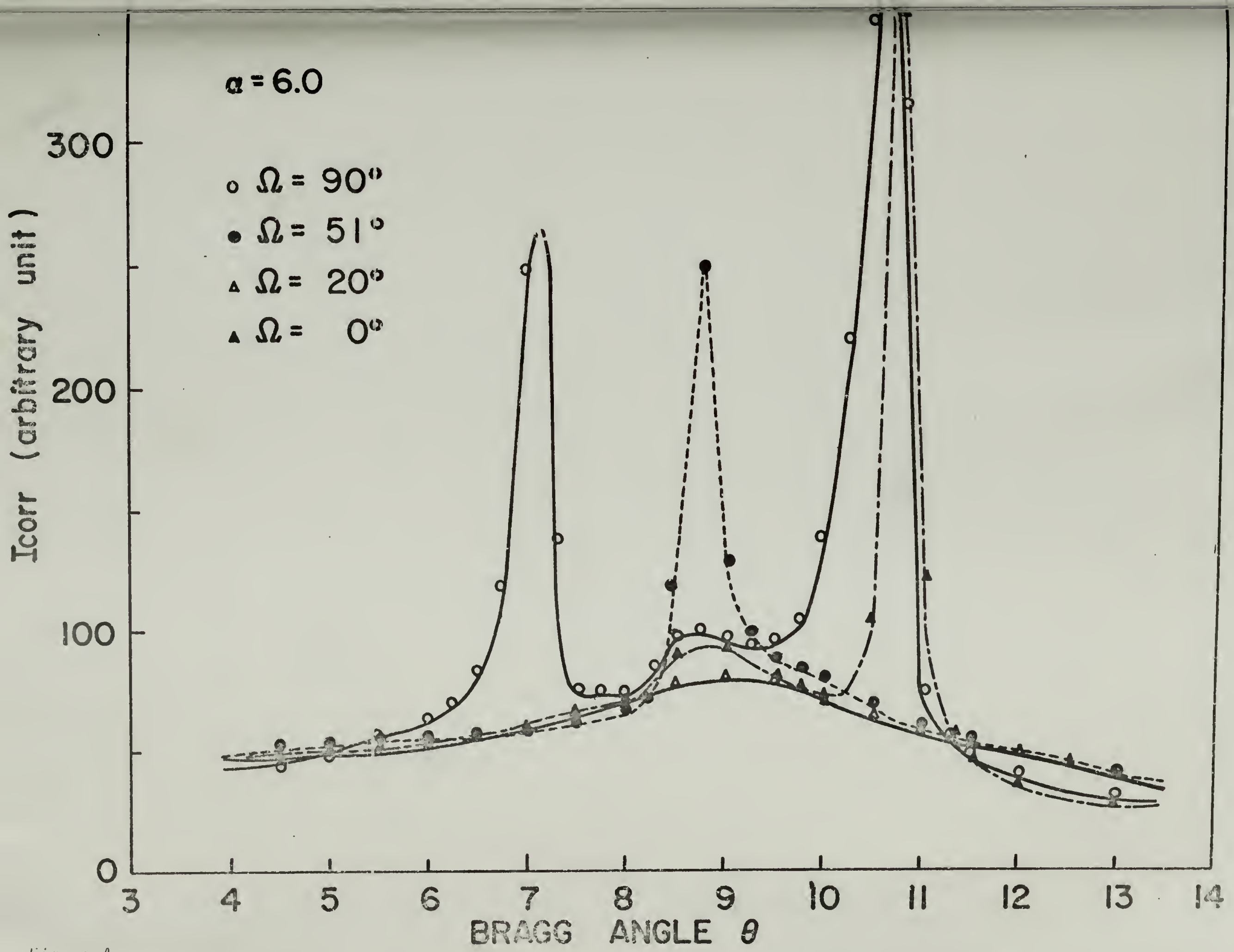
α = 6.0
○ Ω = 90°
● Ω = 51°
△ Ω = 20°
▲ Ω = 0°
Icorr (arbitrary unit)
300
200
100
0
3
4
5
6
7
8
9
10
11
12
13
14
BRAGG ANGLE θ

Figure 4

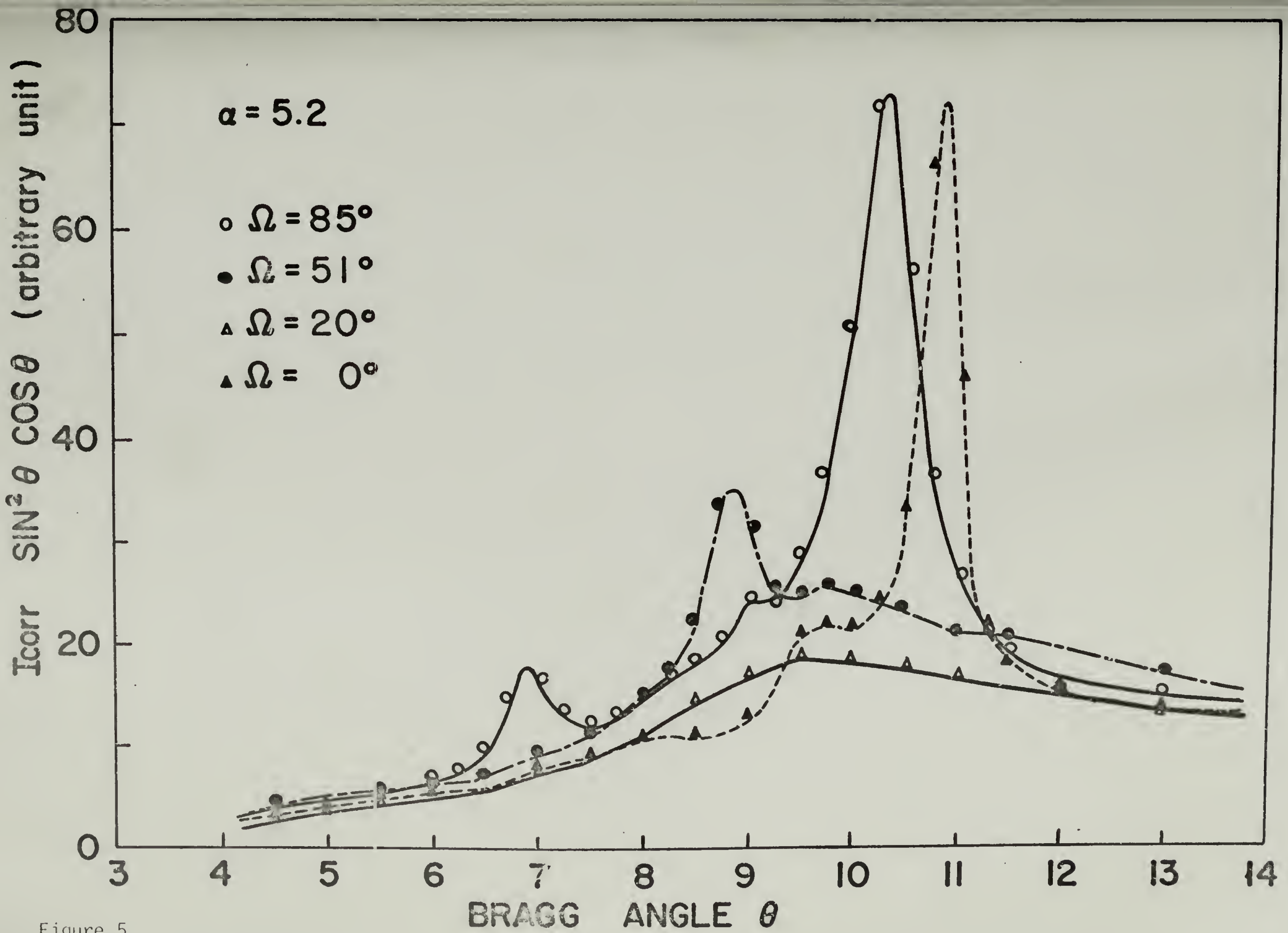
α = 5.2
○ Ω = 85°
● Ω = 51°
△ Ω = 20°
▲ Ω = 0°
Icorr SIN² θ COSθ (arbitrary unit)
0
20
40
60
80
3
4
5
6
7
8
9
10
11
12
13
14
BRAGG ANGLE θ

Figure 5

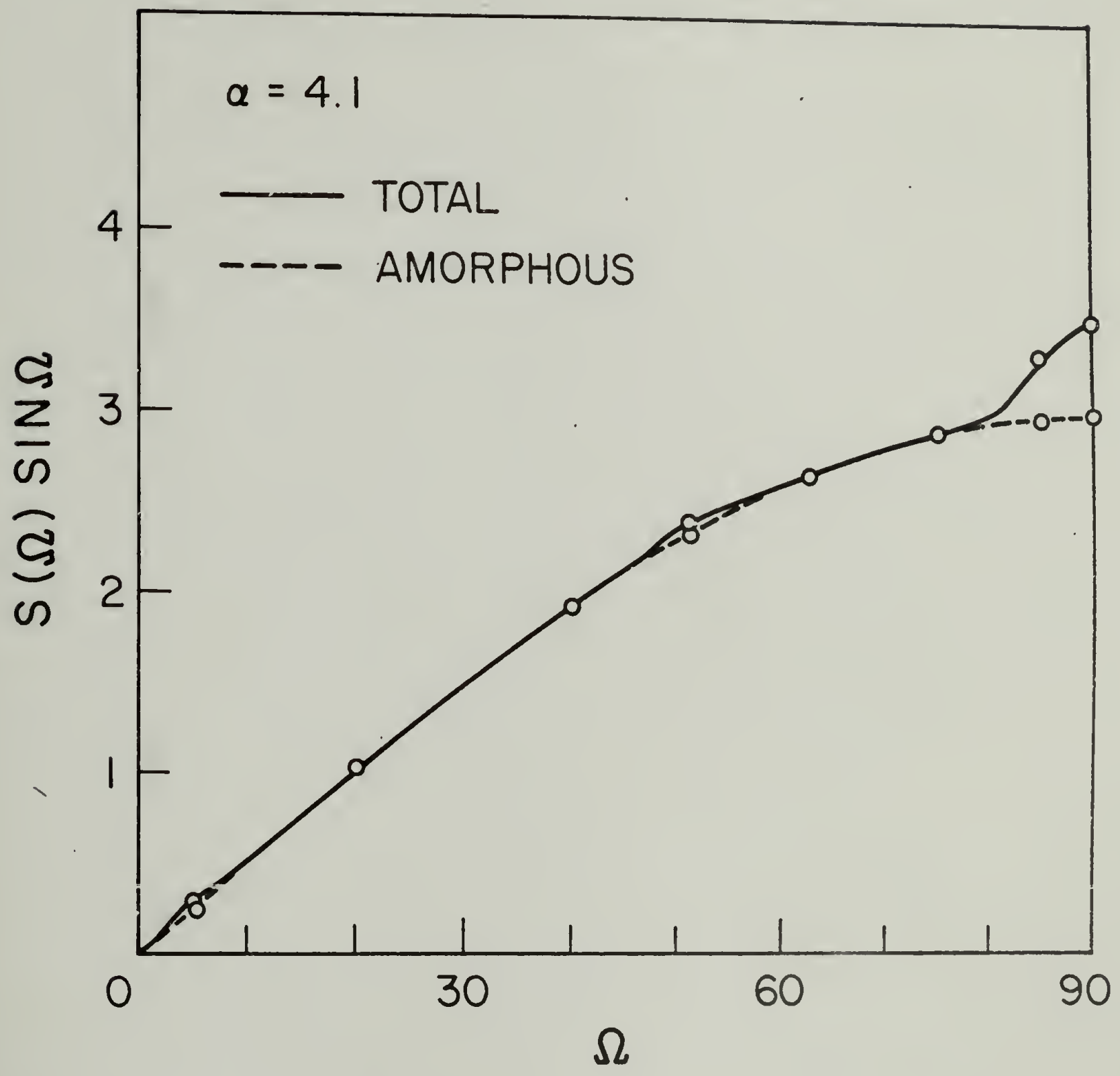

Figure 6

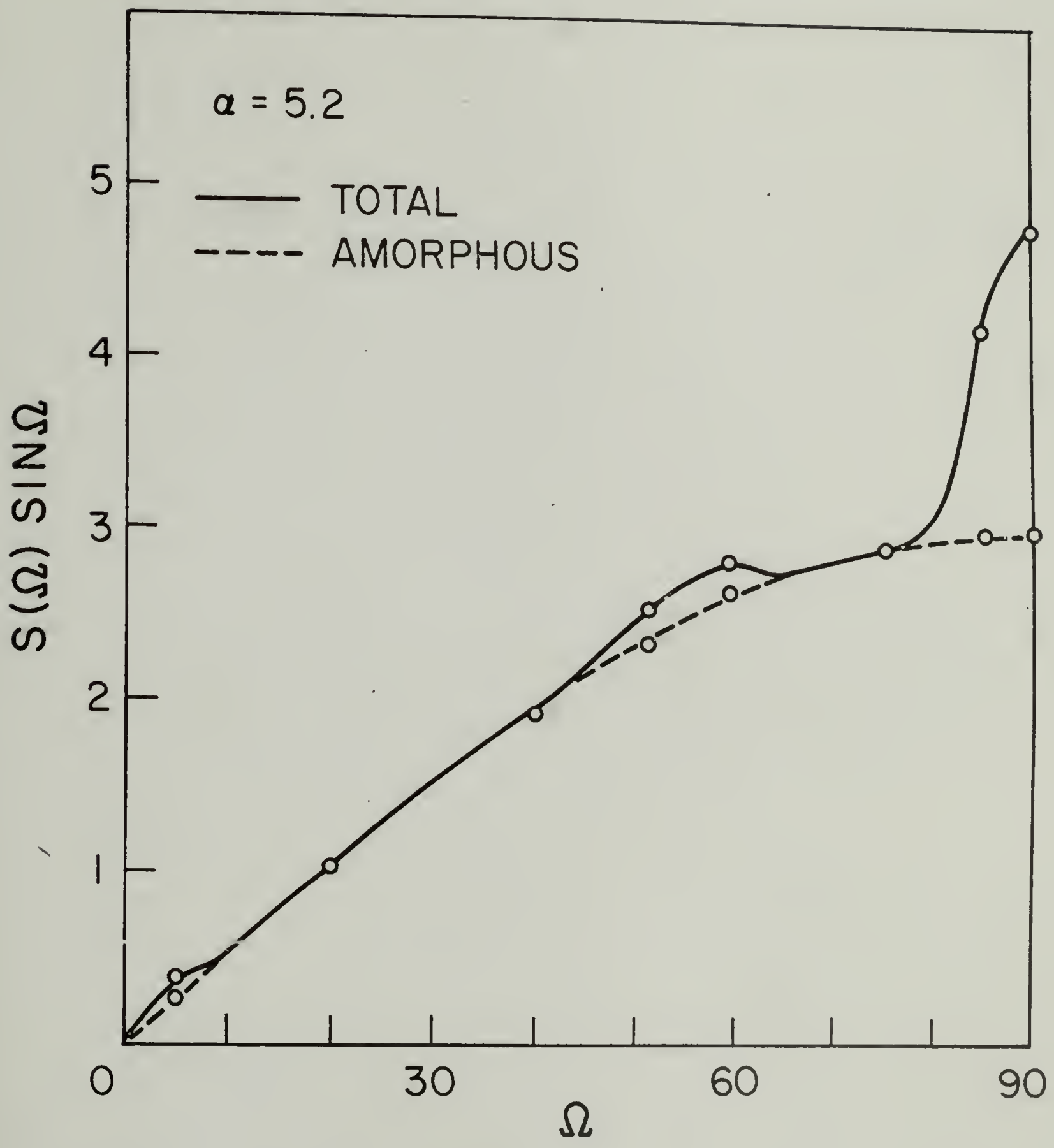

Figure 7

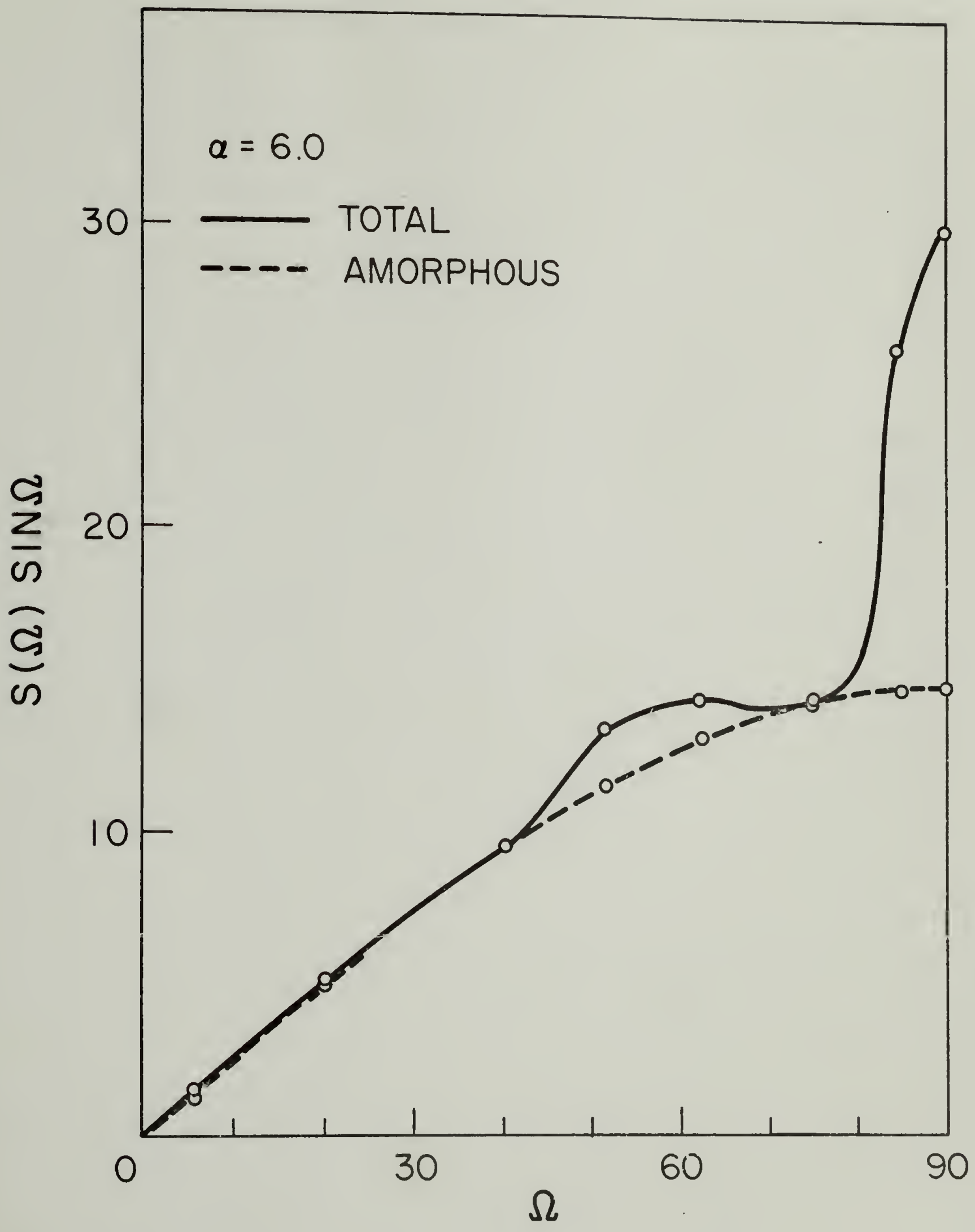

Figure 8

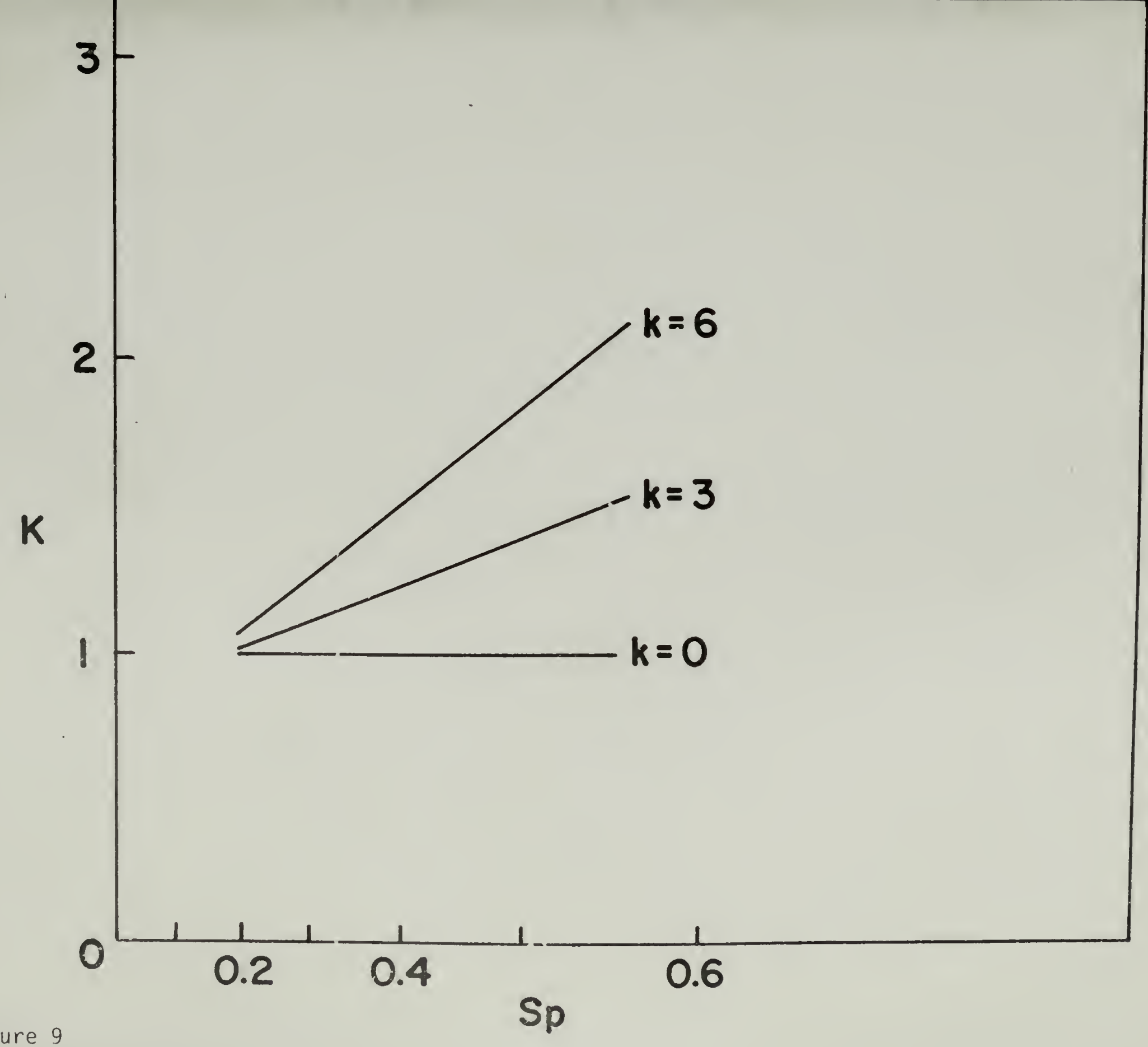

Figure 9

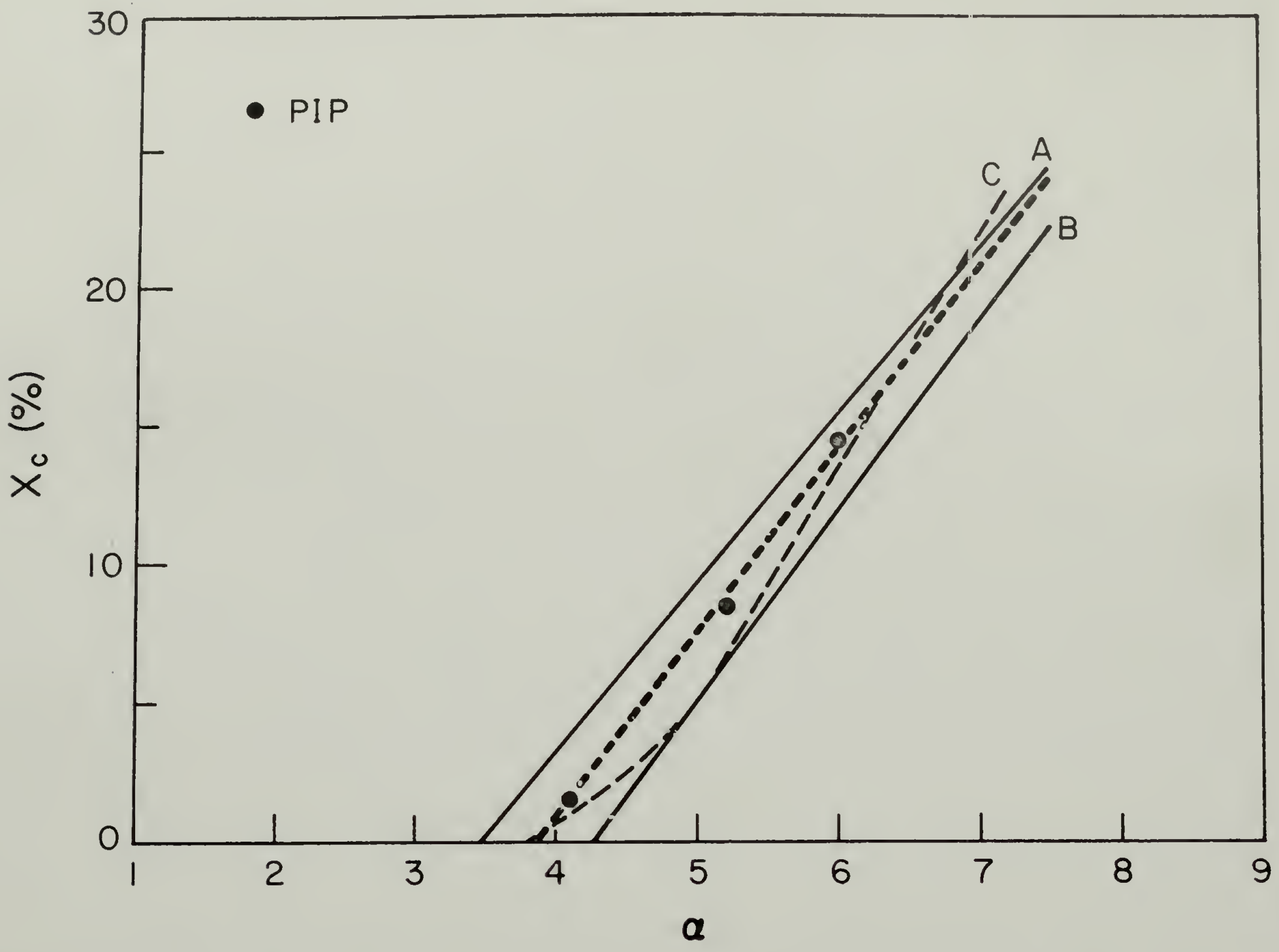

Figure 10

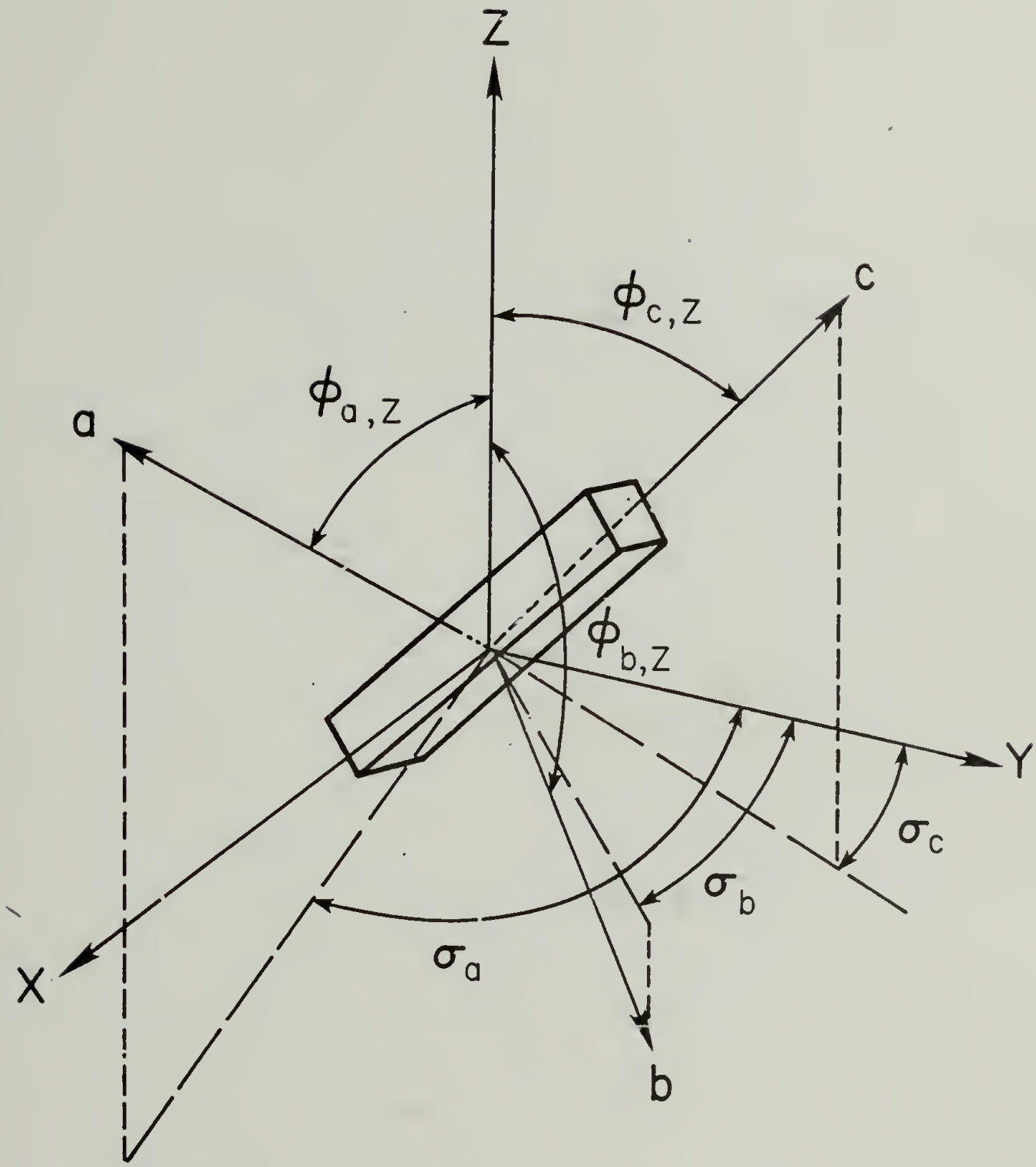

Figure 11

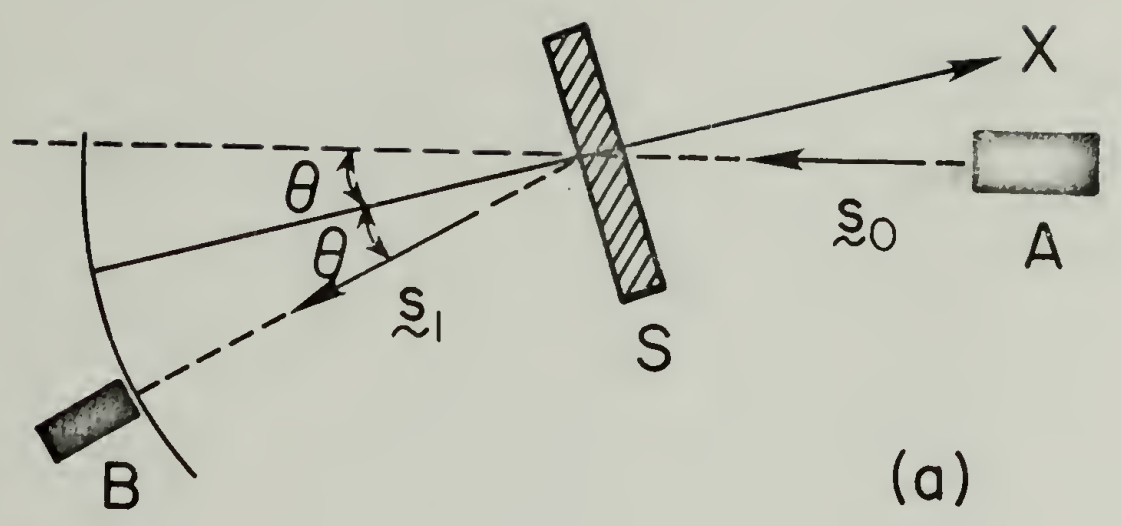

(a)

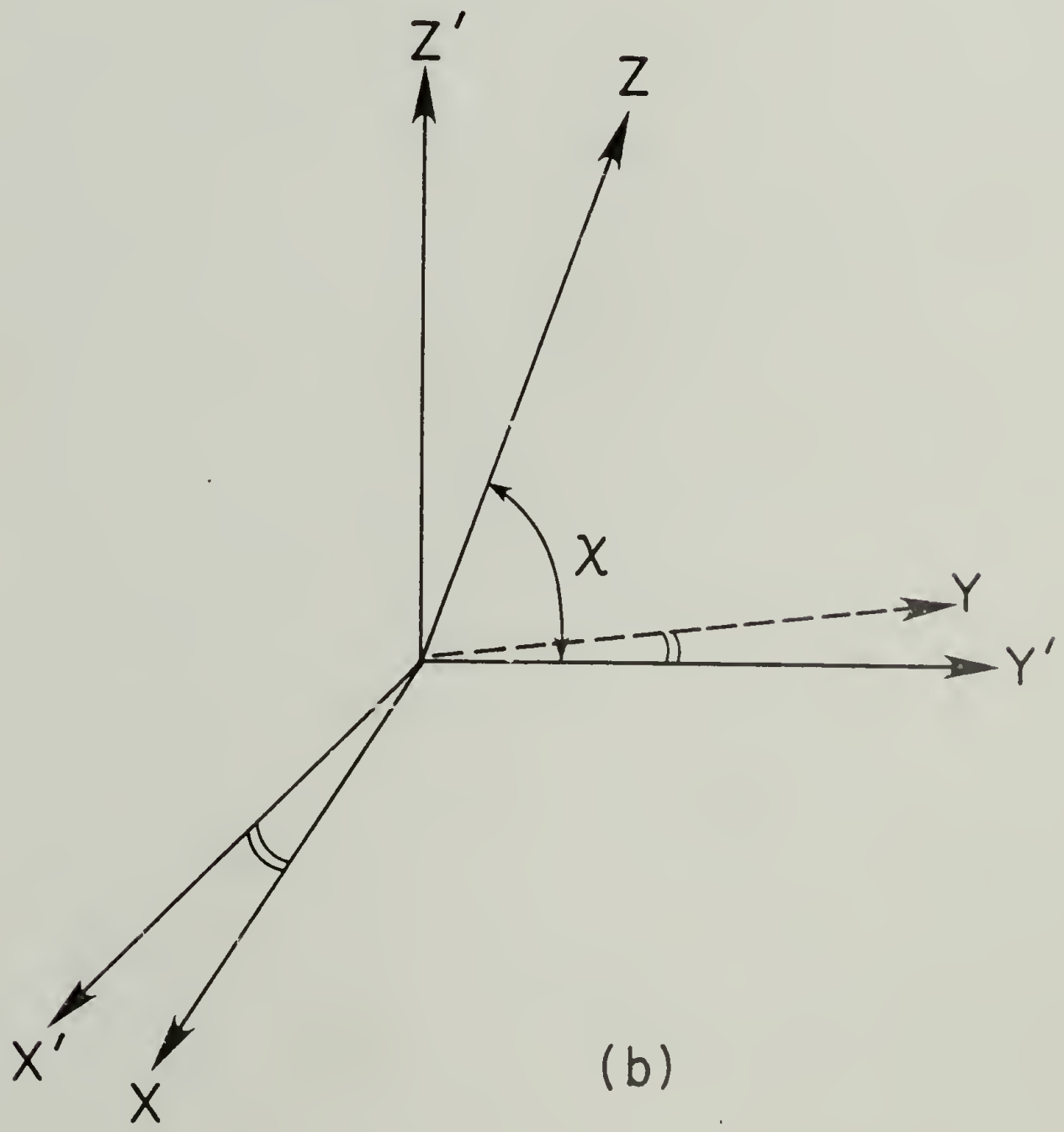

(b)

Figure 12

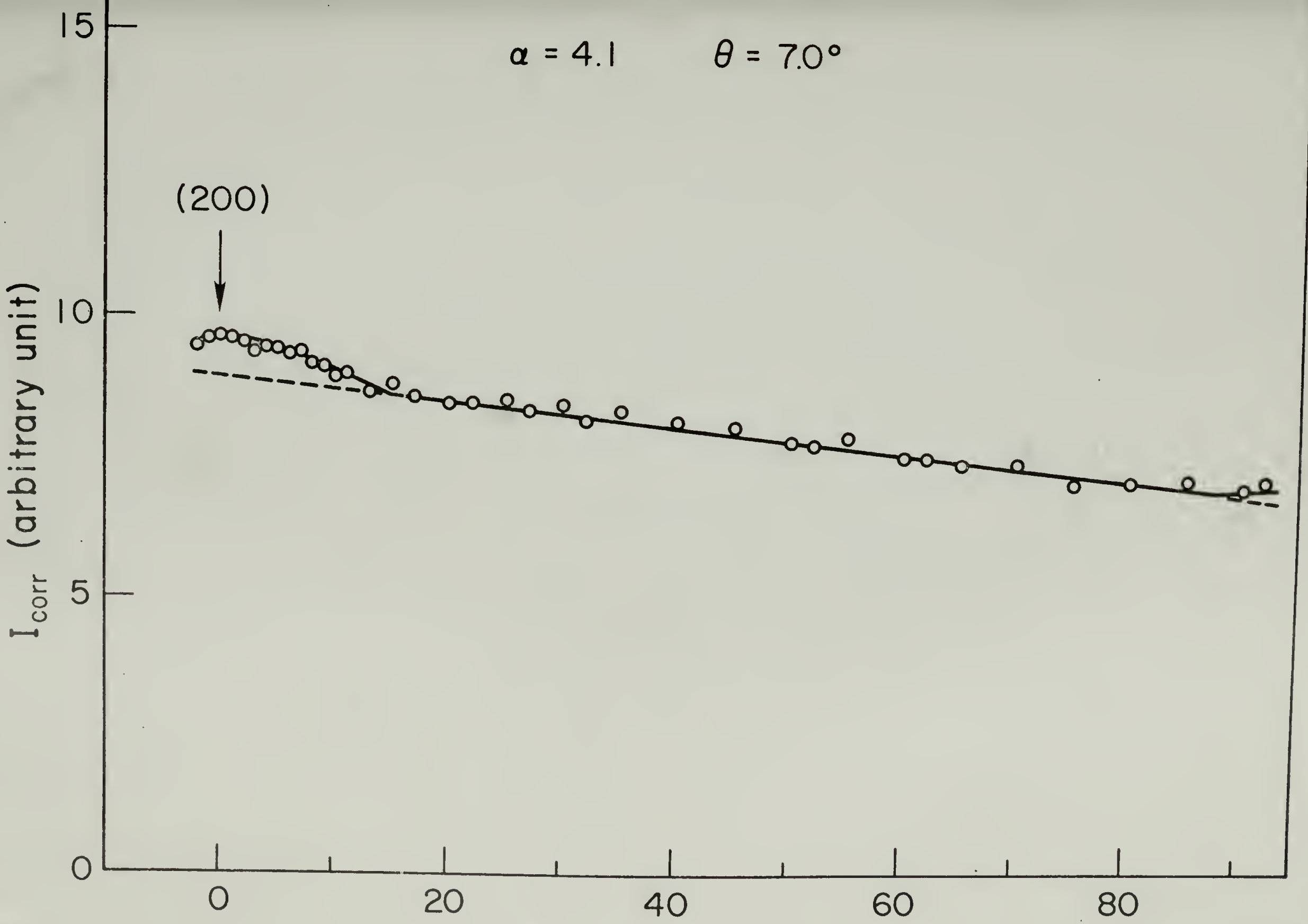
α = 4.1
θ = 7.0°
(200)
I_{corr} (arbitrary unit)
15
10
5
0
0
20
40
60
80
AZIMUTHAL ANGLE Ω

Figure 13

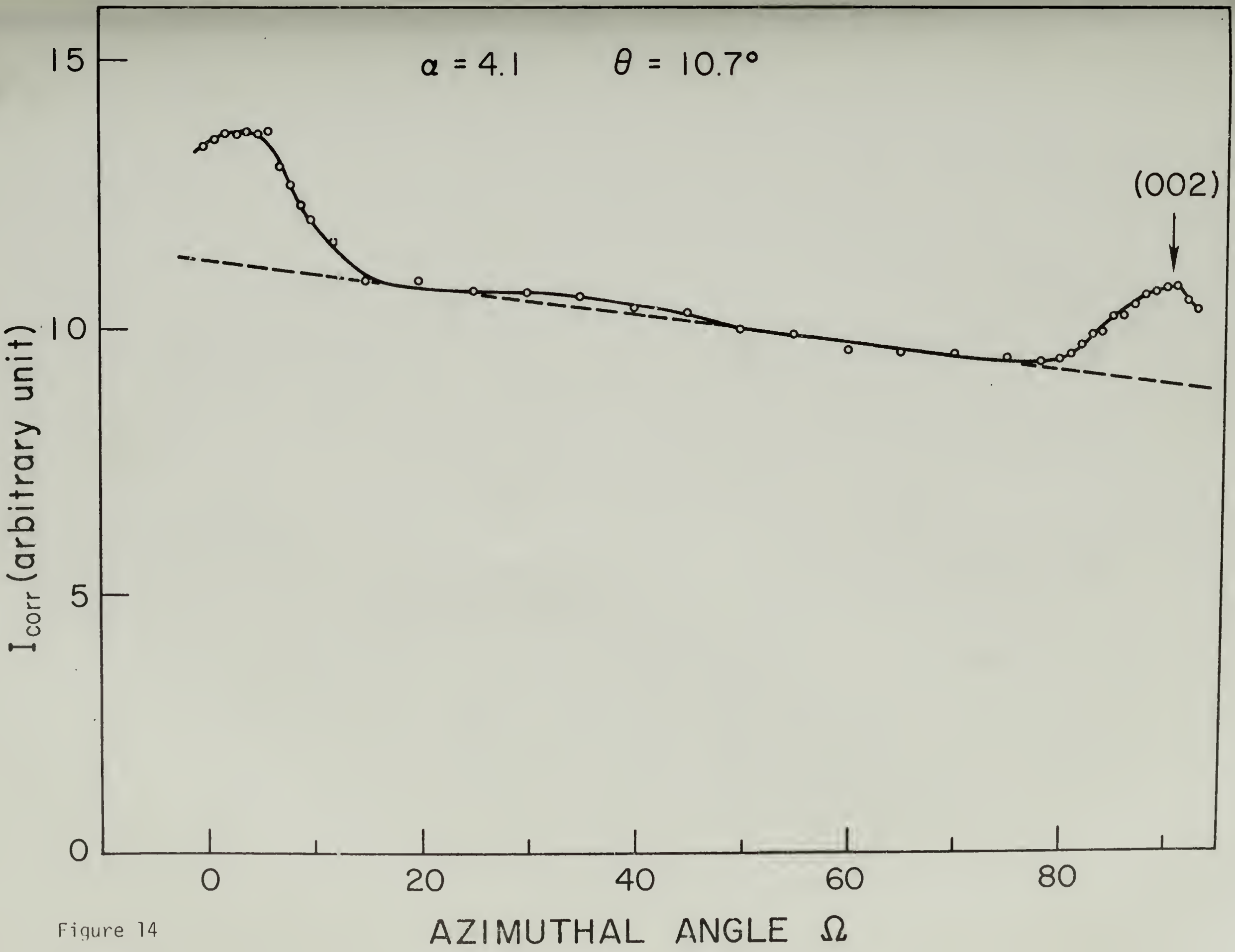
α = 4.1
θ = 10.7°
(002)
15
10
5
0
I_{corr} (arbitrary unit)
0
20
40
60
80
AZIMUTHAL ANGLE Ω

Figure 14

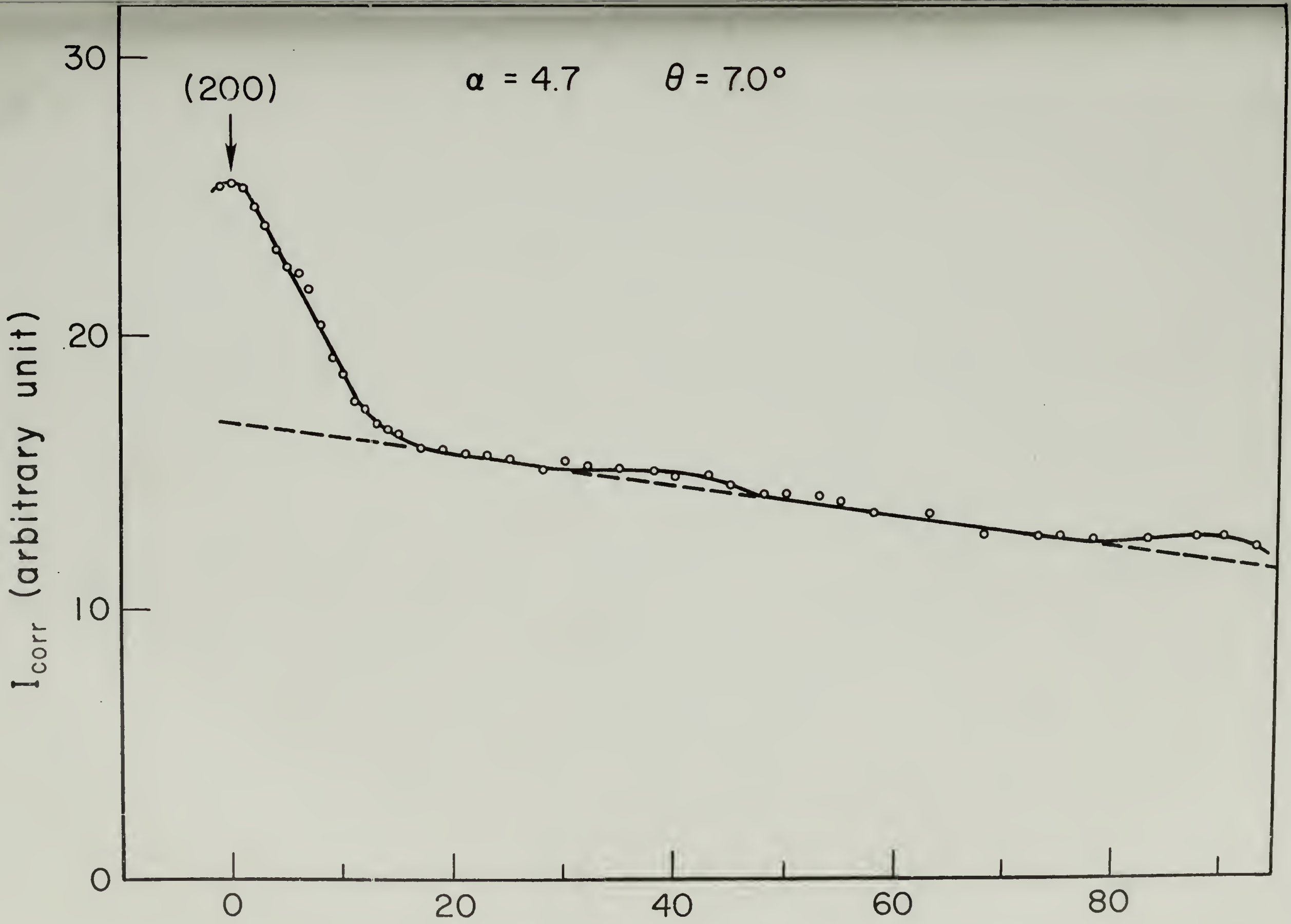
(200)
α = 4.7
θ = 7.0°
30
20
10
0
I_{corr} (arbitrary unit)
0
20
40
60
80
AZIMUTHAL ANGLE Ω

Figure 15

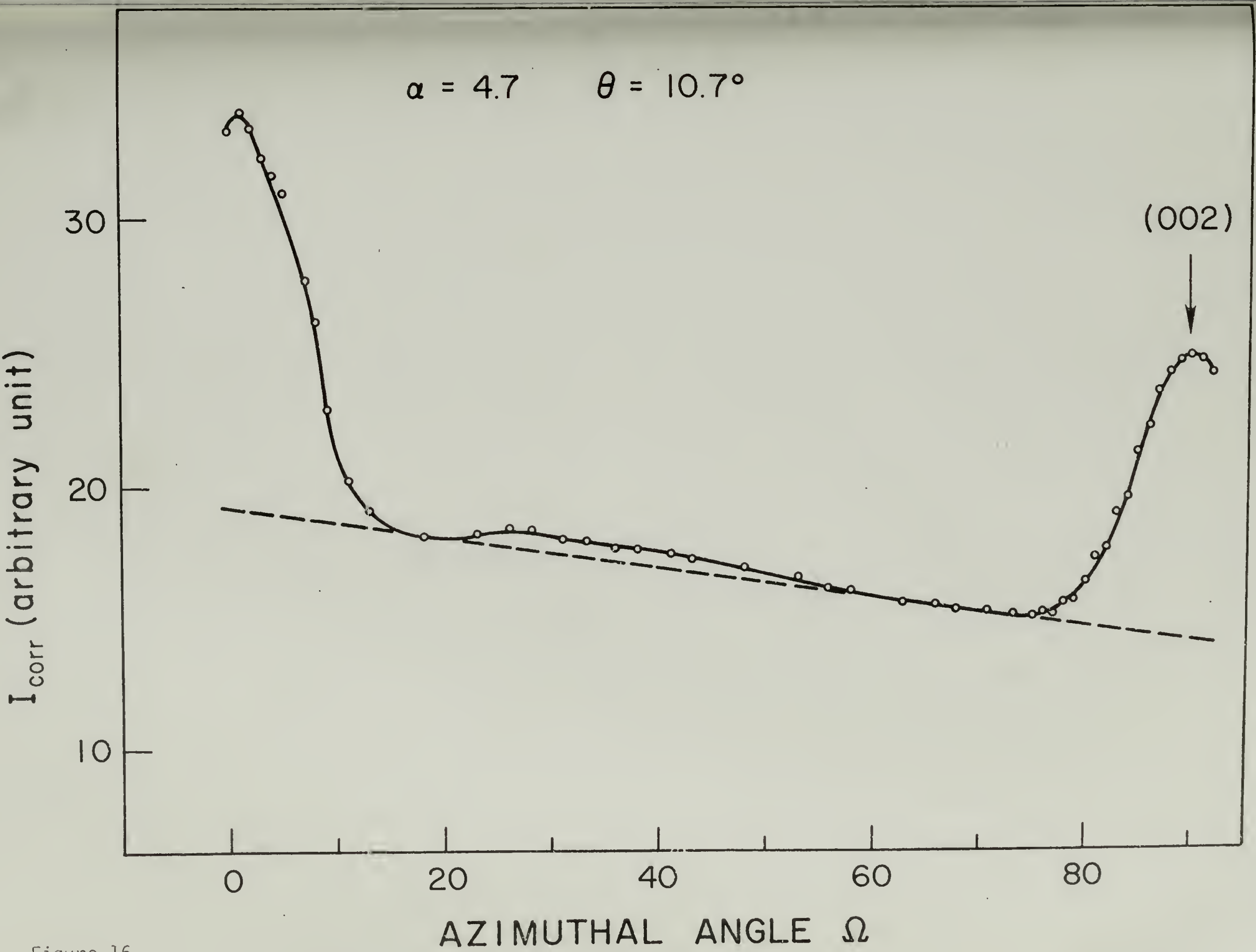
α = 4.7
θ = 10.7°
(002)
30
20
10
I_{corr} (arbitrary unit)
0
20
40
60
80
AZIMUTHAL ANGLE Ω

Figure 16

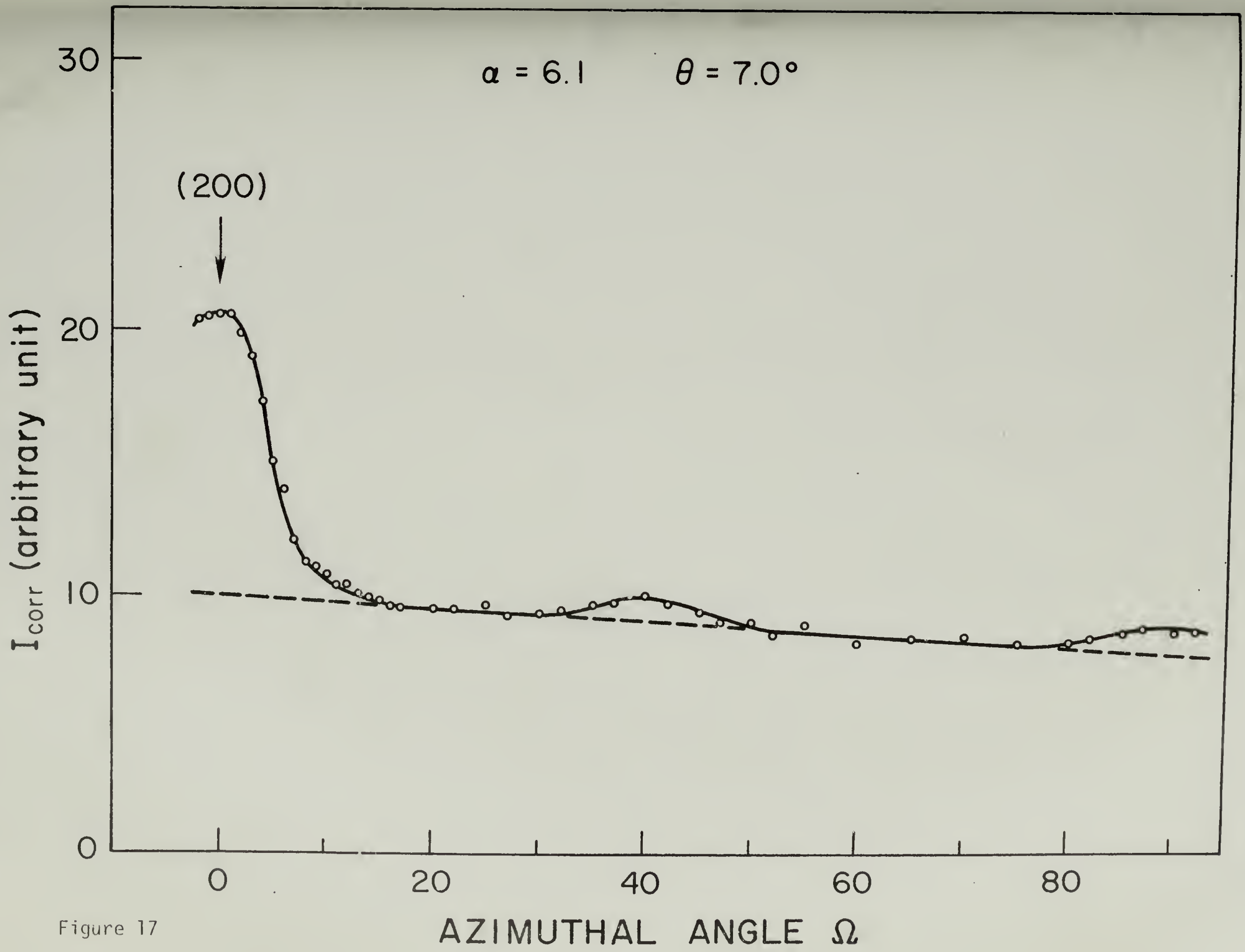
α = 6.1
θ = 7.0°
(200)
30
20
10
0
I_{corr} (arbitrary unit)
0
20
40
60
80
AZIMUTHAL ANGLE Ω

Figure 17

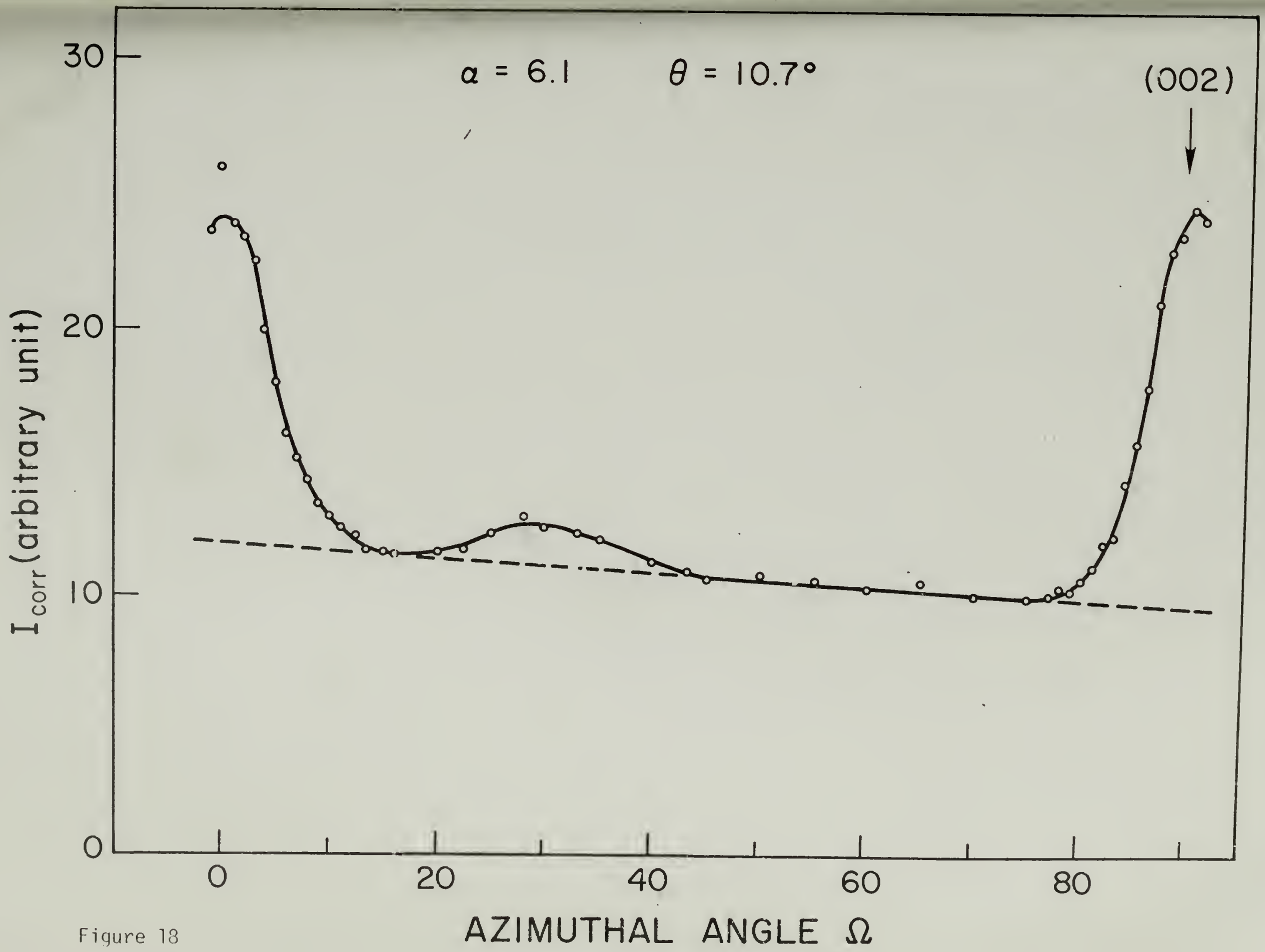
α = 6.1
θ = 10.7°
(002)
30
20
10
0
I_{corr} (arbitrary unit)
0
20
40
60
80
AZIMUTHAL ANGLE Ω

Figure 18

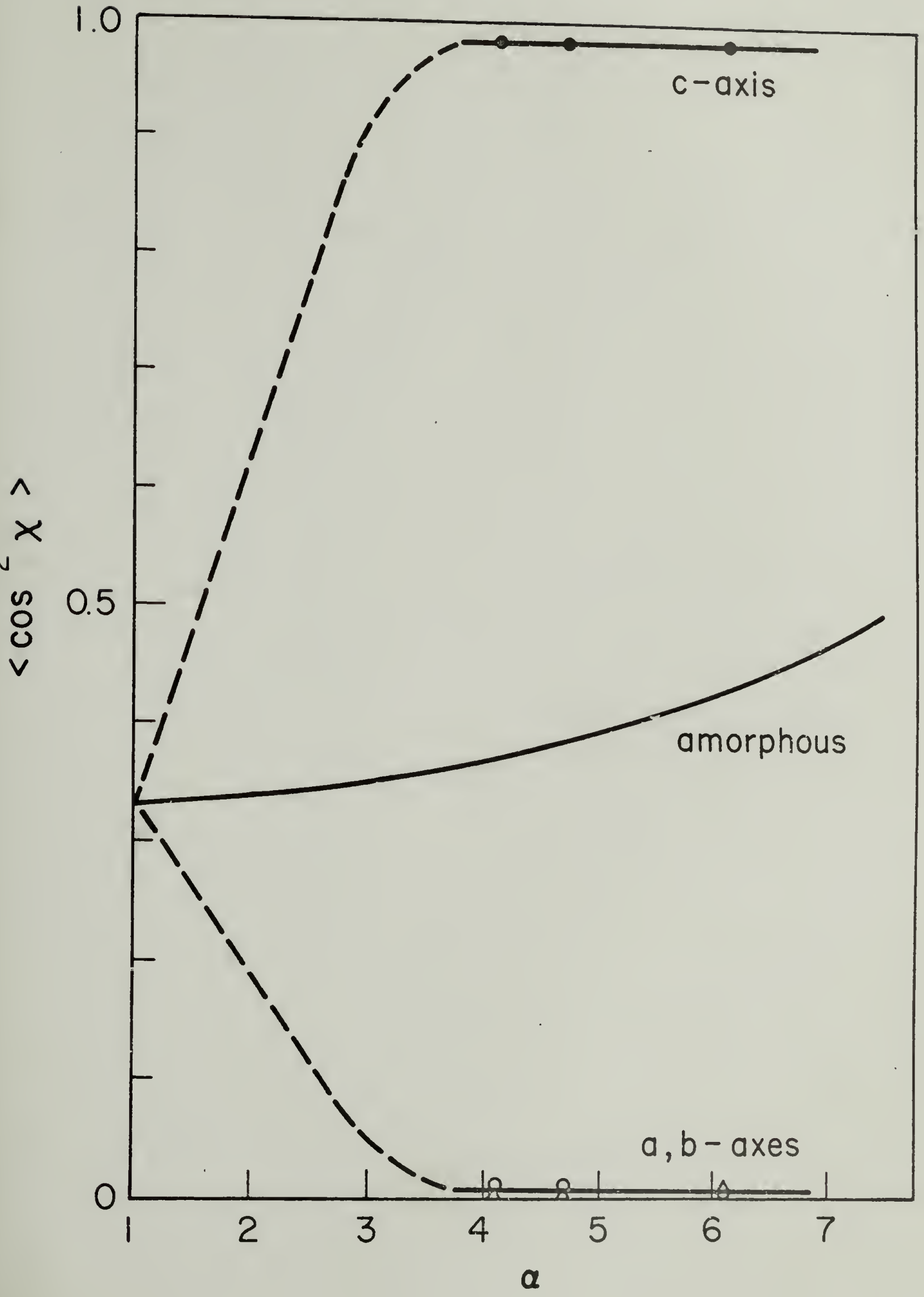
1.0
0.5
0
$\langle \cos^2 \chi \rangle$
c-axis
amorphous
a, b-axes
1
2
3
4
5
6
7
α

Figure 19

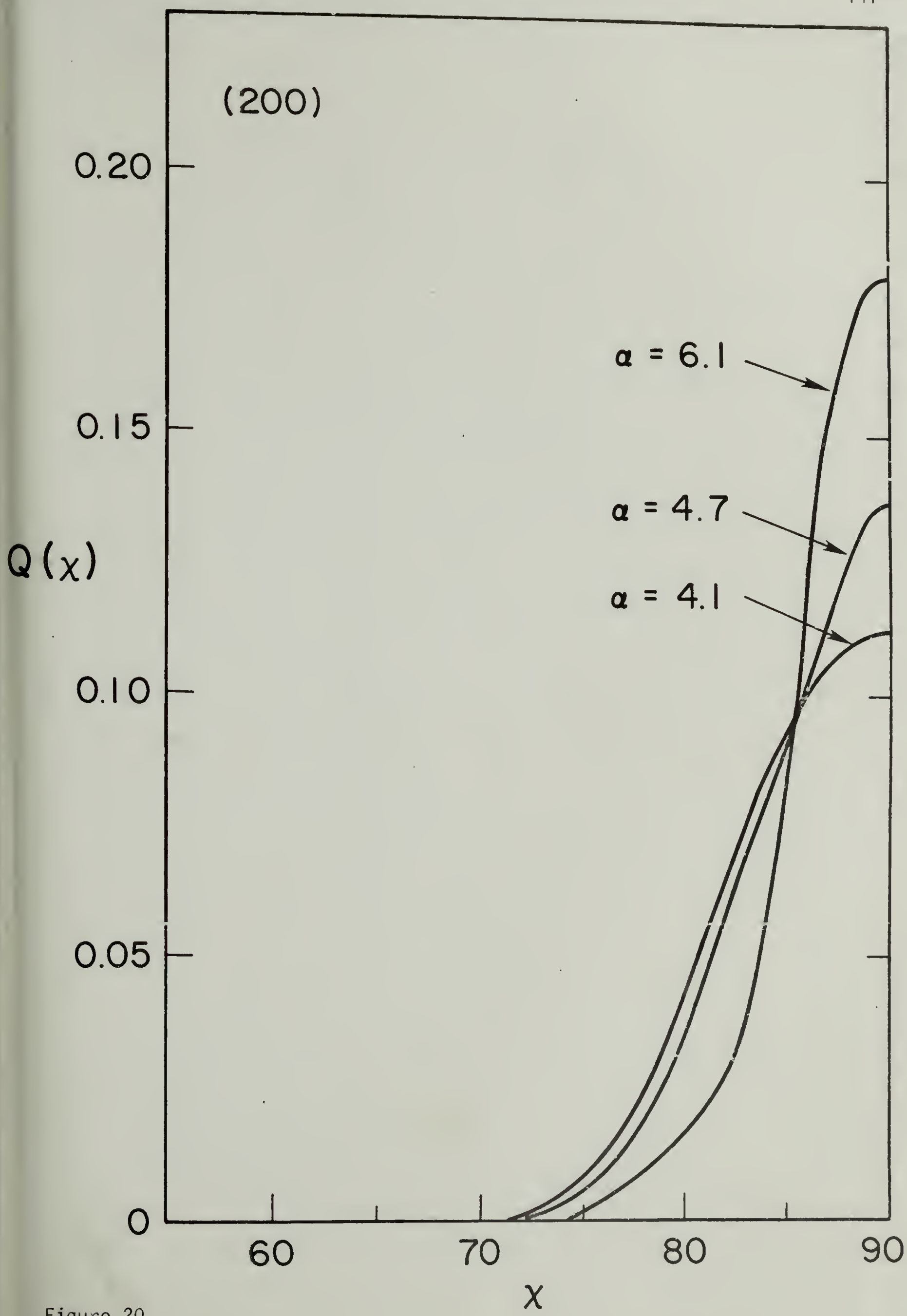

Figure 20

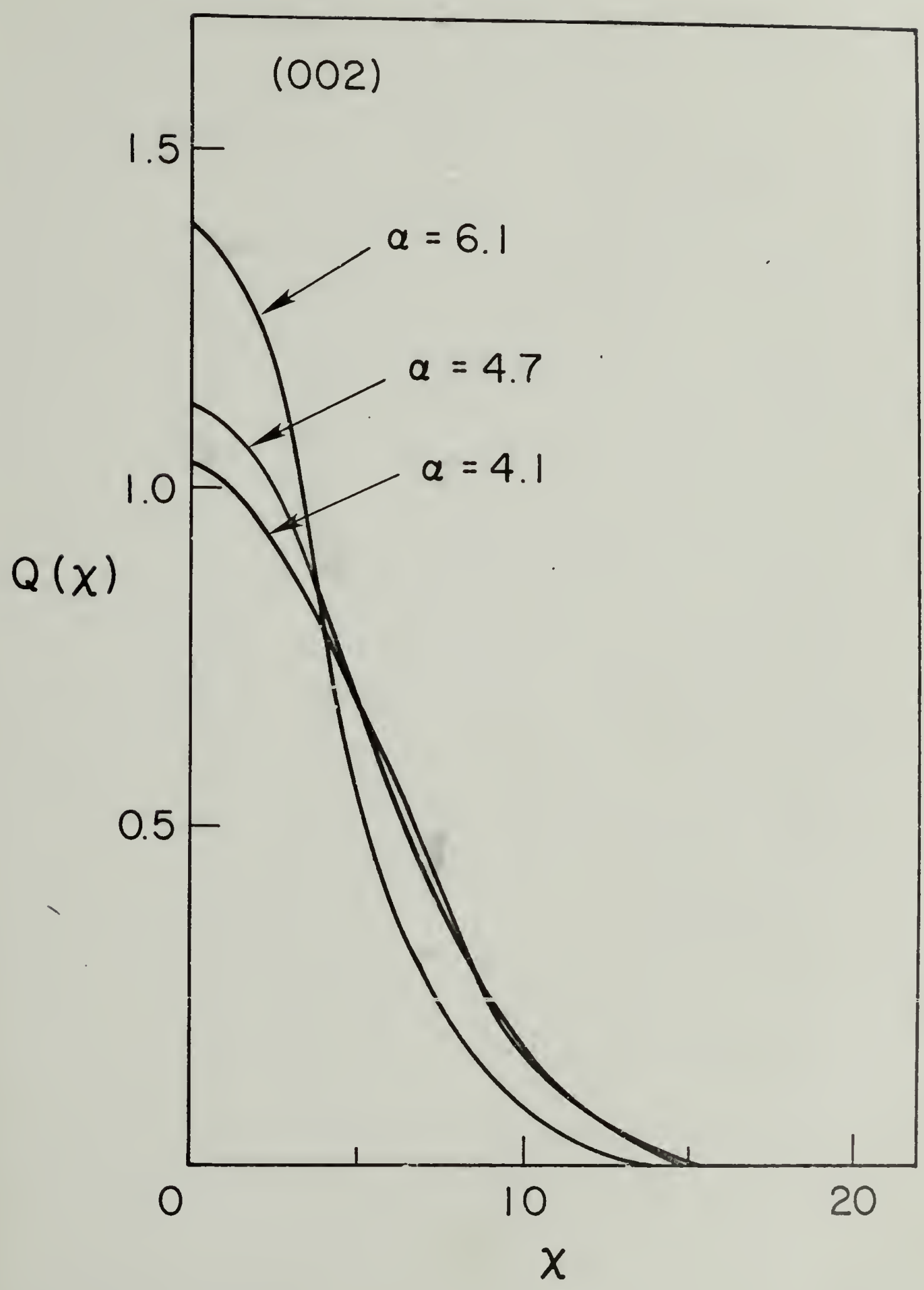

Figure 21

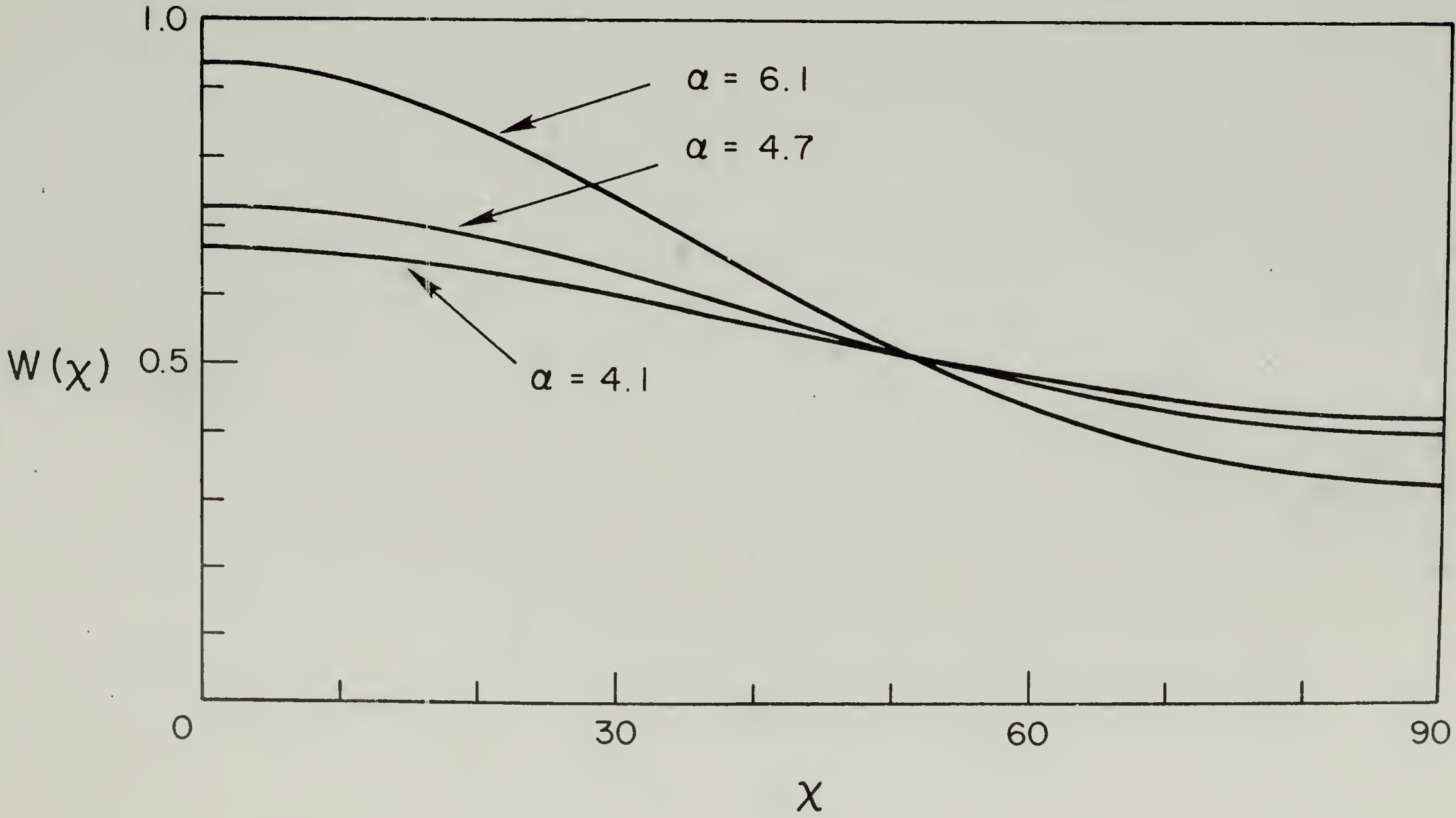

Figure 22

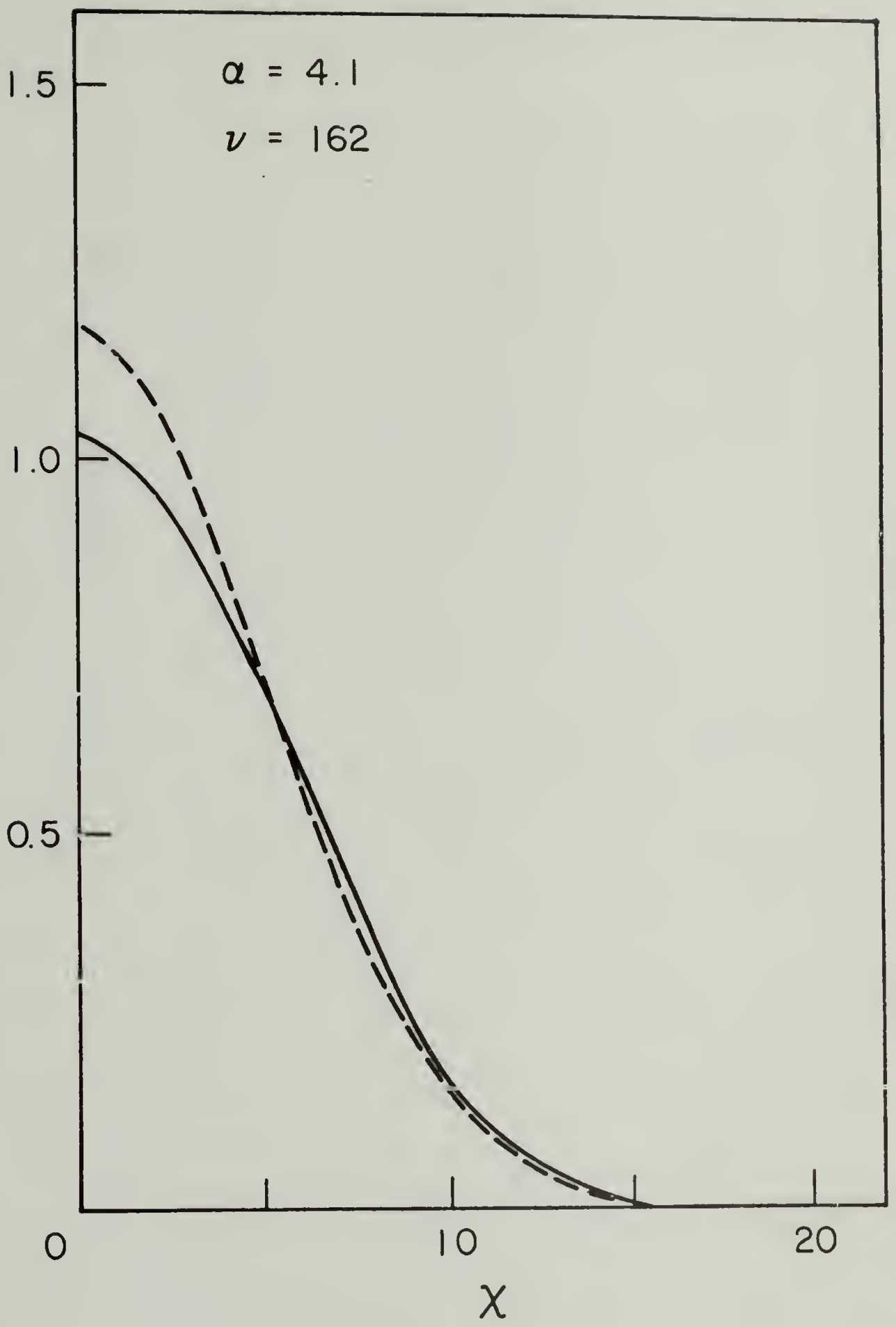

Figure 23

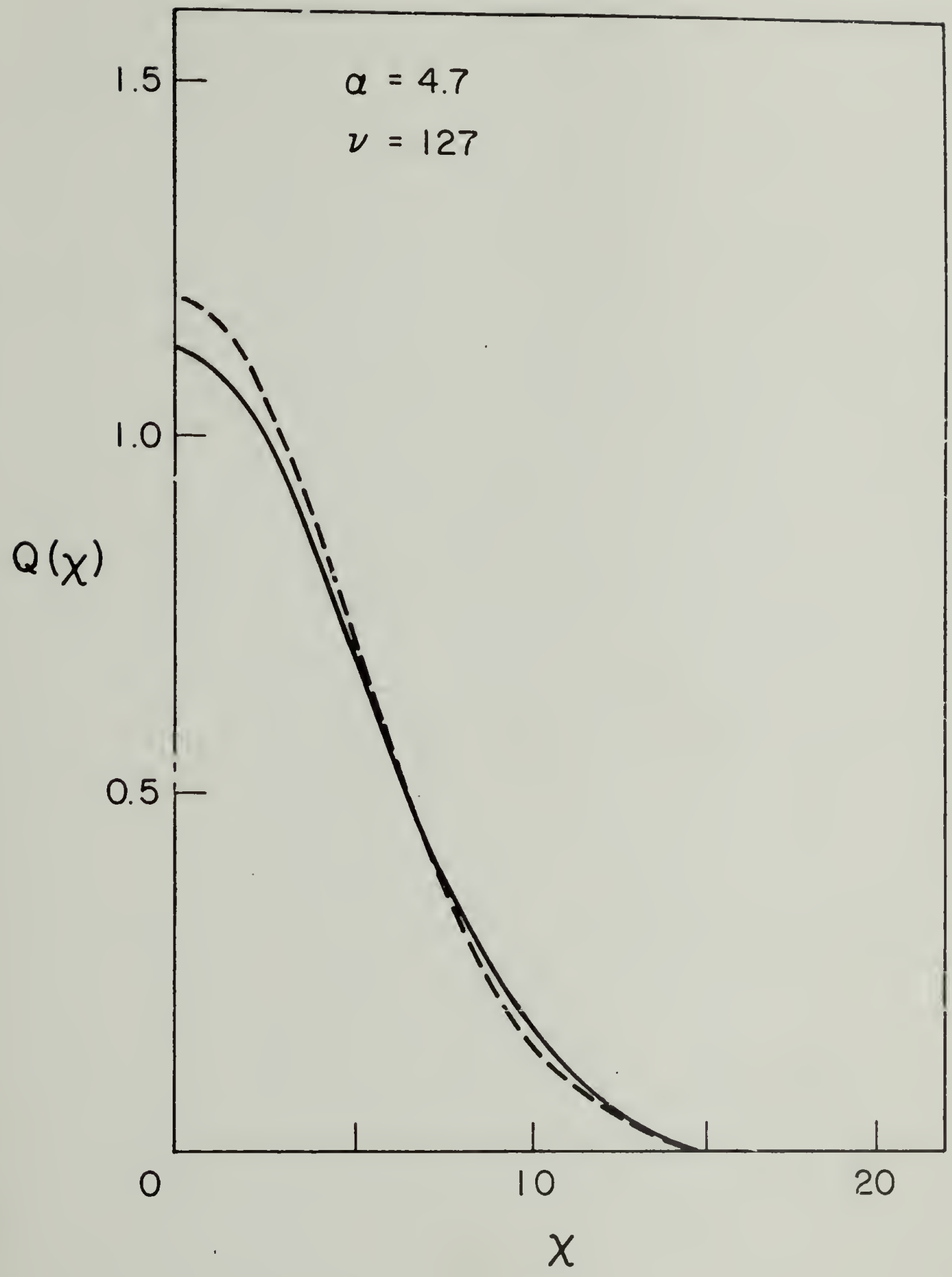

Figure 24

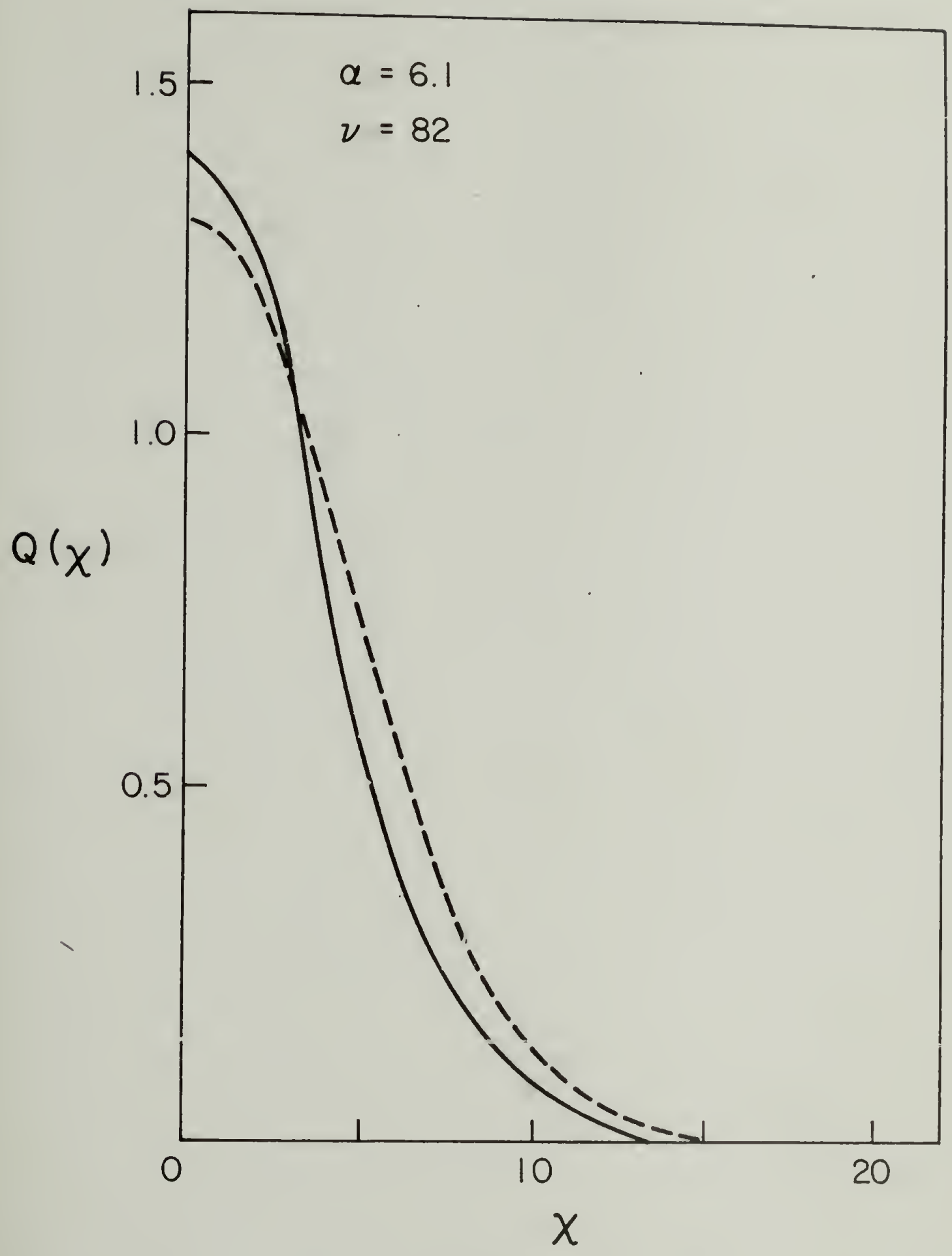

Figure 25

CHAPTER IV

DETERMINATION OF THE CRYSTAL BIREFRINGENCE

Introduction

As shown previously the birefringence, Δ, of a semicrystalline polymer may be described by the equation (1,2)

$$\Delta = \phi_c \Delta_c + (1 - \phi_c) \Delta_{am} + \Delta_f \qquad (1)$$

where ϕ_c is the volume fraction crystallinity and Δ_c and Δ_{am} are the birefringence contributions of the crystalline and amorphous phase. Δ_f is the form birefringence which has been shown to be a 5-10% contribution to the overall birefringence (1,3,4). To evaluate Δ_c one may take experimental means using

$$\Delta_c = \Delta_c^o \quad f_c \qquad (2)$$

where Δ_c^o is the intrinsic birefringence of the crystal and f_c is the orientation function of the optic axis of the crystal.

For polyethylene the value of Δ_c^o can be obtained directly since the crystal is isomorphic with those of n-paraffins which have been studied by Bunn and Daubeny (5). For other crystals, they must be estimated by indirect means (6) such as by calculation from bond polarizabilities as shown in Appendix I. In such calculations a consideration of the internal field effect may be essential and very important, which has been discussed in Chapter II.

The value of Δ_{am} may be given by an equation analogous to Equation (2)

$$\Delta_{am} = \Delta^{o}_{am} f_{am} \tag{3}$$

where Δ^{o}_{am} and f_{am} are the intrinsic birefringence and orientation functions of the amorphous segment.

Substituting Equations (2) and (3) into Equation (1), one obtains

$$\Delta = \phi_c \Delta^{o}_{c} f_c + (1 - \phi_c) \Delta^{o}_{am} f_{am} + \Delta_f \tag{4}$$

By neglecting Δ_f and by rearranging Equation (4)

$$\frac{\Delta}{\phi_c f_c} = \Delta^{o}_{c} + \frac{(1 - \phi_c)}{\phi_c} \frac{f_{am}}{f_c} \Delta^{o}_{am} \tag{5}$$

The birefringence Δ and the crystallinity ϕ_c may be determined generally by conventional methods (7,8). If the orientation functions, f_c and f_{am}, can be obtained by some independent method, for example, x-ray diffraction for f_c and infrared dichroism (9) for f_{am}, then one may plot $\Delta/(\phi_c f_c)$ against $[(1 - \phi_c)/\phi_c]\, f_{am}/f_c$ to give an intercept Δ^{o}_{c} and a slope Δ^{o}_{am}. Such a study has been made by Samuels (10) for polypropylene, by Onogi et. al (11) for polyethylene and by Dumbleton (12) for poly(ethylene terephthalate), in which sonic velocity is used to determine the orientation. Values for polypropylene obtained are $\Delta^{o}_{c} = 0.0291$ and $\Delta^{o}_{am} = 0.0600$. The value of Δ^{o}_{c} is in reasonable agreement with the theoretical calculation (13). For poly-(ethylene terephthalate) the values of 0.220 and 0.275 for Δ^{o}_{c} and Δ^{o}_{am} are obtained. The experimental values show that (14) the birefringence in the

amorphous regions, Δ^o_{am}, is usually higher than that in the crystalline regions, Δ^o_c. This phenomenon has been attributed to the internal field effect (15).

For rubbers one may calculate Δ_{am} using an expression

$$\Delta_{am} = C\ \sigma_{am} \tag{6}$$

where C is the stress-optical coefficient of the amorphous phase and σ_{am} is the stress of the amorphous phase which may be described by (16,17)

$$\sigma_{am} = \sigma/F(\phi_c)$$

$$= \sigma/(1 + 2.5\ \phi_c + 14.1\ \phi_c^2) \tag{7}$$

where σ is the total stress. This approach to evaluate the amorphous contribution was intensively used in Chapter I. Neglecting Δ_f and substituting Equation (2), (6) and (7) into Equation (1), one obtains

$$\Delta = \phi_c f_c \Delta^o_c + \frac{(1 - \phi_c)\ C \cdot \sigma}{(1 + 2.5\ \phi_c + 14.1\ \phi_c^2)} \tag{8}$$

By rearranging Equation (8)

$$\frac{\Delta}{\phi_c f_c} = \Delta^o_c + \frac{(1 - \phi_c)}{(1 + 2.5\ \phi_c + 14.1\ \phi_c^2)}\ \frac{\sigma}{\phi_c f_c} \cdot C \tag{9}$$

If the stress-optical coefficient C is considered to be constant, the plot of $\Delta/\phi_c f_c$ versus $(1 - \phi_c)\sigma/\phi_c f_c\ (1 + 2.5\ \phi_c + 14.1\ \phi_c^2)$ will pro-

duce a value of Δ_c^o from the intercept and a value of C from the slope. Actually the value of C may depend upon the strain as described previously by an equation

$$C = \frac{2B_1 + 2B_2/\alpha}{2C_1 + 2C_2/\alpha} \qquad (10)$$

where B_1, B_2, C_1 and C_2 are constants. Therefore, the method to obtain the value of Δ_c^o described above may suffer an error from the change of C with deformation.

Determination of the Crystal Intrinsic Birefringence

As described in the previous Chapter the crystallinity X_c and the orientation function f_c were measured by x-ray diffraction method. From the results of x-ray measurements and the birefringence data reported in Chapter I, one may determine the value of Δ_c^o. From Figures 8-10 in Chapter I by extrapolating the curves one obtains the values of Δ and σ at about 50 hours after stretching. The corresponding crystallinity and orientation may be obtained from Figures 10 and 19 in Chapter III. They are shown in Table 1.

At $\alpha = 3.89$ the value of X_c from x-ray measurement is negligible, while the birefringence data [Figure 8 in Chapter I] indicates that crystallization occurs at this elongation. This may be demonstrated by the fact that birefringence is more sensitive in detecting and following crystallization under strain than x-ray (6).

The weight fraction crystallinity X_c determined by x-ray measurement may be converted to the volume fraction using

$$\phi_c = \frac{\rho_a X_c}{\rho_a X_c + \rho_c (1 - X_c)} \qquad (11)$$

where ρ_c and ρ_a are the densities of the crystalline and amorphous phases. The values of ρ_c and ρ_a are given previously as 1.007 and 0.91 g/cm^3, respectively.

For determining the value of Δ_c^o, the plotting method expressed by Equation (9) may not be suitable for this present work since only two points (α = 5.0 and 6.0) are available for plotting. The value of Δ_c^o, therefore, was calculated for each α using Equation (8) and the average value was taken as the crystal intrinsic birefringence. In this calculation Equation (15) in Chapter I was used in order to obtain the stress-optical coefficient C. The value of Δ_c^o obtained is 0.224 $\pm$ 0.032.

This value is quite different from that calculated from bond polarizabilities in Appendix I, where a value of 0.130 is obtained using Denbigh's bond polarizabilities (18).

Before discussing this value, the concept of crystallinity should be reconsidered. As described briefly in the General Introduction and Chapter III, the presence of both sharp and diffuse diffraction parts in the x-ray pattern of polymers had once been considered as evidence for a two-phase concept of polymer structure, in which relatively perfect crystallites are dispersed in amorphous regions. However, a number of more recent experimental findings suggest a modification of the earlier notions of polymer structure in order to explain the phenomena of polymer single crystals, chain folding, and lattice dislocation. The new picture of polymer structure may be designated as the crystal defect concept. Is is as yet uncertain whether the new concept will eventually replace the older one, or rather, tend to complement it, but present indications are that it will prove to be complementary (19).

The crystal-defect concept suggests that a portion of the x-ray scattering from the crystalline domains may diffuse and contribute to the so-called amorphous background. Consequently, this raises a question about the simple method by which crystallinity is estimated by separating the total diffraction intensity into sharp (crystalline) and diffuse (amorphous) components (19).

It should also be mentioned that there is a general disagreement in the degree of crystallinity obtained by different methods, such as x-ray diffraction, density, infrared, or NMR (20-23). From these considerations, as described by Alexander (19), the numerical values of crystalline and amorphous contents obtained by well-established and purportedly absolute x-ray techniques are now generally regarded as of doubtful absolute significance. Thus it may be more practical to differentiate the x-ray crystallinity from the crystallinity obtained by other methods. As a result of these problems, increasing preference is shown for describing the degree of three-dimensional order by some relative numerical quantity, which may be termed a crystallinity index (19).

Considering the discussion given above, we now return to the problem of the value of Δ_c^o. The crystallinities reported in Chapter III were obtained by following Ruland's method (24) which considers the lattice imperfections. We assume, however, that the parameter K is 1, which may lead to about 20% error in the estimation of the crystallinity as discussed in Chapter III. If we assume that the real crystallinities are 20% higher than those obtained in Chapter III, the recalculated value of Δ_c^o becomes 0.194 ± 0.025. A factor which may cause a significant error for determination of Δ_c^o is that there are only two experimental points available.

The real value of Δ_c^o could, therefore, be outside of the region indicated by ($\pm$) sign.

For a better determination of Δ_c^o it is desirable to obtain more experimental points at the region of higher crystallinity. In the experiments (10-12) for the determination of Δ_c^o usually the range between 10-45% crystallinity was used. It may be possible to obtain higher crystallinity by stretching more than was used here. An extrapolation of the crystallinity curve shown in Figure 10 in Chapter III indicates that one could obtain about 21% crystallinity at α = 7.0 and 24% at α = 7.5. It should, however, be mentioned that the theoretical maximum extension ratio (25) for the sample used here is probably about 7.5 since the number of statistical segments of the sample are estimated to be about 55-60. In an actual experiment, therefore, the network under very high deformation such as α = 7.5 may suffer some undesirable damage such as chain scission.

The birefringence caused by such high deformation may be remarkably high due to both contributions from high crystallinity and highly oriented amorphous phase, and the turbidity of the sample will increase significantly. The measurement of the birefringence will, therefore, become much more difficult. Actually it was very difficult to measure the birefringence of the sample even at α = 5 or 6, which must have caused some error in the value of the birefringence, and consequently in the calculation of Δ_c^o.

In order to attain higher elongation the use of samples with lower crosslinking density (i.e., larger number of statistical segments) may be considered, provided that the lower crosslinking density does not cause a decrease in the crystallinity due to the lower orientation of amorphous segments prior to the crystallization. However, it is more likely that the

sample with lower crosslinking density may have lower crystallinity at a given elongation as predicted from Flory's theory (26).

It may also be suggested to go to a lower temperature in order to obtain higher crystallinity. This may, however, result in a significant change of crystal morphology. The author feels that the morphology change may induce a change in the internal (electrical) field of the crystalline phase, which will change the birefringence significantly as we have seen in Chapter II. If this is true, the combined use of the data obtained from different temperatures will lead to a totally wrong conclusion.

Recently a question for the use of Equation (7) was raised (27). By considering the predictions of the series and parallel models where the series model would predict that the stress in the amorphous phase is identical with the total stress while the parallel model would predict that the stress is less, we may conclude that the real situation must be somewhere in between these two extreme bounds. The stress in the amorphous phase is, however, not constant but distributed about a filler (crystallite) particle. Consequently there will be a birefringence distribution about a filler particle as described by Ong and Stein (28). Probably a practical way to estimate the effect of amorphous birefringence (or stress) will, therefore, be to integrate the birefringence (stress) contributions about the filler particle over the whole volume of the sample as mentioned by Stein (27). Theory is not yet available to treat this problem. Until this treatment of the problem becomes available, the correction factor $F(\phi_c)$ may be applied as an empirical expression, whose quantitative use may not be justified, indicating that there may be some error due to the use of the empirical expression. If no correction factor is used, that is, if the stress of the

amorphous phase is assumed to be equal to the total stress, the value of Δ_c^o is 0.109 ± 0.035, which is about 15% smaller than that obtained by using the factor $F(\phi_c)$.

It may be expected that in the near future a better value for Δ_c^o of PIP under stress will be obtained by overcoming the difficulties mentioned above. It is believed, however, that the present value of 0.224 is probably a fair evaluation for Δ_c^o. From the data (29) of the birefringence and stress for natural rubber samples stretched at room temperature, the degree of crystallinity was estimated using Equation (8) and the value of 0.224 for Δ_c^o. The crystallinity change at $\alpha = 4.75$ with time is shown in Figure 1. The value of the crystallinity at long time appears to be reasonably consistent with the crystallinity of natural rubber stretched at room temperature (30-32) which are shown in Figure 10 in Chapter III. This agreement may support the value of 0.224 for Δ_c^o.

The definite reason for this disagreement between the experimental and calculated values of Δ_c^o is still uncertain. As we have seen in Chapter II however, the internal field effect may be related to this disagreement.

Discussion

In Chapter I the birefringence method proves at least qualitatively to be sensitive, and convenient to follow the crystallization of the samples under large deformations. It may be expected that the method will be accurate even in the quantitative sense provided that a correct value is used for Δ_c^o. In Equation (11) in Chapter I we used the value of 0.130 for Δ_c^o which was calculated using Denbigh's bond polarizabilities (18). The crystallinity obtained from the equation may, therefore, be considered as

a "relative crystallinity index" and may be meaningful as long as comparison and discussion are made on the same basis.

It may, however, be more meaningful to use a better defined crystallinity index such as that obtained by x-ray measurement. If we use the value of 0.224 for Δ_c^o in order to calculate the crystallinity using Equation (11) in Chapter I, the resulting crystallinity may be considered to be, in principle, equivalent to the crystallinity index obtained by x-ray measurement. Then we can discuss the problems quantitatively on the well defined basis. Since the experimentally determined value of Δ_c^o is about 1.7 times the value used in Chapter I, the crystallinity given by Equation (11) in Chapter I is approximately 70% higher than that obtained using this new value.

The crystallinities with time were recalculated using the data in Figures 8-10 in Chapter I, in which PIP samples were stretched rapidly at room temperature. The calculated values are plotted in Figure 2 for α = 3.89, in Figure 3 for α = 5.0 and in Figure 4 for α = 6.0. It is noted that the new crystallinity curves calculated using the value of 0.224 for Δ_c^o appear qualitatively similar to the old curves (Δ_c^o = 0.130). The crystallinities at α = 5.0 and 6.0 at long time appear to be in the range of crystallinity determined by the x-ray measurement as expected since the value of Δ_c^o (0.224) used here was determined using the crystallinities obtained by x-ray measurement.

These values at α = 5.0 may be compared with those for natural rubbers given in Figure 1. It appears that natural rubber has a higher crystallinity at very short times as compared to PIP. The crystallinity of natural rubber at long time, however, appears to be almost the same as

that for PIP. This may indicate that the rate of crystallization of natural rubber at very short time is probably much higher than that of PIP. Possible reasons for this are that natural rubber is likely to have more impurities which can be used as nuclei and that 3% non-cis-content in PIP may have some effect on nucleation.

The crystallinities at α = 3.89, 5.0 and 6.0 given by Flory's equation (26), described by Equation (18) in Chapter I, appear to be quite high. The possible reasons for this deviation are discussed extensively in Chapter I.

The variation of stress and birefringence following rapid cooling of a sample of PIP to room temperature following stretching to α = 6.0 at 90°C is shown in Figure 15 of Chapter I. From this data one may recalculate the crystallinity using Equation (8) or Equation (11) in Chapter I with the value of 0.224 for Δ_c^o, and using Flory's stress equation and Smith's birefringence equation (33), which are given by Equations (18) and (22) in Chapter I, respectively. A consideration should be made concerning the value of the statistical segment anisotropy of the crystalline phase, $(b_\ell - b_t)_c$. The value of $(b_\ell - b_t)_c$ may be obtained using the equation

$$\Delta_c^o = \frac{2}{9}\pi \frac{(\bar{n}^2 + 2)^2 (b_\ell - b_t)_c}{\bar{n} \quad v_s} \qquad (12)$$

where $\bar{n}$ is the average refractive index of the crystalline phase, v_s is the volume per statistical segment in the crystal. v_s may be calculated from the unit cell structure of cis-1,4-polyisoprene (34,35) and the number of monomer unit per segment which has been obtained as 1.97 in Chapter I. Using $\bar{n}$ = 1.52, one obtains 5.768 x 10^{-25} cm^3. The rest of the parameters

are the same as those used in Chapter I. The results obtained by the three methods are plotted in Figure 5.

It is noted that the value from Equation (11) in Chapter I appears tobe in the range of crystallinity obtained by x-ray measurement. Equation (23) in Chapter I produces slightly lower values, in which the crystallinity at long time is comparable with that obtained by x-ray measurement. The Flory stress relaxation equation, Equation (21) in Chapter I, appears to give high crystallinities compared with the other two methods. By considering the crystallinities obtained by x-ray measurement, one may conclude that the values obtained from Equation (21) in Chapter I are probably too high. Since by using a modified equation such as Equation (21) in Chapter I we consider stress change only during the crystallization and eliminate any deviations from ideal rubber elasticity prior to the crystallization, we may therefore conclude that Equation (21) in Chapter I does not describe quantitatively the stress relaxation due to tne crystallization and may tend to overestimate the effect.

It is well known that the Flory theory may not be applicable at low elongations because of the assumption of perfect orientation of the crystal phase. The theory may therefore be expected to be more applicable at higher elongations such as this experiment in which the orientation function is about 0.98 measured by x-ray. The theory however did not produce reasonable crystallinities. One may suggest that non-Gaussian effect is significant at $\alpha = 6.0$ and is a major reason for the disagreement. It may therefore be worth applying the non-Gaussian stress equation given by Equation (24) in Chapter I in order to study the non-Gaussian effect on the crystallization of PIP. The crystallinities calculated from Equation (24)

are also plotted in Figure 5 (b'). It is noted that there is an appreciable non-Gaussian effect, indicating that the non-Gaussian effect may be one of the major reasons for the disagreement, but not the only reason.

One of the possible reasons for the disagreement is described by Smith (36,37) as follows: "Flory has developed the stress relaxation theory using the assumption that the free energy of crystallization of a network is an absolute minimum. But an absolute minimum in the free energy requires that the vector direction of that portion of a chain passing through a crystallite is such that the retraction force exerted by that chain is reduced by crystallization. There is, however, a finite and perhaps appreciable probability that crystallization of a chain could occur with this direction reversed." The two situations may be visualized by Figures 6 (a) and (b). It is easily seen that the stresses exerted in (a) and (b) may be different. This may be one of the reasons for the disagreement between the crystallinities obtained from Equations (11) and (23) in Chapter I.

Another possible reason for the disagreement may be, of course, attributed to the single pass model of crystallization with perfectly oriented crystals where a chain enters the crystal from the amorphous phase and passes through it without reversing direction. There are, however, many indications (38-40) of the existence of chain folding and superstructure in a stress-induced crystallized natural rubber sample. These phenomenon will cause the deviation from the stress-relaxation predicted by Flory's theory. The deviation will be expected to become larger as crystallization approaches its final stage. This may be a reason for the difference between the values obtained from Equations (11) and (23); that is, that the values become larger as crystallization proceeds.

The Smith's birefringence equation is obtained using the assumptions similar to those used in the derivation of the Flory equation of stress. It is, however, interesting to see that the birefringence theory seems to give fairly reasonable crystallinities. This may be attributed to the same reasons as discussed above. In Figure 6 the stress may be different between (a) and (b), however, the birefringence may not differ significantly because only orientation of the statistical segments is an important factor to the birefringence. Even in the later stages of crystallization, in which chain folding and formation of superstructures probably occur to some extent as long as the orientation of the crystalline phase remains high and constant, the birefringence theory may not be affected significantly. The first term of Smith's birefringence equation, Equation (23) in Chapter I, is an expression of the change in birefringence of the crystalline phase due to crystallization. The rest gives the contribution from the amorphous phase. For a PIP sample the value of $(b_\ell - b_t)_c$ is not small as compared with that of $(b_\ell - b_t)_a$. During crystallization the change of the first term is much larger than that of the second term which can be neglected as a first approximation. The fact that the change in amorphous contribution is not important as compared with that of crystalline contribution may indicate that the perturbation of amorphous phase due to crystallization is really not an important factor for this particular system studied here. It is, therefore, reasonable that non-Gaussian equation gives very similar results to those from the Gaussian equation. In Chapter I the perturbation of the stress-optical coefficient of the amorphous phase was neglected and it was concluded that the error from the assumption appeared to be small. The more quantitative consideration in this chapter confirms again that the

conclusion made in Chapter I is probably correct. The two curves, (a) from Equation (11) and (b) from Equation (23) in Figure 5 show a similar behavior, perhaps because of the relatively small perturbation.

However, if one uses such a polymer whose value of $(b_\ell - b_t)_c$ is relatively small as compared with that of $(b_\ell - b_t)_a$ for the same kind of study as reported here, the situation will not be the same as concluded in this paper. For example, polyethylene and polypropylene are probably such polymers. In this case the first term of Smith's equation becomes no longer a dominant term and the other terms become important. It may therefore be expected that the results from Equation (23) will be different from those of Equation (11). One must take the perturbation effect into the stress-optical coefficient in this case.

We may attempt to fit this recalculated crystallinity to an Avrami type equation (41)

$$X_c = X_\infty [1 - \exp(-k_c t^n)] \qquad (13)$$

where X_∞ is the ultimate crystallinity, k_c is the rate constant, and n is the Avrami exponent. Following the process described in Chapter I, the plot of $\ell n [-\ell n(1 - X_c/X_\infty)]$ vs. ℓnt is given in Figure 7. The value of n is very close to that of 0.93 obtained in Chapter I, which is reasonable because only relative values of crystallinity are required to apply to the Avrami equation.

As shown previously during crystallization the change in birefringence in amorphous phase is not important as compared with that in the crystalline phase. We may, therefore, assume that the change in birefringence is only due to the increase of crystallinity. This may be expressed by

$$X_c = K_B(\Delta - \Delta_o) \tag{14}$$

where K_B is a constant and Δ and Δ_o are the birefringence at time t and the initial birefringence prior to crystallization, respectively. Δ_o can be estimated from Figure 15 in Chapter I by extrapolation. An Avrami plotting was attempted using this equation and the results are also given in Figure 7. The results from this simple approximation agree well with those from Equation (11). This indicates that one may use Equation (14) as a good approximation for kinetic studies of crystallization of polymers, whose properties are similar to cis-polyisoprene which is used here. A corresponding equation for stress may be expressed by

$$X_c = K_s(\sigma_o - \sigma) \tag{15}$$

where K_s is a constant and σ_o and σ are the initial stress prior to crystallization and the stress at time t, respectively. The Avrami plot of the results from this equation is also shown in Figure 7. It is noted from the figure that the slope of the straight lines are very similar, which results in similar value of the Avrami component. The value of the rate constant k_c is, however, slightly different. This may be due to an error on the estimation of the value of σ_o. As a conclusion for this particular system studied here, the simple approximations such as Equations (14) and (15) may be very useful and may be reasonably accurate for the kinetic studies of crystallization.

The variation of crystallinity with temperature on stepwise cooling was also recalculated from the data given in Figures 18 and 19 in Chapter

I by using the value of 0.224 for Δ_c^o. They are plotted in Figure 8, and are qualitatively very similar to the values obtained in Chapter I as expected.

Conclusions

The value of the crystal intrinsic birefringence Δ_c^o was determined experimentally to be 0.224. The reconsideration of the data given in Chapter I shows that the conclusions made in that chapter are generally correct. Furthermore, it is shown in detail that the perturbation of amorphous phase due to crystallization may not be relatively significant and that as a result of this one can even neglect the change in birefringence (and probably also stress) in the amorphous phase for the studies of kinetics of crystallization for the system studied here.

References

1. P. H. Hermans, Contributions to the Physics and Cellulose Fibers, Elsevier, Amsterdam, 1946.
2. R. S. Stein and F. Norris, J. Polym. Sci., 21, 381 (1956).
3. F. A. Bettelheim and R. S. Stein, J. Polym. Sci., 27, 567 (1958).
4. C. Chang, D. Peiffer and R. S. Stein, J. Polym. Sci., Polym. Phys. Ed., 12, 1441 (1974).
5. C. W. Bunn and R. DeDanbeny, Trans. Faraday Soc., 50, 1173 (1954).
6. R. S. Stein, Rheo-Optical Studies of Rubbers, in press.
7. D. A. Keedy, R. J. Volungis and H. Kawai, Rev. Sci. Instr., 32, 415 (1961).
8. L. Mandelkern, Crystallization of Polymers, McGraw-Hill, New York, 1964.
9. R. E. Read and R. S. Stein, Macromolecules 1, 116 (1968).
10. R. J. Samuels, J. Polym. Sci., A-2, 6, 1101 (1968).
11. Y. Fukui, T. Asada and S. Onogi, Polym. J. (Japan), 3, 100 (1972).
12. J. H. Dumbleton, J. Polym. Sci., A-2, 6, 795 (1968).
13. R. S. Stein, D. A. Keedy and J. Powers, J. Appl. Phys., 31, 1911 (1960).
14. R. S. Stein, in U.S-Japan Seminar on Polymer Physics, R. S. Stein and S. Onogi, Eds., Interscience, New York, 1966.
15. R. S. Stein, J. Polym. Sci., A-2, 7, 1021 (1969).
16. H. M. Smallwood, J. Appl. Phys., 15, 758 (1944).
17. E. Guth, J. Appl. Phys., 16, 20 (1945).
18. K. G. Denbigh, Trans. Faraday Soc., 36, 936 (1940).
19. L. E. Alexander, X-Ray Diffraction Methods in Polymer Science, Interscience, New York, 1969.

20. G. Farrow and I. M. Ward, Polymer, 1, 330 (1960).

21. J. J. Brader, J. Appl. Polymer Sci., 3, 370 (1960).

22. H. Hendus and G. Schnell, Kunststoffe, 51, 69 (1961).

23. G. Farrow and I. M. Ward, British J. Appl. Phys., 11, 543 (1960).

24. W. Ruland, Acta Cryst., 14, 1180 (1961).

25. L. R. G. Treloar, The Physics of Rubber Elasticity, Oxford, 2nd. Ed., 1967.

26. P. J. Flory, J. Chem. Phys., 15, 397 (1947).

27. Private communication between Dr. G. Kraus and Prof. R. S. Stein.

28. C. Ong and R. S. Stein, J. Polym. Sci., Polym. Phys. Ed., 12, 1899 (1974).

29. W. Yau, Ph.D. Thesis, University of Mass., Amherst, Mass. (1966).

30. J. M. Goppel and J. J. Arlman, Appl. Sci. Res., A1, 462 (1949).

31. L. E. Alexander, S. Ohlberg and G. R. Taylor, J. Appl. Phys., 26, 1068 (1955).

32. S. C. Nyburg, British J. Appl. Phys., 5, 321 (1954).

33. K. J. Smith, Jr., J. Polym. Sci., A-2, 6, 1723 (1968).

34. C. W. Bunn, Proc. Roy. Soc., A180, 40 (1942).

35. S. C. Nyburg, Acta Crystal., 7, 385 (1954).

36. K. J. Smith, Jr., ACS Polymer Preprint, Vol. 2, No. 2, 337 (1975).

37. Seminar given by K. J. Smith, Jr., University of Mass., 1974.

38. E. H. Andrews, Proc. Roy. Soc., A270, 232 (1963).

39. E. H. Andrews, Proc. Roy. Soc., A277, 562 (1964).

40. W. Yau and R. S. Stein, J. Polym. Sci., A-2, 6, 1 (1968).

41. M. Avrami, J. Chem. Phys., 7, 1103 (1939); 8, 212 (1940); 9, 177 (1941).

42. H. G. Kim and L. Mandelkern, J. Polym. Sci., A-2, 6, 181 (1968).

43. D. Luch and G. S. Y. Yeh, J. Polym. Sci., Polym. Phys. Ed., 11, 467 (1973).

44. A. N. Gent, Trans. Faraday Soc., 50, 521 (1954).

TABLE 1

The Values of Δ, σ, X_c and f_c
Used for the Determination of Δ_c^o

α	$\Delta \times 10^3$	σ kg/cm^2	X_c	f_c
3.89	9.85	36.2	-	-
5.0	25.6	58.0	0.075	0.98
6.0	32.6	78.0	0.140	0.98

Captions for Figures

1) The variation in weight fraction crystallinity of natural rubber with time following rapid stretching at room temperature at elongation ratio of 4.75.

2) The variation in weight fraction crystallinity with time following rapid stretching of PIP samples at room temperature at elongation ratio of 3.89. Values are given which are obtained from the birefringence Equation (11) using the value of 0.224 for Δ_c^o and from Flory's stress equation [Equation (18)].

3) The variation in weight fraction crystallinity at elongation ratio of 5.0.

4) The variation in weight fraction crystallinity at elongation ratio of 6.0.

5) The variation of weight fraction crystallinity recalculated for the data given in Figure 15 in Chapter I using the value of 0.224 for Δ_c^o. (a) from Equation (11), (b) and (b') from Equations (23) and (25), respectively, and (c) and (c') from Equations (21) and (24), respectively. All equations are given in Chapter I.

6) Models for stress-induced crystallite and amorphous chains.

7) Avrami plots of the isothermal crystallization data on PIP given in Figure 15 in Chapter I. O, Δ and ● representing the values from Equation (11) in Chapter I, Equations (14) and (15), respectively.

8) The variation in weight fraction crystallinity with temperature upon stepwise cooling samples of PIP stretched to $\alpha = 4.98$ and $\alpha = 6.51$ at 90°C.

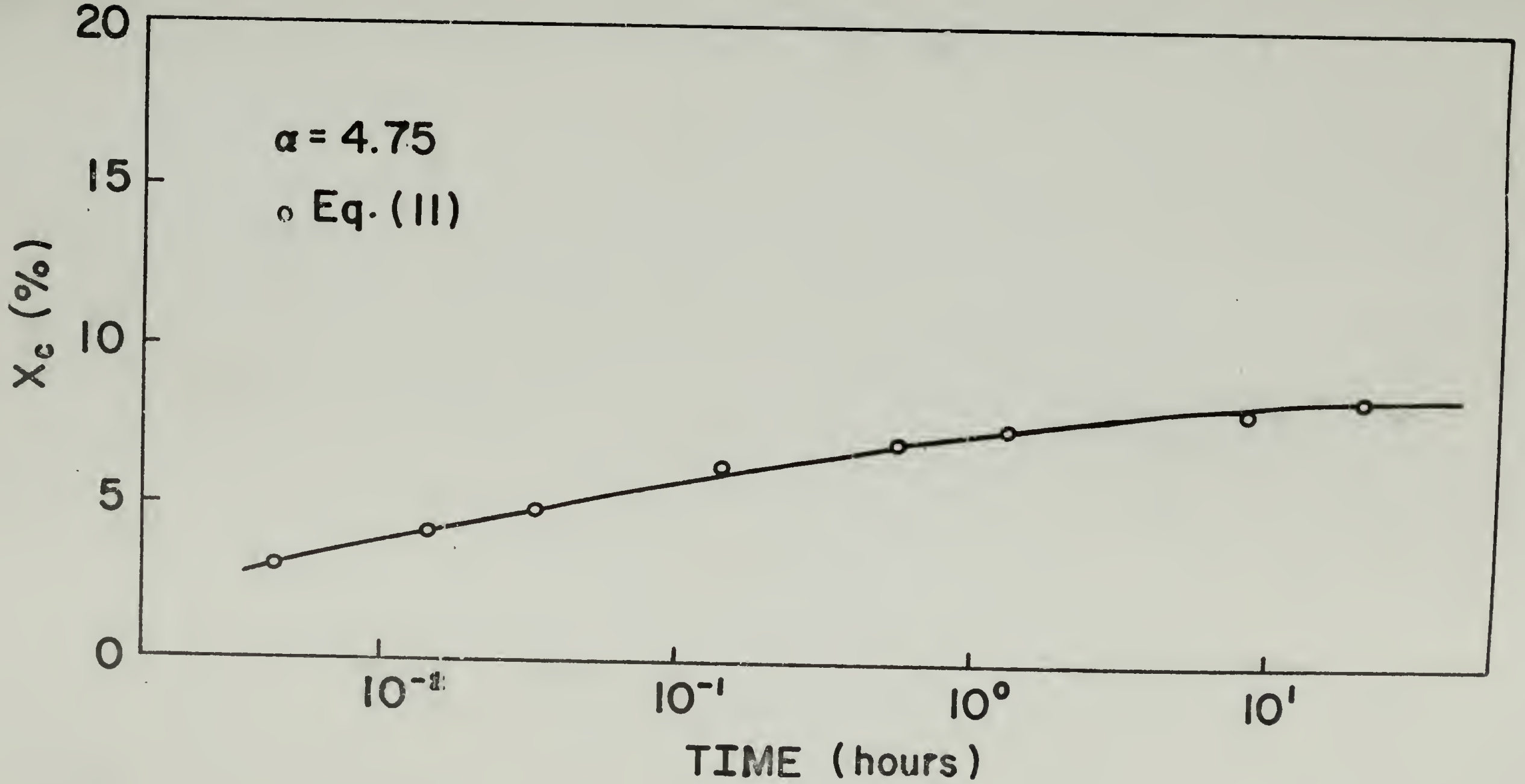

Figure 1

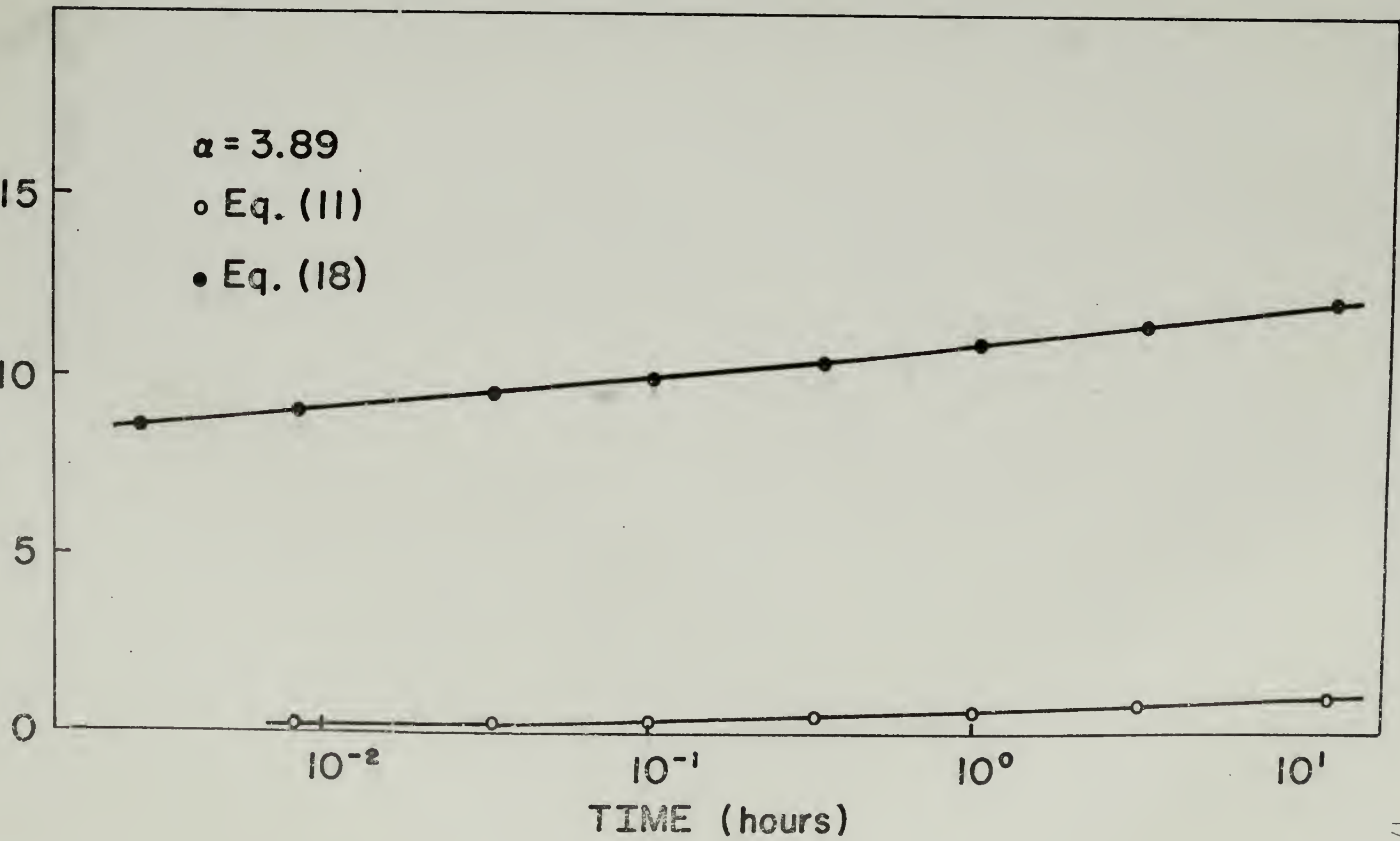

Figure 2

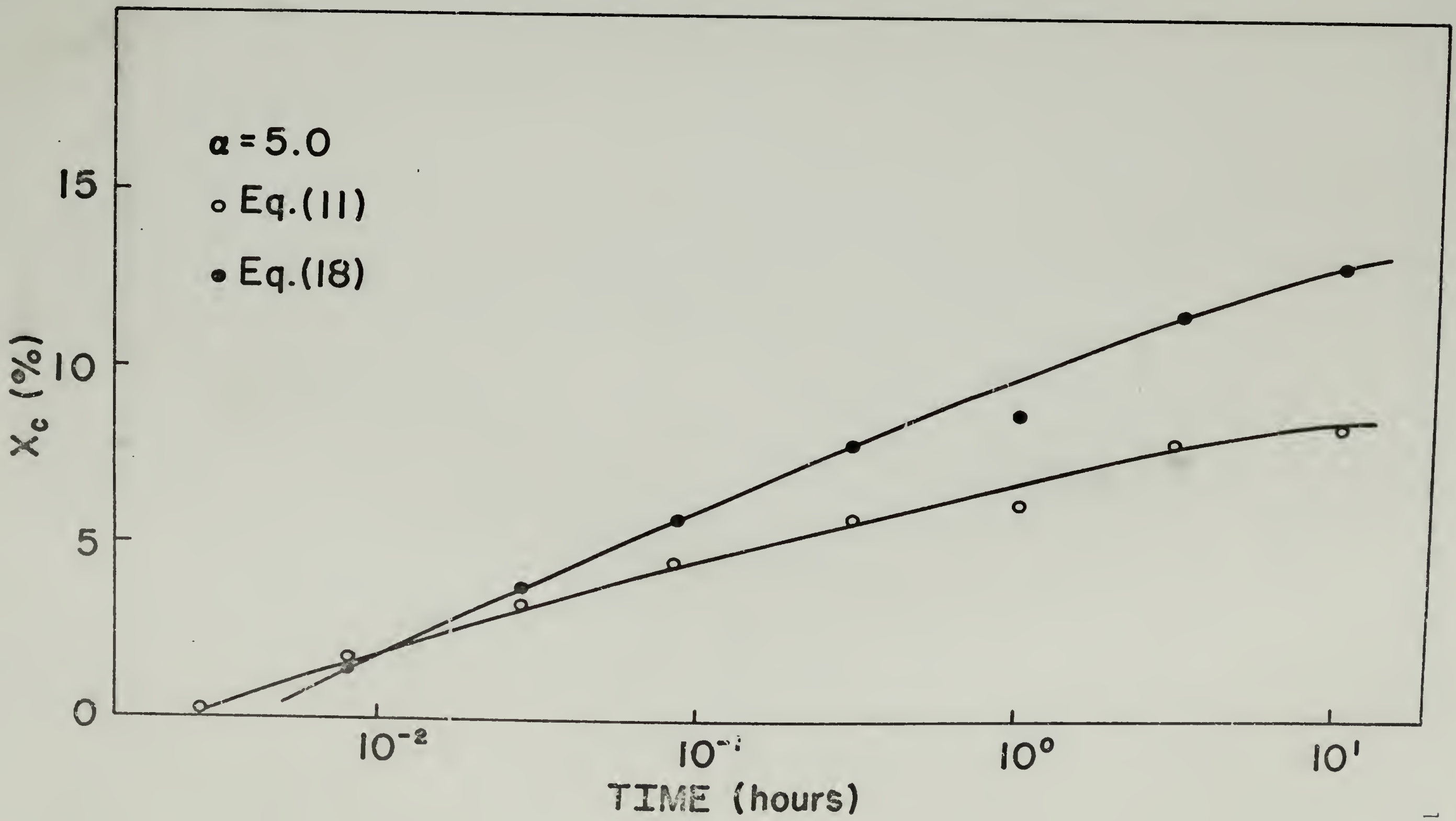

171

Figure 3

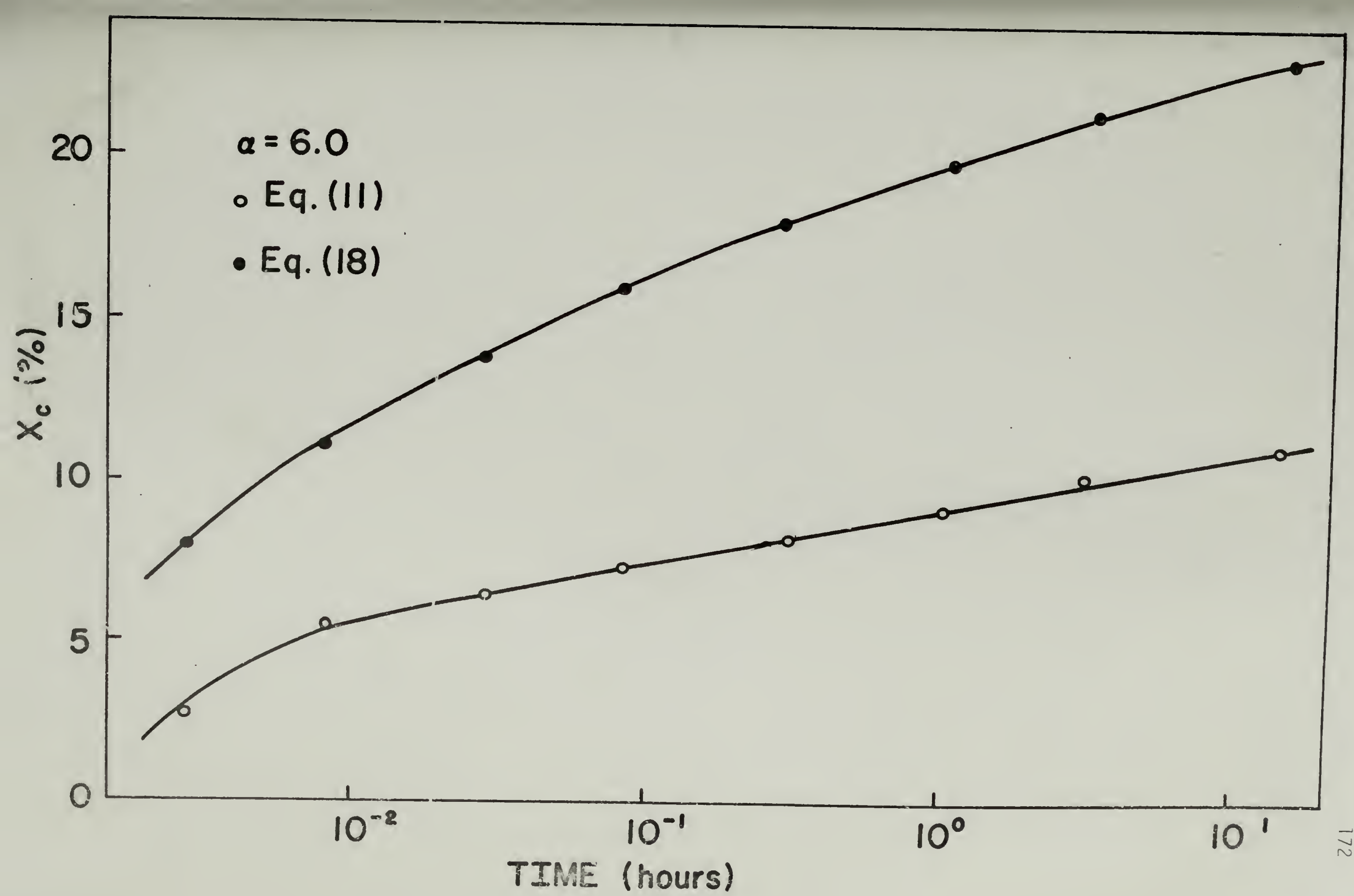

Figure 4

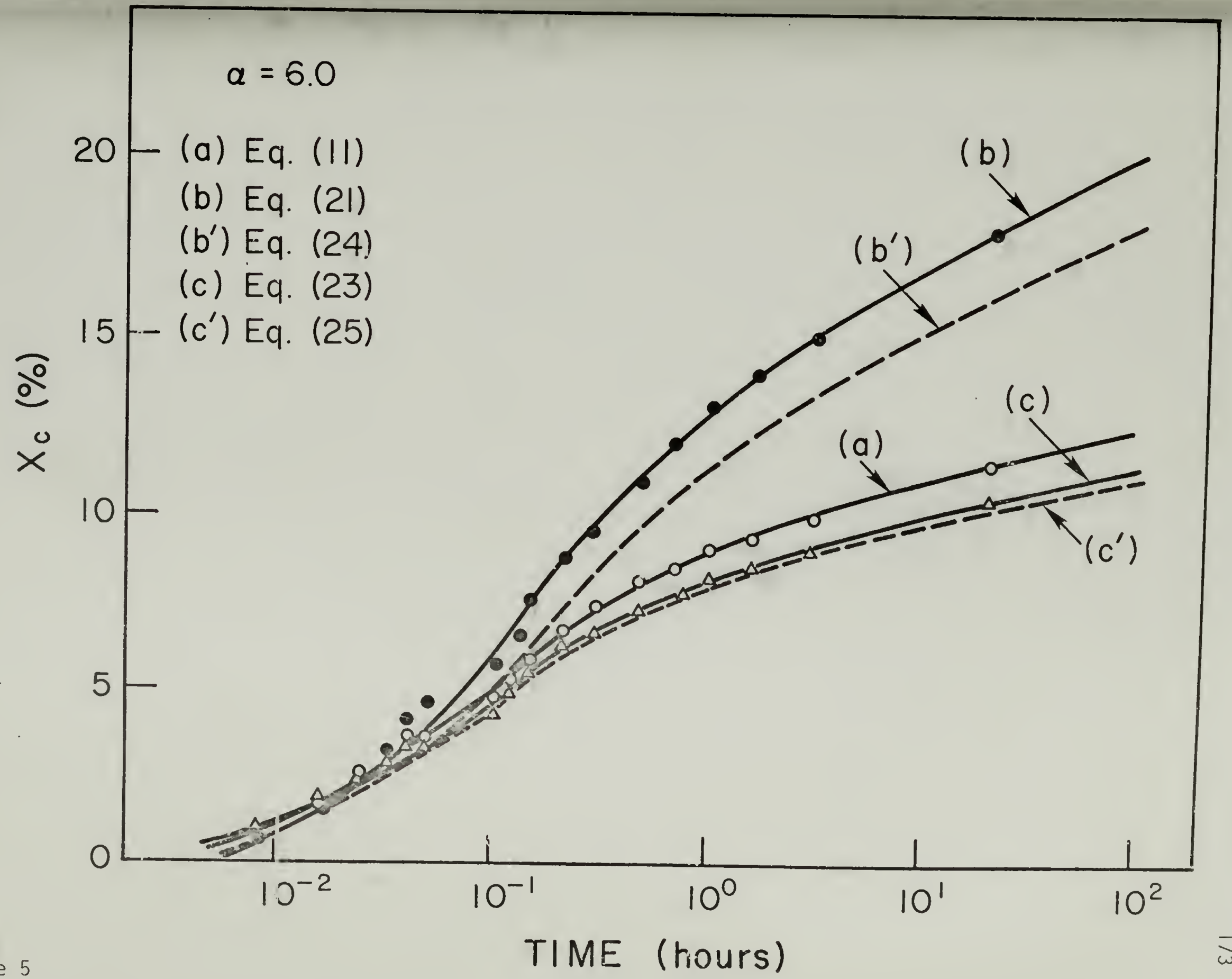
α = 6.0
(a) Eq. (11)
(b) Eq. (21)
(b′) Eq. (24)
(c) Eq. (23)
(c′) Eq. (25)
20
15
10
5
0
X_c (%)
(b)
(b′)
(c)
(a)
(c′)
10^{-2}
10^{-1}
10^{0}
10^{1}
10^{2}
TIME (hours)

Figure 5

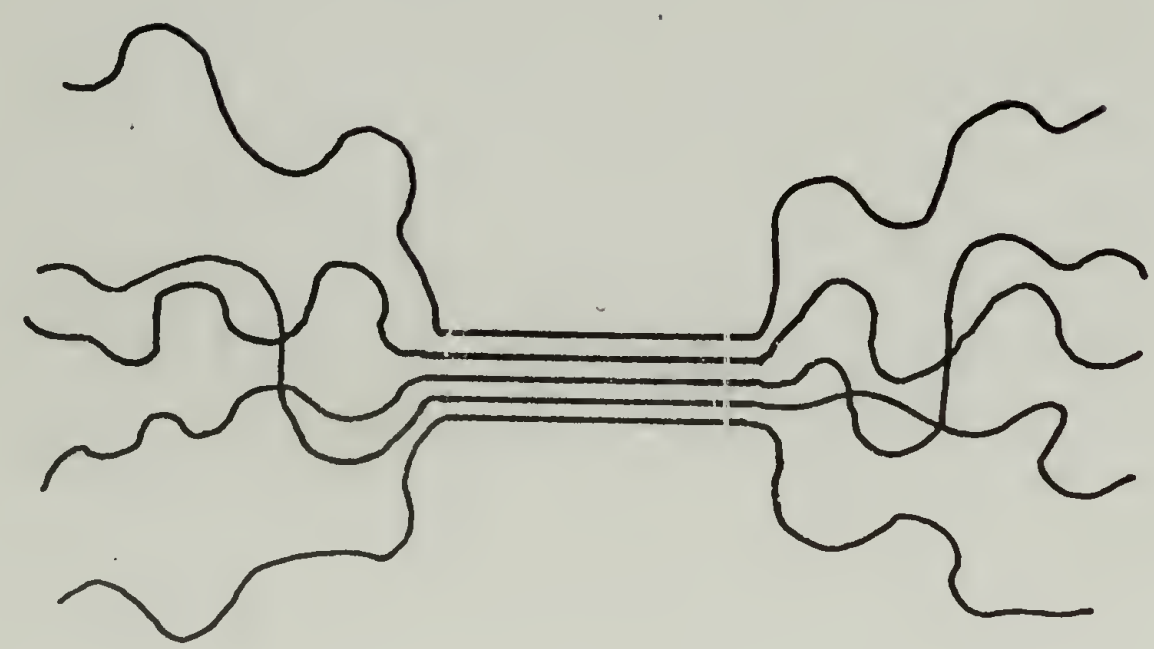

(a)

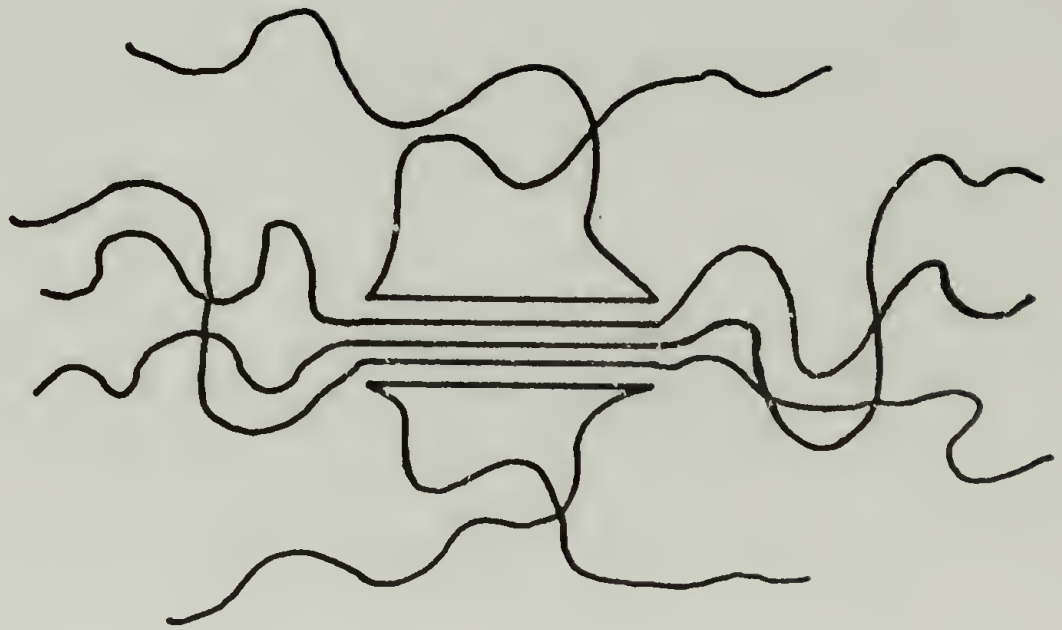

(b)

Figure 6

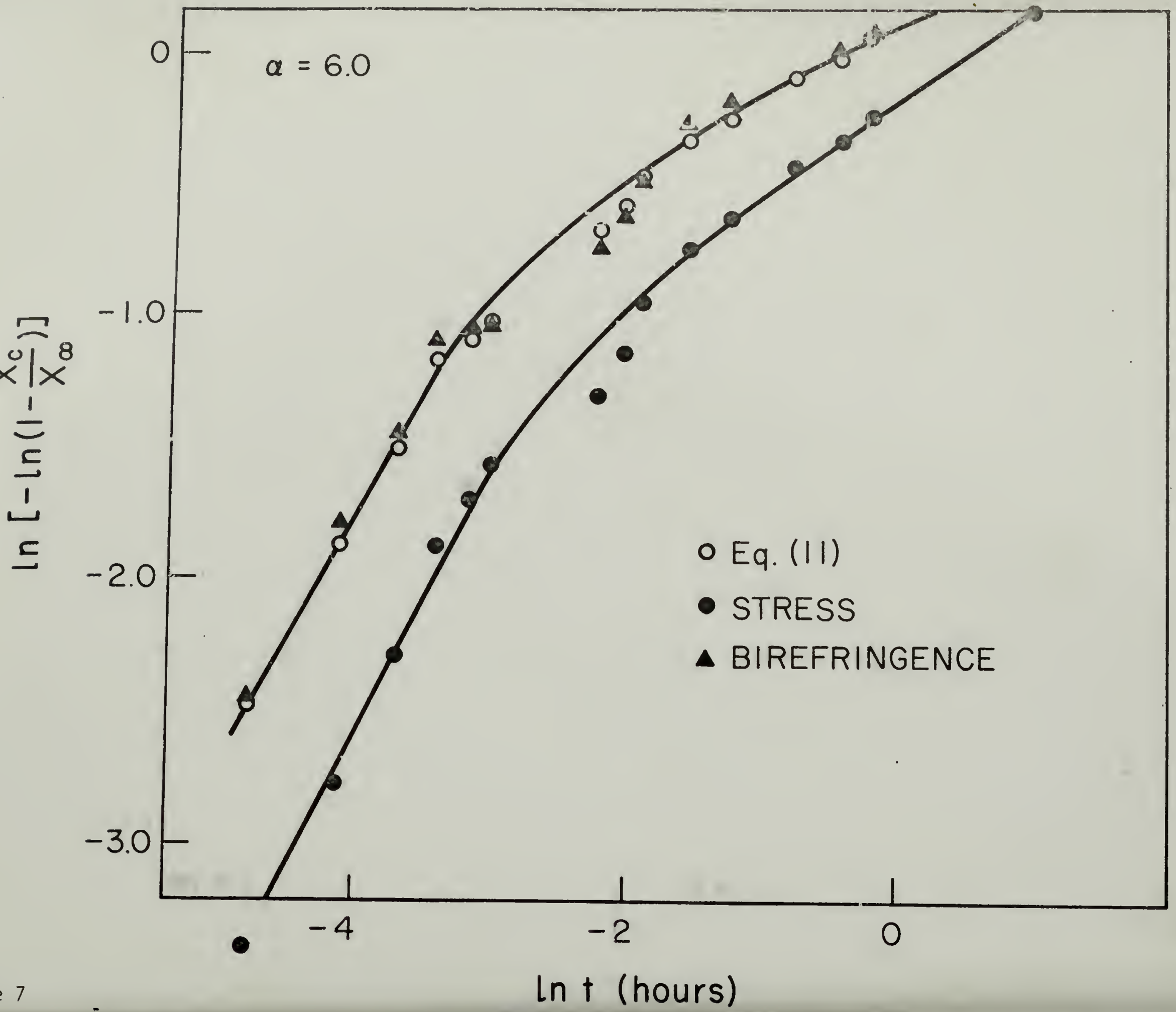
α = 6.0
0
-1.0
-2.0
-3.0
ln [-ln(1-Xc/X∞)]
-4
-2
0
ln t (hours)
Eq. (11)
STRESS
BIREFRINGENCE

Figure 7

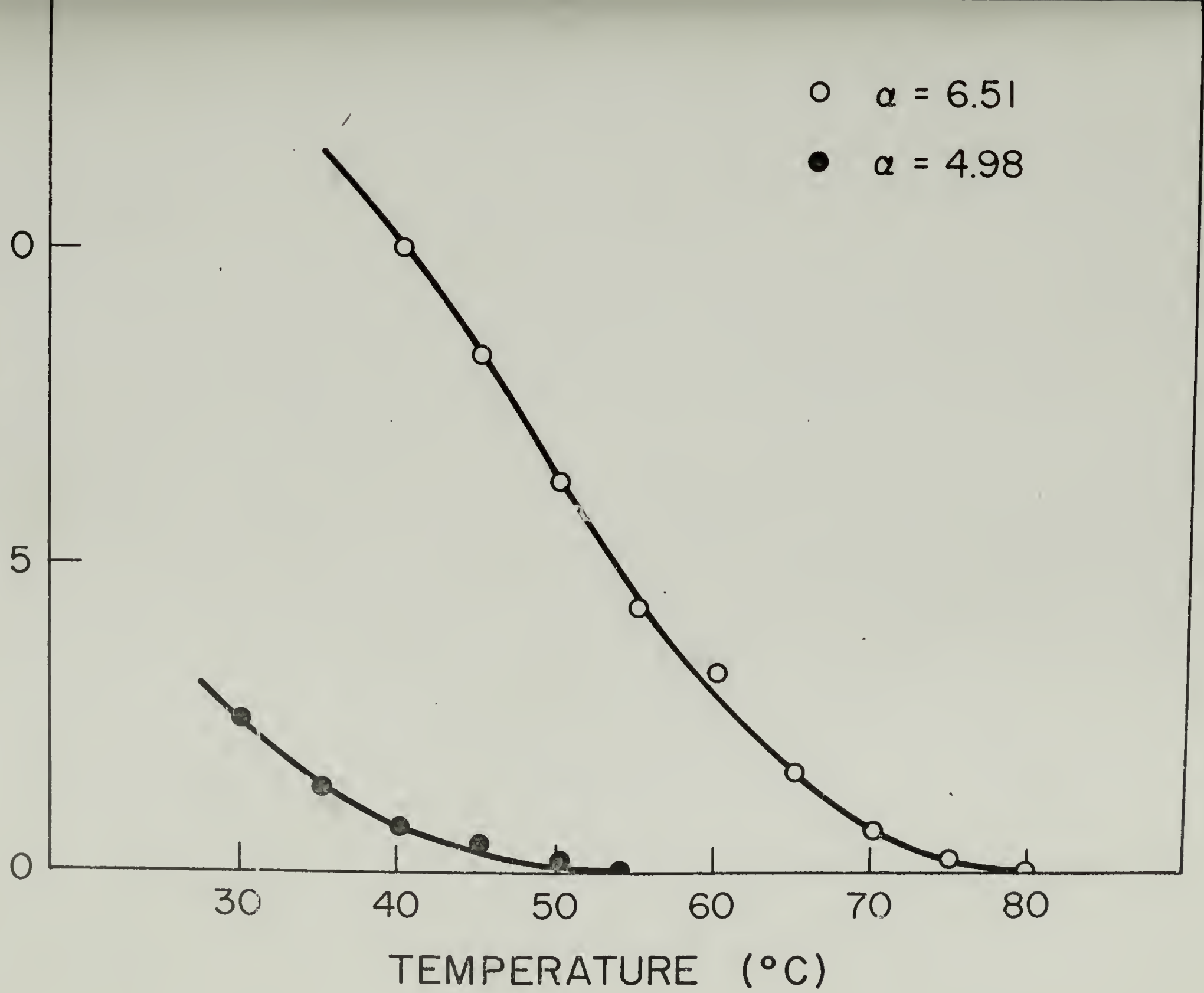

Figure 8

CHAPTER V

LIGHT SCATTERING STUDIES

Introduction

For the last 15 years, the light scattering technique has been developed for the characterization of the structure of crystalline polymers in the solid state. In principle, it permits the characterization of shape, size and orientation of organized assembles of crystallites such as spherulites, rods or shish-kebabs whose dimensions are in the range from approximately 0.5μm to 10μm.

Since a semicrystalline polymer contains optical heterogeneities of dimension comparable to the wavelength of light, it scatters light. In semicrystalline polymers, there are three possible origins for the heterogeneities (1): (i) density fluctuations due to crystallinity, areas of differing density due to statistical fluctuation or voids, (ii) orientation fluctuation due to anisotropy, and (iii) anisotropy fluctuation areas of differing anisotropy. For an example, in the case of natural rubber under strain, it has been reported (2) that the heterogeneities primarily represent fluctuation in the orientation of anisotropic bodies rather than fluctuation in density and that the scattering does not arise from a variation in density, average polarizability, or degree of crystallinity from place to place, but rather from a variation in orientation of anisotropic bodies.

The light scattering from solids can be treated in terms of two limiting types of theories (3). The first of these is referred to as the model approach which calculates the scattering by summing the scattered amplitudes arising from all of the volume elements composing some structural

unit such as a sphere or a rod. This approach has been demonstrated to be useful to explain the morphologies of polyethylene (4) and poly(tetrafluoroethylene) (5) and others (6-7). The second is the statistical approach in which a structure is described in terms of correlation functions describing fluctuations in density and orientation. Each of these methods has its advantages and limitations, and real systems generally lie between the extremes described by these models (3).

The scattering patterns are usually studies in the H_V and V_V modes. In the H_V mode, the polarizer and analyzer are crossed with respect to their polarization directions while in the V_V mode they are parallel. For oriented systems, the stretching direction is usually taken parallel to the polarization direction of the polarizer.

The light scattering studies of stress-induced crystallization have been reported for a few polymers (8-10). For natural rubber (8), intense V_V scattering was found when the crystallization occurred under high strains, which is characteristic of the scattering from the aggregates of dimensions comparable with the wavelength of visible light. Furthermore, it was concluded that the scattering unit consists of an assembly of crystals with their chain axes parallel to the stretching direction, but, in the case of very high elongation, with the fibril axis at a slight angle to the stretching direction. The distance over which the orientation correlation occurred did not vary appreciably with degree of elongation, temperature or time, and the scattering intensity change was mostly related to the change of the degree of crystallinity of the samples.

As for trans-polybutadiene (9), the situation appeared to be more complex because the experiments were carried out under the conditions of low elongations and low temperatures. Consequently the morphology resulting from these conditions was considered to be a combination of a deformed spherulite and a rod-like structure.

Their studies and others (11-15) have demonstrated that the light scattering method is sensitive and convenient to study the morphology of crystalline polymers. The work reported here was done for the study of morphology in stress-induced crystallized rubbers (mainly synthetic cis-1,4-polyisoprene) in the light of the new development of the light scattering technique.

Theories

Since most of this work was carried out by a photographic method, it may be more helpful to use theories based on the model approach. Two basic models for superstructures of crystalline polymers are for spherulites and rods.

The H_V and V_V scattering intensities from an isolated spherulite have been calculated by Stein and Rhodes (4) as

$$I_{H_V}(\theta,u) = K_1 V_0^2 (3/U^3)^2 [(\alpha_r - \alpha_t) \cos(\theta/2) \sin\mu \cos\mu \times (4\sin U - U\cos U - 3SiU)]^2 \quad (1)$$

$$I_{V_V}(\theta,\mu) = K_2 V_0^2 (3/U^3)^2 [(\alpha_r - \alpha_s) (SiU - sinU)$$

$$+ (\alpha_t - \alpha_s) (2sinU - UcosU - SiU)$$

$$+ (\alpha_r - \alpha_t) \cos^2(\theta/2) \cos^2\mu (4sinU - UcosU - 3SiU)]^2 \quad (2)$$

where K_1 and K_2 are constants, α_r and α_t are radial and tangential polarizabilities of the spherulite, respectively, α_s is the average polarizability of the surrounding medium, V_0 is the volume of the spherulite, $U = (4\pi/\lambda')$ $Rsin(\theta/2)$, R is the radius of the spherulite, λ' is the wavelength of the light in the system, θ and μ are the scattering and azimuthal angles, respectively, and SiU is given by

$$SiU = \int_0^U \frac{\sin x}{x} \, dx \quad (3)$$

As seen from Equations (1) and (2), I_{H_V} depends only upon the anisotropy of the scattering element, $(\alpha_r - \alpha_t)$, while I_{V_V} depends not only upon the anisotropy but also upon the optical density fluctuations, $(\alpha_r - \alpha_s)$ and $(\alpha_t - \alpha_s)$. One may determine the radius of the spherulite from the intensity peak position, θ_{max}, by using the expression

$$U = (4\pi/\lambda') R \sin(\theta_{max}/2) = 4.09 \quad (4)$$

Since I_{V_V} depends upon the sign of $(\alpha_r - \alpha_t)$, one can determine whether the spherulite is positive $(\alpha_r > \alpha_t)$ or not from V_V scattering.

The theoretical calculation of light scattered from an isolated rod has also been carried out by Rhodes and Stein (17). Their results for the scattering amplitude are described as

$$E_{H_V} = K_3 L \, \delta \sin\alpha \cos\alpha \sin\phi \, [\sin(kaL/2)/(kaL/2)] \tag{5}$$

$$E_{V_V} = K_4 L \, (\delta \cos^2\alpha + b_t) \, [\sin(kaL/2)/(kaL/2] \tag{6}$$

where K_3 and K_4 are constant, L the length of the rod. δ is the anisotropy of the rod which is given by

$$\delta = b_\ell - b_t \tag{7}$$

where $b_\ell = b_\ell' - b_s$ and $b_t = b_t' - b_s$. b_ℓ' is the longitudinal polarizability of the rod, b_t' is the tangential polarizability of the rod, and b_s is the polarizability of the surroundings. L is the length of the rod. The angle α is the tilt of the rod as measured from the Z axis (stretching direction).

The angle ϕ is formed with the projection of the rod in the xy plane. k is defined as $2\pi/\lambda'$. a is given by

$$a = \sin\alpha \cos\phi (1 - \cos\theta) - \sin\alpha \sin\phi \sin\theta \cos\mu - \cos\alpha \sin\theta \sin\mu \quad (8)$$

For a non-random distribution of rods and no phase relation, one may use a distribution function. The intensity of scattering is then described as

$$I = K \iint N(\alpha,\phi) E^2 \, d\alpha \, d\phi \quad (9)$$

where $N(\alpha,\phi)$ is the distribution function of the rod.

As seen from Equations (5) and (6), H_V scattering depends only upon the anisotropy of the rod, δ, but not upon the polarizability of the surrounding. H_V intensity from the assembled rod will decrease monotonously with increase of scattering angle. On the other hand, V_V scattering depends upon both the anisotropy of the rod and polarizability of the surrounding. By introducing other assumptions, such as a maximum polarizability direction of 45^o with the rod axis, Stein and Rhodes show that the rod model appears to be successful in explaining the observed scattering from both oriented and unoriented polytetrafluoroethylene.

Since their proposals of these theories, a number of developments and improvements for these two models have been made. For example, they are made for three dimensional spherulites (18), for three dimensional rods (7),

for imperfect spherulites (19,20), for the effect of interference between anisotropic scattering entities (21), and for the deformation mechanism (22,23). The many accumulated data and theoretical works show that light scattering is a convenient, fast and interpretable method to study the morphology of a crystalline solid polymer. As pointed out by Stein (3), however, it is apparent that light scattering alone will not suffice to completely characterize the morphology of a polymer film. While the experimental simplicity is attractive, a price is often paid in the difficulty of theoretical interpretation. It will be best if it is used together with all other methods that are available for characterizing a system (3).

Experiments and Discussion

1. Sample Preparation.

A sample of cis-1,4-polyisoprene was prepared by the same method as described in Chapter I. The typical sample thickness was about 10-15 mils. Cis-1,4-polybutadiene (PBD) was Duragen 1203 and believed to have a nominal cis content of 93%. PBD was purified by the same manner as for PIP. The purified PBD was dissolved in benzene (5g/100 ml) along with dicumyl peroxide (DCP) as crosslinking agent and with an antioxidant of 2,6-Di-Tert-Butyl-P Cresol in the proportions: PBD, 100 pts. by weight, DCP, 0.2 pts., and antioxidant, 1 pt. The solution was cast on a teflon-coated pan. These films were crosslinked at 145^{o} and 5000 PSI for 35 minutes in the same press used for PIP.

2. Light Scattering Changes with Elongation.

Samples of PIP and PBD were stretched at room temperature to certain elongations and light scattering patterns were obtained for cross polarization, H_V, as well as parallel polarization, V_V. The photographic apparatus with a Spectra-Physics He-Ne laser has been described elsewhere (16). A schematic diagram of the apparatus is shown in Figure 1. The sample-to-film distance was 11 cm. The patterns of PIP and PBD are shown in Figures 2 and 3.

For PIP it is noted that there is no scattering in the unstretched state indicating that the sample is amorphous. The scattering is first observed about 150% elongation which is at somewhat lower extension than that at which crystallinity is usually detected by x-ray. At 180% elongation, birefringence and stress show small decrease with time as shown in Figure 7 in Chapter I. At around 250-300%, a strong horizontal streak is observed in the V_V pattern, which indicates that rod-like structures are preferentially oriented in the stretching direction. This type of pattern was observed in natural rubber (8) under about 300% strain and polyethylene terephthalate (10) stretched below T_g. The scattering intensity of the V_V pattern is approximately 30-80 times more intense than that of the H_V pattern. (See a footnote on page 206 concerning about this point.)

At higher elongations, new additional four lobes oriented to the equatorial direction appear in the V_V pattern. In the H_V pattern it appears that an important change occurred. It is that the H_V pattern appears to have a maximum in the θ direction at the azimuthal angle of highest intensity,

which is not found at the lower elongations. To confirm this phenomena, a scanning of the intensity along the θ angle was carried out. This was done using an optical multiple channel analyzer (made by Princeton Applied Research) and a result for $\alpha = 6.0$ is shown in Figure 4. It is evident that there is a maximum. This may be indicative of the presence of a spherulitic-type superstructure in the sample. The orientation of the pattern is similar to those obtained from ellipsoidal spherulites as reported by several workers (24-26). Stein and co-workers (27-29) and Samuels (22) have developed light scattering theories to predict patterns from ellipsoidal spherulites. Stretching results in the elongation of the spherulites such that the long axis of these ellipsoidal spherulites is along the stretching direction. Thus, the light scattering pattern is oriented in the direction perpendicular to the direction of stretch. From Figure 2, it appears that as the elongation ratio increases, the morphology in the sample changes from rod-like superstructure to ellipsoidal spherulite. This may, however, be due to the interference between rods rather than due to the formation of ellipsoidal spherulite. At high elongation it is likely that the number of rod-like superstructures increase and that they align fairly regularly. This may cause the interference.

The H_V pattern with a maximum position along the θ direction was not found for natural rubber by Yau (8). The author feels that it is probably due to the insensitivity of the apparatus used ten years ago.

In the V_V pattern, the lobes make about 10° with the equatorial direction. This indicates that the superstructure may be tilted about 10° with respect to the stretching direction. This angle appears to decrease with elongation. For example, this angle becomes about 5° at $\alpha = 7.7$, but complete

alignment may not occur. The existence of the horizontal streak with those lobes may indicate the coexistence of the rod-like superstructures aligned parallel to the stretching direction along with those tilted about 10° with respect to the stretching direction. It is not as yet certain whether the former eventually change to the latter after long time. A picture at 90 days after stretching did not show a significant change of the intensity of the horizontal streak. 90 days, however, may not be long enough for this transition. For natural rubber, Yau observed that this horizontal streak eventually disappears at very high elongations, which does not agree with the results of PIP reported here.

The very high intensity for the V_V scattering as compared with the H_V scattering may be explained using Eqs. (5) and (6). For the H_V scattering, the factor $\delta \sin\alpha \cos\alpha$ in Eq. (5) becomes very small because of the high alignment of the superstructure to the stretching direction (α is very small), while in the V_V scattering the factor $(\delta \cos^2\alpha + b_t)$ is approximately equal to $\delta + b_t = b_\ell$. It is, therefore, very reasonable that the V_V intensity is very high as compared with the H_V intensity. (See Appendix III)

The scattering patterns from PBD stretched at room temperature are given in Figure 3. It is noted that very high elongations are required to cause appreciable scattering. This is reasonable because PBD is much less crystallizable under a given deformation than PIP or natural rubber. It may be difficult to obtain good information from the light s-attering patterns of PBD, however, because they are not as prominent as those of natural rubber or PIP. From these patterns of PBD, valuable information was obtained. By comparing the results of PIP and natural rubber with those of PBD, one may conclude that the light scattering patterns (represented by those at α = 4.9

in Figure 2) are characteristic for a stress-induced crystallized sample at a temperature above the melting temperature of the unstrained sample. As a consequence of this, the mechanism of the crystallization of NR, PIP and PBD under stress may be similar and the resulting crystal morphology will also be similar.

3. Crystallization of Swollen Samples.

For the studies of the effects of the existence of the solvent on the morphology, samples swollen by nitrobenzene were stretched at room temperature. Nitrobenzene was used as a swelling solvent because it was relatively less volatile.

PIP samples were swollen by nitrobenzene at room temperature until an equilibrium was obtained. The degree of swelling may be defined by the ratio of the weight of solvent to the weight of the PIP sample. The average value of the degree of swelling is 210%. A swollen PIP sample was stretched to a certain elongation and a cover glass was put on the surface of the sample to prevent volatilization. The light scattering patterns were taken at 30 minutes after stretching. The elongation ratio was measured in two ways. Two lines were drawn on the sample surface and the distance between the lines was measured before swelling (ℓ^{o}_{dry}) and after swelling (ℓ^{o}_{sw}). After stretching the distance was measured again and the two kinds of elongation ratios, $\alpha_1 = \ell/\ell^{o}_{dry}$, $\alpha_2 = \ell/\ell^{o}_{sw}$, were determined. The patterns are shown in Figure 5.

At $\alpha_2 = 1.0$ ($\alpha_1 = 1.15$), there is no scattering, as expected. The scattering patterns seem to appear as α_2 becomes greater than 2, which is considered to be consistent with the results of dry samples. The light scattering theory predicts that H_V scattering should not be changed because the

H_V scattering depends upon the anisotropy of the scattering element. However, V_V scattering may change because it depends upon both the anisotropy of the element and the polarizability of the surrounding. By the existence of the swelling solvent, the V_V scattering intensity may be changed with the change of the surrounding condition. The shape of the pattern may, however, not be changed if the swelling solvent exists uniformly in the sample. The H_V patterns at $\alpha_2 = 2.72$ ($\alpha_1 = 3.2$) appears to be very similar to that from a dry sample of comparable elongation. At $\alpha_2 = 3.5$ and 4.3, however, additional patterns appear, which are relatively weak, narrow and more oriented to the equatorial direction. The origin of this scattering is not certain, but it must be related to the existence of the solvent because the removal of the solvent by evaporation gives the patterns without narrow scattering, which is exactly identical to that from dry polymer under the corresponding elongation. This type of pattern was not found for natural rubber by Yau. This may be due to the difference of experimental procedures. In his experiment, natural rubber samples were stretched and then swollen by the solvent. He did not observe any appreciable change in the scattering. Another reason for this disagreement may be due to the insensitivity of the apparatus used by him.

In V_V scattering, there is a significant change in patterns. The prominent four lobes no longer exist. Instead, a fan-shaped pattern appears along with an unaffected horizontal streak. As discussed before, the change of the surrounding condition may change the scattering intensity of the V_V pattern. It is expected, however, that the shape of the pattern will be unaffected. A possible reason for the change of the shape of the pattern is

that the superstructure which is tilted about 10^{o} with respect to the stretching direction contains the swelling solvent (nitrobenzene) and that the solvent may not be uniformly contained. Hashimoto, et al. (30), have shown that the internal disorder in rods leads to a decrease in the azimuthal dependence of the pattern. Similar effects of disorder have been studied for a spherulite by Stein and Yoon (21). This conclusion may be applied to the present case. Because of the existence of the solvent, the superstructure is less ordered and this leads to less azimuthal dependence.

It is very interesting that after removal of the solvent by leaving the sample at room temperature for two days, the pattern (Figure 6) becomes very similar to that obtained from a dry sample stretched to the corresponding elongation. The present experiments suggest that the crystallization of a swollen sample is a very interesting phenomena and should be studied further along with other methods in the future.

4. The Effects of the Immersion Liquids.

It has been found (15) that it is necessary to cover the sample by glass microscope slides using an immersion fluid which closely matches the refractive index of the sample in order to minimize the surface scattering. For example (15), the light scattering patterns from teflon and nylon filaments are significantly changed with the refractive index of the oil. In previous experiments, silicone oil with a refractive index of 1.52 was used as the immersion liquid because it does not swell the rubber sample significantly. In the later sections, silicone oil whose refractive index is not 1.52 will be used as a liquid in a heating bath. We must, therefore, examine the effects of the refractive index of the immersion liquid before we carry out further experiments.

Four different silicone oils were used as immersion oils. A sample of PIP was stretched to α = 4.6 at room temperature. The scattering patterns with different silicone oil are given in Figure 7. It is evident that there is no significant change with the change of the refractive index of the immersion oil. One may, therefore, use any silicone oil as an immersion oil for the system studied here.

5. The Scattering Pattern Change in a Strain Cycle.

In order to study the morphological changes of crystalline superstructure in a strain cycle, H_V and V_V light scattering patterns of PIP were obtained at various stages of stretching and retraction.

A sample of PIP was first stretched from 0% to 280% and then to 400%. The sample was then retracted back to 330%, 270%, 210% and 170%. At each elongation, the sample was held for 30 minutes. V_V scattering patterns are shown in Figure 8.

As shown by various methods (8), the crystallization in stretched natural rubber exhibits hysteresis. It is expected that PIP samples show similar effects as natural rubber. In V_V scattering patterns, four lobes can be observed at 210% elongation. When a sample is stretched directly from 0% to 210%, these four-lobe patterns are not observed, as shown in Figure 2. This is apparently due to the so-called memory effect of the crystallization. This kind of phenomena was also found in natural rubber (8) Another sample of PIP was examined by the same procedure. This sample also showed the same phenomena. At 210%, this sample was held for 10 hours and V_V scattering patterns were taken. The result was very similar to that shown

in Figure 8. The intensity, however, appeared to be slightly less. This could be due to some photographic process difference. It is not certain whether this memory effect is permanent as long as the strain is held sufficiently.

As concluded by Yau (8), it appears that there is some degree of irreversibility of formation and disruption of the superstructure upon stretching and retraction and that the structure existing at a given strain does not depend only upon the strain but also upon the entire previous strain history. When we analyze the hysteresis of mechanical properties of stretched rubber, we must consider this memory effect of superstructure along with those of crystallinity, orientation, etc.

6. The Scattering Change During the Secondary Crystallization.

It has been reported (1) that the secondary crystallization process is very slow upon recooling after melting the crystal. In their experiment a natural rubber sample stretched 500% was heated to 93^{o}C and then cooled to room temperature, and the scattering patterns were observed during this period and after cooling. It was found that the formation of the cross-type four-lobe pattern took many hours. If the sample is stretched at room temperature, the development of the four-lobe pattern is observed immediately. Since the author feels this is an interesting phenomena, this type of experiment was repeated using a PIP sample.

A sample of PIP was stretched at room temperature up to α = 4.3. The formation of four lobes in the V_V pattern was observed immediately after stretching. The sample was placed in the silicone oil bath whose temperature

was about 95°C. The temperature was held at 95°C for 15 minutes and then lowered at the rate of 1°C/minute to 40°C, and cooled naturally thereafter. The V_V and H_V light scattering patterns were taken with temperature and time. A main object of this experiment was to confirm the fact that the secondary crystallization (or the development of the four-lobe pattern in V_V scattering) was very slow after the crystal was melted.

For melting the crystal, it was necessary to go to higher temperatures than 95°C, but in many cases PIP samples were broken at such high temperatures. Consequently, 95°C was chosen, which was not high enough for the melt of all of the crystal but sufficiently high to obtain a non-four-lobe pattern. H_V and V_V patterns with time and temperature are shown in Figure 9. It is noted that at 95°C the four-lobe type pattern in V_V scattering disappears, but that some scattering exists. This problem will be discussed in the later section. As temperature decreases, the horizontal streak in V_V scattering becomes intense, as shown by (f) in Figure 9. However, it takes about 56 hours to obtain the development of the four-lobes in V_V scattering as shown by (h). This final pattern appeared to be identical to that obtained before heating. As concluded for natural rubber, the re-development of the four-lobe type pattern in V_V scattering is very slow after its disruption by heating.

A close re-examination of the birefringence data measured by Yau (8) indicates that the increase of the crystallinity during the development of the four lobes is at most 4%. As we have seen in Chapter III, the degree of crystallinity of natural rubber with 400% elongation is approximately 14%. We may, therefore, conclude that most of the crystallization occurs immediately after

the temperature reaches a certain point and that the development of the four-lobe pattern does not correspond to the main part of the crystallization but to the secondary crystallization. It is not as yet certain why the four-lobe formation is so slow after heating, while it appears to be very fast if the sample is stretched at room temperature. This difference may result from the difference of crystallization kinetics between both cases.

7. Change of the Scattering Pattern with Time upon Step-Wise Cooling.

To closely investigate the problems on the origin of the scattering arisen in the previous section and to re-examine the birefringence data obtained in Chapter I, the variation of the scattering pattern with temperature on step-wise cooling was observed by stretching a sample up to α = 5.0 at 110°C and after 15 minutes lowering the temperature in 5° steps. The temperature was kept constant for 15 minutes at each temperature. The results of H_V and V_V scattering patterns are shown in Figure 10.

It is noted that in both H_V and V_V scattering there appears some scattering at 110°C. This may indicate that some scattering elements exist at high temperatures such as 110°C. These scattering patterns are very similar to those obtained at low elongations as shown in Figure 2. This problem will be discussed in the following section.

Both H_V and V_V patterns indicate that there are no significant changes until 75°C. At 50°C the horizontal streak in the V_V pattern appears to become sharper and more intense, and the intensity of the H_V pattern increases as shown by A(d) and B(d) in Figure 10. This change appears to

occur around 60°C. It is very interesting to compare this result with that obtained by the same experimental procedure as in Chapter I. From Figure 20 in Chapter I, the temperature at which the crystallinity is first detected is around 55°C for the sample at α = 4.98. One may, therefore, consider that the occurrence of sharpness and more intensity of the horizontal streak and of more intensity in H_V scattering corresponds to the detection of crystallization by birefringence and stress.

As discussed in the previous section, around these temperatures (such as 40° ~ 50°C), the V_V pattern indicates the superstructure of the rod-like structures with the long axis parallel to the stretching direction. As also discussed previously, it may, however, be difficult to explain satisfactorily H_V scattering by the simple model.

At the lower temperature, the four-lobe type scattering pattern appears in the V_V mode and the intensities of H_V and V_V scattering appear to increase as the temperature is lowered. At 35°C, the V_V scattering may suggest the co-existence of the rod-like structures with their long axis parallel to the stretching direction and with their axis tilted about 10° with respect to the stretching direction.

From these experiments, one may conclude that the strong and sharp horizontal streak in V_V scattering is eventually attributed to the early stage of crystallization which may be considered as a nucleation stage. If this is so, one may further conclude, considering the nucleation process, that in the stress-induced crystallization the nucleation does not occur uniformly or randomly in the amorphous phase but the nuclei (and new-born crystals) have some order in the stretching direction. A similar explanation

was made by Stein, et al. (1), for natural rubber whereby the crystals are correlated in orientation over longer distances in the direction of stretching than in a perpendicular direction. These explanations are similar to that given to account for the scattering from oriented polyethylene (15,31). It is uncertain whether this ordered structure in the stretching direction is equivalent to the γ filament called by Andrews (32) and considered to be so by Stein, et al. (1).

From the x-ray diffraction study, the molecular chains in the crystal are considered to orient close to the stretching direction. If the alignment is complete, there is no H_V scattering at small angles. This may be easily understood from Equation (5). If α is zero, $I = KE^2_{H_V}$ will be zero. The observations in this section and the previous section show the existence of a weak H_V scattering, which may indicate the angle between the chain and stretching direction is small but not zero. As a matter of fact, the x-ray study in Chapter III reveals that the average angle is about 7^o from $\alpha = 4.1$ to $\alpha = 6.1$. The presence of the H_V pattern may, therefore, be due to these crystals which are aligned with their chain axis oriented about 7^o with respect to the stretching direction. It is, however, possible that the H_V scattering may result from the strains imposed upon the amorphous regions by the growth of crystals. As shown by Ong, et al. (33), for a filled polymer, such strains produce birefringence around the filler and the birefringence may cause the scattering. If this is true, it is expected that the H_V pattern will be changed appreciably by swelling because the effect of swelling reduces the amorphous

strain. As observed in the previous section, the H_V patterns did not change significantly. This observation may indicate the possibility of the explanation for the H_V scattering.

From the four-lobe pattern in V_V we consider that the superstructure is tilted about 10^o with respect to the stretching direction. The reason for the tilt of the long axis of the structure with respect to the stretching direction is not clear. As suggested by Stein and Yau (1), this may be related to the analog between the proposed superstructure and that of the pyramidal polyethylene single crystals (34) in which the chain axis is tilted with respected to the plane of the crystal platelet. This is explained on the basis of tilted chains relieving the crowding of chain folds. Furthermore, as mentioned before, there is an indication of the formation of ellipsoidal spherulites. This tilting may relieve some crowding of crystal chains within the superstructure.

All discussion made here explained qualitatively the change of the scattering pattern after crystallization. If the temperature around 55^oC is a real melting temperature, as considered above, what is the origin of the scattering at the higher temperatures shown in (a), (b) and (c) of Figure 10? The problem will be discussed in the following section.

8. Change of the Scattering Pattern during Heating.

A sample of PIP was stretched up to $\alpha = 3.5$ at room temperature and then placed in the silicone oil bath. The bath can be heated at the

rate of 0.5°C/minute. The H_V and V_V patterns are taken with temperature change. They are given in Figure 11.

It is noted that as the temperature increases, the scattering patterns show less azimuthal dependence. It is, however, evident that the V_V pattern still shows the presence of the same scattering until the temperature increases to 80°C. This scattering pattern disappears around 87°C. The H_V pattern shows no scattering at this temperature. This may be considered as a perfect amorphous state. The observation shows that at about 80°C there is an indication of the existence of the scattering which may lead to the existence of a scattering structure. It may be hard to believe that there is some crystal at such a high temperature as 80°C.

For a confirmation of this point, an additional experiment was carried out. Another sample of PIP was stretched to higher elongation (α = 4.2) and the variation of scattering patterns were observed with temperature. They are shown in Figure 12. It appears that at 55°C, as shown by (f) in Figure 12, the four lobes of the V_V pattern exhibit less intensity but there is no significant change in the horizontal streak. At 80°C, shown by (c) and (g), the intensities of the H_V and V_V scattering decrease appreciably, but the shape of the pattern in H_V does not change significantly. In V_V scattering, the four-lobe scattering cannot be recognized and the horizontal streak now becomes less intense. At higher temperature, such as 105°C, both H_V and V_V scattering are very similar to those of low elongations at room temperature. When the temperature rose, the sample was broken.

The breakage of the sample always occurred if the temperature was increased higher than $110^{o}C$. The final stages, as shown in (d) and (h) of Figure 11, could not be obtained at $\alpha = 4.2$, which indicates that the temperature which will produce the perfect non-scattering state will be higher than $105^{o}C$ at $\alpha = 4.2$.

To study the melting temperature, the birefringence may be measured with temperature. Samples of PIP may be stretched at room temperature and held between two small metal plates with small holes by using an epoxy resin (Elmer's EPOXY). Within 5 days, the resin solidified completely and held the sample without any clamps. The metal plates were placed in a Mettler FP2. By using a microscope (Carl Zeiss Light Microscope) in crossed polars, the transmitted intensity was measured with temperature. The rate of temperature increase was $2^{o}C$/minute. The results for $\alpha = 4.0$ and 5.0 are given in Figures 13 and 14, respectively.

Since the transmitted intensity in the crossed polar mode is eventually related to the birefringence of the sample, one may obtain the birefringence change during heating from these measurements. The birefringence values before heating were 1.02 and 10^{-2} and 2.33×10^{-2} for $\alpha = 4.0$ and 5.0, respectively. These values are reasonably consistent with those obtained in Chapter I.

The melting temperature of rubbers under stress may usually be measured by observing the change of the stress or birefringence as temperature is increased. For the stress measurement, the point at which it becomes proportional to the temperature is considered to be an apparent

melting temperature (35,36). For the birefringence method, the point at which the birefringence becomes constant may be considered to be the apparent melting temperature.

In the experiments reported here, it appears that 54^{o} and $84^{o}C$ are approximately the apparent melting temperature for the sample stretched at $\alpha = 4.0$ and 5.0, respectively.

The melting temperature of stretched rubber may be described as

$$\frac{1}{Tm} - \frac{1}{T_m^o} = \frac{R}{2n_s \Delta H} F(\alpha, n_s) \qquad (10)$$

where Tm and T_m^o are, respectively, the thermodynamic melting temperatures for strained and unstrained polymer, R is the gas constant, n_s is the number of statistical segments per crosslinks, ΔH is the molar enthalpy of fusion of statistical segment, and $F(\alpha, n_s)$ may be given by Flory (37)

$$F(\alpha, n_s) = \alpha^2 + 2/\alpha - \alpha \left(\frac{6n_s}{\pi}\right)^{1/2} \qquad (11)$$

and by Krigbaum and Roe (38) (K-R)

$$F(\alpha, n_s) = 3 - \alpha^2 - 2/\alpha \qquad (12)$$

By using the values of ΔH and T_m^o obtained for natural rubber (39), T_m^o may be estimated with elongation. In this calculation, $T_m^o = 16^oC$ and $\Delta H =$ 2160 cal/mole were used. The value was estimated as 70 by the method described in Chapter I. The calculated melting temperature is shown in Figure 15. It was mentioned by Mandelkern, et al. (40), that the K-R equation could not predict the correct range of melting temperature at high elongations. From Figure 15, it is noted that Flory's equation agrees better with those obtained here.

From Figure 15, one important conclusion may be obtained. Equation (11) may not give the exact melting temperature of the PIP sample used here; however, it can give some idea concerning what the melting temperature should be. As reported earlier in this section, the scattering pattern disappears completely at very high temperature, such as 87^oC, for the sample stretched to $\alpha = 3.5$ and it appeared that the temperature for the sample of $\alpha = 4.2$ was higher than 105^oC. Even considering the wide error of Flory's equation, we may conclude that these temperatures cannot be the melting temperature and the melting temperatures must be appreciably lower than these values. If these arguments are correct (the author feels that it is probably so), we now have some scattering patterns above the melting temperature.

One possible origin for this may be impurities within the sample which introduce birefringence around themselves as the sample is stretched. The birefringence may be a reason for this scattering. The scattering for $\alpha = 3.5$ disappears at $87^{o}C$. If this scattering is due to the same impurities and they are destroyed at $87^{o}C$ in the sample of $\alpha = 3.5$, the same phenomena may occur in the sample of $\alpha = 4.2$. As we have seen, however, for the sample of $\alpha = 4.2$, the complete disappearance of the scattering was never obtained up to $105^{o}C$. These considerations lead to a conclusion that this scattering may not be due to the impurities within the sample.

Another possible origin is highly-oriented amorphous aggregates. It is, however, not likely that such aggregates are more stable than crystals. Finally, this scattering may be simply due to very stable crystals which cannot be detectable by stress or birefringence measurements. At the moment it appears that we cannot explain this scattering pattern which could have the same origin for the scattering pattern as observed at low elongations.

Conclusion

It may be concluded that the scattering unit consists of an assembly of crystals with its fibril axis parallel to the stretching direction but, at higher elongations, with the fibril axis at a slight angle to the stretching direction. Within a fibril, crystals may have their axes slightly tilted (less than $\pm 7^{o}$) with respect to the fibril's long axis. There is an indication that at high elongation the H_V scattering has a maximum along e

direction. When a swollen sample is stretched, additional new patterns appear in the H_V scattering whose origin is not certain. In the V_V scattering, the four lobes show no azimuthal dependence. This may be attributed to the disorder within the superstructure because of the existence of the solvent. The four lobes in V_V scattering arise from the secondary crystallization which is very slow after disruption of the superstructure by heating. When PIP sample under 250% strain was heated, the scattering pattern was observed until 87°C. For the sample under 320% strain, the scattering pattern persisted at 105°C. These temperatures are considered to be higher than the melting temperatures of these stretched samples. The origin of this scattering is not as yet certain.

Acknowledgements

The data shown in Figure 4 were obtained by Mr. E. Roche.

References

1. W. Yau and R. S. Stein, J. Polym. Sci., A-2, 6, 1 (1968).
2. W. Yau and R. S. Stein, Polym. Letters, 2, 231 (1964).
3. R. S. Stein, "Optical Studies of the Morphology of Polymer Films," paper presented at the Award Session of the American Chemical Society Meeting, April, 1972.
4. M. B. Rhodes and R. S. Stein, J. Appl. Phys., 31, 1873 (1960).
5. M. B. Rhodes and R. S. Stein, J. Polym. Sci., 62, 587 (1962).
6. G. Adams and R. S. Stein, J. Polym. Sci., A2, 6, 31 (1968).
7. M. Moritani, H. Hayashi, A. Utsuo and H. Kawai, Polym. J. (Japan), 2, 74 (1971).
8. W. Yau, Ph.D. Thesis, University of Massachusetts, Amherst, 1966.
9. Y. Akana, M.S. Thesis, University of Massachusetts, Amherst, 1973.
10. A. Misra, Ph.D. Thesis, University of Massachusetts, Amherst, 1974.
11. G. C. Adams and R. S. Stein, J. Polym. Sci., A2, 6, 31 (1968).
12. R. J. Samuels, J. Polym. Sci., A2, 7, 1197 (1969).
13. R. S. Stein and P. R. Wilson, J. Appl. Phys. 33, 1914 (1962).
14. M. B. Rhodes. D. A. Keedy and R. S. Stein. J. Polym. Sci., 62, S73 (1972).
15. M. B. Rhodes and R. S. Stein, Symposium on Resinographic Methods, Special Technical Publication No. 348, 1963.
16. G. C. Adams, Ph.D. Thesis, University of Massachusetts, Amherst, 1966.
17. M. B. Rhodes and R. S. Stein, J. Polym. Sci., A-2, 7, 1539 (1969).
18. R. Yang and R. S. Stein, J. Polym. Sci., A-2, 5, 939 (1969).
19. C. Picot and R. S. Stein, J. Polym. Sci. 8, 2127 (1970).

20. D. Y. Yoon and R. S. Stein, J. Polym. Sci., Polym. Phys. Ed., 12, 763 (1974).

21. D. Y. Yoon and R. S. Stein, J. Polym. Sci., Polym. Phys. Ed., 12, 735 (1974).

22. R. J. Samuels, J. Polym. Sci., C, 13, 37 (1966).

23. N. Hayashi, Y. Murakami, M. Moritani, T. Hashimoto and H. Kawai, Polym. J. (Japan), 4, 560 (1973).

24. M. B. Rhodes and R. S. Stein, J. Appl. Phys. 32, 2344 (1961).

25. G. Adams and R. S. Stein, J. Polym. Sci., B, 541 (1967).

26. M. J. Wallach, J. Polym. Sci., C, 13, 69 (1966).

27. S. Clough, J. J. van Aartsen and R. S. Stein, J. Appl. Phys., 36, 3072 (1965).

28. R. S. Stein, P. Erhardt, J. J. van Aartsen, S. Clough and M. B. Rhodes, J. Polym. Sci., C, 13, 1 (1966).

29. J. J. van Aartsen and R. S. Stein, J. Polym. Sci., A-2, 9, 295 (1971).

30. T. Hashimoto, N. Hayashi, Y. Murakami and H. Kawai, Polym. J. (Japan), in press.

31. F. Norris and R. S. Stein, J. Polym. Sci., 27, 87 (1958).

32. E. H. Andrews, Proc. Roy. Soc. (London), A270, 232 (1962); J. Polym. Sci., A-2, 4, 668 (1966).

33. C. Ong and R. S. Stein, J. Polym. Sci., Polym. Phys. Ed., 12, 1899 (1974).

34. P. H. Geil, "Polymer Single Crystals," Interscience, New York, 1963.

35. A. Gent, J. Polym. Sci., P-A, 3, 3787 (1965).

36. F. deCandia and V. Vittoria, Makromol. Chem., 155, 17 (1972).

37. P. J. Flory, J. Chem. Phys. 15, 397 (1947).

38. W. R. Krigbaum and R. J. Roe, J. Polym. Sci., A, 2, 4394 (1964).

39. F. deCandia, G. Romano and V. Vittoria, J. Polym. Sci., Polym. Phys. Ed., 11, 2291 (1973).

40. H.-G. Kim and L. Mandelkern, J. Polym. Sci., A-2, 6, 181 (1968).

Captions for Figures

1) Schematic diagram of the photographic light scattering set-up.

2) (A) H_V light scattering patterns of PIP at different elongations. The arrow indicates the directions of both the polarizer and stretching. The length of the arrow is 5 cm. The sample-to-film distance, L, is 11 cm.

Photograph	Elongation Ratio, α	Exposure Time,*** t_{ex} (sec)
(a)	1.0	2
(b)	2.84	2
(c)	3.92	2
(d)	4.9	1.4
(e)	6.93	2

(B) V_V light scattering patterns of PIP at different elongations.

Photograph	α	t_{ex} (sec)***	Density Filter Used, d
(a)	1.0	1/100	1.0
(b)	2.84	1/100	1.0
(c)	3.92	1/100	1.0
(d)	4.9	1/100	1.0
(e)	6.93	2.0	3.0

3) H_V and V_V light scattering patterns of PBD at different elongations. L = 11 cm.

***Note: The exposure time was determined by an old shutter which may have malfunctioned. The intensity ratio given on page 184 was obtained by using a new shutter.

Photograph	α	t_{ex} (sec)***	d
(a)	1.0	1/100	0.6
(b)	1.0	1/100	1.8
(c)	3.4	1/25	0.6
(d)	3.4	1/100	1.2
(e)	6.5	4/25	0.6
(f)	6.5	1/100	1.2
(g)	7.5	1/100	-
(h)	7.5	1/100	0.9

4) Scattering intensity along θ direction at α = 6.0. μ is about 20^{o}. Sample-to-detector distance, 9 cm, and the length of the detector (corresponds to 500 channels) is 1.9 cm.

5) The variation of the scattering patterns of swollen sample stretched at room temperature. L = 11 cm.

Photograph	α_1	α_2	t_{ex} (sec)***	d
(a)	1.15	1.0	1/25	-
(b)	1.15	1.0	1/100	1.8
(c)	3.17	2.71	1/25	-
(d)	3.17	2.71	1/100	1.8
(e)	4.12	3.46	4/25	-
(f)	4.12	3.46	1/100	1.8
(g)	5.00	4.3	1/25	0
(h)	5.00	4.3	1/100	1.8

6) H_V and V_V scattering patterns after removal of the solvent by leaving the sample at room temperature for 2 days. L = 11 cm.

Photograph	t_{ex} (sec)***	d
(a)	4/25	-
(b)	1/100	1.8

7) H_V and V_V scattering patterns with different immersion oil. L = 11 cm. For H_V patterns t_{ex} = 1/100, d = 0.9. For V_V patterns t_{ex} = 1/100, d = 1.8.

8) V_V scattering patterns in a strain cycle. L = 11 cm.

9) The variation of H_V and V_V scattering with time and temperature. For H_V, t_{ex} = 1/60, d = 0.6. For V_V, t_{ex} = 1/125, d = 1.5.

10) (A) The variation of H_V scattering with temperature upon step-wise cooling. All photographs were taken under the same conditions except (d) d = 0.3, (e) d = 0.6 and (f) d = 0.6.

(B) The variation of V_V scattering with temperature upon step-wise cooling. All photographs were taken under the same conditions.

11) The variation of H_V and V_V scattering patterns at α = 3.5 with increase of temperature. For H_V, t_{ex}=1/60, d=0.5. For V_V, t_{ex}=1/125, d=2.1.

12) The variation of H_V and V_V scattering patterns for the sample stretched to α = 4.2 during heating. For H_V,t_{ex}=1/60,d=0.6. For V_V,t_{ex}=1/125,d=2.1.

13) The variation of transmitted intensity with temperature for the sample stretched to α = 4.0.

14) The variation of transmitted intensity with temperature for the sample stretched to α = 5.0.

15) The calculated melting temperatures from Equations (11) and (12) designated as Flory and K-R, respectively. The crossed point indicates the temperature at which no scattering was obtained for the sample stretched at α = 3.5.

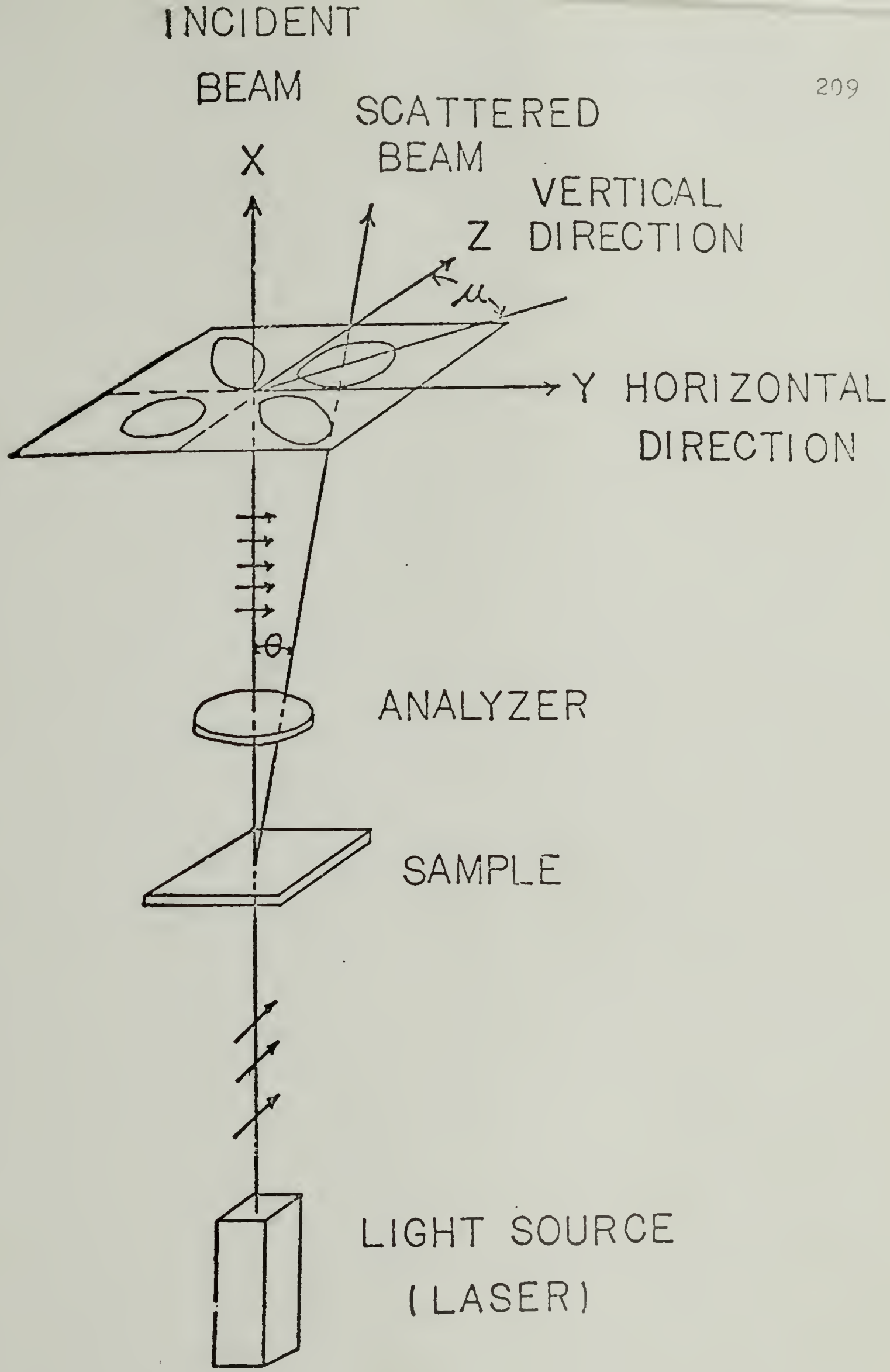
INCIDENT
BEAM
SCATTERED
BEAM
X
VERTICAL
Z DIRECTION
Y HORIZONTAL
DIRECTION
ANALYZER
SAMPLE
LIGHT SOURCE
(LASER)

Figure 1

(a) $\alpha = 1.0$

(b) $\alpha = 2.84$

(c) $\alpha = 3.92$

(d) $\alpha = 4.9$

(e) $\alpha = 6.03$

Figure 2 (A)

V_V

(a) $\alpha = 1.0$ (b) $\alpha = 2.84$ (c) $\alpha = 3.92$

(d) $\alpha = 4.9$ (e) $\alpha = 6.93$

Figure 2 (b)

H_V V_V

(a) α=1.0 (b)

(c) α=3.4 (d)

(e) α=6.5 (f)

(g) α=7.5 (h)

Figure 3

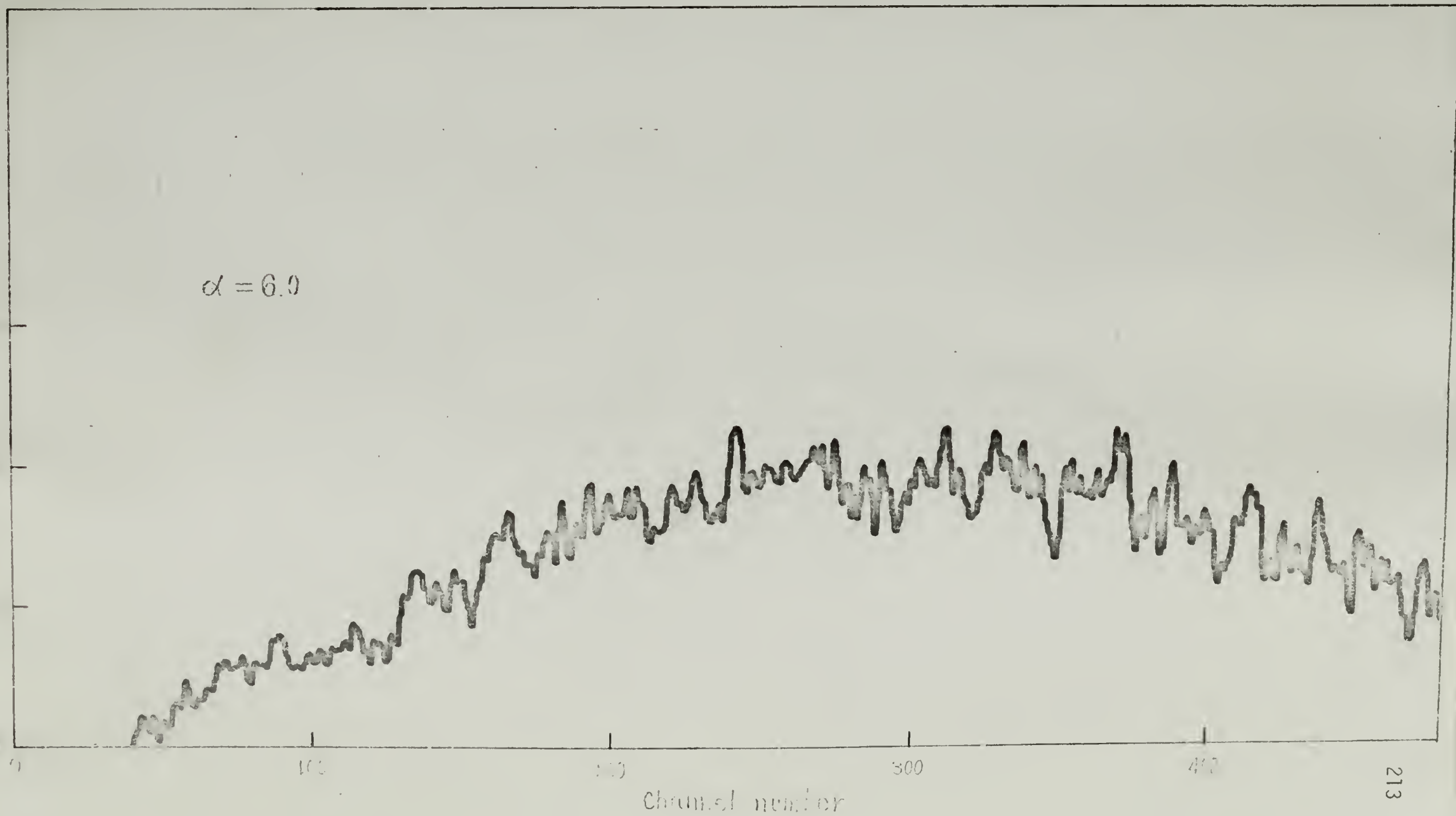

Figure 4

H_V V_V

α_1=1.15

(a) (b)

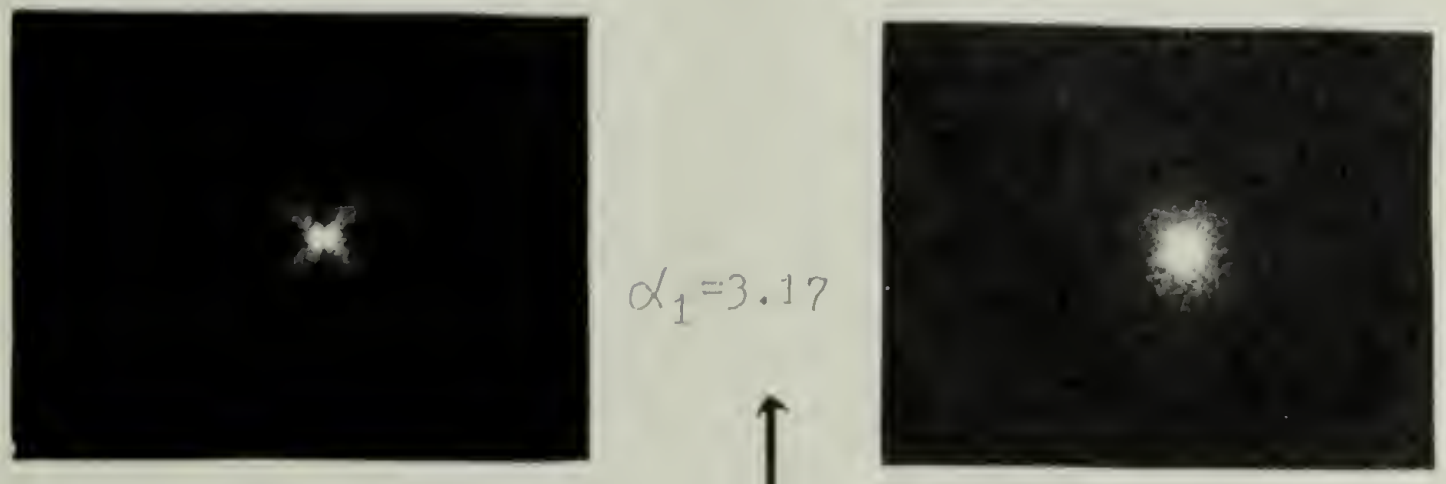

α_1=3.17

(c) (d)

α_1=4.12

(e) (f)

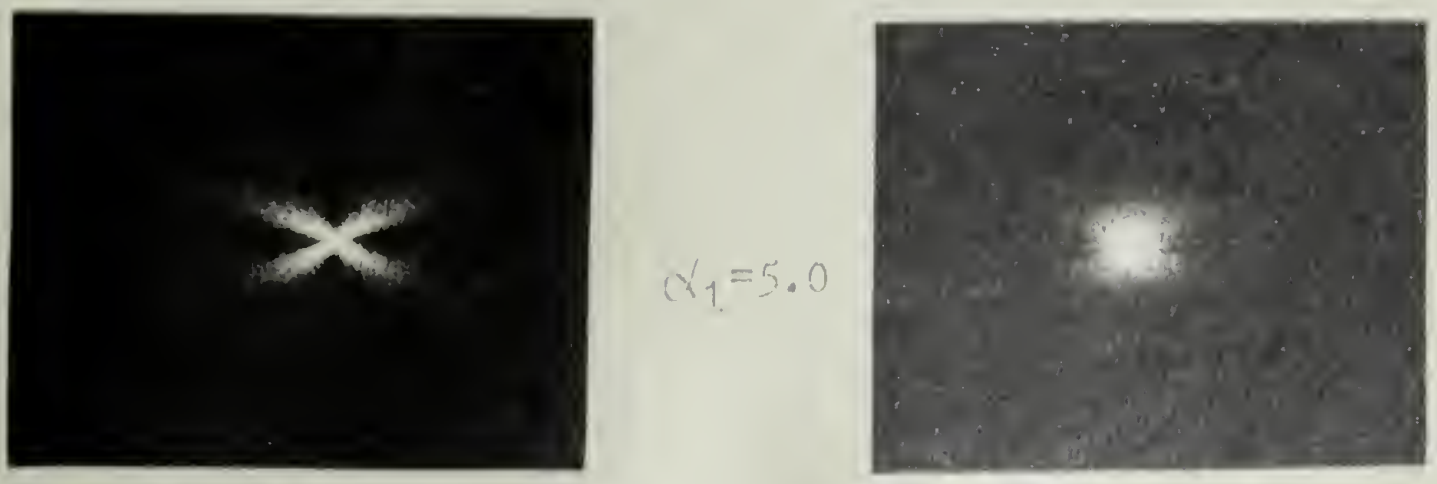

α_1=5.0

(g) (h)

H_V

$\alpha_1 = 4.12$

V_V

Figure 6

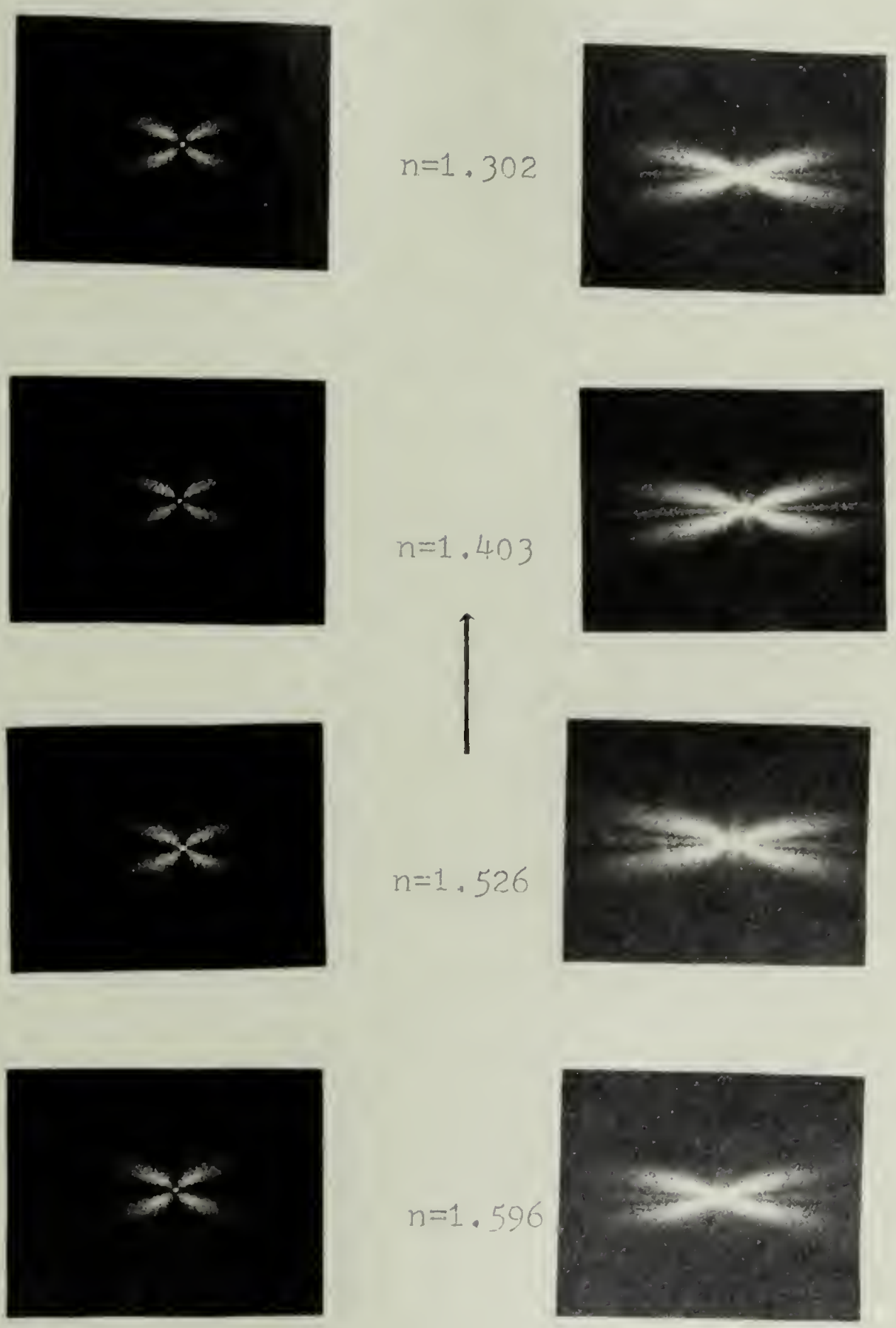

Figure 7

v_V

(a) $\alpha = 3.8$

(b) $\alpha = 5.0$

(c) $\alpha = 4.3$

(d) $\alpha = 3.7$

(e) $\alpha = 3.1$

(f) $\alpha = 2.7$

Figure 8

$\alpha = 4.3$

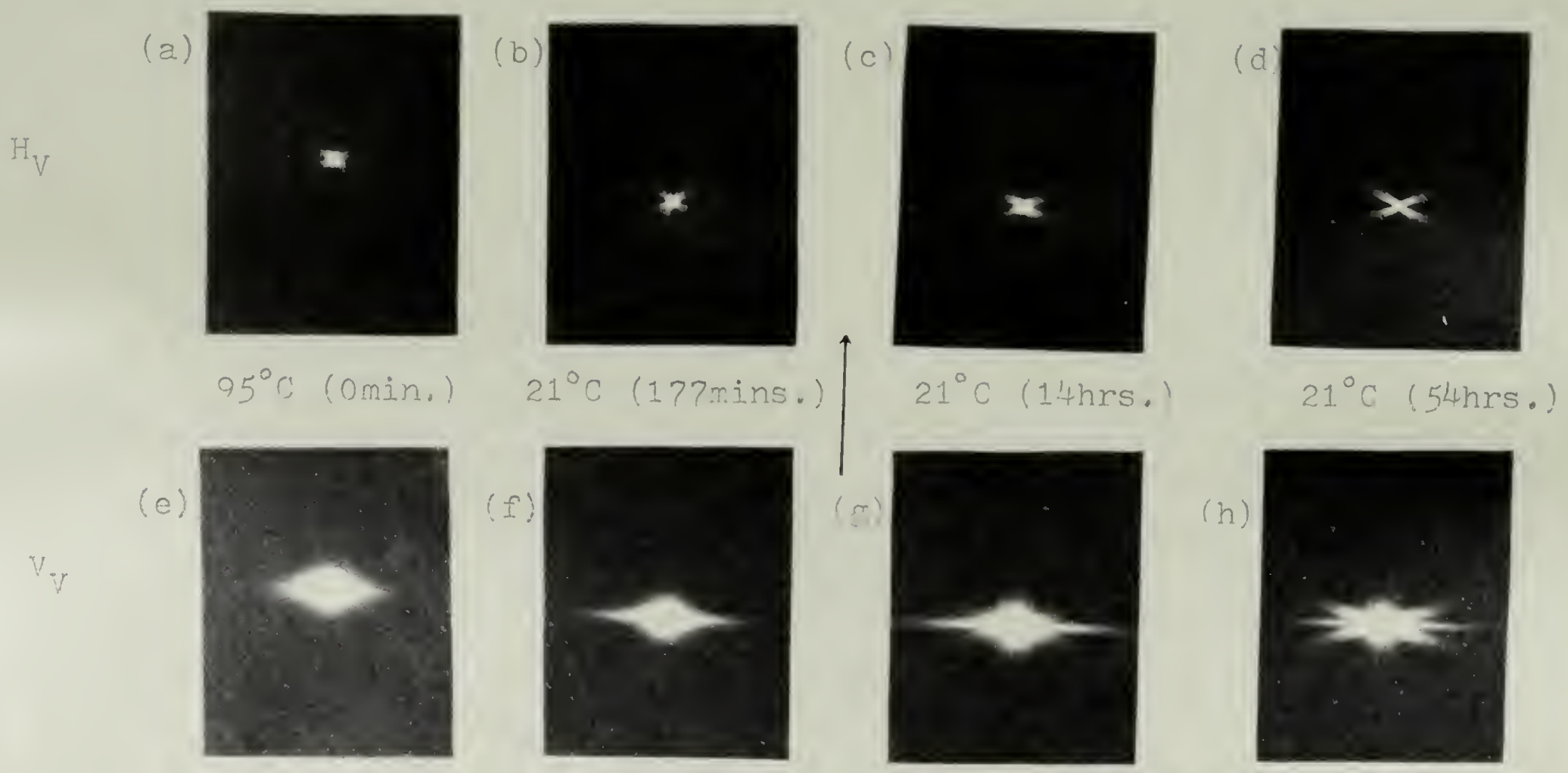

Figure 9

H_y

(a) 110°C (b) 90°C (c) 75°C

(d) 50°C (e) 40°C (f) 35°C

Figure 10 (A)

v_v

(a) 110°C (b) 90°C (c) 75°C

(d) 50°C (e) 40°C (f) 35°C

Figure 10 (B)

$\alpha = 3.5$

(a) (b) (c) (d)

H_V

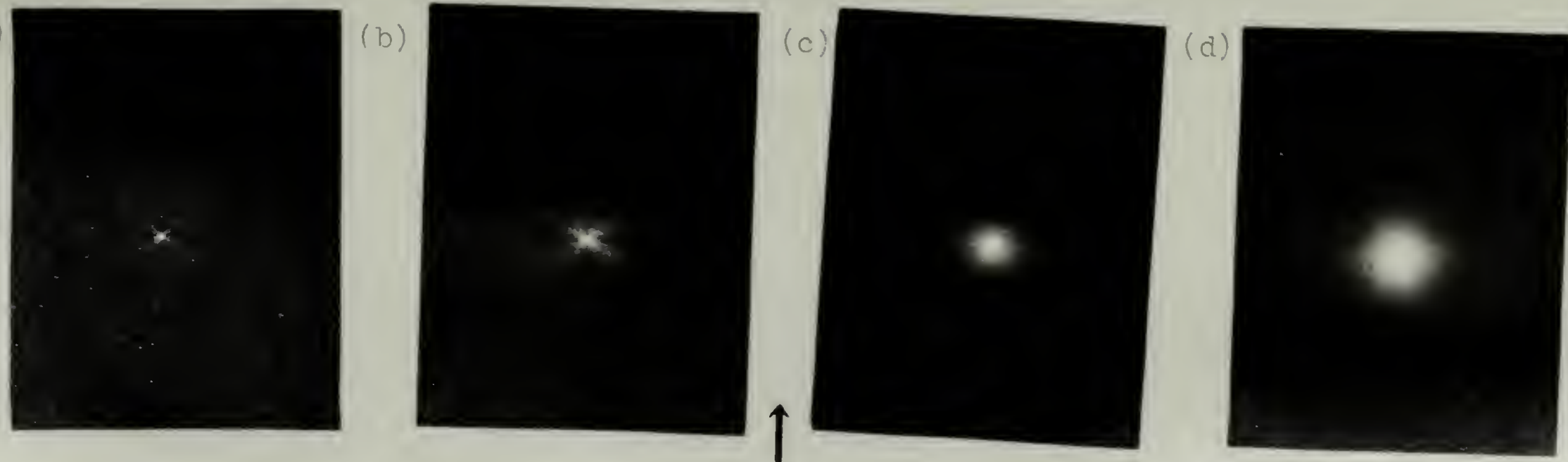

22°C 50°C 80°C 87°C

(e) (f) (g) (h)

V_V

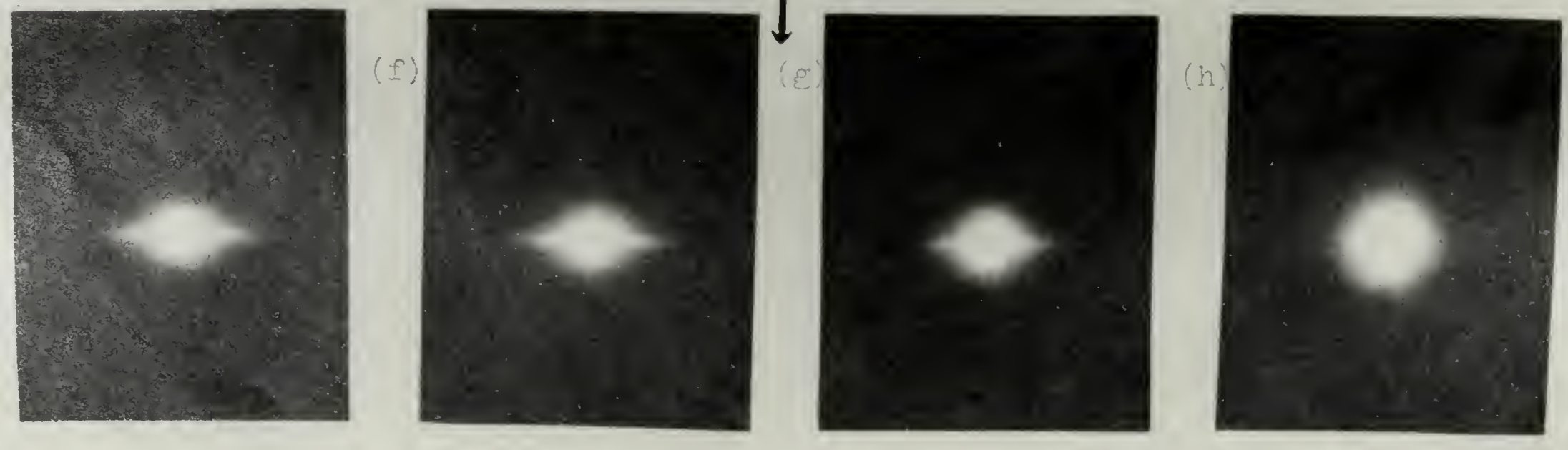

Figure 11

$\alpha' = 4.2$

(a)

(b)

(c)

(d)

V_V

25°C

55°C

80°C

105°C

(e)

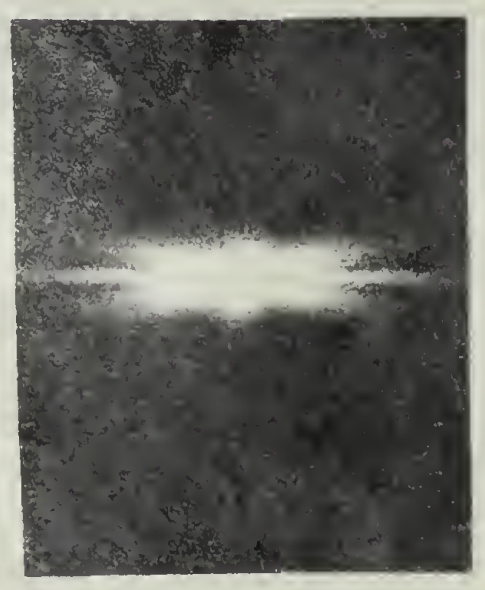

(f)

(g)

(h)

V_V

Figure 12

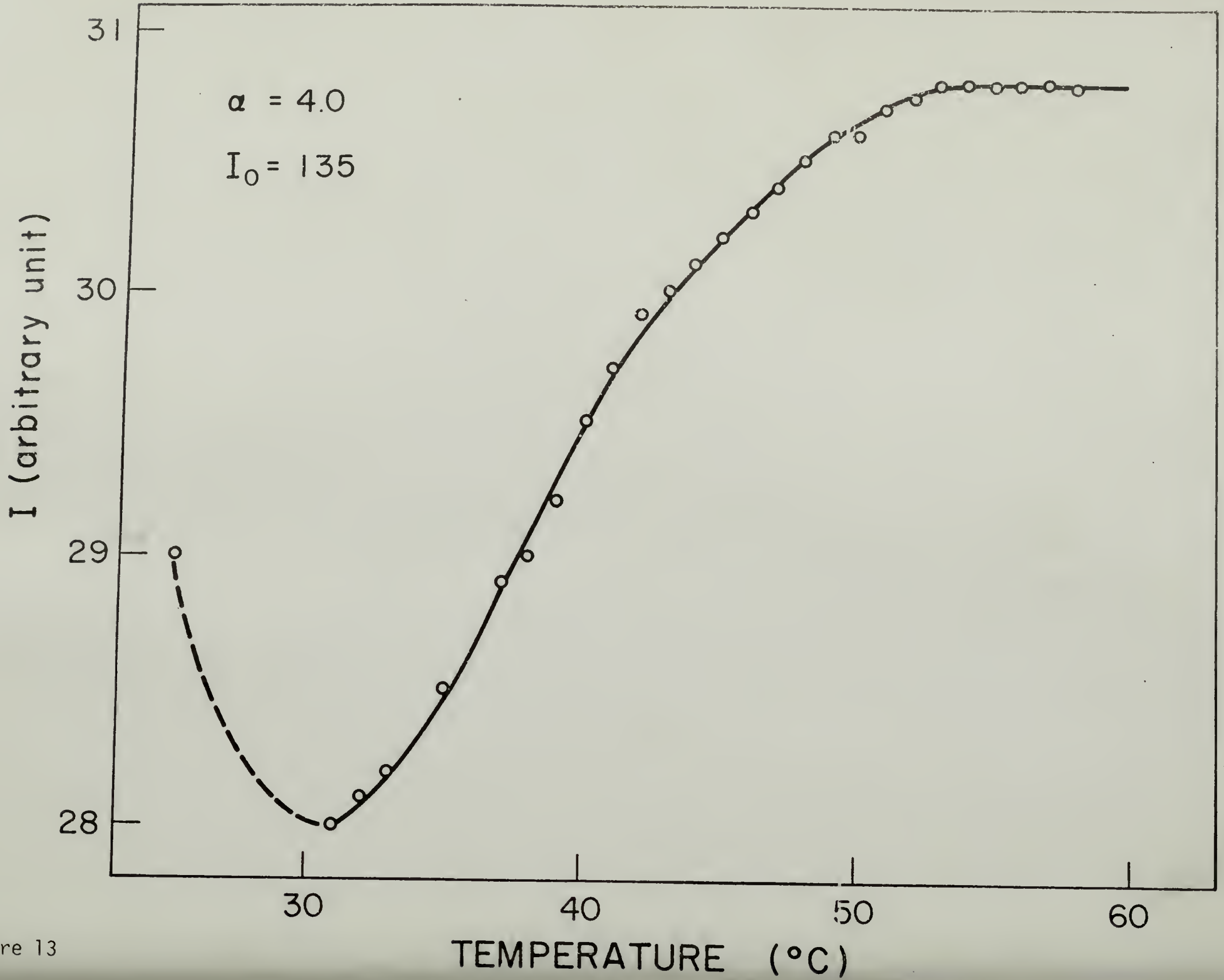
α = 4.0
I_0 = 135
I (arbitrary unit)
31
30
29
28
30
40
50
60
TEMPERATURE (°C)

Figure 13

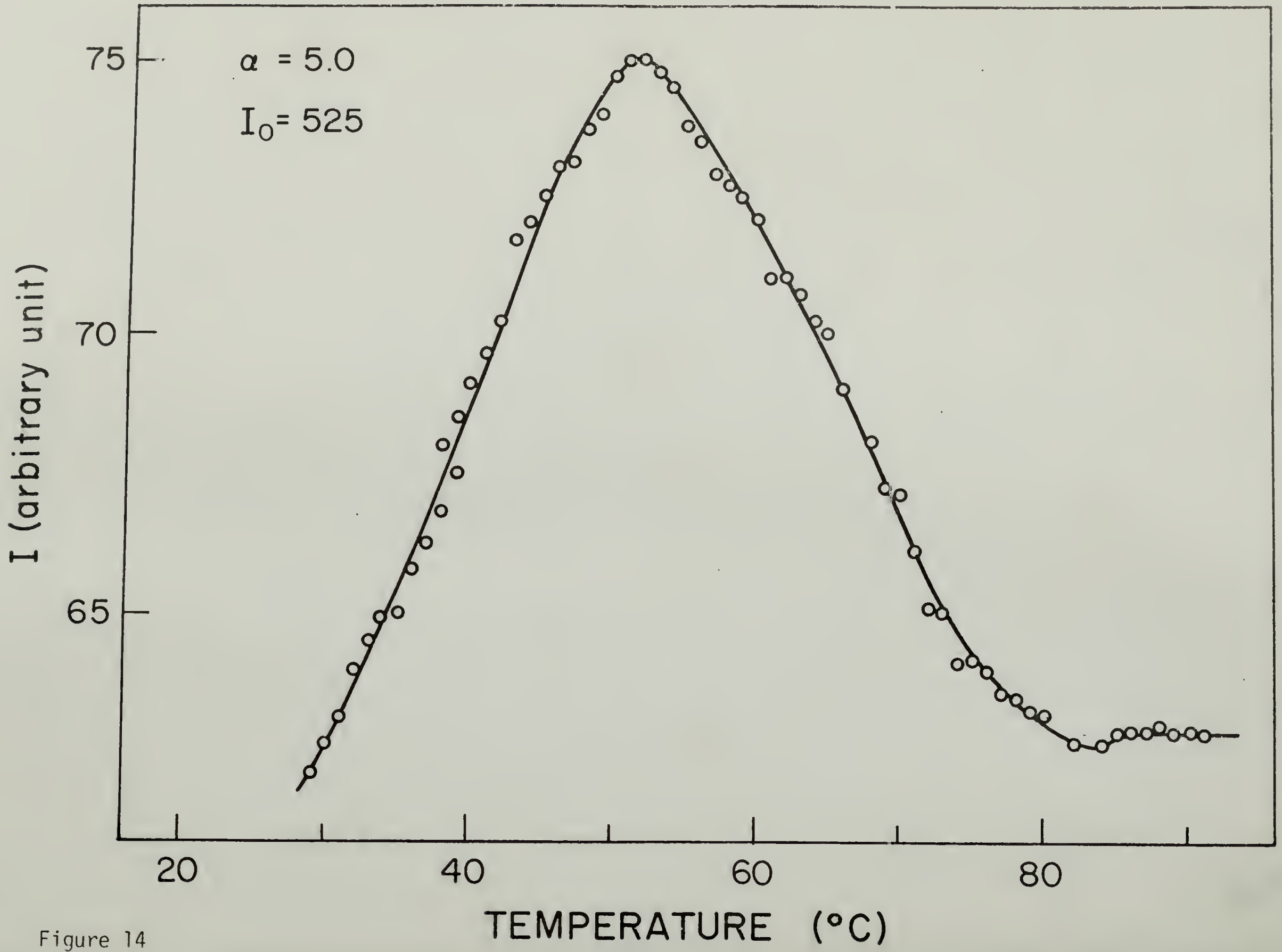

Figure 14

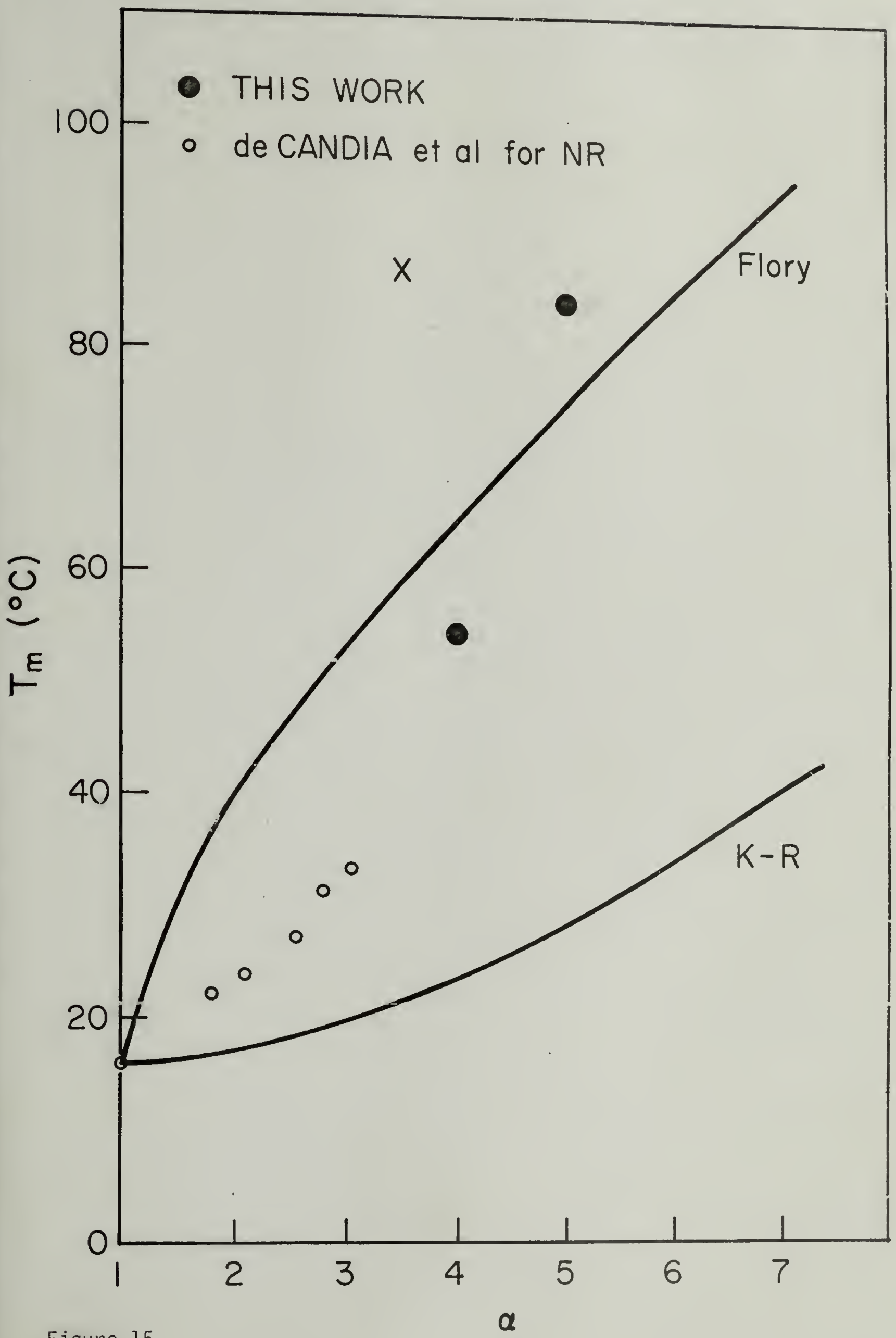
THIS WORK
de CANDIA et al for NR
X
Flory
K-R
100
80
60
40
20
0
T_m (°C)
1
2
3
4
5
6
7
α

Figure 15

APPENDIX I

Calculation of Crystal Intrinsic Birefringence of Cis-1,4-Polyisoprene

The conformation of the molecules in the crystalline unit cell is considered to be different from that in the amorphous phase. Bunn (1) and Nyburg (2) have investigated the molecular structure of the crystalline state of natural rubber.

From an examination of the diffraction data, Bunn (1,3) choses the basic type (b) in Figure 1. The final form is represented in Figure 2. It is to be noted that the bond lengths and valence angles diverge considerably from the normal value and that isoprene units are non-planar, especially with respect to the methyl group, which are some 23° out of the general plane of the remaining four carbon atoms. Finally the two adjacent isoprene units are themselves quite different from each other. Bunn favors a monoclinic cell, having the dimensions

$$a = 12.46\ \text{Å} \quad b = 8.89\ \text{Å} \quad C\ (\text{fiber axis}) = 8.10\ \text{Å} \quad \beta = 92°$$

The proposed cell contains four molecular chains running parallel to the c axis. The repeat distance along the chain axis contains two isoprene units. There are, therefore, eight isoprene units in the unit cell. In Table I the coordinates of carbon atoms and hydrogen atoms in a unit cell are given. For calculating the coordinates of hydrogen atoms it is assumed that the distance of C-H bond is 1.07 Å and that the angle for the tetrahedrally hybridized carbon is 109 1/2°.

Nyburg (2,3) in a later investigation proposed a structure in which the molecules have a conventional configuration but in which any given site may be occupied by either a "left-handed" or a "right-handed" molecule - the left-handed being the mirror image of the right-handed as shown in Figure 3. The unit cell dimensions and the arrangement of the molecules in the unit cell correspond closely to Bunn's model. From these basic concepts Nyburg finally obtained the best agreement with the observed intensities of the diffraction pattern by small variations of the atomic coordinates. His final structure is shown in Figure 1 (c). In Nyburg's structure the isoprene unit, including the methyl group, is strictly planar, and the two isoprene units in the repeating pattern are identical in their bond structure. The middle C-C bond, which is abnormally short, is rotated out of the plane of the isoprene unit by 58°. The final structure is shown in Figure 19 and the coordinates of each atom are given in Table II. For this calculation H_3 in Figure 1 is assumed to be on the plane which the five carbon atoms make and the angle $C_2C_3H_3$ is taken as 118° and the other assumptions are the same as Bunn's case.

The components of polarizability, β_{xx}, β_{yy}, β_{zz} for each monomer unit with respect to a set of coordinate axes OX, OY and OZ, respectively, (where OZ is taken as the direction of chain axis), may be calculated by using the standard equations for the transformation of the polarizability tensors (4) for the individual bond and summing over all bonds. These equations are given as

$$b_{xx} = \xi_\ell \cos^2\theta + \xi_t \sin^2\theta \qquad (1)$$

$$b_{yy} = (\xi_\ell - \xi_t) \sin^2\theta \cos^2\phi + \xi_t \qquad (2)$$

$$b_{zz} = (\xi_\ell - \xi_t) \sin^2\theta \sin^2\phi + \xi_t \quad (3)$$

$$\beta_{xx} = \sum b_{xx} \quad (4)$$

$$\beta_{yy} = \sum b_{yy} \quad (5)$$

$$\beta_{zz} = \sum b_{zz} \quad (6)$$

where ξ_ℓ is the longitudinal bond polarizability, ξ_t is the transverse bond polarizability, θ is the angle between the bond and X axis, ϕ is the angle between the Y axis and the projection of the bond on the YZ plane.

There have been reported several sets of bond polarizabilities, i.e., those of Bunn (5), Vuks (6), Denbigh (7), and of Clement and Bothorel (8). Their values are shown in Table III.

Bunn's values for a C-C bond were obtained from the values of the three refractive indices of n-paraffin. These values, however, are incorrect because of the use of Lorenz-Lorentz internal field as Volkenstein (10) has argued quite convincingly and as shown by Hong et. al (11). By introducing quite simplified assumptions on the internal field of crystalline paraffins, Vuks has obtained bond polarizabilities from the same experimental data as those used by Bunn and Daubeny (12). His calculation may, however, not be exact as Volkenstein has also mentioned (10). Denbigh's values were obtained from the molecular refractions and the Kerr constants of a number of simple compounds investigated in the gas phase. Clement and Bothorel's results were obtained from the depolarization ratios of Rayleigh scattering of pure liquids.

Stein et. al (13) has reported a better agreement between experimental and theoretical birefringence of polypropylene crystal when Denbigh's values were used than when Bunn's were used. Nagai and Ishikawa (14) favored the values of Clement and Bothorel on the study of stress-optical coefficient.

In many papers (9,10,13,14) Bunn's values seem to be discarded or at least not to be suitable to calculate theoretical birefringence from. In this work, therefore, we shall not use Bunn's bond polarizabilities. Although Denbigh's values are mainly used in this work, at present there seems little justification for the choice of Denbigh's value rather than others, as mentioned by Treloar (3). This problem will be discussed in Chapter 2.

The values of β_{xx}, β_{yy} and β_{zz} were calculated from Equations (1)-(6) and given in Table IV for Bunn's model and in Table V for Nyburg's model. The mean anisotropy of polarizability for a repeating unit in the crystal, $(b_\ell - b_t)^o_c = \beta_{zz} - (\beta_{xx} + \beta_{yy})/2$, was also calculated and given in Tables IV and V.

The crystal intrinsic birefringence, Δ^o_c, may be calculated using the differential Lorentz-Lorenz equation (15,16)

$$\Delta^o_c = \frac{2\pi}{9} \frac{(\bar{n}^2 + 2)^2}{\bar{n}} \frac{(b_\ell - b_t)^o_c}{V} \qquad (7)$$

where $\bar{n}$ is the average refractive index of the material and V is the volume per repeating unit. The calculated values of Δ^o_c are given in Table VI.

Since Nyburg's model for PIP crystal is newer and appears to be more reasonable than the Bunn model, the former is used in this work. As for the bond polarizabilities, Denbigh's values, and Clement and Bothorel's values are in general favored in many papers (9,10,13,14).

Calculation of Crystal Intrinsic Birefringence of Cis-1,4-Polybutadiene

The crystal structure of cis-1,4-polybutadiene has been studied by Natta and Corradini (17). Their study shows that the crystal unit cell is monoclinic and that its dimensions are a = 4.60 Å, b = 9.50 Å, c = 8.60 Å (fiber axis) and β = 109°. There are 4 monomer units per unit cell. The model proposed is shown in Figure 4. The atomic coordinates in a unit cell are given in Table VII.

From Equations (1)-(6) we obtained the following values using Denbigh's bond polarizabilities.

$$\beta_{xx} = 6.032, \quad \beta_{yy} = 7.118, \quad \beta_{zz} = 9.221$$

The mean anisotropy of polarizability for monomer unit, $(b_\ell - b_t)^o_c = \beta_{zz} - (\beta_{xx} + \beta_{yy})/2$, is equal to 2.646×10^{-24} cm^{-3}.

In this case the differential Lorentz-Lorenz equation may not be a good approximation for Δ^o_c, because the difference of the polarizabilities is relatively large. Therefore, the original Lorentz-Lorenz equation may be used.

$$\frac{n_i^2 - 1}{n_i^2 + 2} = \frac{4\pi}{3} P_i \qquad (8)$$

where n_i is the refractive index along i direction and P_i is the polarizability along i direction per unit volume. By using Equation (8) we obtain

$$\Delta^o_c = n_z - \frac{n_x + n_y}{2} = 0.286$$

The Optical Intrinsic Birefringences of Other Rubber-Like Polymers

Δ_c^o of syndiotactic 1,2-polybutadiene (SPBD) was also calculated to compare its value with those of PIP and cis-polybutadiene. The crystal structure of SPBD has been studied by Natta and Corradini (18). The unit cell is orthohombic and its dimensions are a = 10.98 Å, b = 6.60 Å and C (fiber axis) = 5.14 Å. There are four monomers per unit cell. In the same manner described before the intrinsic birefringence was calculated using Denbigh's bond polarizabilities as

$$\beta_{xx} = 6.791 \times 10^{-24} \text{ cm}$$

$$\beta_{yy} = 8.076 \times 10^{-24} \text{ cm} \qquad \text{(per monomer unit)}$$

$$\beta_{zz} = 7.504 \times 10^{-24} \text{ cm}$$

$$\Delta_c^o = 0.0054$$

The value of Δ_c^o of SPBD is remarkably small as compared with those of PIP and PBD because the C=C bond of SPBD is almost parallel to OY axis, i.e. b axis, and because there is little contribution of polarizability of the bond to Z direction, i.e. c axis.

The calculated and experimental values of Δ_c^o of several polymers are shown in Table VIII.

Most of the values presented here are obtained by using the Lorentz-Lorenz internal field which is described by Equation (7) or (8). The

Lorentz-Lorenz field may, however, not be a good approximation for the actual internal field in the crystal as pointed out by several workers (10,11,24). This problem will be discussed in detail in Chapter II.

References

1. C. W. Bunn, Proc. Roy. Soc., A180, 40 (1942).
2. S. C. Nyburg, Acta Crystl., 7, 385 (1954).
3. L. R. G. Treloar, The Physics of Rubber Elasticity, Oxford, 1958.
4. D. W. Saunders, Trans. Faraday Soc., 53, 860 (1957).
5. C. W. Bunn, Chemical Crystallography, Oxford Clarenedon Press, 1961.
6. M. F. Vuks, Optika Spectroskopiya, 2, 494 (1957).
7. K. G. Denbigh, Trans. Faraday Soc., 36, 936 (1940).
8. C. Clement and P. Bothorel, J. Chem. Phys., 61, 878 (1964).
9. R. J. Morgan and L. R. G. Treloar, J. Polym. Sci., A-2, 10, 51 (1972).
10. M. V. Volkenstein, Configurational Statistics of Polymeric Chains, Interscience, New York, 1963.
11. S. D. Hong, C. Chang and R. S. Stein, J. Polym. Sci., Polym. Phys. Ed., 13, 1447 (1975).
12. C. W. Bunn and R. Daubeny, Trans. Faraday Soc., 50, 1173 (1954).
13. D. A. Keedy, J. Powers and R. S. Stein, J. Appl. Phys., 31, 1911 (1960).
14. T. Ishikawa and K. Nagai, J. Polym. Sci., A-2, 7, 1123 (1969).
15. H. A. Lorentz, The Theory of Electrons, Dover, New York, 1952.
16. L. Lorenz, Ann. Physik, 11, 70 (1880).
17. G. Natta and P. Corradini, Nuovo Cimento, Suppl. Vol. XV, 11 (1960).
18. G. Natta and P. Corradini, J. Polym. Sci., 20, 251 (1956).
19. R. S. Stein, "Rheo-Optical Studies of Rubbers," in press.
20. Y. Akana, M.S. Thesis, University of Massachusetts, Amherst, Mass. (1973).
21. T. K. Su and R. S. Stein, Bull. Am. Phys. Soc., Ser. II, 20, 340 (1975).

22. T. Kokubo and R. S. Stein, in preparation.

23. G. Kraus and J. T. Gruver, J. Polym. Sci., Polym. Phys. Ed., 10, 2009 (1972).

24. R. S. Stein, J. Polym. Sci., A-2, 7, 1021 (1969).

TABLE I

Numerical Values for Atom Coordinates
for Bunn's Model of the Crystal of PIP

Atom	x	y	z
C_1	9.432	7.414	-0.202
C_2	8.211	8.045	0.421
C_3	8.024	7.770	1.742
C_4	9.270	7.414	2.641
C_5	6.629	7.361	2.171
C_6	9.283	8.526	3.702
C_7	10.529	8.045	4.390
C_8	10.641	7.690	5.694
C_9	9.382	7.992	6.496
C_{10}	12.061	7.788	6.261
H_1	10.311	7.766	0.299
H_2	9.301	6.352	-0.248
H_3	7.534	8.654	-0.101
H_4	9.103	6.469	3.115

H_5	10.160	7.474	2.049
H_6	6.629	6.330	2.454
H_7	6.320	7.960	3.002
H_8	5.947	7.510	1.360
H_9	8.445	8.405	4.357
H_{10}	9.476	9.467	4.643
H_{11}	11.419	8.110	3.773
H_{12}	9.239	9.050	6.501
H_{13}	8.530	7.606	5.980
H_{14}	12.061	7.457	7.281
H_{15}	12.394	8.803	6.216
H_{16}	12.718	7.170	5.686

TABLE II

Numerical Values for Atom Coordinates
for Nyburg's Model of the Crystal of PIP

Atom	x	y	z
C_1	3.078	1.129	1.725
C_2	1.807	1.342	2.479
C_3	1.881	1.662	3.815
C_4	3.177	1.876	4.536
C_5	0.399	1.218	1.904
H_1	3.916	1.475	2.335
H_2	3.189	0.073	1.504
H_3	0.980	1.761	4.357
H_4	3.297	2.924	4.751
H_5	3.988	1.527	3.923
H_6	0.000	0.242	2.144
H_7	-0.230	1.972	2.333
H_8	0.436	1.333	0.841

TABLE III

Bond Polarizabilities ($\times 10^{-24}$ cm^3)

Bond	C-H		C-C		C=C	
Set	ξ_ℓ	ξ_t	ξ_ℓ	ξ_t	ξ_ℓ	ξ_t
Bunn	0.82	0.60	0.97	0.26	2.90	1.07
Vuks	0.71	0.62	1.47	0.06	2.82	1.05
Denbigh*	0.79	0.58	1.88	0.02	2.93	0.99
Clement and Bothorel	0.81	0.59	1.46	0.04	3.69	0.66

*Note: One small modification has been introduced for the C=C (aliphatic) bond by Morgan and Treloar (9). In deriving his values, Denbigh assumed a value of 125° between the C=C and C-H bond in ethylene compared with the now generally accepted value of 120°. Recalculation on the basis of 120° angle gives the corrected values of ξ_ℓ and ξ_t in Table III.

TABLE IV

The Value of β_{xx}, β_{yy} and β_{zz} for
Bunn's Model of the Crystal Structure of PIP
(Per Two Monomer Units)
($\times 10^{-24}$ cm^3)

Set of Polarizabilities	β_{xx}	β_{yy}	β_{zz}	$(\beta_\ell - \beta_t)_c^0 = \beta_{zz} - \frac{\beta_{xx} + \beta_{yy}}{z}$
Vuks	19.116	14.866	19.778	2.787
Denbigh	20.574	15.057	20.696	2.882
Clement and Bothorel	18.393	14.462	21.324	4.897

TABLE V

The Values of β_{xx}, β_{yy}, β_{zz} for
Nyburg's Model of the Crystal Structure of PIP
(Per Monomer Unit)
($\times 10^{-24}$ cm^3)

Set of Polarizabilities	β_{xx}	β_{yy}	β_{zz}	$(\beta_\ell - \beta_t)_c^0 = \beta_{zz} - \frac{\beta_{xx} + \beta_{yy}}{2}$
Vuks	9.788	7.101	10.069	1.625
Denbigh	10.535	7.116	10.536	1.711
Clement and Bothorel	9.365	6.840	10.820	2.717

TABLE VI

The Values of the Crystal Intrinsic Birefringence, Δ_C^O

Set of Polarizability	Bunn's Crystal Model	Nyburg's Crystal Model
Vuks	0.106	0.123
Denbigh	0.110	0.130
Clement and Bothorel	0.186	0.207

TABLE VII

Numerical Values for Atom
Coordinates in the Crystal Unit Cell of Cis-1,4-Polybutadiene

Atom	x	y	z
C_1	-0.487	0.0	-0.589
C_2	0.487	0.0	0.589
C_3	0.200	1.207	1.505
C_4	-0.200	1.207	2.795
C_5	-0.487	0.0	3.711
H_1	0.374	-0.906	1.147
H_2	1.491	0.061	0.223
H_3	0.337	2.178	1.057
H_4	-0.337	2.178	3.244
H_5	-0.374	-0.906	3.153
H_6	-1.491	0.061	4.077

TABLE VIII (19)

Some Calculated Values of Δ_c^o
(Intrinsic Birefringence of Polymer Crystals)

Polymer	Δ_c^o
Polyethylene (12)	0.059
Cis-1,4-Polyisoprene	0.130
Cis-1,4-Polybutadiene	0.286
Syndiotactic-1,2-Polybutadiene	0.0054
Trans-1,4-Polybutadiene (Mod. II) (20)	0.183
Poly-N-Vinyl Carbazole (21)	-0.457
Polyvinyl Chloride (22)	0.089
t-Polypentenomer (23)	0.268

Captions for Figures

1) Basic structure of cis-1,4-polyisoprene molecule (3). (a) Projection normal to plane of isoprene unit. (b,c) Alternative projections parallel to plane of isoprene unit.

2) Configuration of rubber molecule in crystal, seen from two different viewpoints, based on Bunn's model (1). (Bond length in Å).

3) Nyburg's model (2). (a) Isolated molecule. (b) Mirror-related pair of molecules.

4) The crystal structure of cis-1,4-polybutadiene (17).

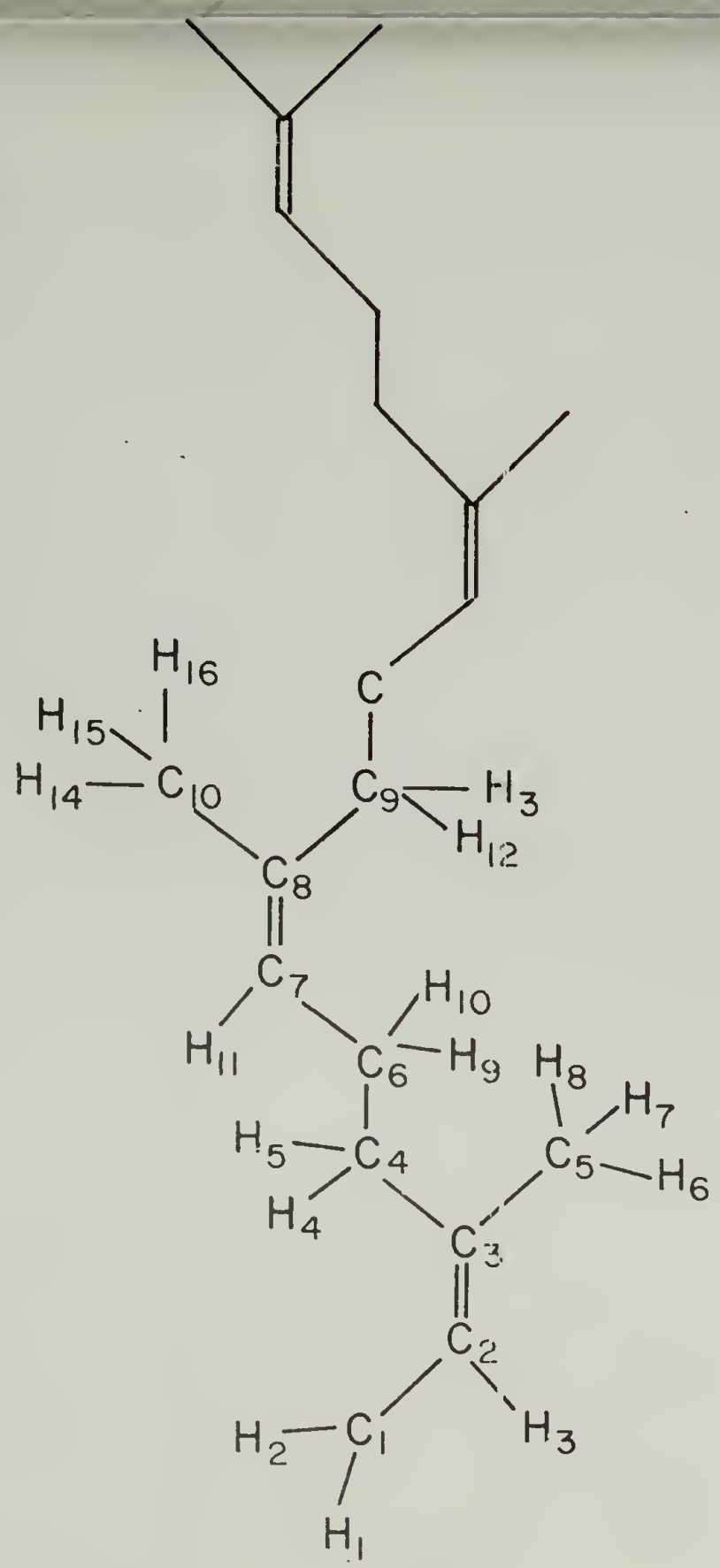
H16
H15
H14
C10
C
C9
H3
H12
C8
C7
H10
H11
C6
H9
H8
H7
H5
C4
C5
H6
H4
C3
C2
H2
C1
H3
H1

(a)

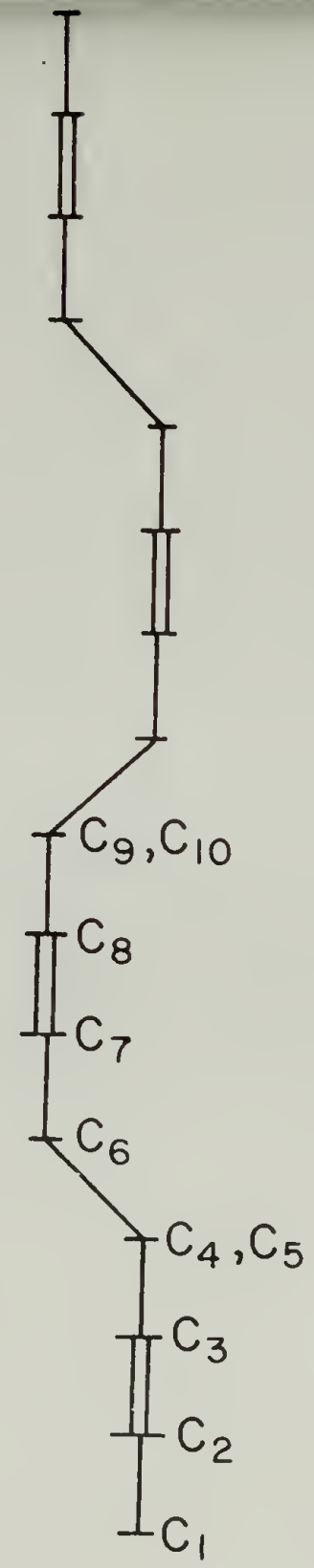
C9,C10
C8
C7
C6
C4,C5
C3
C2
C1

(b)

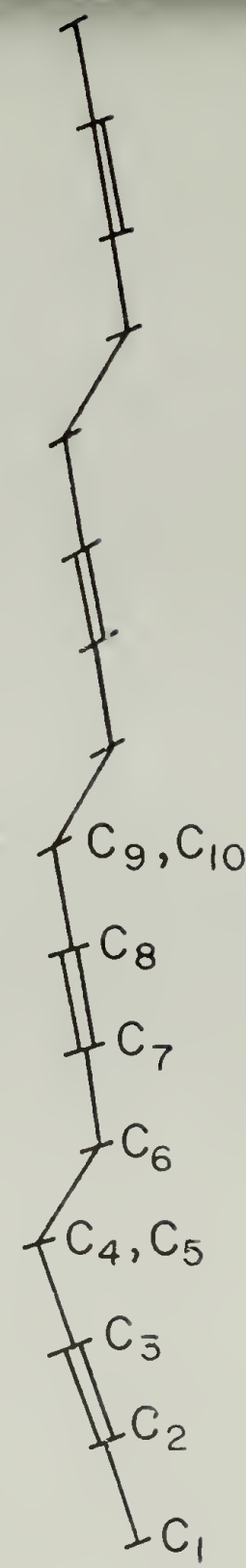
C9,C10
C8
C7
C6
C4,C5
C3
C2
C1

(c)

Figure 1

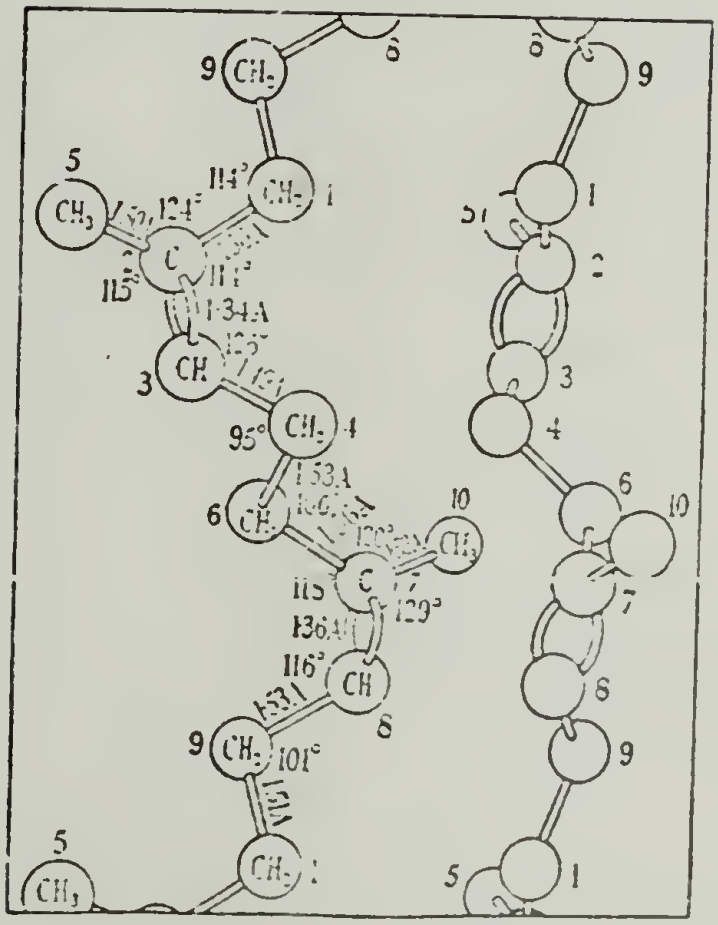
9
CH₂
8
5
CH₃
114°
CH₂
1
124°
C
115°
111°
1.34A
3
CH
95°
CH₂
4
1.53A
6
CH₂
10
CH₃
115
C
129°
1.36A
116°
CH
1.53A
8
9
CH₂
101°
1.51A
5
CH₃
CH₂
1
8
9
1
2
3
4
6
10
7
8
9
5
1

Figure 2

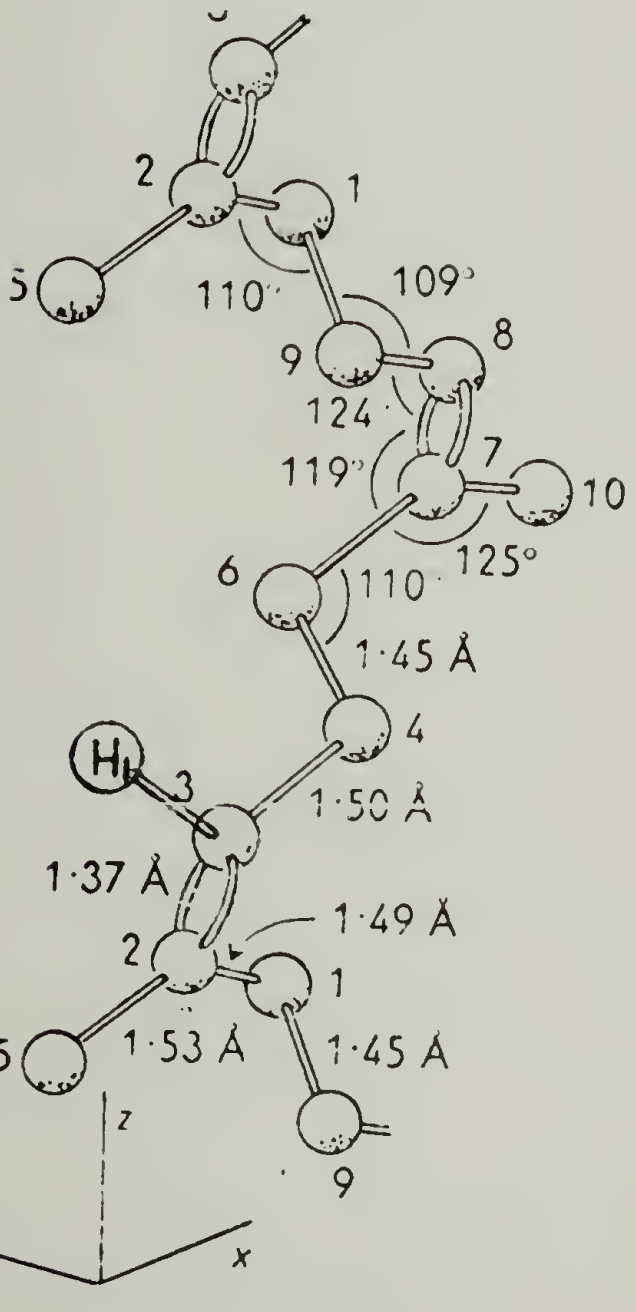
2
1
5
110°
109°
9
8
124°
119°
7
10
6
110°
125°
1·45 Å
4
H
3
1·50 Å
1·37 Å
1·49 Å
2
1
5
1·53 Å
1·45 Å
z
9
y
x

(a)

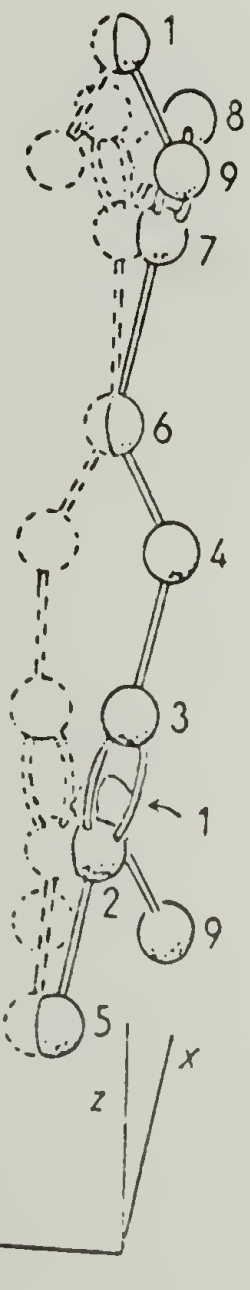
1
8
9
7
6
4
3
1
2
9
5
z
x
y

(b)

Figure 3

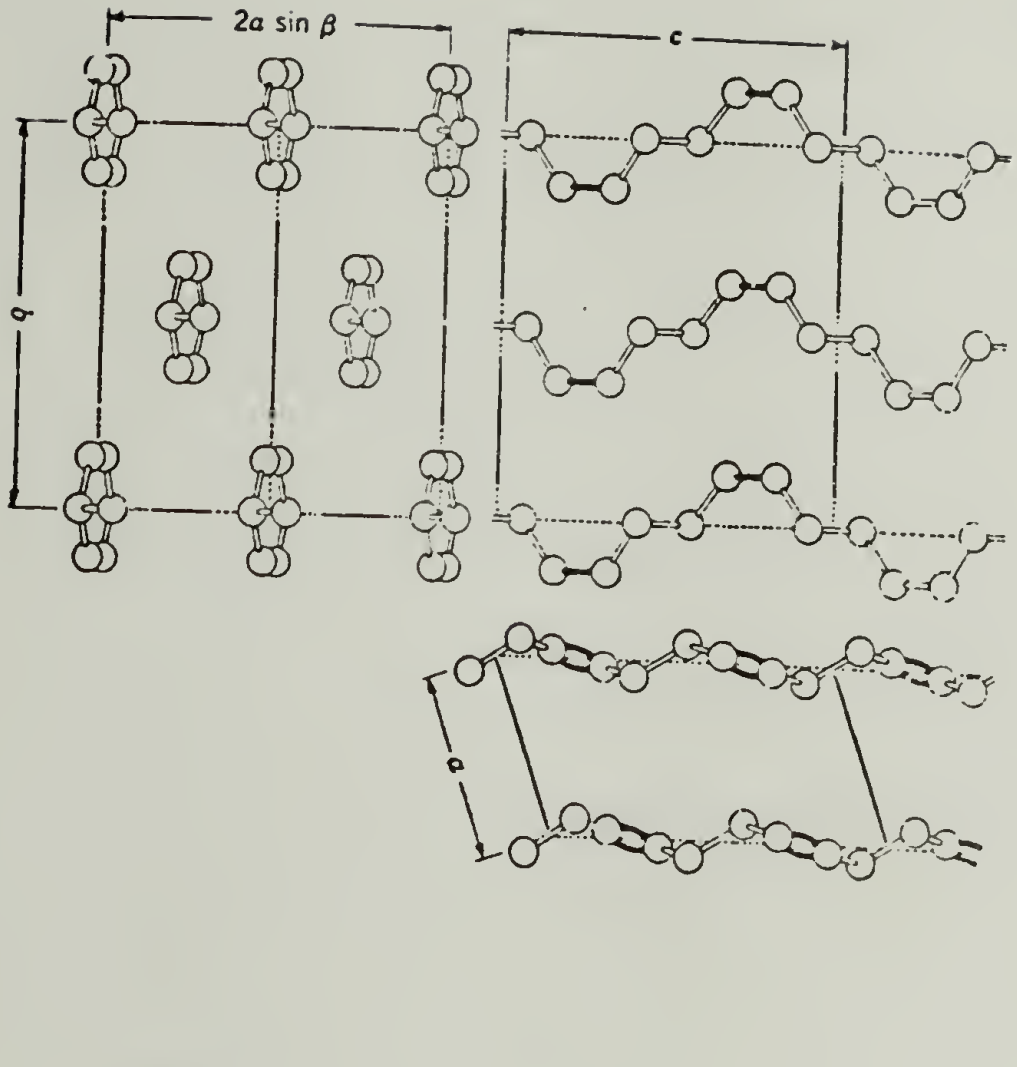

Figure 4

APPENDIX II

Thermal Effects of Extension and Crystallization

Heat Generation on Extension

The fact that when rubber is stretched rapidly its temperature rises has been known for a long time (1,2). If stress-induced crystallization occurs following rapid stretching of a rubber sample to a certain length, the kinetics of the crystallization may be affected by the temperature rise of the sample due to the rapid extension. The rate of crystallization strongly depends upon the crystallization temperature T_c, especially if T_c is near the melting temperature. For an example, it has been reported that (3) for a linear polyethylene the rate of crystallization at 125°C is 60 times higher than that at 129°C. Consequently an estimation of the temperature rise on rapid stretching may be useful to consider its effects on the crystallization.

This phenomenon can be described by thermodynamics. The second law of thermodynamics is represented by an equation (4)

$$dE = dQ + dW \qquad (1)$$

In a reversible process the evolution of heat (-dQ) gives a direct measure of the change of entropy in the process. If heat is evolved on the extension of the material, the entropy change is negative. Conversely, if heat is absorbed, the entropy change is positive.

Assuming that the work is done only by the external force of extension, f, one obtains for isothermal stretching

$$f = \left(\frac{\partial E}{\partial L}\right)_T - T\left(\frac{\partial S}{\partial L}\right)_T \qquad (2)$$

where the quantities E, T, S and L have their usual meaning. If there is no heat exchange with the surrounding medium and if the internal energy of rubber does not depend on deformation, a thermodynamical consideration gives an expression (5)

$$\left(\frac{\partial T}{\partial L}\right)_S = \frac{f}{C_L} = -\frac{T}{C_L}\left(\frac{\partial S}{\partial L}\right)_T \qquad (3)$$

where C_L is the specific heat at constant sample length. Integrating between the limits L_o and L, one finds the temperature change, T:

$$\Delta T = -\frac{T}{C_L}\int_{L_o}^{L}\left(\frac{\partial S}{\partial L}\right)_T dL$$

$$= \frac{1}{C_L}\int_{L_o}^{L} f\,dL \qquad (4)$$

The term $\int_{L_o}^{L}\left(\frac{\partial S}{\partial L}\right)_T dL$ means the entropy change ΔS when the rubber is stretched from the length L_o to L.

The theory of rubber elasticity gives readily the value of ΔS for a Gaussian network as

$$\Delta S = -\frac{1}{2} N_c k\,(\alpha^2 + 2/\alpha - 3) \qquad (5)$$

where N_c is the number of chains per unit volume, k is Boltzmann's constant and α is the elongation ratio. ΔT is then described as

$$\Delta T = \frac{N_c kT}{2CL}\,(\alpha^2 + 2/\alpha - 3) \qquad (6)$$

As an approximation the specific heat at constant length, C_L, may be replaced by the specific heat at constant pressure, C_p. The value of C_p for cis-polyisoprene is 0.437 cal/gC°. The value of N may be determined in the same manner as described in Chapter I. Thus ΔT can be estimated as a function of α. The values of ΔT calculated are given in Table 1.

Equation (4) says that one can also estimate the temperature rise from the force-strain relationship. A typical force-strain curve is given in Figure 1. In this work samples were stretched at a rate of 2000 % per minute. The term $\int fDL$ gives the work done on the total sample (not on unit volume of the sample) and is used to heat up the sample. The values of ΔT calculated from Figure 1 are given in Table 2.

The values in Table 1 are higher than those in Table 2. This is because the values in Table 1 were calculated using the Gaussian rubber elasticity theory, which is now well known to give higher stress than actual value. The estimation in Table 2, therefore, is probably better than in Table 1.

From Table 2 one may conclude for typical samples used in this work that at relatively low elongations the temperature rise upon rapid stretching probably does not have a significant effect on the crystallization which will occur following the stretching. At higher elongations there may be some effect on the crystallization, however, it is considered to be small because of small values of ΔT. If a very highly crosslinked polymer is used, the temperature rise may be significantly large because of its high elastic modulus, which will cause a serious problem on the crystallization kinetics.

In the present estimation it is assumed that the internal energy does not change with deformations. However internal energy changes have been

reported as being typically, for an example, in natural rubber between 10 and 20 % of the total work done (6). Consequently, actual temperature rise will be expected to be slightly smaller than the value estimated here, since energy is apparently absorbed by the rotational isomerization (6).

Heat Generation by Crystallization

If a rubber sample is stretched sufficiently to cause crystallization, the configurational entropy change will not be the only reason for the temperature rise. The latent heat of crystallization will be superposed on the effect due to the entropy change. This phenomenon has been observed by several workers (7-10). This effect due to the crystallization may be a primary reason for the temperature rise. Rubbers which do not crystallize usually do not show the very large temperature rise. For an example, the maximum heating by Hycar OR (butadiene-acrylic nitrile) is less than 2°C (11), which is very small compared with 14°C reported for natural rubber and neoprene (7).

This thermal phenomenon due to the crystallization may be used as an indicator for the process of the crystallization. Mitchell and Meier (12) havestudied the stress-induced crystallization in a rapidly stretched natural rubber by following the heat evolved when the crystallization is initiated.

In this section the temperature rise due to crystallization is estimated in the adiabatic condition. The heat evolved by the crystallization may be described as

$$\Delta Q = -N_c \, mq \, \Delta H_u$$

$$= -N_c \, n_s X_c \, q \, \Delta H_u \qquad (7)$$

where m is the number of segments in the crystalline phase, q the number of monomeric units per segment, ΔH_u the enthalpy of fusion per monomeric unit, X_c the degree of crystallinity and n_s is the number of statistical segments between crosslinks.

The values from 1000 to 1170 cal/mole have been reported as ΔH_u for natural rubber (13,14). Using a value of 1100 cal/mole (1.83×10^{-21} cal/monomer unit) for ΔH_u and typical values for other parameters, which were obtained in Chapter I as $q = 1.98$, $n_s = 97.8$ and $N_c = 4.21 \times 10^{19}$ cm^3, ΔQ can be expressed by

$$\Delta Q = -14.89\ X_c \quad \text{cal/cc} \tag{8}$$

where (-) sign means that the crystallization is an exthermal process. The temperature rise corresponding to the crystallization which is given in Figures in Chapter I was calculated assuming an adiabatic condition from Equation (8). It is shown in Table 3. The values in Table 3 are relatively comparable with the temperature rises reported for natural rubber (12). It is noted that at low elongation ($\alpha = 3.89$) the temperature rise due to crystallization is very small. One may, therefore, conclude that the crystallization at $\alpha = 3.89$ is not significantly affected by the heat liberated by the crystallization itself. At higher elongation ($\alpha = 6.0$), however, there may be some affect of the temperature rise on the crystallization. To deal with this problem, one must consider the heat transfer from the sample to its surrounding materials.

Heat Transfer from A Sample to Air

The adiabatic temperature rise during the crystallization cannot be

neglected at high elongation as demonstrated above. However, the real system is not adiabatic, but the heat can be transferred from the sample to the surrounding media, which is air in this consideration.

We will consider a case that a thin rubber sample is placed vertically in the still air. This problem is so called "heat transfer by free convection" (15). The heat transferred through two surfaces of the sample may be given as (15)

$$2A\ (T_S - T_\infty)\ h\ dt = -C_L\ V dT_S \qquad (9)$$

where A is the surface area, T_S the temperature of the sample at time t, T_∞ the temperature of the air, h is the convection coefficient, and V is the volume of the sample.

Integrating Equation (9) from t = 0 to t = 5, one obtains

$$T_S = T_\infty + (T_0 - T_\infty)\ \exp\left(-\frac{2Aht}{C_L V}\right) \qquad (10)$$

where T_0 is the initial temperature (at t = 0) of the sample. A function J is defined as

$$J(t) = \frac{\Delta T}{\Delta T_0} = \frac{T_S - T_\infty}{T_0 - T_\infty} = \exp\left(-\frac{2Aht}{C_L V}\right) \qquad (11)$$

The value of the convection coefficient h may be cauculated by the methods given elsewhere (15-17). The coefficient h may be described as

$$h = A\ \frac{K}{L}\ (a\ L^3 \Delta T)^B \qquad (12)$$

where K is the thermal conductivity of the air, L is the sample height, and

a is given by

$$a = g \beta \rho^2 C_p / \mu K \tag{13}$$

where g is the acceleration of gravity, β the coefficient of thermal expansion of the fluid (air), ρ the density of fluid, C_p the specific heat of fluid, and μ is the absolute viscosity of fluid. The constants A and B are determined from the value of $(a\ L^3 \Delta T)$.

In the case in which T_o is about 5-20°F (3-10°C) higher than room temperature (25°C), the coefficient h is given by

$$h = 0.344\ (\Delta T)^{1/4} \tag{14}$$

where the unit is BtU/(hr) (ft^2) (°F).

Assuming that the initial temperature difference is 10°F (≃ 5.6°C) and that h does not change during heat transfer, J was calculated as a function of time. It is shown in Figure 2 (a). Actually h does depend upon ΔT. The result considering this factor, however, is not changed significantly as shownin Figure 2 (b).

By comparing Table 3 (α = 6.0) with Figure 2, one may conclude that at later stages of the crystallization there are no heat effects on the crystallization because heat transfer is fast enough not to build up heat within the sample. At very initial stages of crystallization, there seems to be a temperature rise which is small, probably about 1°C. Therefore, one can say that there is no significant heat effect on the crystallization of PIP.

In summary we may conclude that as for the study of the crystallization

of PIP used in this work, we can neglect the heat effect evolved by stretching or following crystallization. This conclusion is attributed to two main factors, which are that (1) the rate of crystallization of PIP is relatively low, and (2) the heat transfer from the sample to the surrounding media is sufficiently fast to remove heat liberated within the sample.

If polymers with very high rates of crystallization and high crystallinity are used for this kind of study, however, there will be a significant effect due to the temperature rise and one will have to take note of this effect to study the real kinetics of the crystallization

References

1. M. Gough, Mem. Lit. Phil. Soc., Manchester, 1, 288 (1805).
2. J. P. Joule, Trans. Roy. Soc., London, 149, 91 (1859).
3. L. Mandelkern, Crystallization of Polymers, McGraw-Hill, New York, 1964.
4. W. J. Moore, Physical Chemistry, Prentice-Hall, New Jersey, 1962.
5. M. Volkenstein, Configurational Statistics of Polymeric Chains, Interscience, New York, 1963.
6. M. C. Shen, D. A. McQuarrie and J. L. Jackson, J. Appl. Phys., 38, 791 (1967).
7. S. L. Dart, R. L. Anthony and E. Guth, Ind. Eng. Chem., 34, 1340 (1942).
8. S. L. Dart and E. Guth, J. Chem. Phys., 13, 28 (1945).
9. J. B. Ehrbar and C. G. Boissonas, Rubber Chem. Tech., 28, 675 (1955).
10. M. P. Votinov and E. V. Kuvshinskii, Rubber Chem. Tech., 29, 1209 (1956).
11. L. R. G. Treloar, The Physics of Rubber Elasticity, Oxford, 1958.
12. J. Mitchell and D. Meier, J. Polym. Sci., A-2, 6, 1689 (1968).
13. D. E. Roberts and L. Mandelkern, J. Amer. Chem. Soc., 77, 781 (1955).
14. F. deCandia, G. Romano and V. Vittoria, J. Polym. Sci., Polym. Phys. Ed., 11, 2291 (1973).
15. A. I. Brown and S. M. Marco, Introduction to Heat Transfer, McGraw-Hill, New York, 1958.
16. H. Grober, U. Grigull and J. Moszynski, Fundamentals of Heat Transfer, McGraw-Hill, New York, 1961.
17. A. J. Chapman, Heat Transfer, Macmillan, New York, 1960.

TABLE 1

Temperature Rise Upon Adibatic Stretching

α	ΔT (°C)
1	1
2	0.3
3	1.1
4	2.2
5	3.6
6	5.4
7	7.5

TABLE 2

Temperature Rise Upon Adiabatic Stretching

α	ΔT (°C)
1	0
2	0.1
3	0.5
4	0.9
5	1.5
6	2.3

TABLE 3

Adiabatic Temperature Rises by the Crystallization Shown in Figures in Chapter 1

Time (sec)	X_c	ΔT (°C)
	$\alpha = 6.0$	
10	0.036	1.4
30	0.076	2.9
100	0.085	3.1
300	0.097	3.6
1080	0.109	4.1
3600	0.121	4.5
11400	0.135	5.1
54000	0.148	5.5
	$\alpha = 3.89$	
10	0	0
30	0.002	0.0^{7}_{5}
120	0.004	0.1^{5}_{9}
360	0.005	0.1^{9}_{6}
1200	0.007	0.2^{6}_{4}
3600	0.009	0.3^{4}_{5}
11700	0.012	0.4^{5}_{0}
45600	0.016	0.6^{0}

Captions for Figures

1) Force-strain curve of a sample stretched at a rate of 2000% per minute.

2) The variation of J calculated from Equation (11); (a) h given by Equation (12) is assumed to be constant; (b) actual h is used.

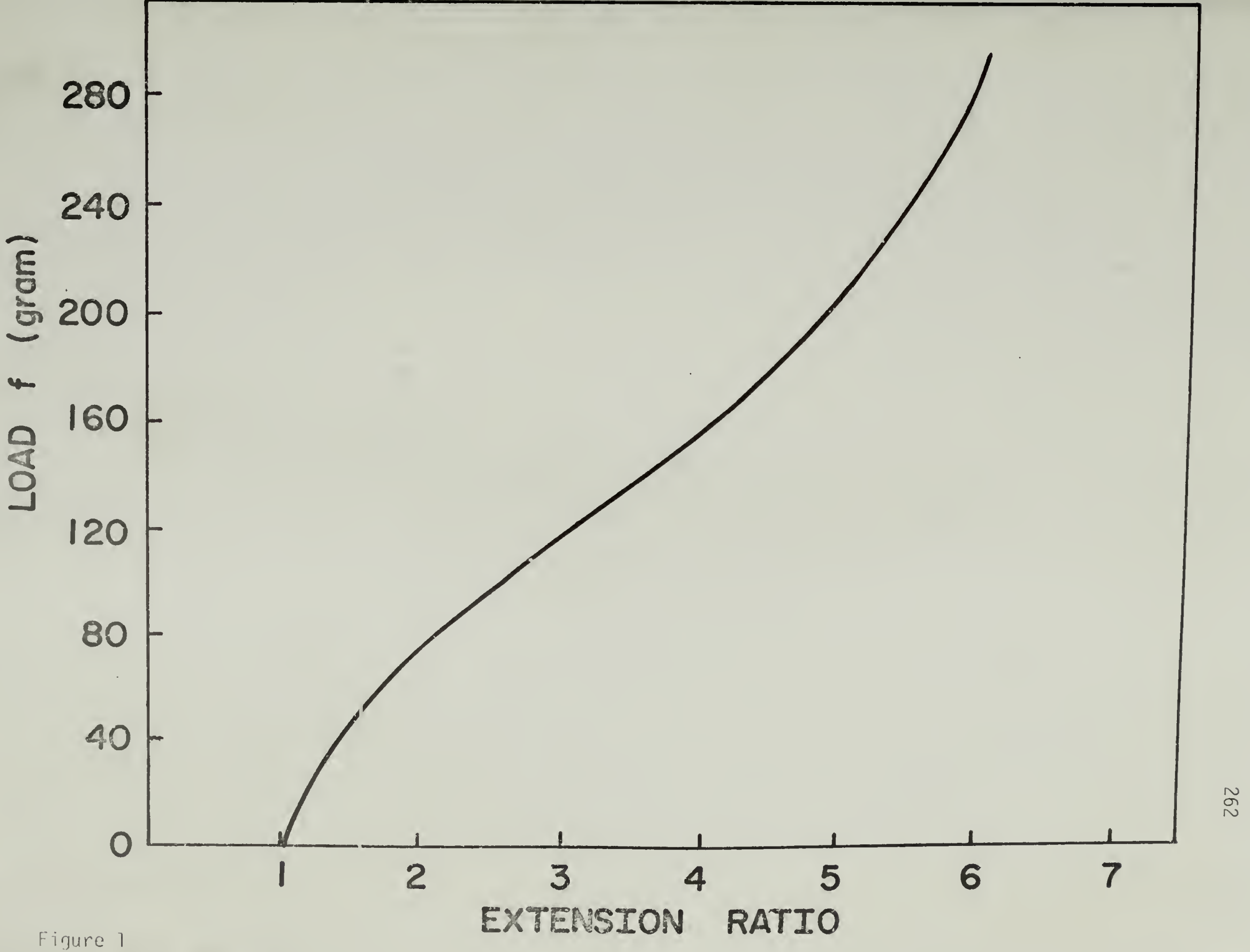
LOAD f (gram)
280
240
200
160
120
80
40
0
1
2
3
4
5
6
7
EXTENSION RATIO

Figure 1

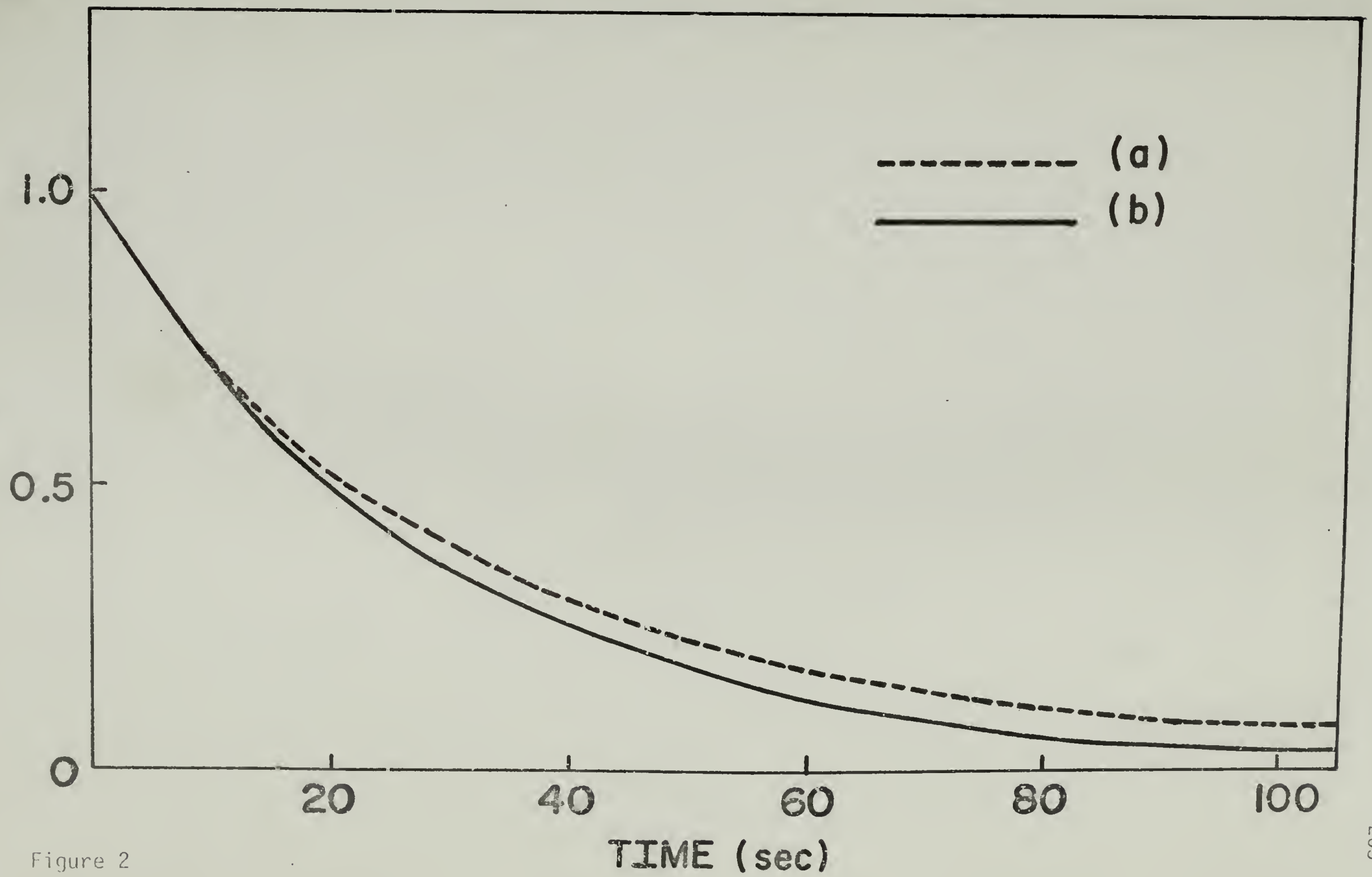

Figure 2

APPENDIX III

Intensities of The H_V and V_V Scattering

The ratio of the H_V and V_V scattering intensities from a rod may be described as

$$\frac{I_{V_V}}{I_{H_V}} = \frac{(\delta \cos^2\alpha + b_t)^2}{(\delta \sin\alpha \cos\alpha)^2} \qquad (1)$$

where δ, α and b_t are given in CHAPTER V.

The average polarizability of the amorphous phase may be calculated using Clement and Bothorel's bond polarizabilities. The value per unit volume is 0.07276. The average polarizability of the crystalline phase may be obtained using the result in APPENDIX I. The value is 0.08033. By assuming that $X_c = 0.14$ ($\phi_c = 0.128$), one may obtain the value of the average polarizability of the surrounding, which is 0.07373.

The longitudinal and tangential polarizabilities of the rod may be obtained from the result in APPENDIX I. They are 0.09648 and 0.07225, respectively. Then, the value of δ and b_t are 0.02423 and - 0.00148, respectively. From the x-ray studies in CHAPTER III, α is determined to be approximately 7°.

The value of I_{V_V}/I_{H_V} may be obtained from Eq. (1), it is about 58. This result is in reasonably good agreement with the value obtained by the photographic method. The Denbigh's bond polarizabilities give a value of 85. The contribution due to the density fluctuation to the total intensity is about - 6% and 13% for Clement and Bothorel's and for Denbigh's polariza-

bilities, respectively. One may, therefore, conclude that the most scattering arises from the fluctuation in the orientation of anisotropic bodies.